

UNCLASSIFIED

AD NUMBER

AD384477

CLASSIFICATION CHANGES

TO: unclassified

FROM: confidential

LIMITATION CHANGES

TO:

Approved for public release, distribution  
unlimited

FROM:

Controlling DoD Organization: Air Force  
Rocket Propulsion Lab., Edwards AFB, CA.

AUTHORITY

30 Sep 1979 per Grp-4 document marking;  
Air Force Rocket Propulsion Lab ltr dtd 5  
Feb 1986

THIS PAGE IS UNCLASSIFIED

# **SECURITY MARKING**

---

**The classified or limited status of this report applies to each page, unless otherwise marked.**

**Separate page printouts MUST be marked accordingly.**

---

**THIS DOCUMENT CONTAINS INFORMATION AFFECTING THE NATIONAL DEFENSE OF THE UNITED STATES WITHIN THE MEANING OF THE ESPIONAGE LAWS, TITLE 18, U.S.C., SECTIONS 793 AND 794. THE TRANSMISSION OR THE REVELATION OF ITS CONTENTS IN ANY MANNER TO AN UNAUTHORIZED PERSON IS PROHIBITED BY LAW.**

**NOTICE: When government or other drawings, specifications or other data are used for any purpose other than in connection with a definitely related government procurement operation, the U. S. Government thereby incurs no responsibility, nor any obligation whatsoever; and the fact that the Government may have formulated, furnished, or in any way supplied the said drawings, specifications, or other data is not to be regarded by implication or otherwise as in any manner licensing the holder or any other person or corporation, or conveying any rights or permission to manufacture, use or sell any patented invention that may in any way be related thereto.**

~~CONFIDENTIAL~~

AFRPL-TR-67-204

September 1967

(Title Unclassified)

ADVANCED PROPELLANT STAGED-COMBUSTION FEASIBILITY PROGRAM

Final Report, Phase II

R. J. Kuntz, PE, R. G. Sjogren, et al.

Aerojet-General Corporation

AD384477

Prepared for

AIR FORCE ROCKET PROPULSION LABORATORY

Air Force Systems Command

Research and Technology Division

United States Air Force

Edwards Air Force Base, California 93523

OCT 15 1967

SPECIAL HANDLING REQUIRED

NOT RELEASABLE TO FOREIGN NATIONALS

The information contained in this document will not be disclosed to foreign nationals or their representatives.

0961

~~CONFIDENTIAL~~

## **REPRODUCTION QUALITY NOTICE**

**This document is the best quality available. The copy furnished to DTIC contained pages that may have the following quality problems:**

- **Pages smaller or larger than normal.**
- **Pages with background color or light colored printing.**
- **Pages with small type or poor printing; and or**
- **Pages with continuous tone material or color photographs.**

**Due to various output media available these conditions may or may not cause poor legibility in the microfiche or hardcopy output you receive.**

☐ **If this block is checked, the copy furnished to DTIC contained pages with color printing, that when reproduced in Black and White, may change detail of the original copy.**

~~CONFIDENTIAL~~

Report 10785-F, Phase II

LEGAL NOTICE

"When U.S. Government drawings, specifications, or other data are used for any purpose other than a definitely related Government procurement operation, the Government thereby incurs no responsibility nor any obligation whatsoever, and the fact that the Government may have formulated, furnished, or in any way supplied the said drawings, specifications, or other data, is not to be regarded by implication or otherwise, or in any manner licensing the holder or any other person or corporation, or conveying any rights or permission to manufacture, use, or sell any patented invention that may in any way be related thereto."

~~CONFIDENTIAL~~

(This page is Unclassified)

~~CONFIDENTIAL~~

AFRPL-TR-67-204

September 1967

(Title Unclassified)

ADVANCED PROPELLANT STAGED-COMBUSTION FEASIBILITY PROGRAM

Final Report, Phase II

R. J. Kuntz, PE, R. G. Sjogren, et al.

Report 10785-F, Phase II

Prepared for

AIR FORCE ROCKET PROPULSION LABORATORY  
Air Force Systems Command  
Research and Technology Division  
United States Air Force  
Edwards Air Force Base, California 93523

SPECIAL HANDLING REQUIRED

NOT RELEASABLE TO FOREIGN NATIONALS

The information contained in this document will not be disclosed to foreign nationals or their representatives.

GROUP 4
DECLASSIFIED AT 1 YEAR INTERVALS, UNCLASSIFIED AFTER 12 YEARS
ALL INFORMATION CONTAINED HEREIN IS UNCLASSIFIED EXCEPT WHERE SHOWN OTHERWISE
EXCEPT WHERE SHOWN OTHERWISE, THIS INFORMATION IS UNCLASSIFIED
EXCEPT WHERE SHOWN OTHERWISE, THIS INFORMATION IS UNCLASSIFIED
EXCEPT WHERE SHOWN OTHERWISE, THIS INFORMATION IS UNCLASSIFIED

~~CONFIDENTIAL~~

0203T

~~CONFIDENTIAL~~

Report 10785-F, Phase II

FOREWORD

This is the summary final report submitted in partial fulfillment of Contract AF 04(611)-10785. The program had two Air Force managers, Mr. Richard Weiss/AFRPL, originally, and Capt. J. F. Ensminger/AFRPL who later succeeded him. This report contains a summary of major accomplishments and a discussion of technical progress of Phase II of the program. Phase I of the program is covered by another final report, AFRPL-TR-66-4, and the experimental  $H_2O_2$  heat-transfer work spanning both phases is presented in special report AFRPL-TR-66-263. The period of performance covered by the Phase II final report is from December 1965 to July 1967.

The Advanced Propellant Staged-Combustion Feasibility Program was conducted by the Advanced Storable Engine Division of Liquid Rocket Operations, Aerojet-General Corporation, Sacramento, California, under the direction of Mr. R. Beichel. Technical and managerial control was provided by Mr. R. J. Kuntz, PE, Project Manager. Mr. R. G. Sjogren was the Project Engineer.

Contributors to this report, in addition to those noted on the title page, included the following Aerojet personnel:

Hardware Design:	G. V. Brereton
Engine Transient Cooling Characteristics:	R. L. Even
	P. F. Farr
	S. D. Mercer
Performance Analysis:	J. I. Ito
Heat-Flux Analysis:	W. J. Bailey
	M. J. Ditore
	H. I. Siegel
	J. J. Williams
Combustion Stability:	D. A. McCallister
	K. K. Wong
Catalyst Pack Operation Analysis:	C. J. O'Brien

~~CONFIDENTIAL~~

(This page is Unclassified)

~~UNCLASSIFIED~~  
UNCLASSIFIED

Report 10785-P, Phase II

FOREWORD (cont.)

In addition, we would like to acknowledge the help of Mr. J. M. McCarrick of the Food Machinery and Chemical Corporation for supplying valuable technical assistance with regard to catalysts for peroxide decomposition.

This technical report has been reviewed and is approved.

Capt. J. P. Ensminger  
USAF Program Manager

~~UNCLASSIFIED~~  
UNCLASSIFIED



# UNCLASSIFIED

Report 10785-F, Phase II

## UNCLASSIFIED ABSTRACT

The major objective of this program was the definition of problems associated with the use of 98% hydrogen peroxide ( $H_2O_2$ ) and Alumizine-43 in a staged-combustion rocket engine system. In the cooled version of the engine conceived, all of the  $H_2O_2$  is used to regeneratively cool a secondary combustor (in which Alumizine-43 is burned) before the  $H_2O_2$  passes through the preburner catalyst pack and the turbine. Conditions associated with operating this engine cycle that require investigation are (1) the ability of  $H_2O_2$  to cool the secondary combustor, (2) integrity of the catalyst (activity, durability) at higher temperature, (3) heat-transfer characteristics of 98% peroxide, and (4) the effect that thermal decomposition of  $H_2O_2$  vapor may have on the engine design. The program was divided into two phases. Phase I (of six months duration) consisted of design and analysis, 98%  $H_2O_2$  experimental technology, and critical hardware procurement for Phase II. This phase of the contract was conducted from June to December 1965. The results of Phase I indicated that 98%  $H_2O_2$  would be a satisfactory coolant and oxidizer for an Alumizine-fueled engine.

Phase II was initiated immediately following the conclusion of Phase I and consisted of a series of 20,000-lbf preburner and staged-combustion evaluation tests. The Phase II technical achievements included the completion of a  $H_2O_2$  experimental heat-transfer program, a preburner test program, and a staged-combustion test program. Satisfactory operation of a 98%  $H_2O_2$  preburner was demonstrated at throughputs from 48 to 108.2 psim for two catalyst configurations. Staged combustion at 3000 psia with 98%  $H_2O_2$ /Alumizine-43 was demonstrated satisfactorily with two secondary injector concepts. Heat-transfer data on critical areas of the chamber and throat were obtained. The experimental performance of the propellant combination was determined over a range of mixture ratios with two different  $L^*$  chambers. The performance of 90%  $H_2O_2$ /Alumizine-43 was determined and compared to the 98%  $H_2O_2$ /Alumizine-43 propellant combination.

v

UNCLASSIFIED

UNCLASSIFIED

Report 10785-F, Phase II

TABLE OF CONTENTS

	<u>Page</u>
I. Introduction	1
A. Program Description and Background	1
B. Statement of Work for Phase II	2
C. Summary of Accomplishments	5
D. Organization of Report	8
II. Engine Transient Cooling Characteristics	9
A. Introduction and Summary	9
B. Technical Discussion	11
III. Preburner Evaluation	29
A. Program Objectives and Approach	29
B. Technical Discussion	30
1. Hardware	30
2. Method of Testing	41
3. Test Facilities	51
4. Preburner Test Description and Results	58
5. Test Data Analyses	78
IV. Staged-Combustion Evaluation	89
A. Program Objectives and Approach	89
B. Technical Discussion	91
1. Hardware	91
2. Method of Testing	114
3. Staged-Combustion Test Description and Results	129
4. Performance Analysis	194
5. Heat-Flux Analysis	226
6. Test Data Analysis	243
V. Conclusions	247
VI. Recommendations	250

UNCLASSIFIED

# UNCLASSIFIED

Report 10785-F, Phase II

## TABLE OF CONTENTS (cont.)

### APPENDIXES

	<u>Page</u>
I Shutdown Transient Equations and Computer Programs	255
II A Description of the Interaction Theory Method of Performance Analysis	278
III A Method for Evaluating Chamber Heat Loss	285
IV A Method for Evaluating Chamber Friction Loss	289

### TABLE LIST

<u>Table</u>	<u>Page</u>
I Preburner Design Parameters	32
II Advanced Propellant Staged-Combustion Feasibility Program--Preburner Operation	59
III Oxidizer Valve Bypass Operation	68
IV 20,000-lbf Staged-Combustion Engine Design Parameters	92
V Comparison of Vane-Type Injector Designs	104
VI Advanced Propellant Staged-Combustion Feasibility Program--Staged-Combustion Operation Results	130
VII Performance Summary--Advanced Propellant Program	195
VIII Predicted 100K Engine Performance--Advanced Propellant Staged-Combustion Program	221
IX Position of Thermocouple Tips for Test 1.2-02-AAC-004	227
X Position of Thermocouple Tips for Tests 1.2-03-AAC-001, 003, and 007	227
XI Engine Operating Parameters, Tests 1.2-03-AAC-001 and 003	229

viii

UNCLASSIFIED

# UNCLASSIFIED

Report 107P5-F, Phase II

## FIGURE LIST

<u>Figure</u>		<u>Page</u>
1	Program Organization	3
2	Shutdown Transient Analysis	13
3	Reduced Valve Transients, Advanced Staged-Combustion Engine	16
4	Advanced Staged-Combustion Engine Flow System Shutdown Transient--Both Valves Closed Simultaneously in 0.5 sec	17
5	Advanced Staged-Combustion Engine Chamber Wall Shutdown Transient--Both Valves Closed Simultaneously in 0.5 sec	18
6	Advanced Staged-Combustion Engine Flow System Shutdown Transient--0.1-sec Oxidizer Delay, Both Valves Closed at 0.5 sec	20
7	Advanced Staged-Combustion Engine Chamber Wall Shutdown Transient--0.1-sec Oxidizer Delay, Both Valves Closed at 0.5 sec	22
8	Advanced Staged-Combustion Engine--Chamber Wall Analysis	24
9	Advanced Staged-Combustion Engine--Shutdown Transient for Thin Coating	26
10	Advanced Staged-Combustion Engine--Shutdown Transient for Tungsten Coating	27
11	H <sub>2</sub> O <sub>2</sub> Preburner	33
12	Decomposition Temperature of Peroxide	36
13	Instrumentation of Preburner Assembly	40
14	Propellant Circuit Schematic--H <sub>2</sub> O <sub>2</sub> Preburner	43
15	J-1 Low Frequency Stability Analysis	47
16	Gain-Phase Plot of J-1 Preburner with Turbine Simulator	49
17	Gain-Phase Plot of J-1 Preburner without Turbine Simulator	50
18	Partial Cutaway of Intensifier	52
19	H <sub>2</sub> O <sub>2</sub> Intensifier--Oxidizer End	53
20	H <sub>2</sub> O <sub>2</sub> Intensifier--Gaseous Nitrogen End	54
21	Preburner Performance after FS-1, Test 1.2-01-AAC-001	60
22	Preburner Performance before FS-1, Test 1.2-01-AAC-001	61

UNCLASSIFIED

# UNCLASSIFIED

Report 10785-F, Phase II

## FIGURE LIST (cont.)

<u>Figure</u>		<u>Page</u>
23	Preburner Performance after FS-1, Test 1.2-01-AAC-002	62
24	Preburner Performance before FS-1, Test 1.2-01-AAC-002	63
25	Preburner Performance--Test 1.2-01-AAC-003	64
26	Preburner Performance--Test 1.2-01-AAC-004	65
27	Preburner Performance--Test 1.2-01-AAC-005	66
28	Preburner Installation, Test Stand J-1	67
29	Preburner Turbine Simulator after Test 1.2-01-AAC-001	70
30	Preburner Aft View of Outlet Plate after Test 1.2-01-AAC-001	71
31	Preburner Inlet Plate after Test 1.2-01-AAC-003	75
32	Catalyst-Pack Postfire, Test 1.2-01-AAC-003	76
33	Catalyst-Pack Temperature Profiles--Low Throughput	79
34	Catalyst-Pack Temperature Profiles--High Throughput, SN 001	81
35	Catalyst-Pack Temperature Profiles--High Throughput, SN 002	83
36	Combustion Dynamics Parameters	87
37	H <sub>2</sub> O <sub>2</sub> /Alumizine-43 Staged-Combustion TCA	94
38	Comparison of Alumizine-43 K <sub>w</sub> with Hydro Lab K <sub>w</sub>	95
39	Tubular Injector	96
40	Multinozzle Injector	98
41	Vane-Type Injector--Mod I	100
42	Mod I Vane-Type Injector Face--Before Modification	101
43	Mod I Vane-Type Injector--After Modification	103
44	Heat-Flux Transducer Installation	107
45	Secondary Combustor	108
46	Predicted Chamber Heat-Flux Transducer Temperature Transient	110
47	Predicted Throat Heat-Flux Transducer Temperature Transient	111
48	TCA Instrumentation	113
49	98% H <sub>2</sub> O <sub>2</sub> /Alumizine-43 Performance Parameters versus Mixture Ratio	118

x

UNCLASSIFIED

# UNCLASSIFIED

Report 10785-F, Phase II

## FIGURE LIST (cont.)

Figure		Page
50	Regression Rate of Tungsten	120
51	Thermochemistry of 98% $H_2O_2$ /Alumizinc-43 System in Presence of Tungsten at 6000°F	122
52	Variation of Oxidation of Tungsten with Temperature	124
53	Comparison of Delivered $I_s$ vs Theoretical $I_s$ , 98% $H_2O_2$ /Alumizinc-43 (Vane Injector Only)	132
54	Percent Theoretical $I_s$ vs MR for 90 and 98% $H_2O_2$ /Alumizinc-43	132
55	Staged-Combustion Flow Schematic	134
56	Staged-Combustion System Performance, Test 1.2-02-AAC-001	136
57	Staged-Combustion Catalyst Pack Temperature Profiles, Test Series 1.2-02-AAC	137
58	TCA Installation on Test Stand J-1, Test 1.2-02-AAC-002	139
59	Staged-Combustion System Performance, Test 1.2-02-AAC-002 (Plot B)	141
60	Staged-Combustion System Performance, Test 1.2-02-AAC-002 (Plot A)	142
61	Ablative Chamber Viewed from Injector after Test 1.2-02-AAC-002	143
62	Staged-Combustion System Performance, Test 1.2-02-AAC-003	145
63	Mod X Vane-Injector Face after Tests 1.2-02-AAC-002 and -003	147
64	Postfire Contour after Tests 1.2-02-AAC-002 and -003	148
65	Staged-Combustion System Performance, Test 1.2-02-AAC-004 (Plot A)	150
66	Staged-Combustion System Performance, Test 1.2-02-AAC-004 (Plot B)	151
67	Filter Particle Sampler	152
68	Tubular-Injector Face after Test 1.2-02-AAC-004	153
69	Inlet Side of Tungsten Throat after Test 1.2-02-AAC-004	154
70	TCA Installation on Test Stand J-1, Test 1.2-03-AAC-001	157
71	Staged-Combustion System Performance Test, Test 1.2-03-AAC-001	158
72	Catalyst Pack Performance, Test 1.2-03-AAC-001	160

UNCLASSIFIED

# UNCLASSIFIED

Report 10735-F, Phase II

## FIGURE LIST (cont.)

<u>Figure</u>		<u>Page</u>
73	Throat and Exit Cone, Postfire, Test 1.2-03-AAC-001	161
74	Chamber, Postfire, Test 1.2-03-AAC-001	162
75	TCA Installation on Test Stand J-1, Test 1.2-03-AAC-002	164
76	Staged-Combustion System Performance Test 1.2-03-AAC-002	165
77	Mod III Vane Injector after Test 1.2-03-AAC-002	166
78	Catalyst Pack Performance, Test 1.2-03-AAC-002	168
79	Staged-Combustion System Performance, Test 1.2-03-AAC-003	170
80	Mod II Vane Injector after Test 1.2-03-AAC-003	172
81	Throat and Exit Cone, Postfire, Test 1.2-03-AAC-003	173
82	Catalyst Pack Performance Test 1.2-03-AAC-003	174
83	Staged-Combustion System Performance, Test 1.2-03-AAC-005	177
84	Catalyst Pack Performance Test 1.2-03-AAC-005	179
85	Staged-Combustion System Performance, Test 1.2-03-AAC-007	180
86	Catalyst Pack Performance, Test 1.2-03-AAC-007	182
87	CC (Combustion Chamber) Heat-Flux Transducer Temperature, Test 1.2-03-AAC-007	183
88	CE (Throat Entry Section) Heat-Flux Transducer Temperatures, Test 1.2-03-AAC-007	184
89	CT (Throat) Heat-Flux Transducer Temperatures, Test 1.2-03-AAC-007	185
90	Staged-Combustion System Performance, Test 1.2-03-AAC-008	187
91	Catalyst Pack Performance, Test 1.2-03-AAC-008	189
92	Staged-Combustion System Performance, Test 1.2-03-AAC-010	191
93	Modified Tubular Injector, Postfire, Test 1.2-03-AAC-010	192
94	Catalyst Pack Performance, Test 1.2-03-AAC-010	193
95	Effect of Mixture Ratio versus Efficiency	196
96	Particle Mass Distribution versus Particle Diameter	202
97	Effect of Mixture Ratio on Gas-Particle Loss	203
98	Effect of Operating Mixture Ratio on the Theoretical Combustion Temperature with and without Aluminum Combustion	205

UNCLASSIFIED

# UNCLASSIFIED

Report 10785-F, Phase II

## FIGURE LIST (cont.)

<u>Figure</u>		<u>Page</u>
99	Effect of Mixture Ratio upon Energy Release Efficiency	208
100	Effect of Fuel Vaporization Rate upon Energy Release Efficiency	209
101	Effect of Mixture Ratio upon Fuel Vaporization Rate	210
102	Estimated and Experimental Combustion Efficiency	215
103	Estimated and Experimental Specific Impulse Efficiency	217
104	Estimated and Experimental Specific Impulse Normalized Efficiency	219
105	Effect of Nozzle Position on Two-Phase Flow Performance Loss	223
106	Effect of Mixture Ratio and Particle Size on Two-Phase Flow Performance Loss	224
107	Thermodynamic Properties of Silver-Infiltrated Tungsten	230
108	Combustion Chamber Heat-Flux Transducer Temperature Histories, Test 1.2-02-AAC-004	231
109	Throat Heat-Flux Transducer Temperature Histories, Test 1.2-03-AAC-001	232
110	Combustion Chamber Heat-Flux Transducer Temperature Histories, Test 1.2-03-AAC-001	233
111	Throat Heat-Flux Transducer Temperature Histories, Test 1.2-03-AAC-003	234
112	Throat Heat-Flux Transducer Temperature Histories, Test 1.2-03-AAC-007	235
113	Comparison of Temperature for Throat, Tests 1.2-02-AAC-001 and -003	236
114	Temperature Transient During Steady State--Throat Section, Test 1.2-03-AAC-001	239
115	Temperature Transients During Steady State--Chamber Section, Test 1.2-03-AAC-001	240

x111

UNCLASSIFIED



# UNCLASSIFIED

Report 10785-F, Phase II

## SECTION I

### INTRODUCTION

#### A. PROGRAM DESCRIPTION AND BACKGROUND

(U) High-chamber-pressure liquid rocket engines incorporating the staged-combustion cycle and using storable liquid propellants such as  $N_2O_4$  and 50% UDMH-50% hydrazine have been under evaluation for some time. Mission and growth-potential studies indicated that the performance of this engine system can be increased significantly by using as propellants gelled mixtures of hydrazine and aluminum powder with either  $N_2O_4$  or 98%  $H_2O_2$  as the oxidizer. Further studies indicated that  $H_2O_2$  provides significant advantages over  $N_2O_4$ , because  $H_2O_2$  requires only a monopropellant preburner (which reduces the complexity of the propulsion system); provides "on-board" life support and subsystem capability; and offers the possibility of further performance increases through the use of gelled mixtures of hydrazine with beryllium powder or light metal hydrides.

(U) In this advanced engine system, all of the  $H_2O_2$  is decomposed when passing through a preburner catalyst bed; the decomposed  $H_2O_2$  is a hot gas (oxygen and steam) that is capable of driving a turbine to drive the fuel and oxidizer turbopumps. The turbine exhaust then passes through a secondary injector where the fuel is added to be burned in the combustion chamber. The engine system may or may not be cooled, depending on design requirements. In the cooled version, the  $H_2O_2$  first passes through the coolant jacket of the combustion chamber before entering into the preburner catalyst bed. Other cooled variations are possible (e.g., parallel flow circuits for the coolant jacket and the preburner). In the uncooled version, a tungsten-lined, graphite heat-sink chamber would be used for the combustor.

(U) The combined use of  $H_2O_2$  and metalized propellants in a high-pressure staged-combustion engine system required further development in various areas of

UNCLASSIFIED

UNCLASSIFIED

Report 10785-F, Phase II

I. A. Program Description and Background (cont.)

technology: a high-temperature catalyst bed for the decomposition of 98%  $H_2O_2$  had to be developed; the ability to burn metalized propellants and to realize high performance efficiency had to be demonstrated; and the feasibility of absorbing anticipated high heat fluxes in the combustion chamber had to be established. An exploratory development program, divided into two phases, was therefore initiated at Aerojet-General Corporation under the direction of the Air Force Rocket Propulsion Laboratory, Edwards AFB, California. Organization and task structure of this program are shown in Figure 1.

(U) Phase I was primarily concerned with the evaluation of  $H_2O_2$  as a prospective oxidizer and with a comparison of problems associated with the use of  $H_2O_2$  or  $N_2O_4$ . At the conclusion of Phase I, it was determined that (1)  $H_2O_2$  can be used as a regenerative coolant for a high-pressure rocket engine, (2) the prospective materials of construction for such an engine are compatible with 98%  $H_2O_2$  having a temperature as high as 270°F, and (3) an experimental high-temperature catalyst, under study at Food Machinery and Chemical Corporation (FMC) is acceptable for use in the preburner. The technical effort during Phase I is summarized in Ref. 1.

B. STATEMENT OF WORK FOR PHASE II

1. Task I--Extended 98%  $H_2O_2$  Convective Heat-Transfer Experiments

(U) Convective heat-transfer experiments were to be performed to evaluate the effect of tube material, velocity, heat flux, operating pressure, and other parameters on the regenerative cooling characteristics of 98%  $H_2O_2$ . Tests were to be conducted to evaluate the repeatability of test data and to determine the effect of duration on the heat-transfer characteristics of 98%  $H_2O_2$ . Long-duration tests were to be conducted for durations up to 10 min of cumulative running time to determine possible changes in the cooling

UNCLASSIFIED

UNCLASSIFIED

Report 10785-F, Phase II

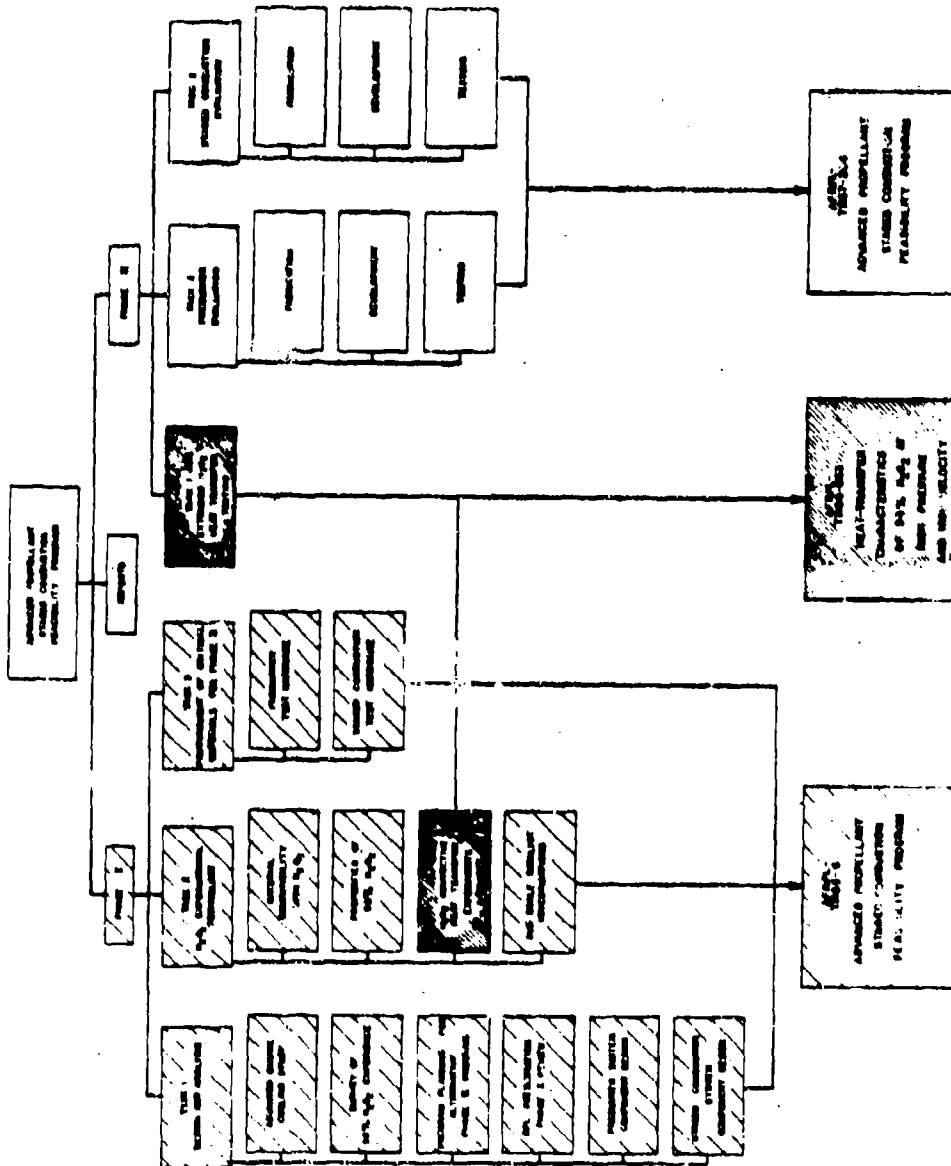


Figure 1. Program Organization

UNCLASSIFIED

# UNCLASSIFIED

Report 10785-F, Phase II

## I. B. Statement of Work for Phase II (cont.)

capability of 98%  $H_2O_2$  as a function of time. These tests were to be operated at various levels of heat input, covering the range of approximately 55 to 80% of the short-duration burnout heat flux. Inconel 718 was to be used for the tube test sections except in those tests in which tube material was to be evaluated. Material evaluation tests were to be conducted with Type 347 stainless steel.

(U) The transient cooling requirements for start, shutdown, and restart of a characteristic  $H_2O_2$  cooled engine were to be evaluated to obtain design criteria and identify potential problem areas.

### 2. Task II--Preburner Evaluation

(U) Tests were to be conducted with a preburner component using 98%  $H_2O_2$  as a monopropellant. Catalyst beds of two different throughput ( $H_2O_2$  load) configurations were to be evaluated during this phase of the program, and an evaluation was to be made of the resultant decomposition gas temperatures. Satisfactory operation of the preburner assembly was to be demonstrated at a chamber pressure of approximately 4000 psia as a prelude to Task III. The preburner was to be sized to permit passage of the total oxidizer flow required for a thrust chamber assembly with a thrust of approximately 20,000 lb at sea level.

### 3. Task III--Staged-Combustion Evaluation

(U) Staged-combustion tests were to be conducted at approximately 20,000 lbf. All testing was to be conducted at approximately 3000-psia chamber pressure in the secondary combustion chamber. A stationary pressure dropping device was to be installed between the preburner and secondary combustor to create a pressure drop. The  $H_2O_2$  monopropellant preburner from Task II was to

UNCLASSIFIED

CONFIDENTIAL

Report 10785-F, Phase II

I, B, Statement of Work for Phase II (cont.)

be used to generate decomposed  $H_2O_2$  gas as the oxidizer for the secondary combustor. The fuel for the secondary combustor was to be Alumazine-43 conforming to the available military specification, MIL-P-27412. All hardware was to be uncooled. At least two different injector concepts for the secondary combustor were to be evaluated. The best injector from this testing was to be used for evaluating the effect on performance with a different chamber length ( $L^*$ ). Data were to be obtained to evaluate specific impulse and combustion efficiency performance; specific impulse efficiency of at least 87% of theoretical was a program goal. The assembly was to be instrumented with high-frequency transducers and temperature probes to evaluate combustion stability and heat flux characteristics, respectively.

C. SUMMARY OF ACCOMPLISHMENTS

1. Extended 98%  $H_2O_2$  Heat-Transfer Experiments

(U) The detailed results of the heat-transfer tests conducted under this task are reported in Ref. 2. It was found that the short-duration burnout heat flux characteristics of 98%  $H_2O_2$  were independent of operating pressure and material. However, the long-duration burnout tests indicated that the allowable heat flux, as a function of velocity, must be reduced to approximately 65% of that obtained in short-duration burnout testing. This phenomenon existed in high-pressure tests, and because of the limitations of the test program, it was not determined whether a long-duration burnout phenomenon exists at low pressure.

(U) The transient cooling requirements for a  $H_2O_2$  regeneratively cooled chamber at the 100,000-lbf thrust level were evaluated. It was determined that a potential transient cooling problem could exist during the shutdown of such an engine, and that the required propellant phasing and flow

Page 5

CONFIDENTIAL

(This page is Unclassified)

# CONFIDENTIAL

Report 10783-F, Phase II

## 1. Summary of Accomplishments (cont.)

Control for this condition should be studied to determine the requirements for start, shutdown, and restart. The study indicated that the shutdown transient was the most severe but found that safe shutdown of such an engine could be accomplished if the instantaneous mixture ratio for the engine were allowed to shift toward the oxidizer-rich side and the turbine flow were controlled independently from the jacket coolant flow.

## 2. Task II--Preburner Evaluation

(U) High-pressure decomposition of 98%  $H_2O_2$  was demonstrated over a pressure range of 4150 to 4500 psi with throughputs ranging from 48 to 108 psim. This was accomplished by using two different sized catalyst packs made from a high-temperature catalyst material (compressed screen configuration) developed by Food Machinery and Chemical Corporation. It was found that predictions for the catalyst depth, which were made as a result of the subscale catalyst test conducted under Phase I of this contract, were valid. An active catalyst depth of less than 1 in. successfully decomposed all of the  $H_2O_2$  at the high operating pressure. It was also found that stable pack operation could be achieved with relatively low pressure drop (approximately 50 psi). From the temperature profile obtained during testing, it was determined that pure silver screens can be utilized at the entry of the pack to initiate decomposition without excessive silver melting. This means that the higher cost, high-temperature catalyst can be used in smaller quantities than previously anticipated.

## 3. Task III--Staged-Combustion Evaluation

(C) Fourteen high-pressure staged-combustion tests were conducted with  $H_2O_2$  and Aluminine at pressures ranging from 2650 to 3050 psi and at mixture ratios of 0.49 to 0.83 (oxidizer to fuel ratio). The desired program performance goal of 87% of theoretical  $I_p$  was exceeded during all valid tests

CONFIDENTIAL

## C. Summary of Accomplishments (cont.)

but one. An  $I_p$  efficiency range of from 89 to 93% was demonstrated for the mixture ratio range studied, and the peak at 93%  $I_p$  was achieved at a mixture ratio of 0.72 and at a chamber pressure of 3050 psia. Two basic injector configurations were evaluated. One used a vane principle in which small tubes were attached to the trailing edge of the vanes, and the second type used relatively large tubes injecting the fuel axially into the combustion chamber. Performance information was obtained from all valid tests, and heat-flux measurements were made to determine the transient heat-transfer characteristics of this propellant combination. The performance evaluation indicated that performance efficiency increases with higher mixture ratios. These data confirm analytical predictions which indicated that a greater percentage of theoretical performance can be achieved with mixture ratios slightly above the optimum theoretical mixture ratio value. The performance data from tests of the two injector configurations clearly demonstrate that high combustion efficiency is achieved from fine dispersion of the Alumizine into the oxidizer-rich gas.

(U) The tests conducted comparing 70-in.  $L^*$  with 40-in.  $L^*$  chambers tend to indicate that higher combustion efficiency can be obtained with the 70-in.  $L^*$  chamber. However, two of the three tests conducted with the 40-in.  $L^*$  chamber were at a lower mixture ratio and the injector pattern was degraded by plugging of some of the fuel injection tubes. The highest performance achieved during all testing was at a mixture ratio of 0.72 with a 40-in.  $L^*$  chamber. Adjustments were made in the data of the two tests conducted at low mixture ratio in an attempt to compensate for the maldistribution of the propellant. It must be concluded from all of the tests conducted that 40-in.  $L^*$  is sufficient to obtain high combustion efficiency with this propellant combination when a high performance injector is used. There are also indications that less  $L^*$  is required at a higher mixture ratio than at a lower mixture ratio.

**CONFIDENTIAL**

~~CONFIDENTIAL~~

CONFIDENTIAL

1. C. Summary of Accomplishments (cont.)

(U) The measurements made of heat flux in the combustion chamber indicated good agreement with Colburn equations.

(U) The performance characteristics of 90%  $H_2O_2$ /Alumizine-43 were also evaluated. It was found that no performance efficiency degradation should be anticipated by a drop in  $H_2O_2$  concentration. I<sub>g</sub> efficiency of 90% was demonstrated using a modified version of the large tube injector.

D. ORGANIZATION OF REPORT

(U) This report follows the general outline of the Statement of Work. The three major tasks were: engine transient cooling characteristics, preburner evaluation, and staged-combustion evaluation. Each of these sections stands alone with its own introduction, summary, and technical discussion. The conclusions drawn from this Phase II of the contract can be found in Section V. Recommendations, based on the conclusions, can be found in Section VI followed by appendixes and references.

~~CONFIDENTIAL~~

(This Page is Unclassified)



# UNCLASSIFIED

Report 10785-F, Phase II

## SECTION II

### ENGINE TRANSIENT COOLING CHARACTERISTICS

#### A. INTRODUCTION AND SUMMARY

(U) A high-pressure staged-combustion engine using  $H_2O_2$  and Alumazine as propellants, can be designed to use either a cooled or uncooled (heat sink) combustion chamber. One of the cooled versions of this engine would use the  $H_2O_2$  as a regenerative coolant. The heat-transfer characteristics of 98%  $H_2O_2$  were determined in Phase I of this contract. These studies indicated that 98%  $H_2O_2$  can accept high heat fluxes, and the short-duration burnout heat flux is strictly a function of coolant velocity and appears to be independent of the coolant static pressure.

(U) Regeneratively cooled, high-pressure combustion chamber design studies were also made at the 100,000-lbf thrust level. These studies indicated that such a combustion chamber would require a thermal barrier (coating) to separate the tube wall from the hot combustion gas and thus limit the tube wall temperature to an acceptable operating level. For more information concerning this design and the heat-transfer characteristics of  $H_2O_2$ , see Ref. 1 and 2.

(U) Many liquid rocket engines have been developed in which a mono-propellant has been used for coolant of the combustion chamber. Transient cooling problems could occur because of improper propellant phasing during the start and shutdown of the engine. Such problems exist for two reasons: (1) the heat flux in the combustion chamber during the engine transients is not directly proportional to the transient coolant velocity, and (2) during shutdown, residual heat in the cooling jacket can cause a bulk temperature rise in the coolant that can subsequently result in thermal decomposition. These problems are further aggravated by the energy stored in the required thermal barrier.

UNCLASSIFIED

# UNCLASSIFIED

Report 10785-F, Phase II

## II. A. Introduction and Summary (cont.)

(U) The purpose of this study was to analyze the shutdown transient of a 100,000-lbf engine combustion chamber, operating at a steady-state pressure of 3000 psi, to determine the propellant phasing required to eliminate the possibility of coolant tube failure. It was considered that if the shutdown transient could be accomplished satisfactorily, the start and restart conditions could also be solved. To this end, a transient thermal analysis of the combustion chamber was conducted to indicate feasible modes of engine shutdown.

(U) Two types of analyses were conducted as part of the shutdown investigation. In the first type, various valve resistance transients were assumed, the engine flows and pressures were calculated, and the results were used for wall cooling analyses at the throat of a thrust chamber with a thin metal-oxide coating. The engine was assumed to have only simple resistance valves in the fuel and oxidizer lines. It was found that the high thermal resistance of the coating, which is required to meet steady-state tube wall temperature limits, forces the heat flux to the coolant to decay slowly, relative to the coolant flow decay as long as the combustion gas recovery temperature remains high. As a result, a severe tube wall burnout condition develops as the shutdown transient proceeds. To reduce the combustion gas temperature, an oxidizer shutdown delay was used to increase the secondary combustor mixture ratio. However, it was found that the oxidizer lag which the postulated engine system can accommodate without excessive preburner pressure and turbine speed during shutdown is not sufficient to eliminate the burnout problem. It became apparent that the simplified engine control system would not produce the proper flow control for a safe engine shutdown. However, a modified control system, in which the turbine flow and coolant flow are independently controlled, should satisfy the requirements for the shutdown transient. The flow requirements for such a control system were evaluated in the second part of the study. This investigation was oriented toward establishing the mixture ratio transient required to solve the burnout problem.

UNCLASSIFIED

UNCLASSIFIED

Report 10765-F, Phase II

## II, A, Introduction and Summary (cont.)

For this purpose a typical pressure decay transient was assumed on the basis of the previous system studies without oxidizer shutdown lag. A mixture ratio transient reaching 15 (oxidizer to fuel) in 0.5 sec was found which yields decreasing wall temperatures and no degradation of the burnout margin during the shutdown for the thin coating. In addition, the coating surface temperature decay was such that a critical temperature-mixture ratio combination exists for only 0.1 sec. Therefore, the prescribed transient will cause little or no erosion and/or oxidation of the coating.

(U) Preliminary analysis of a tungsten-coated (thick coating) tube wall revealed that the increased heat capacity of this coating significantly aggravates the shutdown burnout problem, thus dictating that a faster increase in the secondary combustion mixture ratio would be required than that needed for the thin coating.

## B. TECHNICAL DISCUSSION

(U) The shutdown transient analysis was accomplished in two parts: engine flow analysis and local chamber wall analysis. Fuel and oxidizer valve resistance transients were the forcing functions for the flow model, which defines four engine flow rates: (1) the coolant or oxidizer flow, (2) the fuel flow, (3) the turbine flow, and (4) the secondary combustor flow. At any instant during the shutdown transient, the turbine flow exceeds the oxidizer flow, and the secondary combustor flow is greater than the sum of turbine and fuel flows because of the pressure transients in the preburner and secondary combustor. A computer program was designed to determine these pressure transients, as well as the turbine speed, using backward time differences to represent the differential equations involving these variables. The resulting engine system equations were solved iteratively at each time step using an outer iteration loop which adjusts the two pressures simultaneously and an inner iteration loop

UNCLASSIFIED

UNCLASSIFIED

Report 10700-F, Phase II

## II, B, Technical Discussion (cont.)

to determine the fuel flow rate. Details of the engine system model are given in Appendix I, Section A, and the computer program is described in Appendix I, Section B.

(U) The results of the engine flow analysis were used as the input to a local-chamber-wall computer program. Analysis of local tube wall and coating temperatures and heat fluxes was based on an approximate integral method of solution of the corresponding one-dimensional conduction equations. Quadratic temperature distributions with time-dependent coefficients were assumed in both the tube wall and coating. The resulting transient energy balances were written in terms of the average coating and tube wall temperatures (see Appendix I, Section C). However, solution of these equations<sup>(1)</sup>, coupled with the assumed temperature distributions, provided transient temperatures and heat fluxes across the chamber wall at a given axial position. In this study, only the throat was evaluated because the most severe heating condition exists in this area.

(U) Figure 2 shows schematically the interrelation of the parts of the analysis and the evaluation of shutdown criteria from them. Two local thrust chamber criteria were satisfied in detail in this investigation: the coating-tube wall interface temperature must not exceed its steady-state value, and burnout-heat-flux ratio<sup>(2)</sup> must not exceed its steady-state value. As noted in Figure 2, two additional criteria must also be considered. First, the combustion chamber mixture ratio must be correlated with the coating surface temperature so that erosion or oxidation of the coating is negligible. Because this criterion cannot be specified in detail at this time, the investigation

(1) Again the implicit backward difference method was used, as described in Appendix I, Section D.

(2) Burnout-heat-flux ratio is defined as the predicted heat flux divided by the heat flux at which tube burnthrough will occur under the existing flow conditions.

UNCLASSIFIED

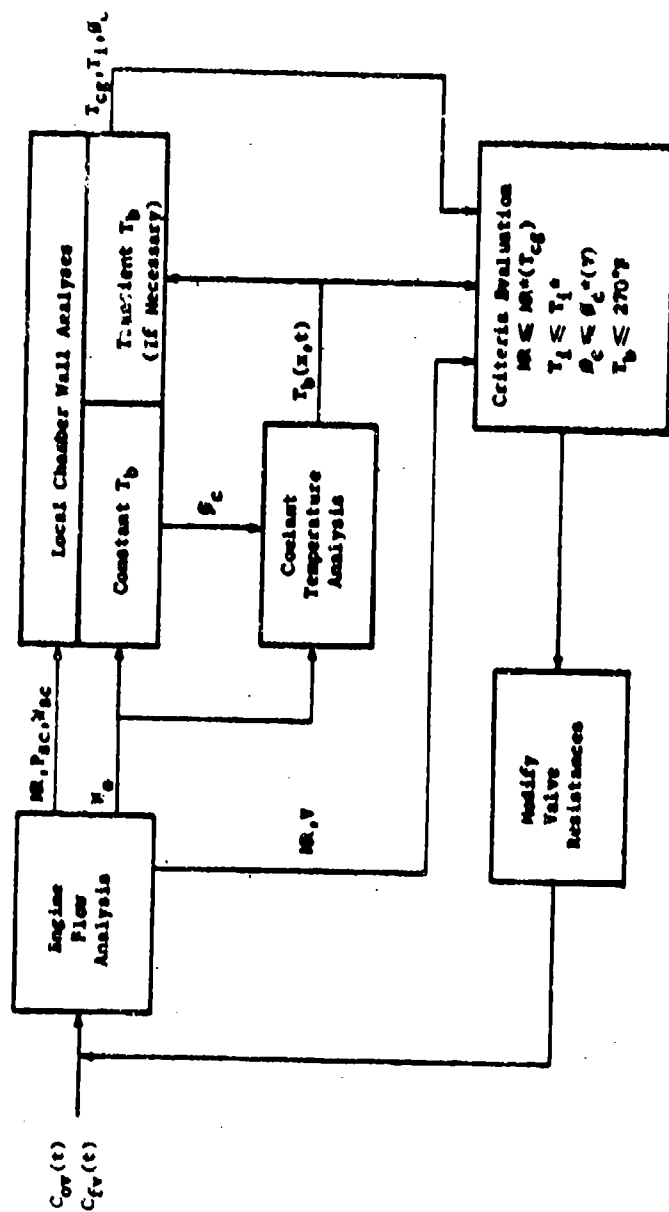


Figure 2. Shutdown Transient Analysis

# UNCLASSIFIED

Report 10785-F, Phase II

## II. A. Technical Discussion (cont.)

sought to minimize the coating surface temperature for mixture ratios above stoichiometric. Second, the coolant bulk temperature must not exceed approximately 270°F in order to prevent thermal decomposition of the  $H_2O_2$ . This requirement was not evaluated explicitly, because it is so closely related to the burnout criterion. Inasmuch as the burnout-heat-flux ratio and the bulk temperature rise are both controlled by the ratio of coolant heat flux to coolant velocity, it was assumed that the thermal decomposition criterion is met if the burnout is satisfied. (3) Section E of Appendix I indicates how the transient bulk temperatures can be calculated for an explicit evaluation of the thermal decomposition criterion.

(U) System limitations were also considered, because an increasing mixture ratio in the combustion chamber could result in an increase in turbine pressure ratio, thus causing an increase in turbine speed and correspondingly an increase in preburner pressure. Several engine shutdown concepts were evaluated, assuming various oxidizer- and fuel-valve resistance transients. These cases clearly showed the interaction of the various system components during shutdown and, particularly, the potential heat-transfer problem areas in the secondary combustor during the shutdown transient.

(U) Two chamber designs, one with a thin metal-oxide coating and one with a thick tungsten coating, were considered in the analysis of shutdown transients. A satisfactory secondary-combustor flow transient has been determined for a thin ( $\approx 0.020$ -in.-thick) coating, but the more complex problem of a thick tungsten coating (with a higher heat capacity) was not thoroughly analyzed.

(U) The engine flow system and chamber-wall analyses conducted during this contract are discussed in the following paragraphs.

(3) This consideration also permitted use of steady-state bulk temperatures as a good approximation in the local chamber-wall analysis.

UNCLASSIFIED

# UNCLASSIFIED

Report 10785-F, Phase II

## II, B, Technical Discussion (cont.)

### 1. Engine Flow System Analysis

(U) The computer program was used to evaluate several engine flow conditions. In each case studied, it was assumed that shutdown is complete when the pressure in the combustion chamber decreases to 10% of the steady-state value. This assumption was necessary to ensure that the calculated transients do not approach zero and invalidate the system equations.

(U) Although many transients have been investigated, only two cases are discussed in detail in this report, because they clearly show the system response during shutdown and because they define the problem areas. In the first case, both valves were closed simultaneously in 0.5 sec; in the second case, the closing of the oxidizer valve was delayed 0.10 sec, but both valves were still closed by 0.5 sec. The valve resistance transients for both cases are shown in Figure 3. Because resistance was specified as a ratio of values during the transient to values during steady state, the same ratio was applicable to both the fuel and the oxidizer valve in the first case considered.

(U) The results of closing both valves simultaneously are shown in Figures 4 and 5. Figure 4 shows the resulting flow-system transients. As will be noted, the transients appear reasonable, and the mixture-ratio excursion in the secondary combustor has been confined to a narrow region between 1.0 and 1.26, which is consistent with the coating erosion criterion. Of particular interest is the fact that very little departure from steady state occurs until about 0.15 sec; at this time, the resistance of the valves increases by a factor of 10. The assumed initial valve resistances were very small compared to those of the total system and thus a large change was required to affect the flow system.

UNCLASSIFIED

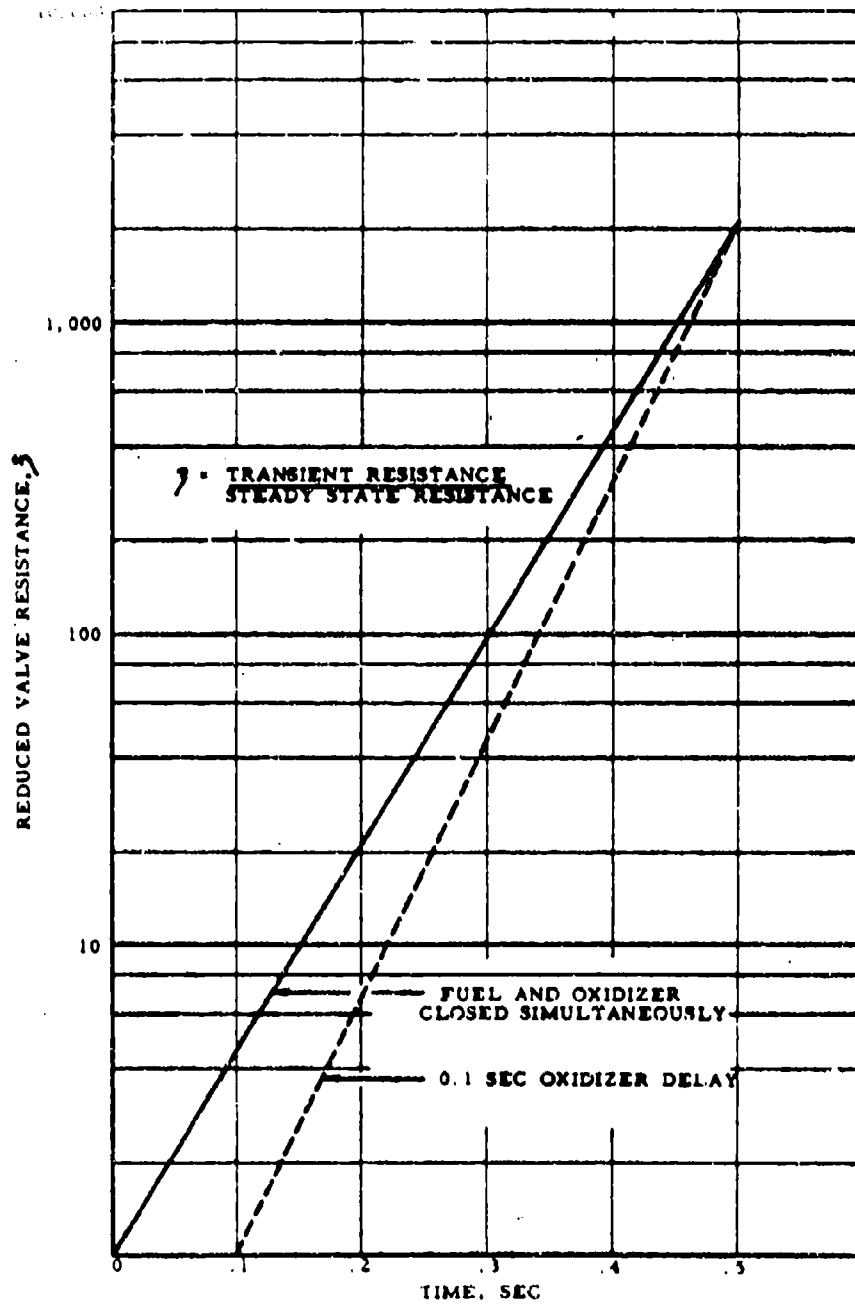


Figure 3. Reduced Valve Transients, Advanced Staged-Combustion Engine



UNCLASSIFIED

July 25, 1972, Rev. 1.0

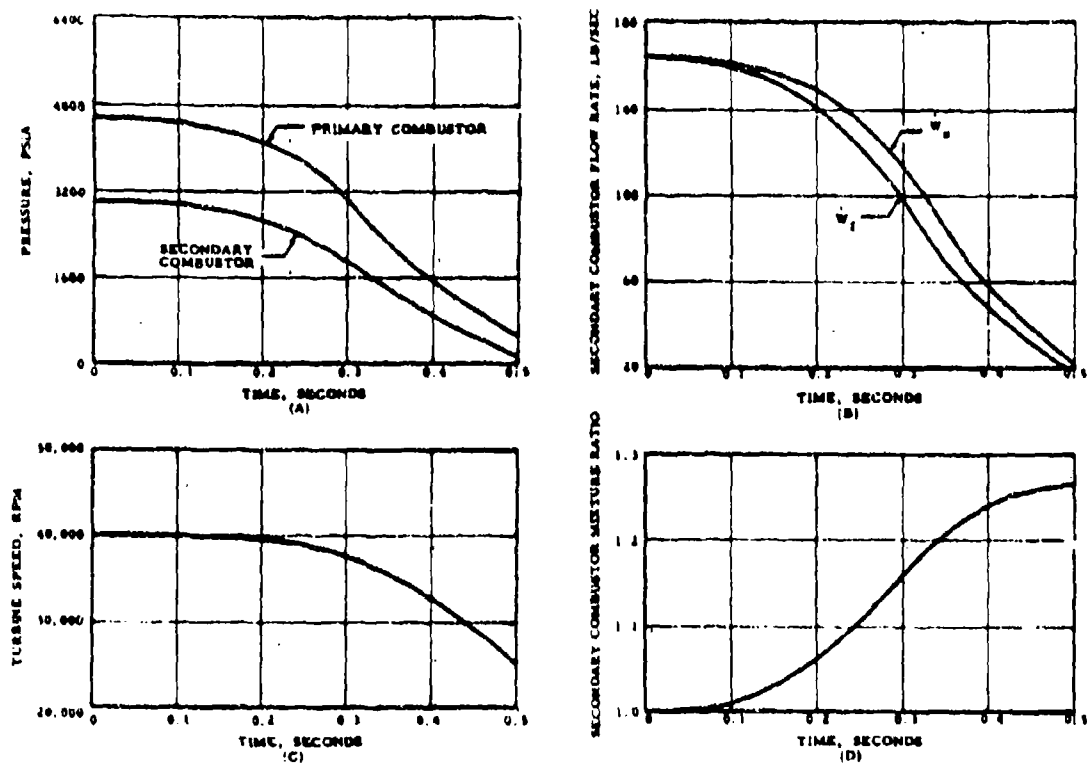


Figure 4. Advanced Staged-Combustion Engine Flow System Shutdown Transient--Both Valves Closed Simultaneously in 0.5 sec

UNCLASSIFIED

UNCLASSIFIED

Report 10785-F, Phase II

NOTE: 1. LOCATION AT THROAT  
2. THIN COATING (0.001 IN.) CASE

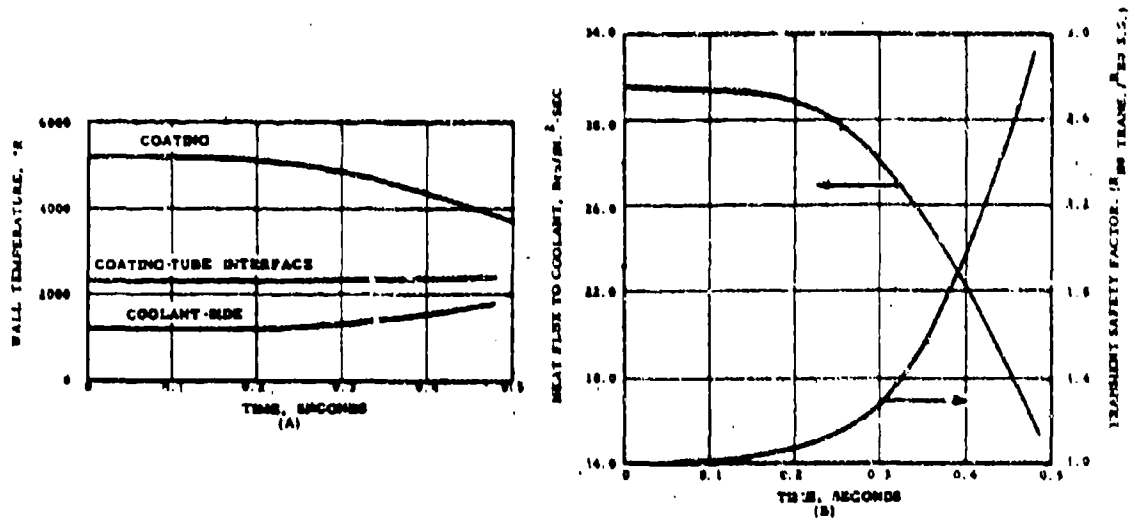


Figure 5. Advanced Staged-Combustion Engine Chamber Wall Shutdown Transient--Both Valves Closed Simultaneously in 0.5 sec

UNCLASSIFIED

## II. B, Technical Discussion (cont.)

(U) Figure 5 shows the thermal response of the secondary-combustor wall (at the throat) with the thin oxide coating. The plot of wall temperatures indicates that the coolant-side wall temperature ( $T_L$ ) approaches 1500°F, which could produce  $H_2O_2$  decomposition; the temperature of the coating ( $T_C$ ) decreases satisfactorily and the temperature at the interface between coating and tube (interface temperature,  $T_I$ ) remains almost constant. Another parameter of interest was the combustion chamber burnout safety factor (Figure 5, Plot B). It can be seen from the curve that a tube burnout is predicted although the inside heat flux (to the coolant) appears to be dropping satisfactorily. The term "safety factor" is defined as the ratio of the transient burnout-heat-flux ratio normalized to the steady-state burnout-heat-flux ratio.

(U) Although the above valve resistance transients are satisfactory for the flow system, the combustion chamber would fail because of the burnout phenomenon. Because of the high thermal resistance of the coated wall relative to the gas-side and liquid-side convection resistances, the heat flux to the coolant decreased at a much slower rate than the coolant flow. This can be altered by increasing the mixture ratio early in the shutdown transient until the combustion-gas recovery temperature is reduced. The mixture ratio is increased by simply discontinuing fuel flow and continuing oxidizer flow (oxidizer lag on shutdown).

(U) As indicated above, the case selected for discussion is one in which the oxidizer valve is delayed 0.1 sec and both valves are closed at 0.5 sec. The valve resistances during the transient for this case are also shown in Figure 3. Figure 6 shows the engine flow-system response to this transient. It should be noted that the oxidizer flow, preburner pressure, and turbine speed increase above their steady-state values during shutdown. This abnormality was caused by the fact that, in the flow system considered,

# UNCLASSIFIED

Report 10785-F, Phase II

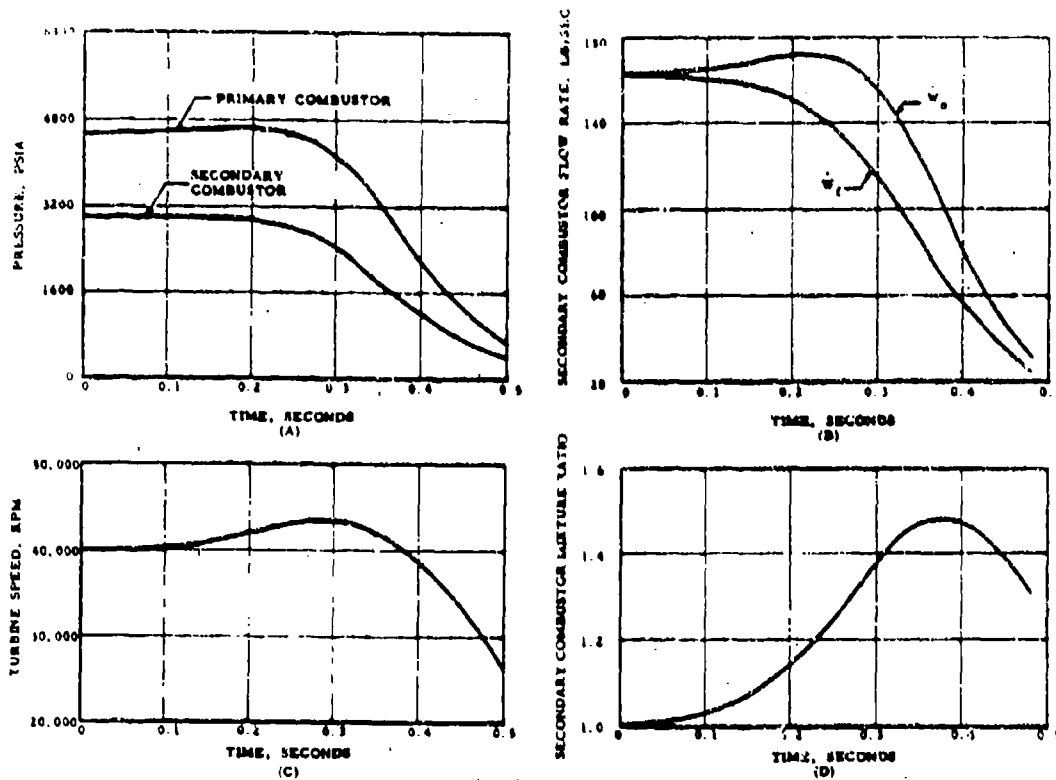


Figure 6. Advanced Staged-Combustion Engine Flow System Shutdown Transient--0.1-sec Oxidizer Delay, Both Valves Closed at 0.5 sec

UNCLASSIFIED

UNCLASSIFIED

REPORT 10705 P, 11

11, B, Technical Discussion (cont.)

All the oxidizer passes through the turbine. Thus, since the work required to drive the fuel pump is reduced with decreasing fuel flow, the turbine tends to overspeed and pumps more oxidizer at a higher outlet pressure. It was therefore decided to confine both turbine overspeed and excess chamber pressures to no more than 10% of their steady-state values. The particular case evaluated, in which oxidizer flow is delayed 0.1 sec, very closely approaches these limits and is discussed to show the maximum effect on the assumed flow system that can be produced by valve sequencing. Modifications of the system hydraulics are possible to permit bypass control, but such variations were not evaluated.

(U) The thermal response of the chamber wall for the oxidizer lag case is shown in Figure 7. It should be noted that wall temperatures and safety margins are satisfactory until midway through the transient. A further shift to higher mixture ratios is necessary to control the remainder of the transient.

(U) No modifications to the flow system have been investigated because the primary objective of this study was an investigation of the thermal aspects of engine shutdown. Subsequent effort was concentrated on specifying a satisfactory shutdown transient purely on the basis of heat-transfer characteristics of the combustion chamber. This transient, in turn, may be used as a guide to determine the flow-system modifications that are required to achieve a satisfactory shutdown.

2. Additional Chamber-Wall Analyses

(U) Two approaches to the thermal-barrier problem were evaluated. The first, included in the initial shutdown calculations, considered a mixture of metal and metal oxides with low thermal conductivity. Inasmuch as a coating with a specified thermal resistance is required to satisfy the

UNCLASSIFIED

# UNCLASSIFIED

Report 10785-F, Phase II

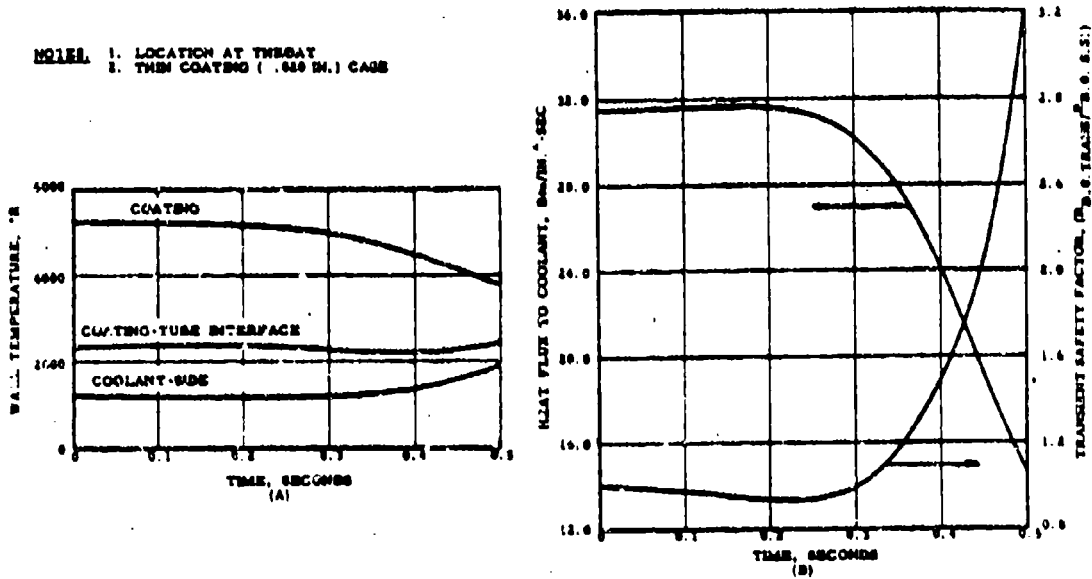


Figure 7. Advanced Staged-Combustion Engine Chamber Wall Shutdown  
Transient--0.1-sec Oxidizer Delay, Both Valves Closed  
at 0.5 sec

UNCLASSIFIED

UNCLASSIFIED

Report 10785-E, Phase II

## II. B. Technical Discussion (cont.)

steady-state temperature limitations of the tube wall, this thermal barrier is quite thin and consequently has a low heat capacity. The second approach considered the use of pure tungsten. Since the thermal conductivity of tungsten is higher than that of the oxide coating, the tungsten coating must be thicker to limit the steady-state heat flux to the coolant jacket. Also, the thick tungsten coating is a good thermal heat sink and thus increases the required oxidizer lag on shutdown. The transient requirements for the thin coating during shutdown were determined first because they may be evaluated more easily and served as a guide for the more difficult task of evaluating the thick tungsten coating.

### a. Thin Coating

(U) A study was made to determine the mixture-ratio excursion required during the shutdown transient for a chamber with a thin coating. For purposes of this study, the assumed pressure transient was that discussed earlier for the case of closing both valves simultaneously. Neglecting the energy stored in both the tube wall and the coating, steady-state equations may be used to predict wall temperatures, heat fluxes, and safety margins for any assumed operating conditions. These quasi-steady calculations were used to obtain an initial estimate of the mixture ratio excursion required for a constant normalized burnout heat flux safety factor of 1.0; the resultant curve of mixture ratio versus relative chamber pressure is shown in Figure 8.

(U) A parametric study was then conducted using the thermal section of the computer program and the assumed pressure transient, using the quasi-steady calculations of Figure 8 as a guide. The final calculated mixture ratio transient at shutdown, which resulted in an essentially constant burnout safety factor of 1.0, is also shown in Figure 8. The magnitude of

UNCLASSIFIED

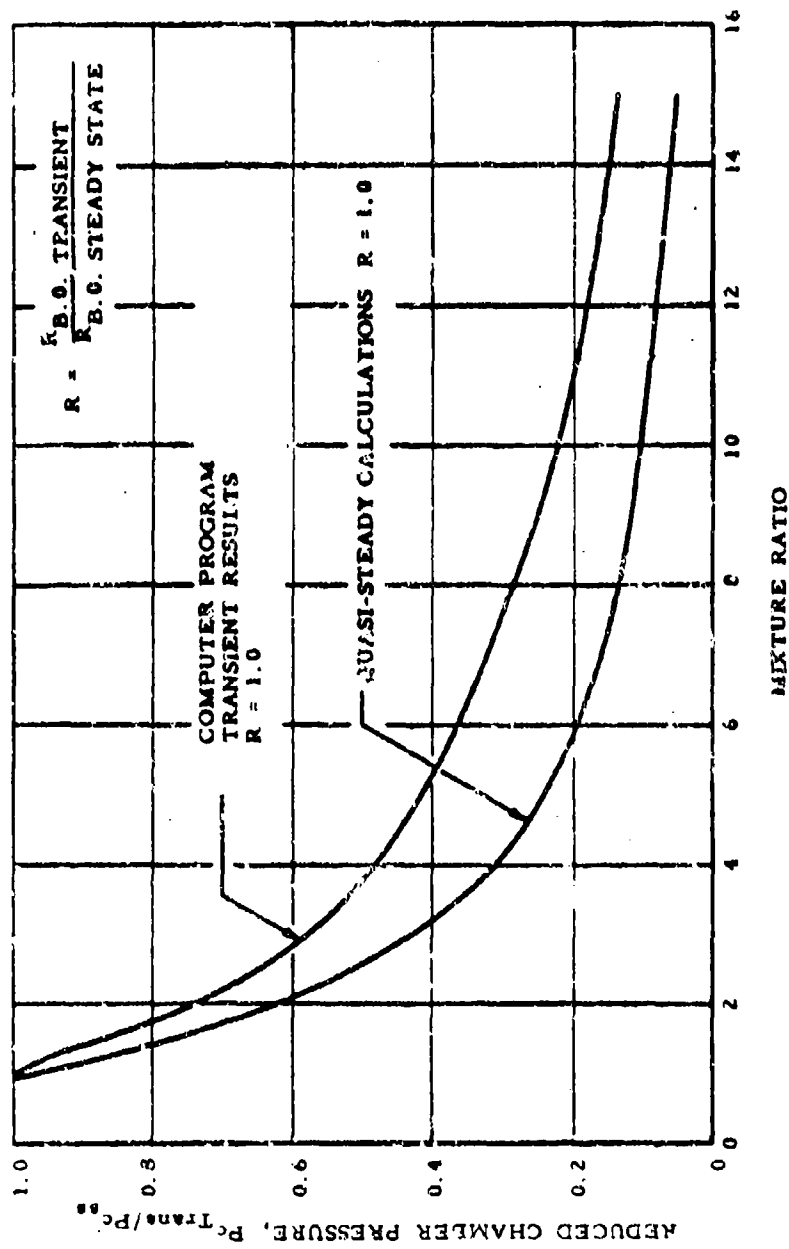


Figure 2. Advanced Staged-Combustion Engine--Chamber Wall Analysis



UNCLASSIFIED

Report 10785-F, Phase II

II. B. Technical Discussion (cont.)

the mixture-ratio shift required when changing from quasi-steady to transient conditions should be noted; it indicates the effect of the tube wall and coating energy storage.

(U) Figure 9 shows the required flow conditions during the transient for the combustion chamber as well as the thermal response of the chamber wall. The flow during the transient (Figure 9, Plot A) indicates that a mixture-ratio excursion from 1.0 (steady-state condition) to a final value of 15 is required at the end of the engine shutdown. As indicated above, the normalized safety factor related to burnout is essentially constant at 1.0. Of particular interest is the plot of wall temperatures (Figure 9, Plot B), which indicates that all temperatures are decreasing throughout the transient. The surface temperature of the coating is reduced to about 3800°F as the chamber mixture ratio passes through stoichiometric, and remains between 2500 and 3800°F for only 0.1 sec. Thus, the prescribed transient appears to be satisfactory and will cause little or no erosion and/or oxidation of the coating.

b. Thick (Tungsten) Coating

(U) The thick coating was studied by using the flow transient specified for the thin coating; the results are shown in Figure 10. It will be noted that the chamber burnout-heat-flux factor reaches a peak of about 1.6, which is not acceptable. The reason for the peak is shown clearly in the plot of incident heat flux and heat flux to the coolant during shutdown. The difference between the two values is the rate of change of energy stored in the wall; this energy is absorbed by the coolant during the transient. To reduce the heat flux to the coolant, the incident flux to the wall must be reduced much earlier in the shutdown; this can be accomplished only by a more rapid mixture-ratio excursion during the transient.

UNCLASSIFIED

UNCLASSIFIED

Report 10785-F, Phase II

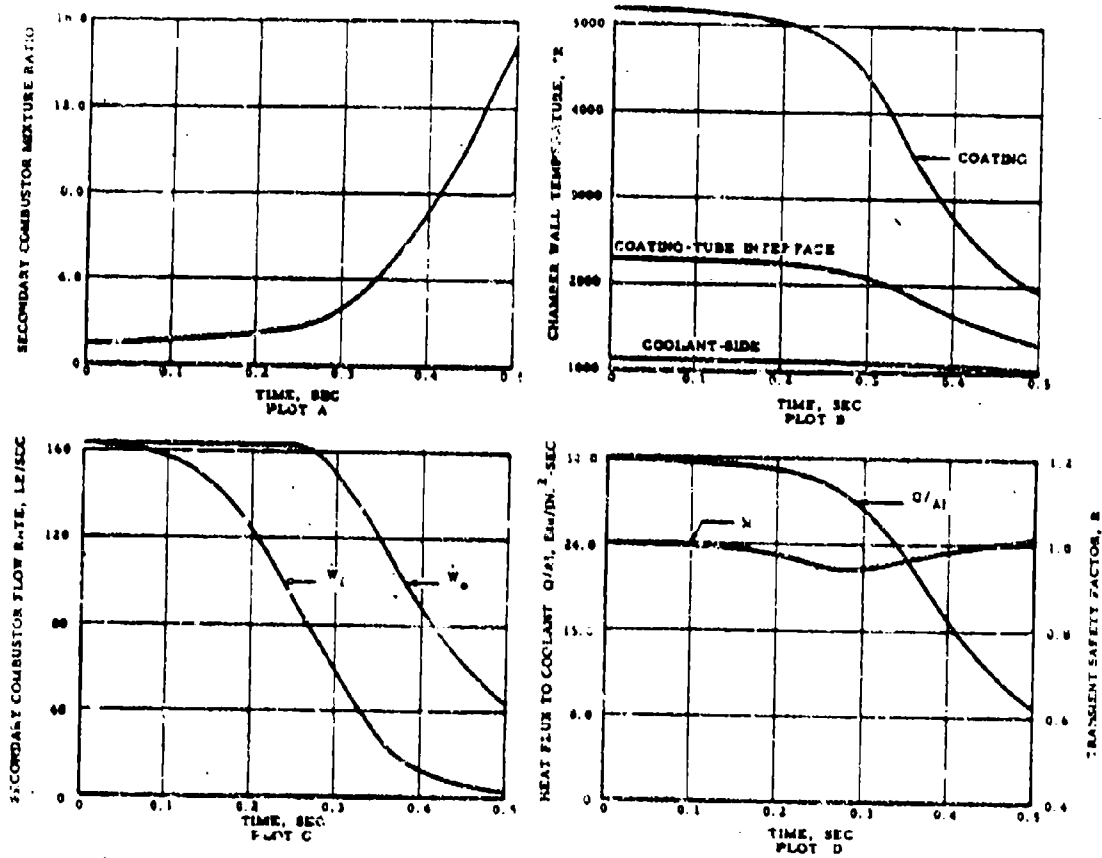


Figure 9. Advanced Scaged-Combustion Engine--Shutdown Transient for Thin Coating

UNCLASSIFIED

UNCLASSIFIED

Report 10735-R, Phase II

NOTE: LOCATION AT THROAT

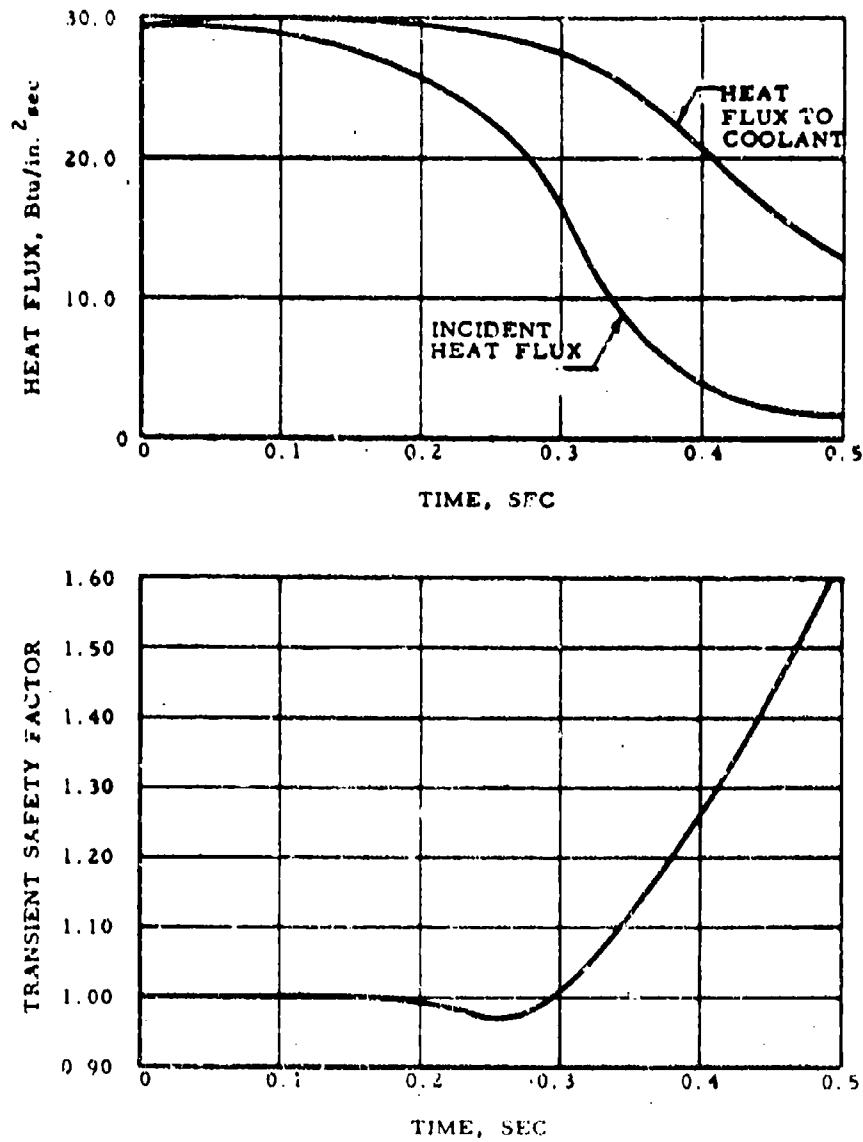


Figure 10. Advanced Staged-Combustion Engine--Shutdown Transient  
for Throttle Cutting

Page 27

UNCLASSIFIED

# UNCLASSIFIED

Report 10785-F, Phase II

## II. B. Technical Discussion (cont.)

(G) This study indicates that a 100,000-lbf thrust level  $H_2O_2$  regeneratively cooled chamber with a thin protective thermal barrier can be shut down safely if peroxide coolant flow is controlled independently of turbine flow. However, the specific conditions for the actual engine system require further study to accurately define the control system requirements to obtain safe shutdown modes.

UNCLASSIFIED

# UNCLASSIFIED

Report 10785-F, Phase II

## SECTION III

### PREBURNER EVALUATION

#### A. PROGRAM OBJECTIVES AND APPROACH

(U) The preburner evaluation portion of this program had as its principal objective the demonstration of high-pressure (4000 psi) catalytic decomposition of 98%  $H_2O_2$ . Other objectives were to evaluate the effect of bed loading (throughput)<sup>(4)</sup> on the catalyst behavior characteristics such as temperature profile, stability, and pressure drop. The preburner evaluation program was to culminate in the demonstration of a high-pressure catalyst assembly capable of producing a stable flow of homogeneous hot oxidizer gas for staged combustion with Alumizine-43.

(U) This section confines itself to a discussion of the five tests that were necessary to develop the preburner. Preburner results obtained during the staged-combustion evaluation are presented in Section IV of this report.

(U) The basic intent of the overall program was to demonstrate, at a thrust level of 20,000 lbf, the feasibility of a 98%  $H_2O_2$ /Alumizine-43 propellant system. The goal of this portion of the program is to provide a workable  $H_2O_2$  preburner for subsequent staged-combustion use to aid in fulfilling that intent. With these premises as guidelines the approach taken was to perform all the high-pressure tests with uncooled, rugged hardware and employ only short-duration tests to obtain the desired data.

(U) In keeping with this philosophy, hardware with at least a safety factor of 2 was designed (Ref. 1) and fabricated. The preburner design was based upon existing high-temperature catalyst technology and incorporated design

(4) Throughput is an expression for flow rate through a catalyst pack and is expressed in psim: 
$$\frac{\text{pounds of peroxide}}{\text{square inches of catalyst pack frontal area} \times \text{minutes}}$$

# UNCLASSIFIED

Report 10785-F, Phase II

## III. A, Program Objectives and Approach (cont.)

features recommended by FMC<sup>(5)</sup> and tested on a subscale basis during Phase I of the contract (Ref. 1). It was the intent of the preburner program to conduct a test evaluation to certify, not develop, a catalyst material. Fortunately, the Age Catalyst Company of Buffalo, New York, in conjunction with FMC, had developed the Ageite series of high-temperature hydrogen peroxide decomposition catalyst materials prior to the inception of this program. Therefore, this approach could logically be taken and the usable throughput range of the catalyst packs could be and were experimentally determined.

(U) In support of the preburner evaluation, certain supplementary engineering investigations were conducted. These included a theoretical evaluation of the probability of low-frequency instability occurring as a result of system-coupled effects, the evaluation of an actual low-frequency instability occurrence (Test 1.2-01-AAC-005), a start transient and preburner operation analysis, and analysis of catalyst performance.

## B. TECHNICAL DISCUSSION

### 1. Hardware

#### a. General

(U) In designing the preburner assembly, the governing philosophy was to design components to obtain a maximum in operational flexibility and simplicity. Also, because the program was concerned primarily with evaluation of an advanced propellant system, not hardware development, hardware ruggedness and dependability were accentuated. These design objectives were implemented by maintaining the same bolt hole circle size, seal size, bolt size, and bolt

<sup>(5)</sup> Food Machinery and Chemical Company, supplier of electrolytic 98%  $H_2O_2$ .

UNCLASSIFIED

UNCLASSIFIED

Report 10785-F, Phase II

III, B, Technical Discussion (cont.)

length throughout both the preburner assembly and the secondary combustor. The previously mentioned minimum safety factor of 2/1 was maintained throughout the structure.

b. Preburner Structural Design

(U) Design parameters for the preburner assembly are shown in Table I. The preburner configuration was designed to cover two different throughput ranges. These throughputs were nominally 40 psia (low throughput configuration) and 80 psia (high throughput configuration). The preburner assembly was designed so that the two catalyst configurations matched the interfaces of the adjacent components.

(U) The preburner assembly in its final form is shown in Figure 11. Preburner design was based both upon recommendations and consultation with Mr. McCormick of Food Machinery and Chemical Company and upon the data derived in the subscale catalyst program conducted during Phase I of this program (Ref. 1). The latter program strongly influenced pack design parameters such as pack length, screen orientation, and screen selection.

(U) The catalyst pack is made up of an entrance manifold, entrance orifice plate, catalyst screen (active and passive), and an exit orifice plate.

(U) Stainless steel (Series 347) was used as the material of construction for all preburner components. This material was selected because of its excellent structural properties at high temperature and its compatibility with  $H_2O_2$ . The catalytic decomposition temperature of 98%  $H_2O_2$  is approximately 1800°F. However, exposure to this temperature would produce only transient heating effects in the preburner structure, because of the short duration

UNCLASSIFIED

# UNCLASSIFIED

Report 10785-F, Phase 11

TABLE I  
PREBURNER DESIGN PARAMETERS

<u>Parameter</u>	<u>Symbol</u>	<u>Units</u>	<u>Value</u>	
			(Low)	(High)
Throughput at MR = 0.5 <sup>(a)</sup> (nominal design point)	TP	psia <sup>(b)</sup>	40	80
Throughput at MR = 1.0 (off-design maximum)	TP	psia	61	122
Oxidizer flow at MR = 0.5	$\dot{W}_O$	lbm/sec	22.0	
Oxidizer flow at MR = 1.0	$\dot{W}_O$	lbm/sec	33.7	
Chamber pressure	$P_{PC}$	psia	4500	
Gas temperature	$T_{CP}$	°F	1750	

- (a) MR refers to the thrust chamber mixture ratio of total weight flows of 98% H<sub>2</sub>O<sub>2</sub> to Alumazine-43.
- (b) Pounds per square inch of catalyst pack frontal area times minutes.

UNCLASSIFIED



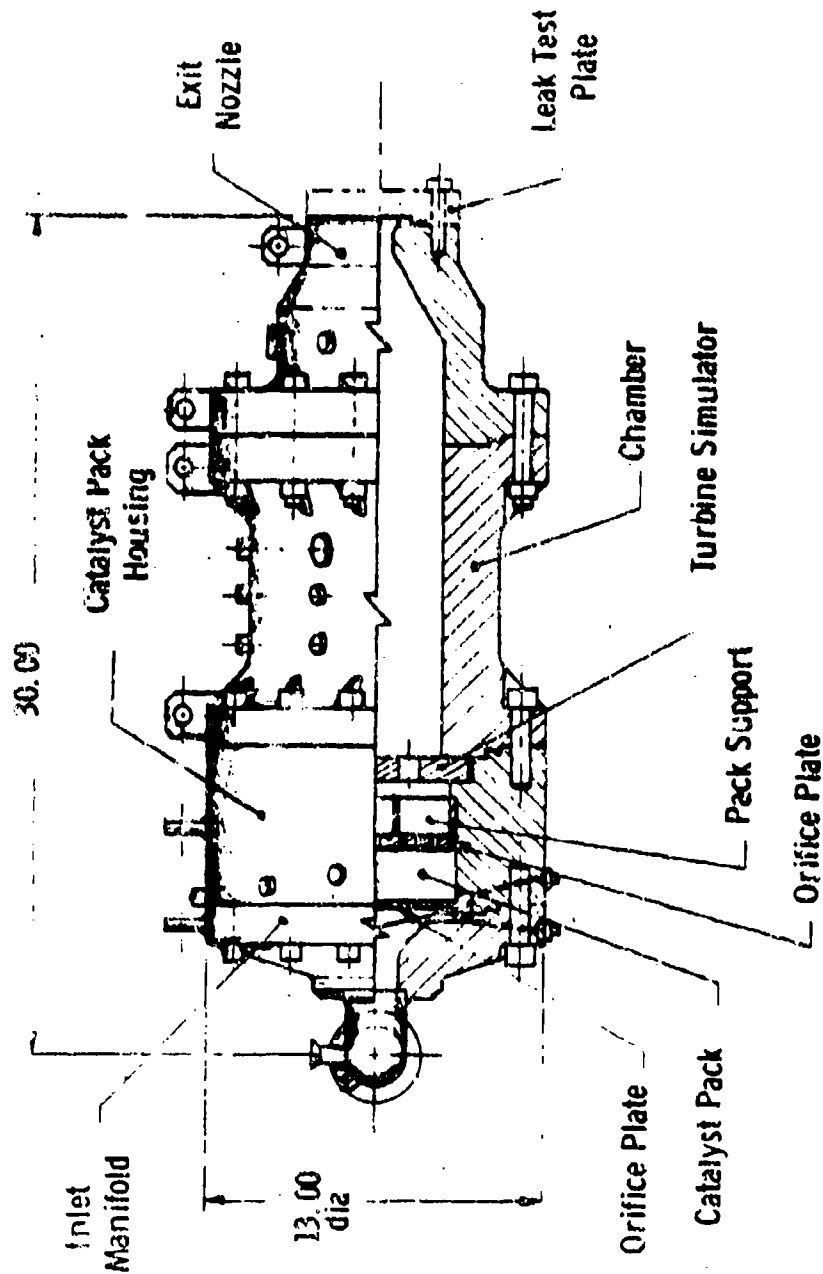


Figure 11.  $H_2O_2$  Preburner

# UNCLASSIFIED

Report 10785-F, Phase II

## III. B, Technical Discussion (cont.)

(5.0 sec) of the tests. The inlet manifolds, catalyst housings, chambers, and nozzles were all machined from forged CRIS 347. The remaining components were fabricated from CRIS 347 plate, bar, or tubing.

(U) High-pressure Conoseal<sup>(6)</sup> joints, were incorporated into the preburner as the flange seals. This type of metal-to-metal seal has previously been used successfully in other Aerojet high-pressure component test programs. Thus, no elastomer-type seals were used in any of the liquid  $H_2O_2$  circuits.

(U) As shown in Figure 11, a seven-orifice turbine simulator was designed using the compressible gas-flow through-orifice relationship described in Ref. 3. The turbine simulator reduces the pressure from a level of between 4000 and 4500 psia (depending on balance requirements) at the catalyst pack outlet, to a level of about 3000 psia--the desired operating pressure for the secondary combustor. The pressure drop is similar to that anticipated for a turbine in an engine.

(U) To perform preburner testing, a back-pressure nozzle was also designed and fabricated (see Figure 11). This nozzle, in conjunction with the turbine simulator, allowed accurate simulation of the staged-combustion oxidizer flow and pressure conditions.

(U) The assembly also incorporated a chamber section which served as a gas flow straightening section. Gas turbulence anticipated at the outlet of turbine simulator could cause poor  $H_2$  distribution and oxidizer-rich zones across the face of the injector which in turn could produce erosion of

<sup>(6)</sup> Conoseal is the trade name for a metal gasket produced by the Marman Division of the Aeroquip Corporation, Los Angeles, California.

UNCLASSIFIED

## 1.1. B. Technical Discussion (cont.)

downstream ablative and tungsten components. The inside diameter of the chamber, 5.0 in., was selected to maintain a gas velocity of about Mach 0.3, in keeping with current design practice for gas generators.

## c. Catalyst Pack Design

(U) The catalytic decomposition of 98%  $H_2O_2$  is an exothermic reaction in which the temperature of reaction is almost entirely a function of peroxide concentration and feed temperature. Pressure appears to have little effect although this has not been conclusively demonstrated. Figure 12 shows the relationship of decomposition temperature to concentration and feed temperature. Decomposition temperatures in the range of 1750 to 1800°F may be anticipated. If pressure has an effect, the decomposition temperature can be expected to be closer to 1800°F. Therefore, pure silver screens which perform very well with 90%  $H_2O_2$  cannot be used as the sole catalytic material for 98%  $H_2O_2$  because the melting point of silver is 1760°F. Other higher-temperature catalytic screens must be used, particularly in the high-temperature zone of the catalyst pack. Silver may be used in the forward end of a pack to assist in the initiation of the decomposition since this portion of the pack remains relatively cool.

(U) Two axial flow catalyst pack configurations were designed. Both of these incorporated high-temperature catalyst materials which effectively resisted the temperatures encountered from 98%  $H_2O_2$  decomposition. These catalyst materials, Ageite 220 and Ageite 225, are under a patent secrecy order<sup>(7)</sup> and their composition cannot be revealed at this time. The two configurations were: (1) a low throughput pack to cover the peroxide loading range of 40 to 61 psim; and (2) a high throughput pack to cover the range 80 to

<sup>(7)</sup> United States Patent Office Secrecy Order covering patent application Serial No. 473,326, Decomposition Catalyst, by James C. McCormick.

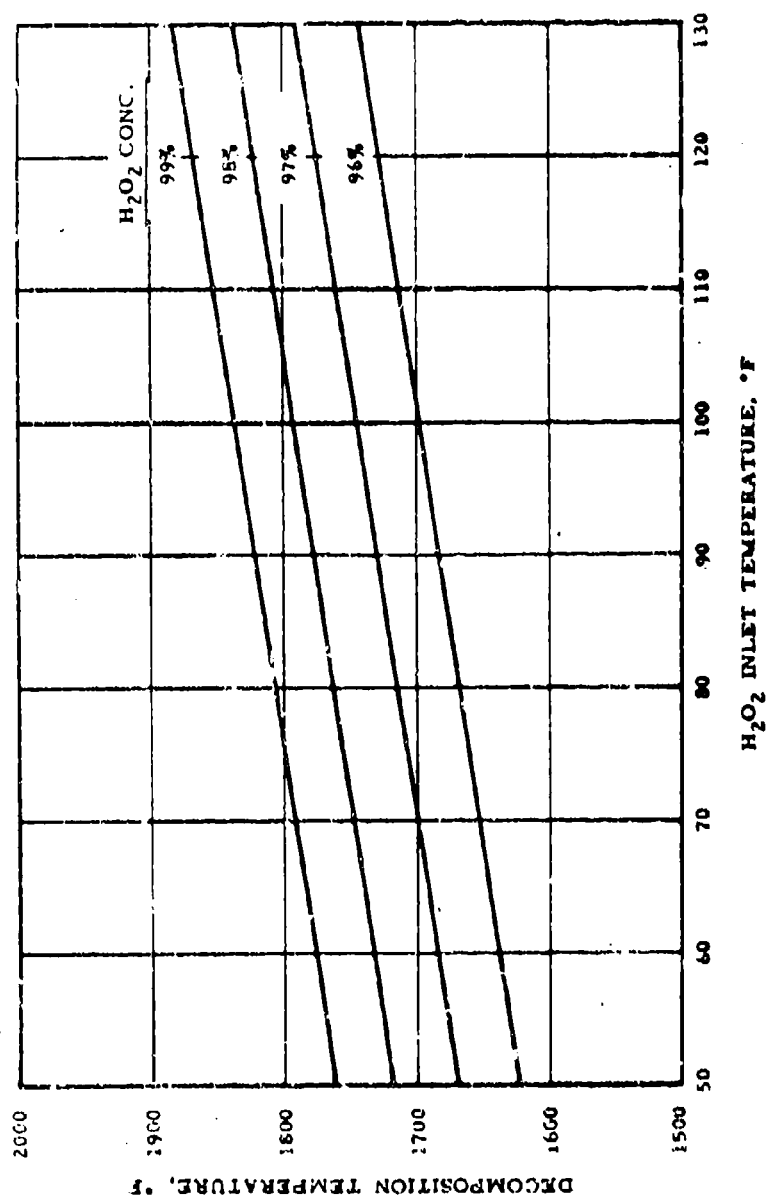


Figure 12. Decomposition Temperature of Peroxide

## III, 8. Technical Discussion (cont.)

122 psim. They were 6.50 and 4.58 in. in diameter, respectively. (Note: 40 and 80 psim correspond to an MR of  $H_2O_2$ /Alumazine-43 of 0.5 while 61 and 122 psim correspond to an MR of 1.0.)

(U) The design of the axial catalyst packs and certain other features of the preburner configuration were based on existing high-temperature catalyst technology provided by the Food Machinery and Chemical Company, the supplier of electrolytic 98%  $H_2O_2$ , and the subscale catalyst evaluation conducted during Phase I of the program (Ref. 1). From these two sources, such parameters as catalyst depth, throughput, catalyst pack compression, pressure drop, and the number of active screens were derived.

(U) Several important design considerations were taken into account based on the above cited experience. First, the introduction of the liquid peroxide into the pack was found to be very important. Excessive volume in the inlet manifold could lead to unstable behavior during the decomposition reaction. On the other hand, excessive velocity in the inlet manifold could produce unequal distribution of peroxide flow into the pack. These undesirable effects were countered in several ways. The kinetic effects of the peroxide entering the manifold at 21 ft/sec were eliminated through the use of baffle plate located directly opposite the inlet line (see Figure 11). Next, the volume in the manifold was contoured to maintain 7 to 10 ft/sec  $H_2O_2$  velocity across the inlet plate to the catalyst pack and to minimize manifold volume. Finally, the inlet plate was drilled in a uniform pattern of holes to yield about 25% open area and give equal distribution of liquid peroxide as it passed into the pack.

(U) The catalyst pack itself was composed of a compressed mass of die-cut screens corresponding to the diameter required for low throughput (40 psim) and high throughput (80 psim). Details of the screen arrangement may

## III, B, Technical Discussion (cont.)

be found in Section III,B,5. The active screens, 20-mesh silver and 20-mesh Agelite, were placed in the forward end of the pack to initiate the decomposition reaction. These screens were alternately interspersed with 14-mesh inert nickel-manganese screens. It was possible to use a fairly tight mesh size in this part of the pack and thereby realize a relatively high catalyst surface area, because the peroxide was still in the liquid phase. The lower portion of the pack was made up of 12-mesh nickel and 14-mesh nickel-manganese screens which act as thermal catalyst to sustain the reaction. The anticipated pressure drop was about 60 psi.

(U) The screens were compressed with a load to induce a compaction of 4000 psi. Experience (as previously noted) indicated that pack stability was dependent on the maintenance of this compression during operation. Consequently, the length of the pack was measured while the pack was being compressed in a precision hydraulic operated press. When the pack was inserted into the preburner housing, Type 347 stainless-steel shims were used at the forward end to maintain the depth corresponding to that measured during the compression operation. A soft aluminum spacer was also used at the forward end to absorb possible thermal growth during firing.

(U) The active screens were interspersed with nickel-manganese screens to also prevent flow of the softer, active metals into each other during compression and operation. This technique was successful in maintaining a high catalytic surface area.

(U) Two anti-channel baffles were used to prevent channeling of the peroxide along the sides of the catalyst pack. Split rings made of 347 CRES, resembling piston rings, were inserted between the screens at strategic points in the pack prior to pack compression.

## III, 5, Technical Discussion (cont.)

(U) The catalyst depth was selected based upon a correlation discussed in Section II, B, 5. The test results indicate that the pack depth selected was proper.

(U) The pack was supported by a drilled multiorifice exit plate having an open area of 30% and a heavy "wagon-wheel" support structure to resist thermal and load stresses during preburner operation. Spacers were included in the design between the "wagon-wheel" and the exit plate to permit large changes in catalyst pack depth.

## d. Instrumentation Provisions

(U) The placement of instrumentation is shown schematically in Figure 13. The preburner was fully instrumented to measure the following functions during each test.

(1) Temperature measurement--sheathed chromel-alumel TC's at:

- (a) Inlet manifold to catalyst pack.
- (b) At least four stations in pack to obtain a temperature profile as a function of catalyst depth.
- (c) Pack outlet.
- (d) At least three locations in chamber section.
- (e) Entry to nozzle.

NOTE: P - PRESSURE  
 O - OXIDIZER  
 J - INLET MANIFOLD  
 T - TEMPERATURE  
 CP - CATALYST PACK  
 PN - PREBURNER NOZZLE  
 PC - CHAMBER  
 FN - DESIGNATOR FOR HIGH FREQUENCY TRANSDUCER  
 BLK - BLANK

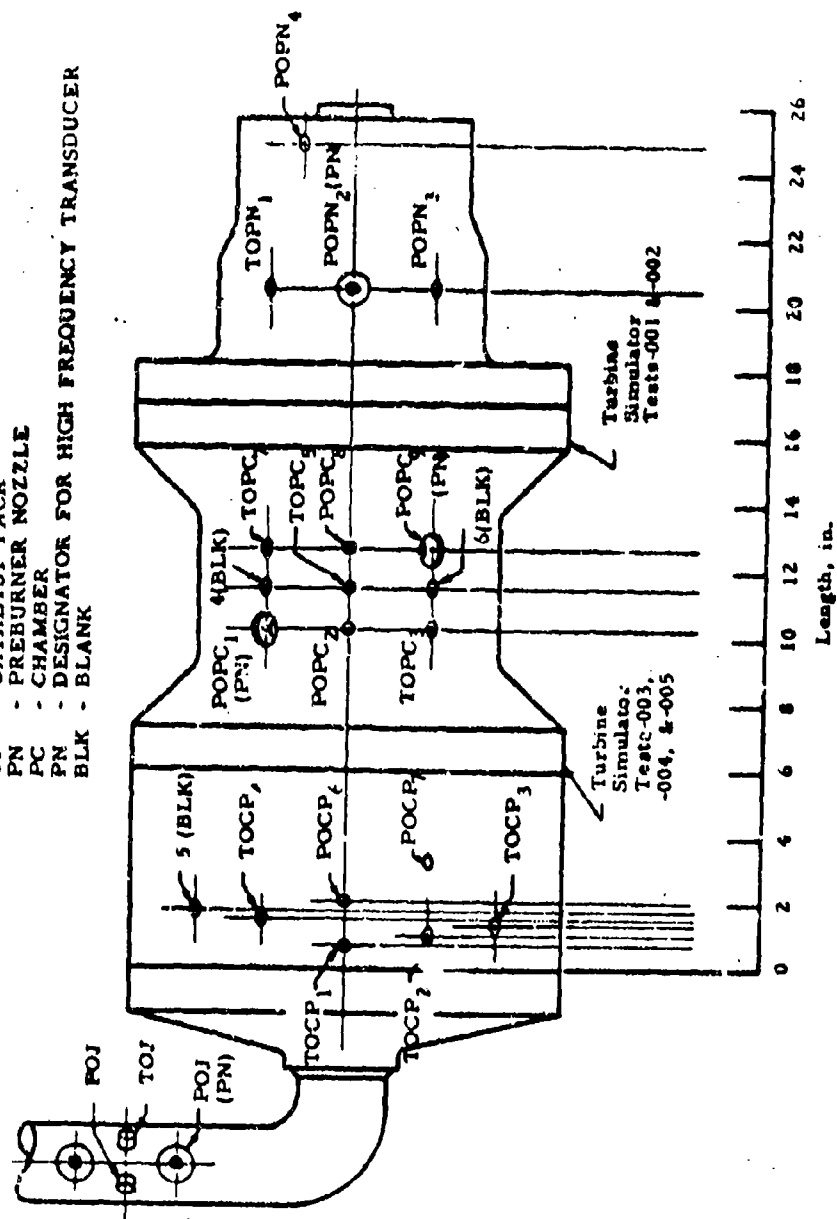


Figure 13. Instrumentation of Preburner Assembly



## III. B, Technical Discussion (cont.)

(2) Pressure measurement--Taber<sup>(8)</sup> transducers at:

- (a) Inlet manifold.
- (b) Outlet pack.
- (c) At least two locations in chamber.
- (d) Entry to nozzle.
- (e) Entry to nozzle.

(3) High frequency capacitance-type transducer--Photocon<sup>(9)</sup> Model 307, wat.

- (a) Inlet manifold.
- (b) Two locations in chamber.
- (c) Entry to nozzle.

All instrumentation ports were located in the upper portions of the hardware to obtain self draining, and prevent accumulation or trapping of peroxide.

2. Method of Testinga. Preburner Start Transient and Operation Analysis

(U) An analysis to evaluate the starting requirements and operation of the preburner was conducted. This analysis took the following factors into consideration:

<sup>(8)</sup> Taber transducers, a product of Taber Instrument Corporation, North Tonawanda, New York, 14120.

<sup>(9)</sup> Photocon transducers, a product of Photocon Research Products, Pasadena, California.

## III, B, Technical Discussion (cont.)

(1) The servo-controlled intensifier system (Figure 14) uses the discharge pressure as the control feedback signal.

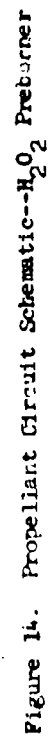
(2) The catalyst may fail to initiate decomposition of the  $H_2O_2$  with the predetermined rising pressure schedule.

(3) Pulse starting of the catalyst would not be feasible, because the high supply pressure would produce excessive flow during the time prior to initiation of decomposition of the  $H_2O_2$ .

(U) Start transient malfunction-shutdown criteria were based upon the "no-ignition" factor. Because the feed system was on closed-loop pressure control, the preburner was started at low pressure (about 300 psia) and low flow rate (about 2 to 3 lbm/sec) by using a small valve and orifice that bypassed the main thrust chamber valve. The chamber pressure which would result from  $H_2O_2$  decomposition was estimated, and a pressure switch was set near this value to make contact within a specified time period so that chamber flooding could be prevented. The pressure switch then initiated a timer that was programed to allow the catalyst to heat by decomposition of the bleed  $H_2O_2$ . Upon completion of the heating-up period, 2 to 3 sec in duration, the supply pressure to the preburner was increased linearly from 300 psi to about 4500 psia. The main thrust chamber valve opened simultaneously. The pressure rise (also called staging and ramping elsewhere in this report) was timed for 1.0 to 1.5 sec.

(U) A second pressure switch preset at 3500 psia was included in the system as an indicator that decomposition of the  $H_2O_2$  was sustained throughout the pressure ramp. Failure of this pressure switch to actuate within a specified time period automatically initiated the shutdown sequence. Thus, a flooding condition was avoided.

PORT 10.0, -R, Phase II



14:40 43

UNCLASSIFIED

UNCLASSIFIED

Report 10785-F, Phase II

(II), B, Technical Discussion (cont.)

(U) The requirements for obtaining intensifier flow control rather than pressure control were also evaluated. The analysis indicated that an analog simulation of the intensifier system would be needed to evaluate the various methods of generating the flow feed-back signal to the servo-valve system which controls nitrogen flow on the gas side of the differential piston. (See next section for a description of the test facility.) Costs were estimated for completion of this analysis, for procurement of a modified control network, and for checkout of the system. Cost analysis indicated this modification to be significantly beyond the scope of the program. It was also determined that this type of control was not necessary for the preburner testing since no throat erosion would be expected. Throat erosion estimates for the secondary combustor indicated that the throat diameter would change insignificantly in the short-duration tests planned. Therefore, the more sophisticated flow control system did not appear warranted. Test experience confirmed this conclusively.

(U) Preburner operation was also examined for the flow conditions needed to increase staged-combustion mixture ratio from 0.5 to 1.0. These oxidizer flow rates were 22.0 and 33.7 lb/sec, respectively. The design, as presented in Ref. 1, was based upon a nominal catalyst pack throughput preburner. At a mixture ratio of 1.0, these throughputs increase to 61 and 122 psim, respectively.

(U) The possibility of bypassing a portion of the  $H_2O_2$  around the pack and thermally decomposing the peroxide in the hot-gas stream was also considered. This concept is entirely feasible and affords a means of avoiding excessively high catalyst bed throughputs. Diluent testing in the Phase I subscale catalyst program (Ref. 1), in which it was attempted to attenuate gas temperature by injecting 98%  $H_2O_2$  downstream of the catalyst pack, showed that bypassed flows, as high as 30%, would thermally decompose completely. A diluent injector, previously designed for the preburner system, would be employed to inject the bypassed peroxide, if it became necessary to resort to this method. (Later, it was not necessary.)

UNCLASSIFIED

# UNCLASSIFIED

Report 10785-F, Phase II

## III. B. Technical Discussion (cont.)

(U) The pressure schedule for the preburner testing considered a 4300-psia supply pressure to the  $H_2O_2$  manifold. Pack pressure drop depending on throughput and pack length was expected to range from 60 to 150 psi, giving a preburner chamber pressure of about 4400 psia. The desired pressure downstream of the turbine simulator was about 3075 psia. A pressure drop of approximately 1300 psi could be expected to occur across the turbine simulator, and therefore, the  $H_2O_2$  manifold pressure was set accordingly. The manifold pressure was adjusted, based upon actual pressure drop across the turbine simulator, to maintain the 3075-psia pressure level.

### b. System Dynamics Analysis

(U) "Chugging", or low-frequency combustion instability in liquid rocket engines, is caused by the interaction of pressure and weight-flow oscillations in the combustion process and engine feed system. This analysis was conducted to investigate the stability characteristics of the preburner coupled to the J-1 intensifier feed system and to identify potential problems that would require system modification. Figure 14 is a schematic of the feed system, and Figure 11 shows the preburner with the back-pressure nozzle attached.

(U) An analytical model of the preburner system was developed using analog networks to represent the feed system and catalyst components. The concept of hydraulic impedance, which parallels the concepts of electrical transmission line theory, was used to define the frequency response characteristics of the feed system and chamber elements. Flow or pressure fluctuations are either attenuated or amplified in the system according to the impedance properties as seen from the decomposition zone.

UNCLASSIFIED

# UNCLASSIFIED

Report 10785-F, Phase II

## III, B, Technical Discussion (cont.)

(U) Thus, the impedances that must be evaluated for the stability analysis are (1) the upstream liquid feed system impedance, and (2) the downstream gas-side impedance. These impedances are composed of equivalent inductances, capacitances, and resistances, which are, in turn, functions of the feed system geometry and the fluid properties. The problem is thereby reduced to the analysis of a linear electrical circuit corresponding to the preburner system.

(U) A convenient method of studying the stability of this system is the signal flow graph (Figure 15), which is a graphical representation of the set of Laplace-transform equations describing the circuit. The flow graph is merely used as an aid in visualizing the cause-and-effect relationships between pressure oscillations in the circuit under study.

(U) A steady-state stability equation is derived from the graph by reducing the graph to a single gain from input to output. This reduction of the flow graph is equivalent to solving the set of simultaneous linear algebraic equations by successive substitution. The procedure for graphical reduction is well documented in Ref. 4 and 5.

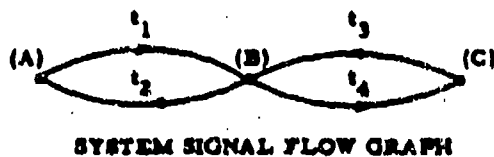
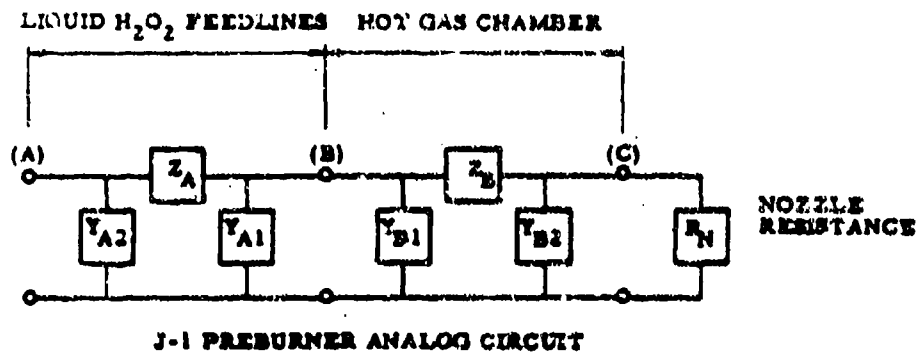
(U) A single gain term, which is the ratio of output to input, is obtained as a result of the reduction. A digital computer program is used to evaluate this gain numerically as a function of frequency over the frequency range of interest. The gain thus evaluated is a measure of the amplification or attenuation of an oscillatory pressure originating in the decomposition zone, transmitted through the upstream and downstream impedances, and then reflected back to the decomposition zone.

(U) Not only must the magnitude of the gain be equal to or greater than one, but the input and output must also be in phase in order for the system to sustain oscillations. The resultant open-loop transfer function

UNCLASSIFIED

UNCLASSIFIED

Report 10/55-2, Phase II



$$F_D = 1 - T_D = 0$$

where  $T_D = t_1 t_2 + t_3 t_4 = \text{open-loop transfer function}$

SYSTEM STABILITY EQUATION

Figure 15. J-1 Low Frequency Stability Analysis

UNCLASSIFIED

# UNCLASSIFIED

Report 10785-F, Phase II

## III, B, Technical Discussion (cont.)

was plotted on a gain-phase diagram to display the results. For the signal flow graphs used in this analysis, Nyquist's stability criterion states that a closed-loop system is stable if the open-loop gain is less than unity when the open-loop phase is  $0^\circ$ . In control system analysis, stability is normally ensured if the open-loop gain is 0.5 (-6 db) or less at the  $0^\circ$  phase angle, and the open-loop phase lag is  $30^\circ$  or more when the gain is 0 db<sup>(10)</sup>.

(U) The results of the stability analysis are presented graphically in Figures 16 and 17. Two cases were considered at an MR of 0.5 and steady-state operation: (1) without turbine simulator and (2) with turbine simulator. Both cases display gain-phase characteristics which indicate stability in accordance with Nyquist's stability criteria. Also, in both cases, the gain steadily decreases with increasing frequency due to the capacitance of the chamber gases. With the additional resistance of the turbine simulator (case 2), the gains are generally lower, indicating a more stable system. From these results, it was concluded that the J-1 preburner system would be stable over the frequency range from 0 to 500 cps.

---

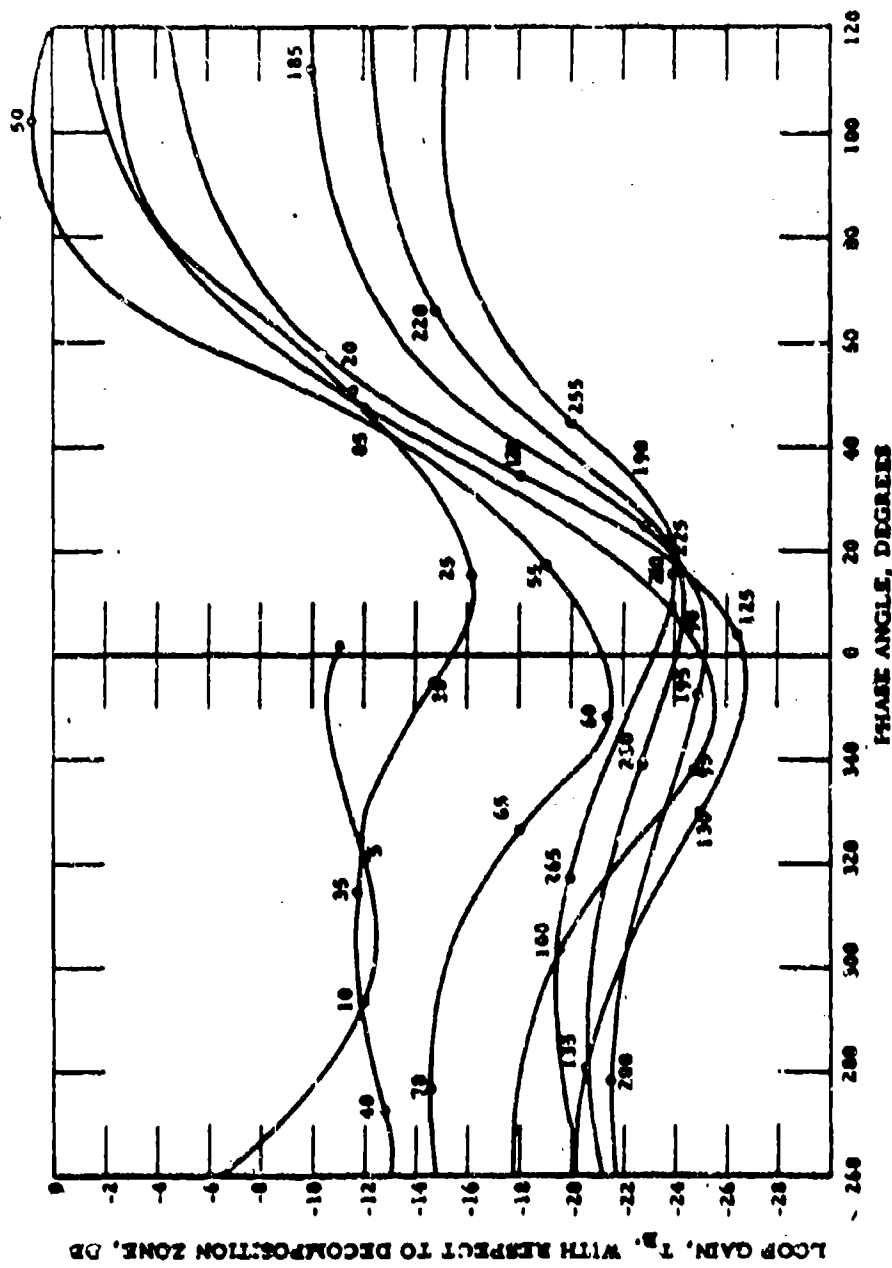
(10) In the signal-flow-graph method of analysis, the characteristic equation is one minus the open-loop transfer function is equal to zero, whereas in the block diagram type of analysis, it is one plus the open-loop transfer function is equal to zero.

UNCLASSIFIED



UNCLASSIFIED

Report 10781-F, Phase II



Page 49

UNCLASSIFIED

Figure 16. Gain-Phase Plot of J-1 Preburner with Turbine Simulator

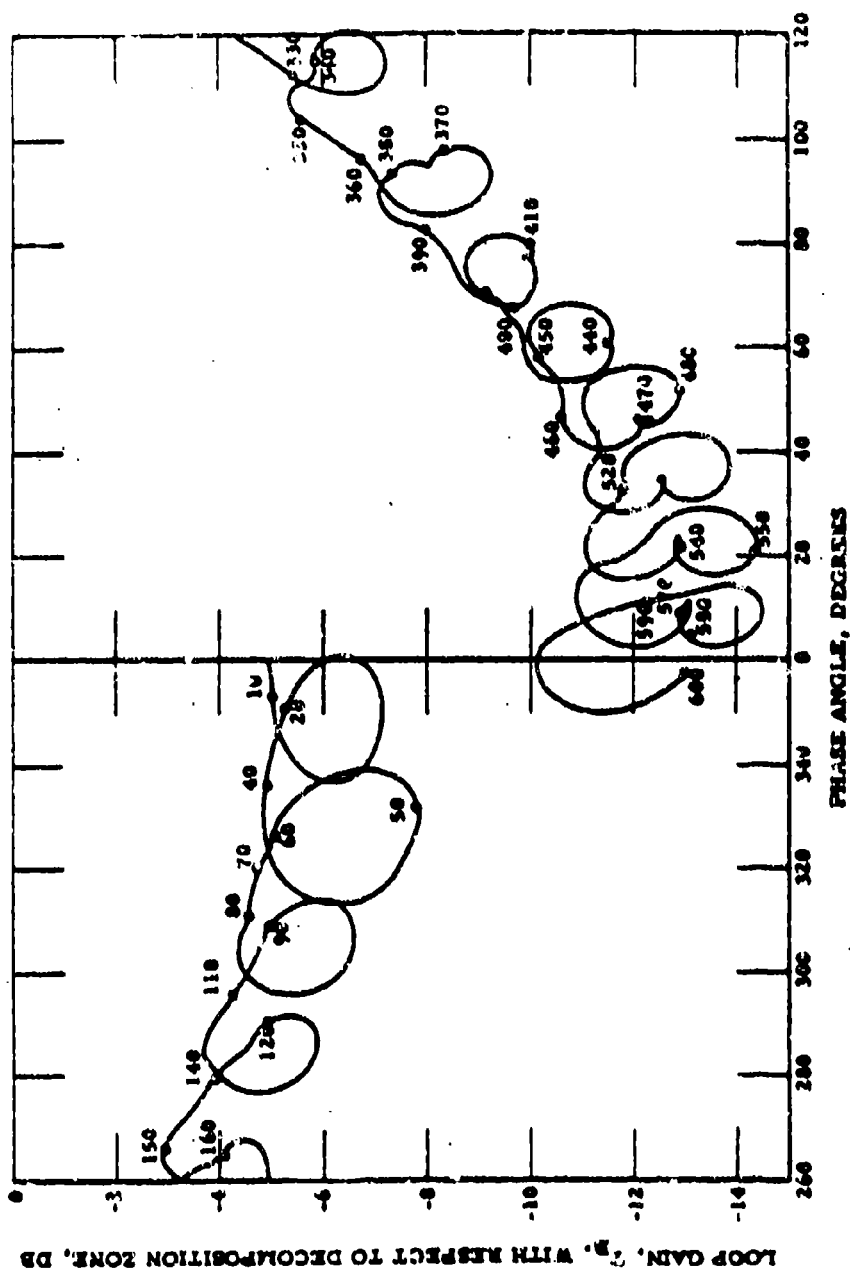


Figure 17. Gain-Phase Plot of J-1 Preburner without Turbine Simulator

# UNCLASSIFIED

Report 10785-F, Phase II

## III, B, Technical Discussion (cont.)

### 3. Test Facilities

(U) All Phase II test activities were conducted on Test Stand J-1. The test facility consists of a test bed with thrust measurement capability, an intensifier system to deliver propellants to the hardware at the required pressures and flow rates, a gaseous nitrogen cascade storage and transfer system, and a control room in which is housed instrumentation, recording, and monitoring equipment. Test Stand J-1 is part of a larger test complex devoted to altitude testing and the evaluation of exotic propellant systems and unique hardware concepts.

#### a. Test Stand J-1

(U) The test stand consists of a flexure-mounted horizontal test bed rated at 20,000 lbf of thrust. Thrust is measured with a dual-bridge load cell. The error in thrust measurement is less than 0.5% and repeatability is 0.15% above 10,000 lbf of thrust.

(U) Propellants are supplied to the hardware mounted on the test bed at pressures up to 5000 psig by two dual-piston pressure intensifiers which have a deliverable capacity of 80 gal each. The intensifiers have a 3 to 1 mechanical advantage; i.e., the gas-side piston has three times the area of the propellant side piston. Therefore, for example, 1500-psig gaseous nitrogen pressurization of the large piston will develop 4500-psig propellant pressure. Figure 18 shows the intensifier in partial cutaway. Figures 19 and 20 show the oxidizer intensifier installation. The fuel intensifier system is similar.

(U) The oxidizer side of the system is Class 2 with respect to 98%  $H_2O_2$  service from the intensifier through the oxidizer thrust chamber valve. Class 2 is an arbitrary classification applied to certain materials

UNCLASSIFIED

UNCLASSIFIED

Report 107 5-F, Phase II

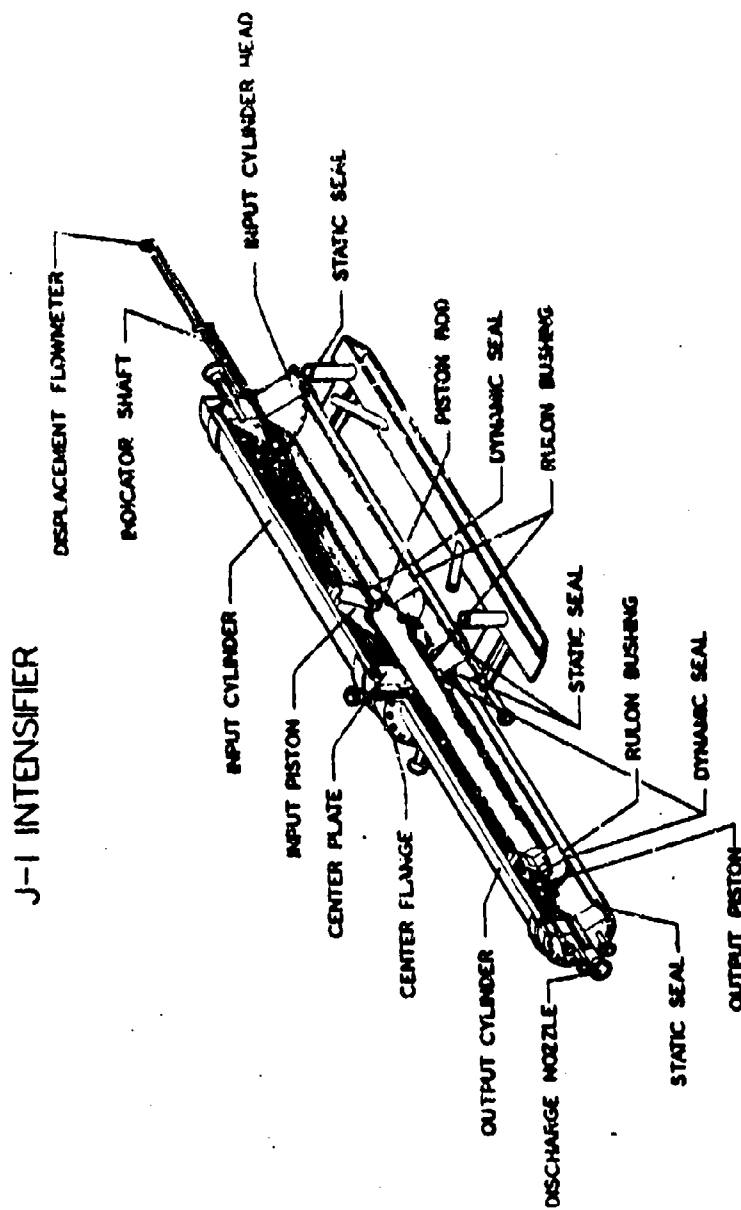


Figure 18. Partial Cutaway of Intensifier

UNCLASSIFIED

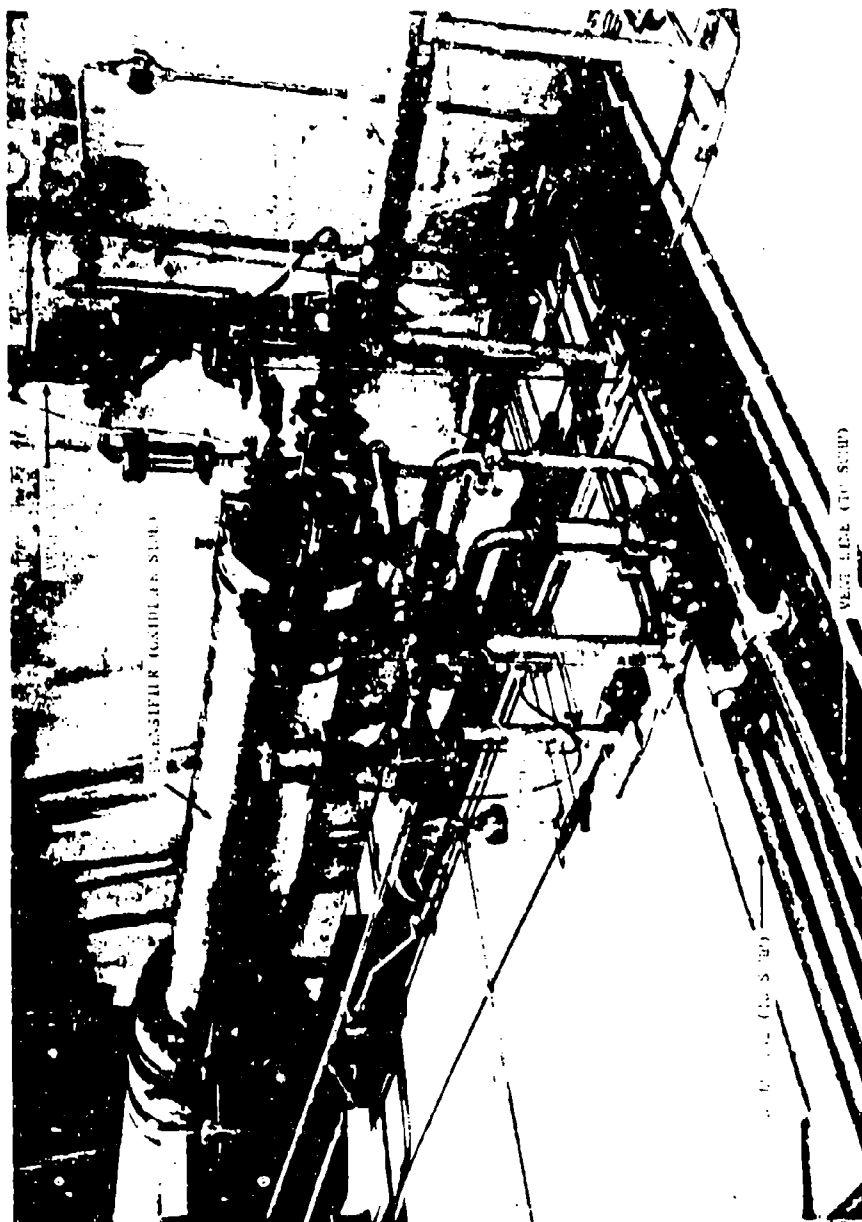


Figure 19.  $4\text{O}_2$  Intensifier--Oxidizer Pna

UNCLASSIFIED

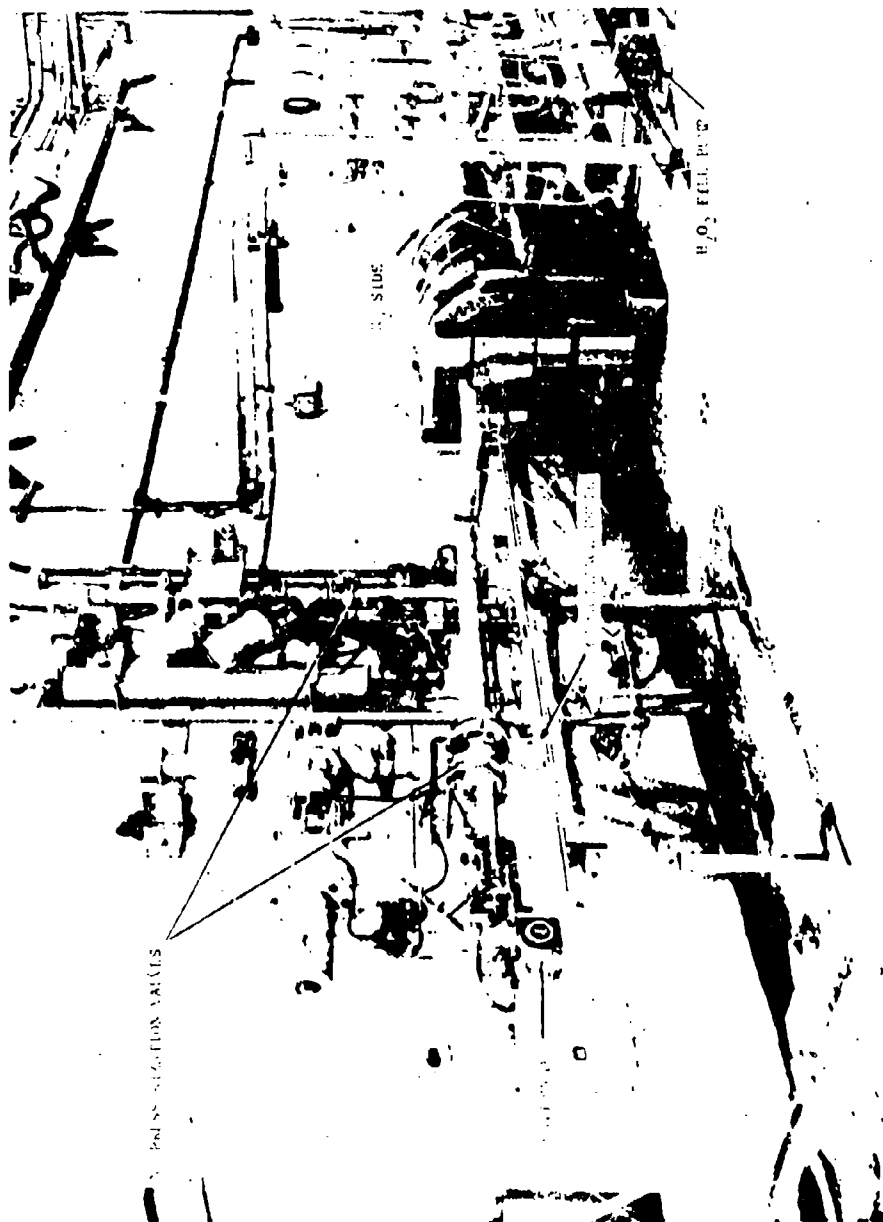


Figure 20.  $H_2O_2$  Intensifier--Gaseous Nitrogen End

UNCLASSIFIED

UNCLASSIFIED

Report 10785-F, Phase II

III, B, Technical Discussion (cont.)

of construction that are satisfactory for repeated short-time contact with 98%  $H_2O_2$  (Ref. 6). The classification of materials is based upon field results and upon laboratory evaluation of materials exposed to high concentration  $H_2O_2$ . Typical materials which fulfill this classification after they have been properly machined, cleaned and passivated include CRES 302, 316, 321, 347, Teflon, and Rulon-P. <sup>(11)</sup>

(U) Gaseous nitrogen is supplied to the intensifiers from a 3500-psig, 103,000-scf cascade and storage system. Inlet pressures to the intensifiers are controlled by servo-operated flow control valves with a closed-loop feedback system on pressure control. Each intensifier is fitted with two flow control valves which are operated separately to obtain a wide range of propellant pressure rise rates, pressures, and flows.

b. Instrumentation

(U) The J-Zone complex has an instrumentation system consisting of the following:

(1) Strain gage--24 strain gage channels with a maximum error of 0.5% of the measured value are available. The high-pressure transducers used on this program were of the balanced-bridge strain-gage type.

(2) Thermocouples--48 channels, basically designed to handle chromel-alumel, with a maximum error of 1% of the measured value, operate through a temperature-controlled 32°F reference bath.

(3) Flow measurement--Three methods of flow measurement were used on this program:

(11) Rulon-P, a filled Teflon material, a product of Dixon Corporation, Bristol, Rhode Island.

UNCLASSIFIED

## III, B, Technical Discussion (cont.)

(U) (a) Turbine-type magnetic flowmeters were mounted directly in both the fuel and oxidizer delivery lines. The primary purpose of the flowmeters was to provide preliminary posttest data. The signals from the flowmeters are conditioned with integrator units to convert from ac to dc for digital tape and strip chart recording. The ac signal is recorded on the oscillograph.

(U) (b) Linear potentiometers, with a maximum error of 0.4% of the measured value, are mounted on each intensifier to measure displacement of the piston. Measurement of an impressed dc voltage is similar to the methods used to measure valve traces, and the voltage change as a function of time is directly related to flow. This flow measurement method was used as a secondary or back-up flow measurement system.

(U) (c) Capacitance-type probes with a limited 24-in. travel were used as the primary flow measurement system, and all performance data contained in this report, unless otherwise noted, are based on measurements with these devices. These probes are accurate to within 0.4%. Probes are ac excited and are converted to a dc output for digital recording.

(U) (4) Time event measurement and control functions--The timers are R/C type. Valve movement is determined through the use of rotary or linear potentiometers which have had a dc voltage impressed upon them. Switch position changes are recorded through the switch contact.

(U) (5) High-frequency measurement and recording--A 32-channel Minneapolis-Honeywell Model 7600 recorder with a 0.4 to 20 kc frequency response can be utilized with capacitance, strain gage and/or crystal type sensing elements. For this program, water-cooled capacitance-type transducers were used.



## III. B. Technical Discussion (cont.)

(U) (6) Recording devices--The recorders are divided into two basic groups, analog and digital. The analog recorders are strip chart recorders, oscillographs, visual gages, and time-event recorders. The digital system is the analog-to-digital converter (ADC) and the digital tape recorder. The ADC is the primary means of recording because of the high degree of precision ( $\pm 0.1\%$  one count) and data reproduction capability by a computer. The strip chart is a low-response (1.0 cps) recorder used primarily for viewing "kill" parameters during test and to provide preliminary posttest data. The oscillographs are used to record low and medium frequency parameters (2000 cps) and monitor the occurrence of low-frequency instability. Visual gages are used for observation of test stand parameters that do not have to be recorded. Among the specific recording and monitoring devices used on this program were:

- (a) Oscillograph--18 channel
- (b) Oscillograph--36 channel
- (c) Strip chart recorders--12
- (d) Visual gages--12
- (e) 72-channel analog to digital conversion (ADC) system
- (f) Time interval counter, 10 channel (Berkeley)
- (g) TV closed circuit, 2 displays
- (h) Hot stylus recorder, 4 channel (Sanborn), setup of flow control and valve position.

(U) (7) All instrumentation is calibrated before and after each test by imposing a dc voltage in step increments over the range of the transducer.

## III, B, Technical Discussion (cont.)

4. Preburner Test Description and Results

(U) Three 98%  $H_2O_2$  preburner tests were conducted with the low-throughput (6.50-in.-dia) catalyst pack, and two were made with the high-throughput (4.58-in.-dia) catalyst pack. The objective of these tests was to demonstrate satisfactory operation of the preburner at oxidizer throughputs in each pack corresponding to staged-combustion mixture ratios of 0.5 and 1.0 for 98%  $H_2O_2$  and Alumisine-43. The results of this series of tests are summarized in Table II. Figures 21 through 27 show the results graphically. The location of instrumentation is shown in Figure 13. The instrumentation designators correspond to those used in the legends of the graphic displays of the preburner data. Figure 14 is a schematic of the propellant circuit. The preburner, with leak-test plate in place on the nozzle exit as it was installed on the test stand, is shown in Figure 28.

(U) To ensure satisfactory start of the system prior to opening of the main thrust chamber valve, a bypass valve was installed to allow a small amount of flow (2 to 3 lbm/sec) to enter the catalyst pack at a low preset pressure (375 to 500 psia) of the intensifier. This low flow rate permitted the initiation of  $H_2O_2$  decomposition and the preheating of the pack to a temperature between 1600 and 1700°F prior to staging (or ramping) to full flow and pressure conditions. Table III summarizes the bypass operation. On the first two tests, the bypass sequence was controlled manually. Main flow staging was manually initiated when a temperature gage downstream of the catalyst pack indicated 1000°F. In the final three tests, the entire sequence was controlled automatically.

(U) The flow conditions and parameters for each test are summarized below. The catalyst pack operation is discussed in the following section.

**TABLE II**

**ADVANCED PROPELLANT STAGED-COMBUSTION FEASIBILITY PROGRAM  
PREBURNER OPERATION 'U)**

[illegible]

2. The results are averaged over a 5-year interval, the first after beginning of study state, the second at the mid-point of study state, and the third near the end of study state.

3. The difference between two 500-gal. samples is 2.5.

4. Based on 500 gal. with 1000-type computer.

5. The estimated standard PPS decomposition expenditures.

CONFIDENTIAL

Report 10785-F, Phase II

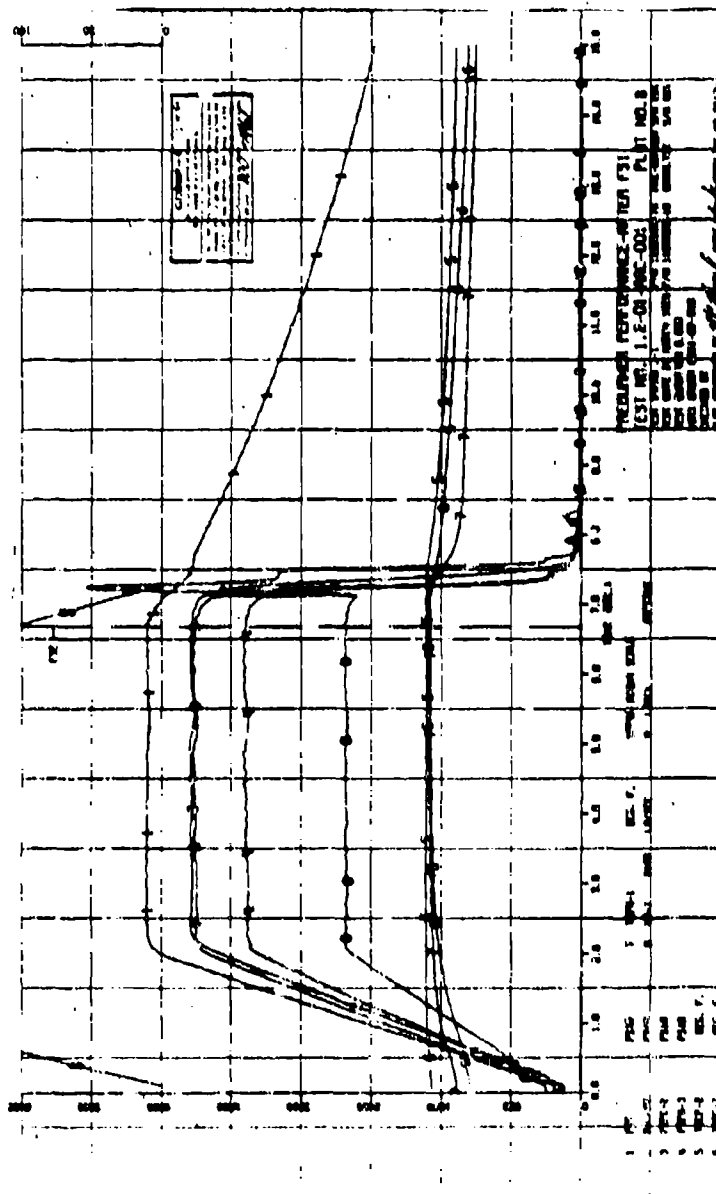


Figure 21. Preburner Performance after FS-1, Test 1.2-01-AMC-001 (u)

CONFIDENTIAL

**CONFIDENTIAL**

Report 10785-r, Phase II

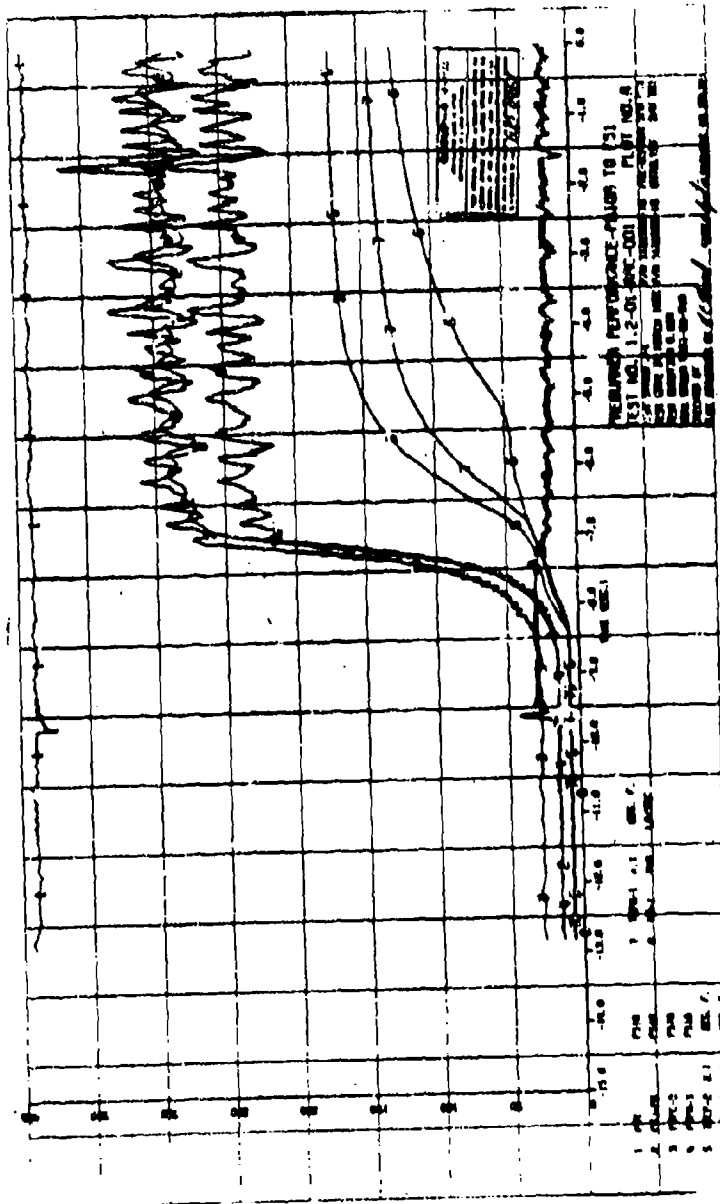


Figure 22. Preburner Performance before PS-1, Test 1.2-01-AAC-001 (u)

**CONFIDENTIAL**

CONFIDENTIAL

Report 10785-F, Phase II

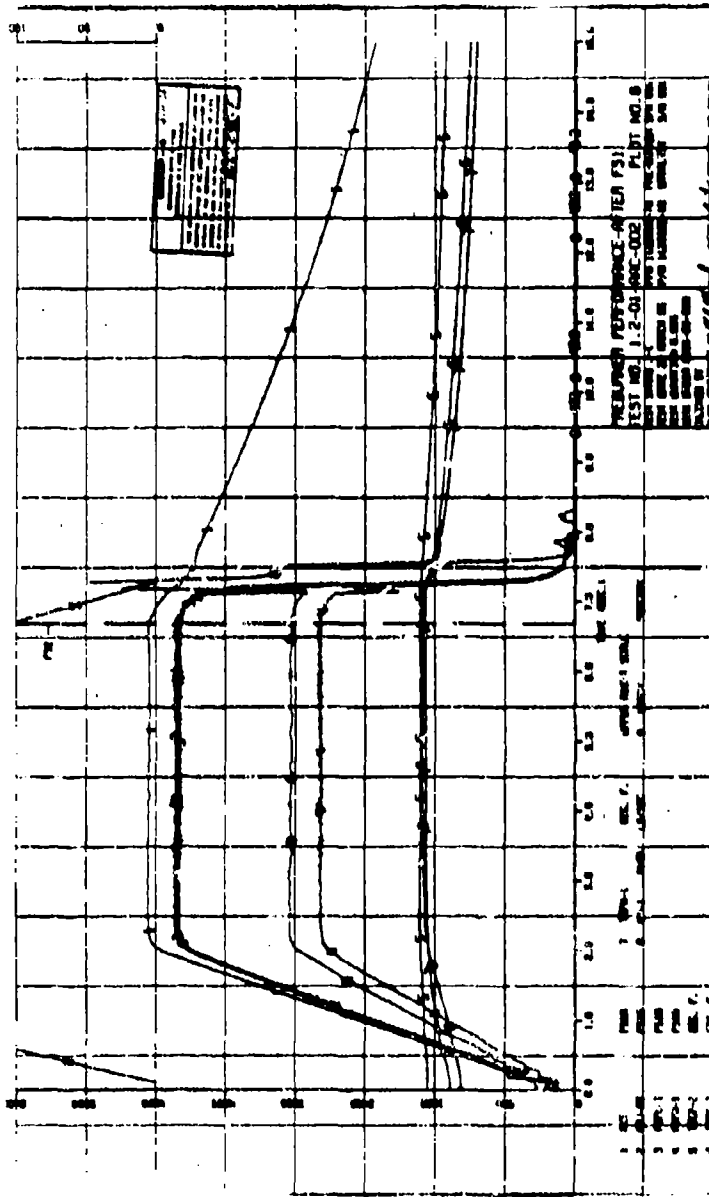


Figure 23. Preburner: Performance after FS-1, Test 1.2-01-AMC-002 (u)

CONFIDENTIAL



CONFIDENTIAL

Report 10785-F, Phase II

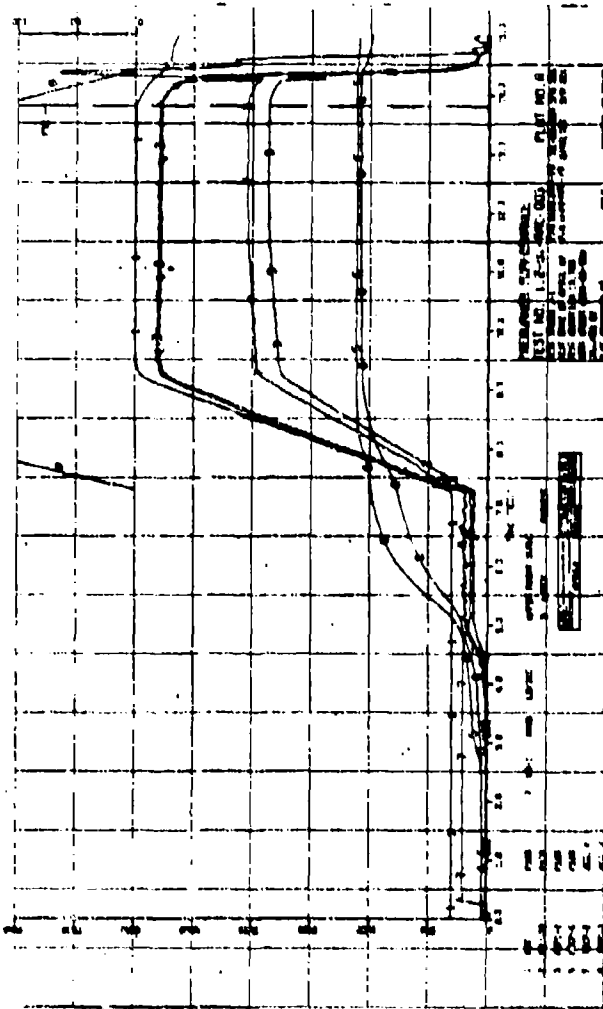


Figure 25. Preburner Performance--Test 1.2-01-AAC-003 (u)

CONFIDENTIAL



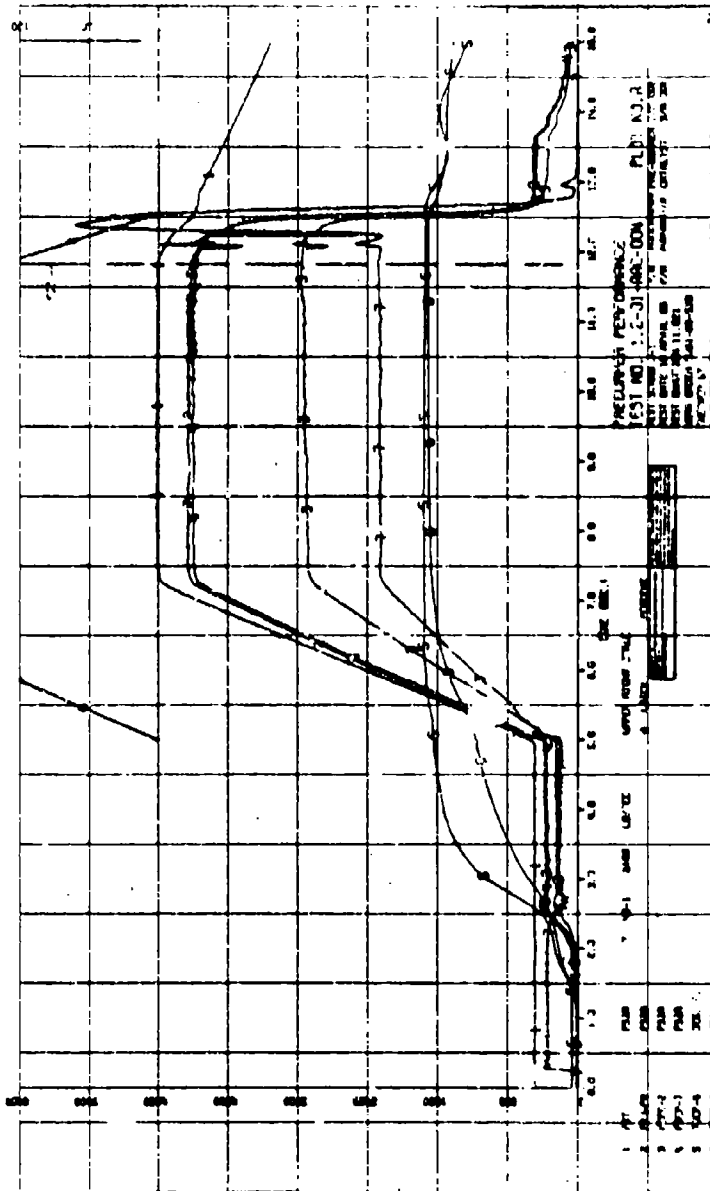


Figure 26. Preburner Performance--Test 1.2-01-AAC-004 (u)

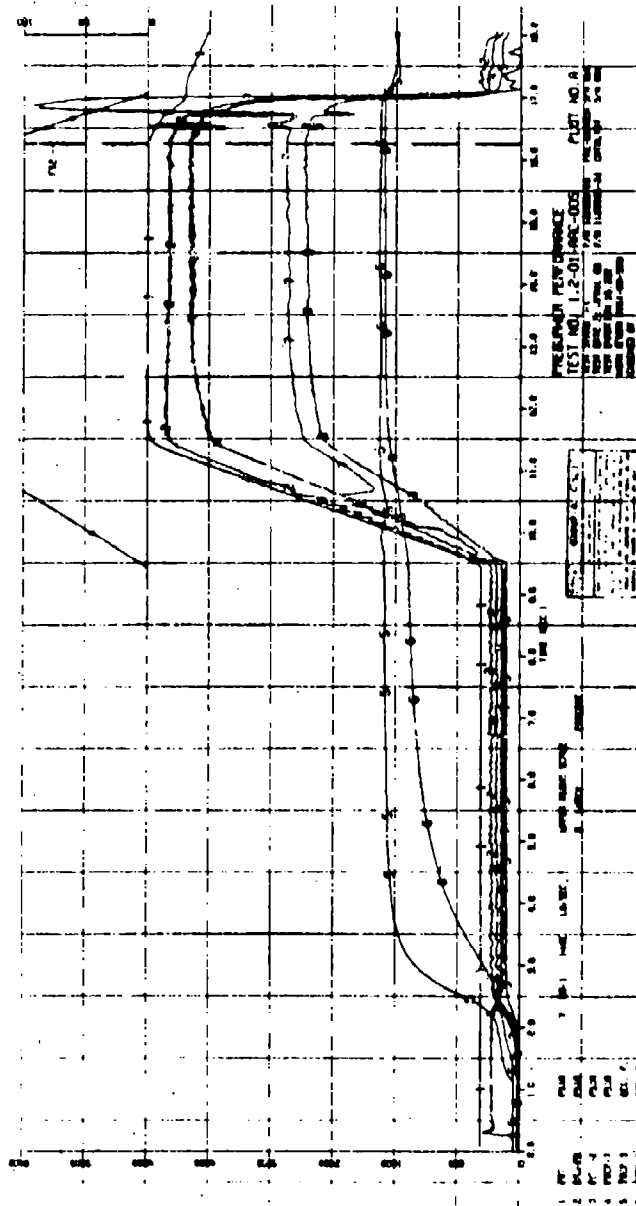


Figure 27. Preburner Performance--Test 1.2-01-AAC-005 (u)

**CONFIDENTIAL**

CONFIDENTIAL

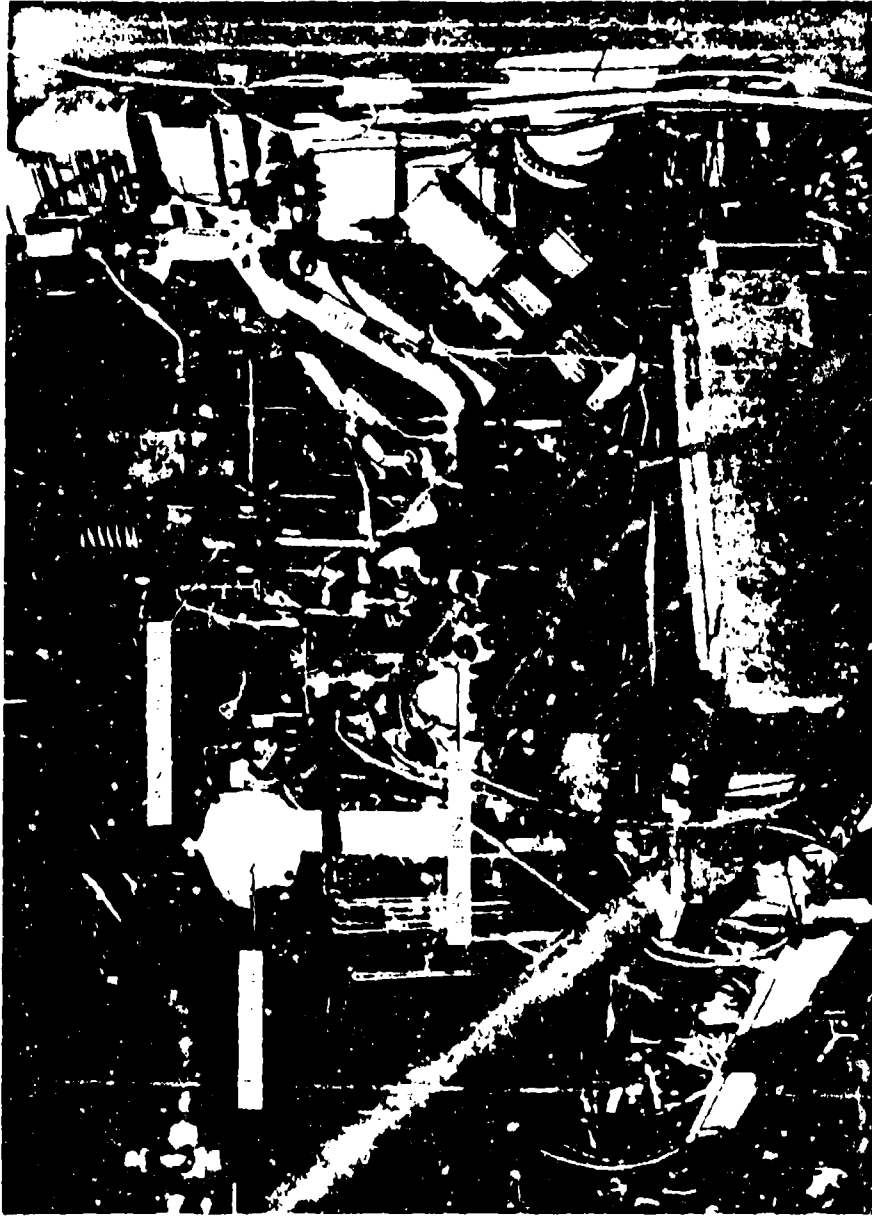


Figure 24. Helmer Installation, Test Stand J-1

CONFIDENTIAL

TABLE III

## OXIDIZER VALVE BYPASS OPERATION (U)

Test No.	Initiation Time Sec	Time to* 1600°F Sec	Bypass Flow lbm/sec	Booster Press. psia	Temp at Staging °F	Time From Initiation To Stage, sec
001	0.00	4.00	1.38	376	1713	8.70
002	0.93	8.00	2.25	431	1688	11.27
003	1.00	4.80	2.37	492	1591	5.00
004	0.00	2.92	2.16	485	1640	3.70
005	0.00	2.57	2.08	497	1750	8.62

\* 1600°F SELECTED BECAUSE THIS ASSURES GREATER THAN 90% DECOMPOSITION HAS OCCURRED.

## III, B, Technical Discussion (cont.)

## a. Test 1.2-03-AAG-001

(C) The objectives of this test were to check out the system and to operate the low-throughput preburner at a nominal throughput of 40 psim, corresponding to an  $H_2O_2$ /Aluminine-43 mixture ratio of 0.5. As noted in Table II, a throughput of 46.3 to 46.7 psim was achieved. A lower-than-desired pressure drop (383 versus 1400 psi) through the turbine simulator accounts for the increased flow rate and for the higher secondary chamber pressure ( $P_n$ ). Desired secondary chamber pressure for staged-combustion operation is 3000 to 3100 psia. A pressure of 3801 to 3843 psia was obtained. Otherwise, preburner operation was satisfactory. A pressure of 4400 psia and decomposition temperatures of 1771 to 1779°F were achieved over a steady-state period of 3.26 sec (steady-state operation was defined as that period of time over which the chamber pressure was in excess of 90% of full  $P_c$ ).

(U) Staging of preburner supply pressure to the desired operating pressure was initiated manually after sufficient temperature was indicated. Ramp (stage) time for this test was 2.0 sec, and ramping was linear, as shown in Figure 21. Preburner performance prior to ramping is plotted in Figure 22.

(U) Figure 29 shows the upstream side of the turbine simulator. The deposit of silver on the surface is a common occurrence with packs containing silver screens. Figure 30 is an aft view of the interior of the chamber just downstream of the catalyst pack. Note the silver spattered on the exit orifice plate. Also, observe the thermocouples that protrude into the chamber to measure the temperature gradient of the gas.



Figure 29. Preburner Turbine Simulator after Test 1.2-01-AAC-001

Page 70

**CONFIDENTIAL**

(This Page Is Unclassified)

**CONFIDENTIAL**

Report 1C785-F, Phase II

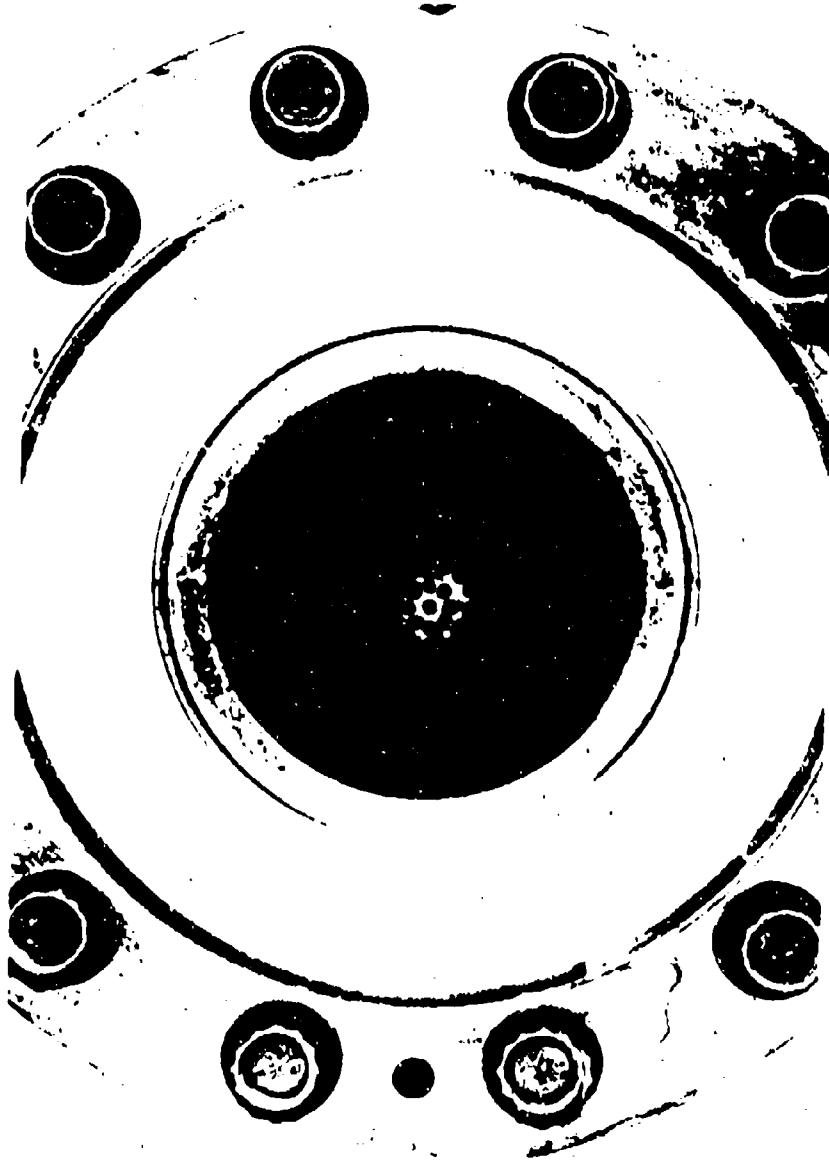


Figure 30. Preburner Aft View of Outlet Plate after Test 1.2-01-AAC-001

Page 71

**CONFIDENTIAL**

(This Page is Unclassified)

III, B, Technical Discussion (cont.)

b. Test 1.2-01-AAC-002

(U) The main objective of the second test was to demonstrate the capability of the low-throughput preburner to operate at a throughput of 61 psim, corresponding to an  $H_2O_2$ /Aluminine-43 mixture ratio of 1.0. This objective was met. Test results are shown in Table II and Figures 23 and 24.

(C) The preburner was sequenced in the same manner as in Test 001. A new turbine simulator, resized for the increased flow rate, was used. A pressure drop of 1617 to 1628 psi through the simulator was obtained. This produced a secondary chamber pressure of 2908 to 2917 psia. Chamber pressure downstream of the catalyst pack remained at about 4535 psia, during the 5.18 sec of steady-state operation. The maximum decomposition temperature was 1788°F.

(U) The slightly higher pressure drop through the turbine simulator also accounts for the lower throughput obtained. However, a throughput of 59 psim (instead of 61 psim) is considered sufficient for demonstrating satisfactory preburner operation at or near an oxidiser flow rate corresponding to a mixture ratio of 1.0.

c. Test 1.2-01-AAC-003

(U) The objectives of this test were to check out automatic operation of the preburner firing sequence and to evaluate the effects of locating the turbine simulator closer to the catalyst pack. The test was conducted satisfactorily with the low-throughput pack, at a throughput of about 59 psim.

(U) Completely automatic operation includes the low-pressure and low-flow bypass of the main propellant valve in the engine sequence. The



# CONFIDENTIAL

Report 10785-F, Phase II

## III, B, Technical Discussion (cont.)

bypass flow was sequenced to continue for 2.5 sec after the thrust-chamber pressure switch closed at 240 psia. This time delay was selected on the basis of results obtained in Tests 001 and 002, which showed that a pack temperature of at least 1600°F was reached after this time interval. This temperature ensures that  $H_2O_2$  decomposition exceeding 90% has occurred, thus reducing the possibility of flame-out during staging to full flow and pressure.

(U) The turbine simulator was moved upstream to a position closer to the catalyst pack (at the base of the catalyst-pack housing) because of turbulence noted on Tests 001 and 002 just downstream of the orifice plate. This turbulence could cause unfavorable recirculation patterns and poor mixture ratio distribution in the secondary injector during staged-combustion testing.

(C) Decomposition temperatures of 1792 and 1798°F and chamber pressures of 4454 to 4477 psia were achieved over a steady-state period of 5.11 sec. However, secondary chamber pressure (POPC-2, Figure 25) increased from 2896 to 3001 psia over the first 2.5 sec of steady-state operation before stabilizing. Pressure drop across the orifice plate fell correspondingly, from 1581 to 1456 psi. Flow (WO-1, Figure 25) also increased from 31.8 to 32.7 lbm/sec. As later demonstrated in Test 003, described subsequently, this behavior was corrected by subjecting the turbine simulator to a longer preheat during the peroxide bypass cycle of the sequence. Apparently, dimensional changes in the simulator orifices occurred during transient heating (which is still present during a portion of the chamber steady-state period) and caused flow and pressure-drop variations.

(U) Following this test, the hardware was disassembled and examined. The turbine simulator and the catalyst aft orifice plate and its support were plated with silver in a manner similar to that observed on

CONFIDENTIAL

## 111, B, Technical Discussion (cont.)

Test 001. The inlet plate (Figure 31) showed the effects of allowing the pack to cool down by natural convection. Heat soak-back occurred and produced characteristic discoloration of the plate, as shown. (After the pack was cooled to about 300°F, 10 gal of distilled water was flushed through the preburner to remove residual peroxide.) The Teflon O-ring used to seal the pack inlet plate to the housing was not found, and probably melted after the first test. Absence of the ring apparently did not affect the operation of the preburner on Tests 002 and 003. A posttest photograph of the catalyst pack is shown in Figure 32. Note the flow of silver (light areas) around the periphery of the pack and in the vicinity of the anti-channel baffles. The pack also bore evidence of some oxidation, evidently caused by the water purge and by condensation. (The pack diameter is 6.50 in.)

## d. Test 1.2-01-AAC-004

(C) The principal objective of this test was to demonstrate satisfactory operation of the high-throughput catalyst pack at 80 psia. The test was satisfactory, with a steady-state period of 5.30 sec, a pressure of 4400 psia, and pack decomposition temperatures of 1742 to 1752°F. Throughput was about 82 psia, which would result in a 98%  $H_2O_2$ /Alumazine-43 mixture ratio of 0.5 for an advanced engine utilizing these propellants.

(U) Pressure-drop variations through the turbine simulator also occurred in this test, but were not as pronounced as on the previous test (see Figure 26, POPC-7 and POPC-2).

(U) On this test, posttest purge with nitrogen gas ( $N_2$ ) was substituted for the cooling down and distilled-water purge used on the previous three tests. The  $N_2$  purge was successful in eliminating overheating of the pack.

UNCLASSIFIED

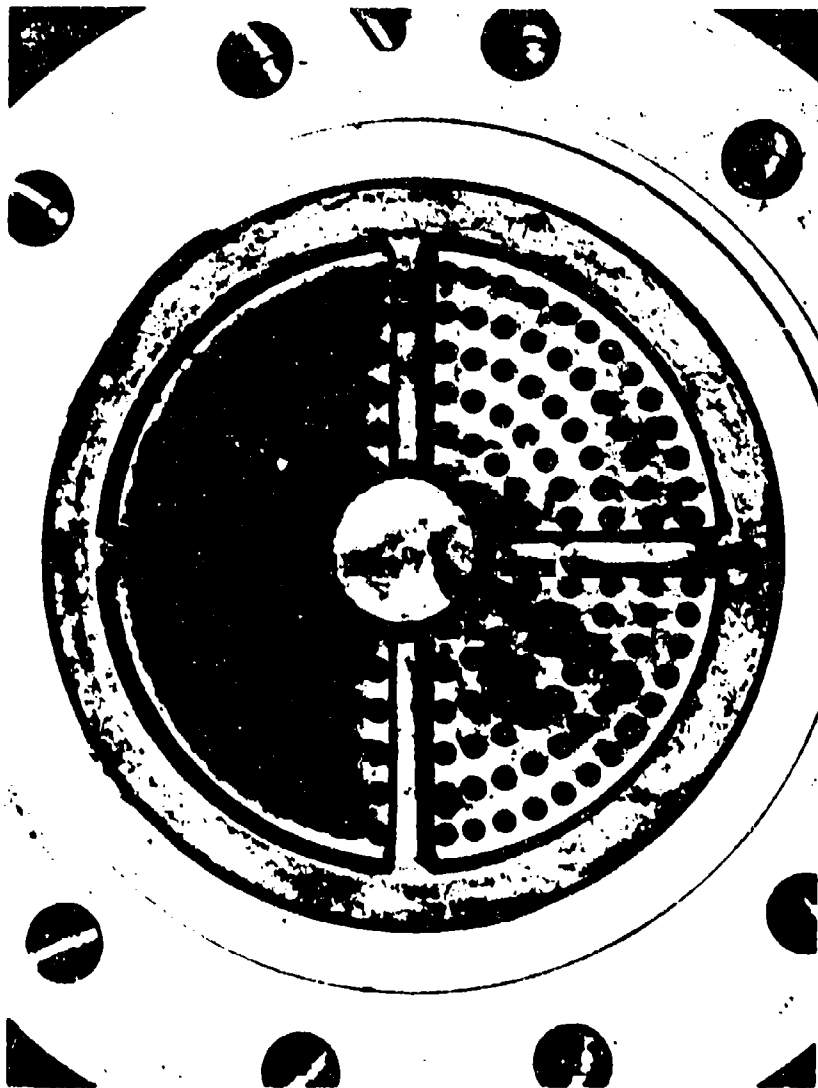


Figure 31. Preburner Inlet Plate after Test 1.2-01-AAC-003

Page 75

UNCLASSIFIED

UNCLASSIFIED



Figure 32. Catalyst-Pack Postfire, Test 1.2-01-AAC-003

UNCLASSIFIED

CONFIDENTIAL

Report 10785-F, Phase 11

III, B, Technical Discussion (cont.)

(C) Thermocouples were located in the chamber about 5 in. downstream of the turbine simulator (at depths equal to a quarter radius, a half radius, and a full radius into the chamber) in the same radial plan (TOPC-4, 5, and 6, Figure 13) to determine if any temperature gradient occurs across the chamber. The temperatures at the half-radius and full-radius thermocouples were essentially equal throughout the run. During disassembly of the hardware after the test, it was found that the quarter-radius thermocouple did not protrude into the chamber, and therefore recorded only the temperature of the metal wall.

(U) Some low-frequency perturbations were encountered during this test, as indicated by the pressure traces in Figure 26. It was determined that pack compression was not maintained when the pack was installed into the chamber because of a machining deficiency in the housing and manifold. The loss of pack compression was considered to be the probable cause of the mild low-frequency perturbations observed.

e. Test 1.2-01-AAC-005

(C) This test was performed to demonstrate the performance of the high-throughput catalyst pack at a throughput of 122 psia, corresponding to a 98%  $H_2O_2$ /Alumizine-43 mixture ratio of 1.0. In addition, an attempt was made to correct the pressure-drop variation in the turbine-simulator orifice plate by lengthening the duration of the bypass flow of  $H_2O_2$  from 2.5 to 7.5 sec after actuation of the low-pressure thrust-chamber pressure switch. As mentioned previously, this produced an essentially constant pressure drop (1458 to 1473 psi) through the orifice plate over the entire steady-state period. Therefore, it can be concluded that the turbine simulator requires somewhere between 2.5 to 7.5 sec of preheat to stabilize the orifice size and thereby ensure constant flow and pressure drop.

CONFIDENTIAL

## III, B, Technical Discussion (cont.)

(U) During the test, two periods of low-frequency instability (or chugging) were encountered. The first of these occurred during staging to operating pressure (see Figure 27). The frequency was 45 cps, with peak-to-peak pressure fluctuations of 500 psi in the inlet manifold to the catalyst pack as well as just downstream of the pack. The instability appeared to have originated in the catalyst pack, which displayed an inordinately high pressure drop compared to previous test results (see Traces 2 and 4 in Figure 27). The measured pressure drop at the start of steady-state operation was 550 psi and this leveled off to 300 psi approximately 2 sec later. At this point, a second instability was initiated and continued for the remainder of the test at a frequency of 100 cps. This is discussed in Paragraph 5,c, below.

(U) The high pressure drop through the catalyst pack was caused by the installation of a greater number of screens (which had been added to the pack to improve activity), in combination with recompression of the total pack. Since the final compression was greater than that of a pack with new screens only, this increased compression caused more flow restriction. Pack modifications and composition are discussed in Paragraph 5,a, below.

(C) A throughput of 108 psia was attained over a steady-state period of 5.41 sec. Because of the high pressure drop through the catalyst pack, chamber pressure was only 4145 to 4224 psia and secondary pressure was correspondingly lower, 2681 to 2791 psia. The remaining parameters are summarized in Table II and Figure 27.

5. Test Data Analyses

## a. Catalyst Performance Results

(U) The first three tests utilized the low-throughput catalyst pack shown in Figure 33. This pack was compacted at 4000 psi. The pack showed

CONFIDENTIAL

Report 10785-F, Phase II

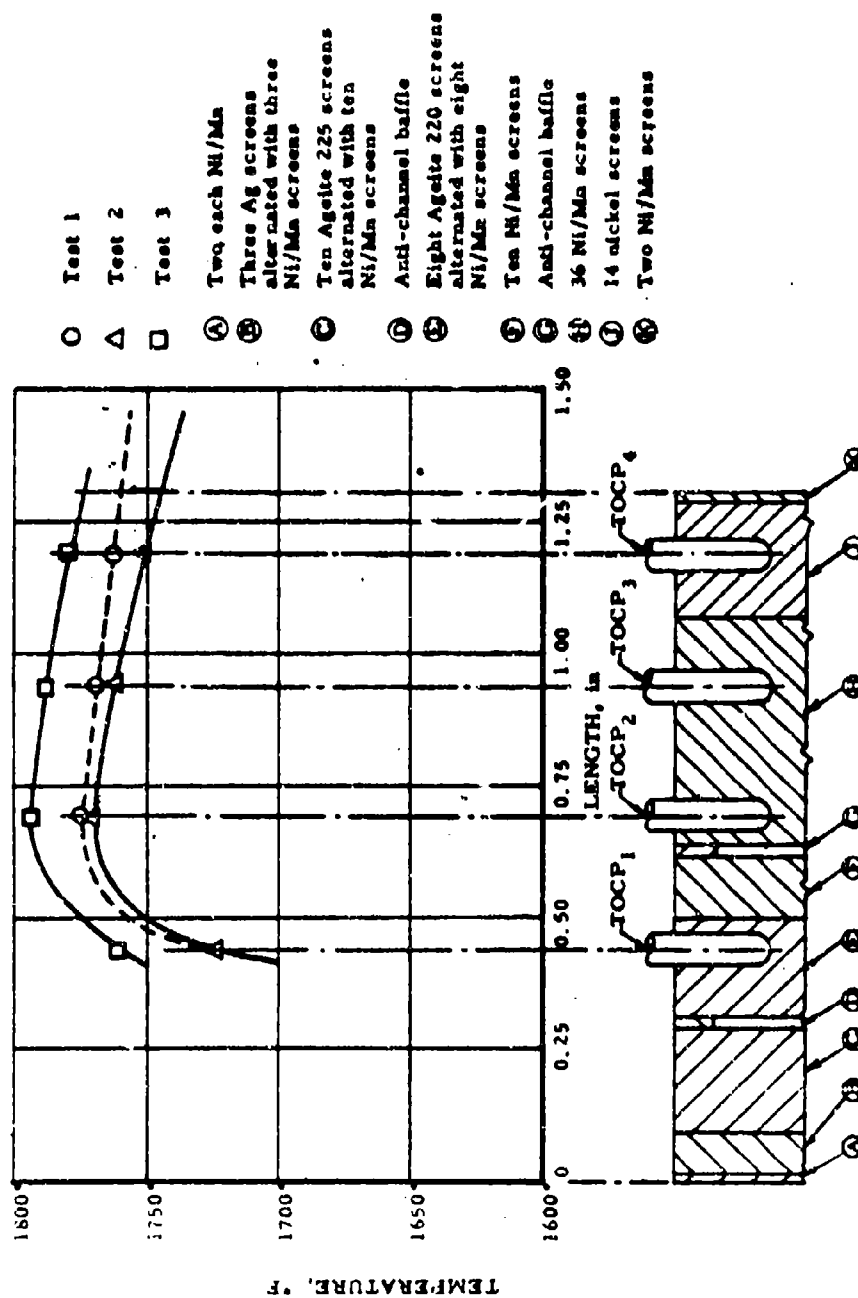


Figure 33. Catalyst-Pack Temperature Profiles--Low Throughput (u)

CONFIDENTIAL

# CONFIDENTIAL

Report 10785-F, Phase II

## III, B, Technical Discussion (cont.)

some drop-off in initiation activity (Table III) but apparently lost none of its operating activity, as indicated by similar decomposition profiles across the pack from test to test. It is possible that the drop-off in initiation activity may have been caused by the presence of residual purge water. (Ten gallons of water were passed through the hardware after testing to remove any residual  $H_2O_2$ .) The water also left a deposit of rust on the chamber wall, on portions of the pack, and on the inlet and outlet plates. Figure 33 also shows the temperature profiles across the pack for the three tests.

(U) The pressure drop through the low-throughput pack was very low and remained nearly constant during operation. This probably was the result of the pack's unique design feature: all active screens, which are relatively soft, were alternated with relatively hard nickel-manganese screens. This lamination apparently prevented any cohesion (or flow) of the soft metal at the high operating temperatures, which would otherwise tend to plug the pack and result in increased pressure drop. Also, the absence of any low-frequency oscillations on the second and third tests indicates that pack compaction and integrity were maintained.

(U) The high-throughput catalyst pack used for Test 004 was constructed as shown in Figure 34. It should be noted that none of the more active Ageite-225 screens, which were used in the low-throughput catalyst pack, were used in this pack. These screens were unavailable when the test was prepared.

(U) The pack performed satisfactorily with the low starting flow, and a temperature profile was established with the maximum at Thermocouple 4. However, as flow and pressure were increased, temperature at the first three thermocouple locations in the pack declined. This continued over the balance of the steady-state period, as shown in Figure 34. It was

Page 80

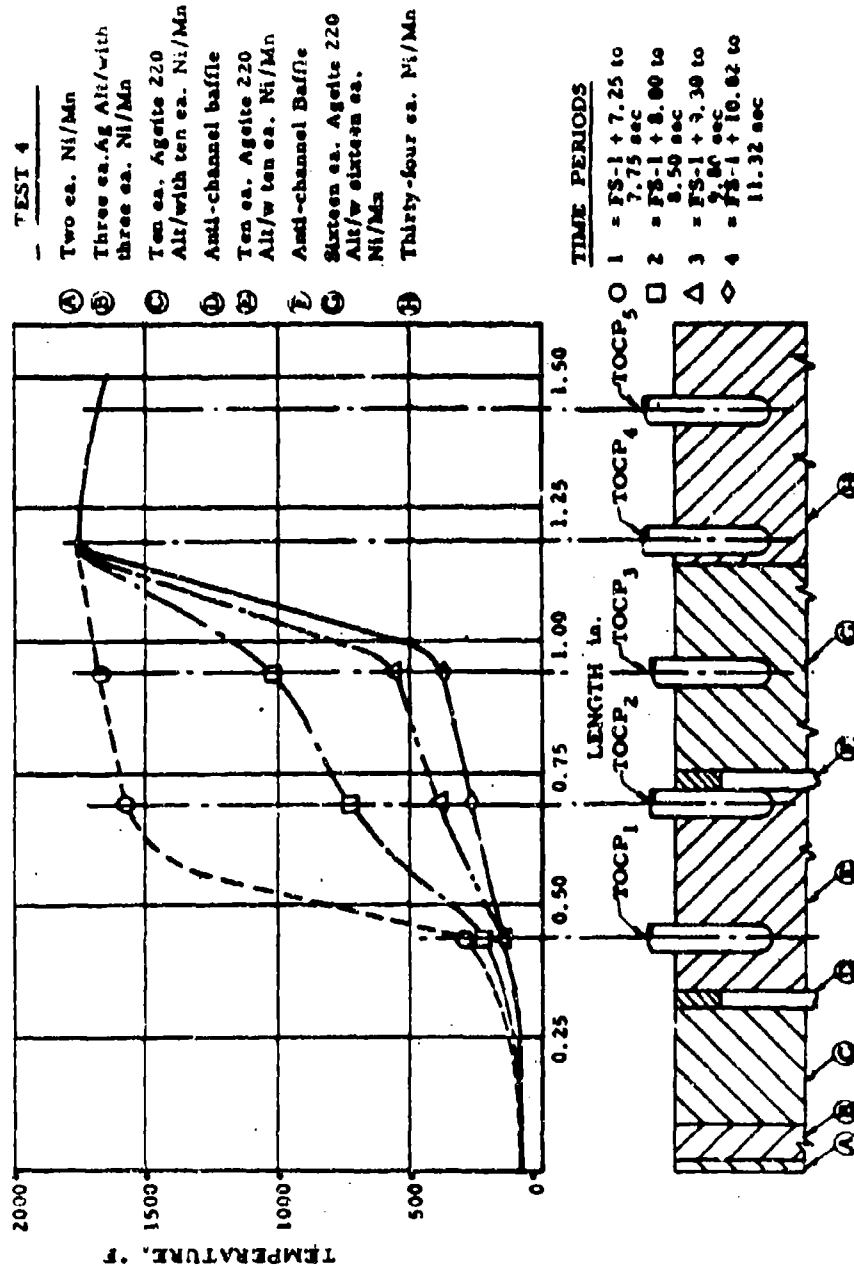
CONFIDENTIAL

(This Page is Unclassified)



CONFIDENTIAL

Report 10785-F, Phase II



Page 81

CONFIDENTIAL

Figure 34. Catalyst-Pack Temperature Profiles--High Throughput, SN 001 (u)

## III, 8, Technical Discussion (cont.)

believed that had the more active Ageite-225 screens been present the changes in temperature profile during the steady-state period of this test could have been avoided.

(U) Because of the decomposition-temperature drop in the active portion of the pack (as opposed to the experience with the low-throughput pack), it was decided to add five Ageite-225 screens, which were reported by FMC to be more active than Ageite-220. Two more Ageite-220 screens were also added, bringing the total number of active screens to 46 compared with 39 on Test 004 (see Figure 35).

(U) The new screens together with the used pack were recompressed. In addition, a bolt torque in excess of that used on previous assemblies was required to install the pack in the chamber.<sup>(12)</sup> Consequently, the increased bolt torque together with the precompressed condition of the pack caused excessive pack compression and resulted in an increase in the pack-pressure drop; the maximum temperature station shifted to Thermocouple 3.

## b. Catalyst Performance Analysis

(U) Decomposition of  $H_2O_2$  in a catalyst pack is initiated at the pack entrance and progresses to completion as a function of throughput, pressure drop, static pressure, and catalyst depth.

(U) The location of complete decomposition can be predicted in terms of catalyst length as shown in Equation 1,

$$L_2 = L_1 \left( \frac{TP_2}{TP_1} \right) \left( \frac{P_1}{P_2} \right) \quad (\text{Eq 1})$$

(12) Note: For Test 004, the compression of the pack in the chamber was less than 3000 psi because of an error in machining the seal-gland surfaces.

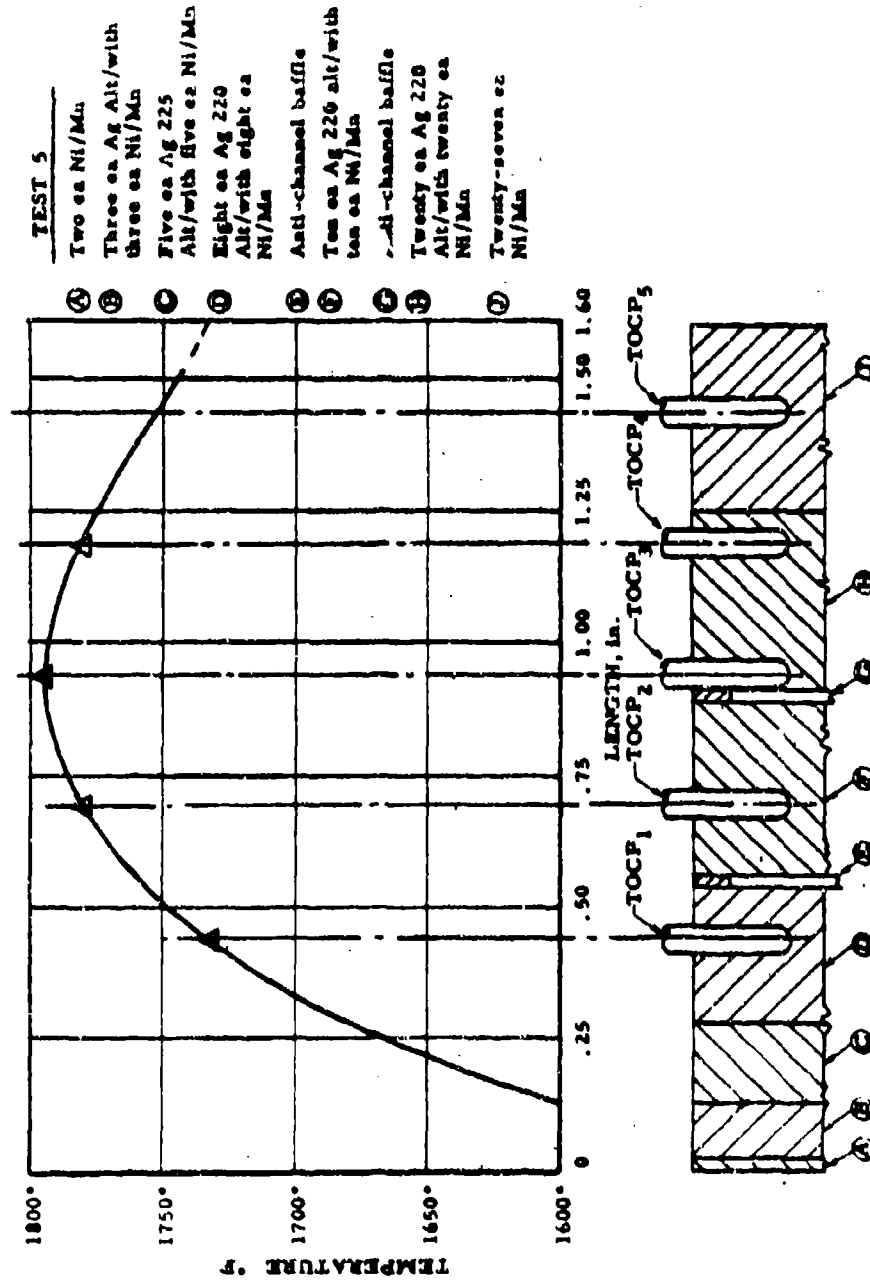


Figure 35. Catalyst-Pack Temperature Profiles--High Throughput, SM 002 (u)

## III, B, Technical Discussion (cont.)

where  $L$  refers to the distance from the pack entrance to the location of maximum gas temperature,  $TP$  is the throughput in psim,  $P$  is the chamber pressure in psia, and subscripts 1 and 2 refer to two different operating conditions. Other factors, such as pack compression, can modify the result of Equation 1, as described below.

(U) It is interesting to compare the observed increase in  $L$  during the test series, through the use of the relationship (Equation 1) developed during Phase I of the program (Ref. 1). Complete decomposition occurred between 0.5 and 0.7 in. (Figure 33) in Tests 001, 002, and 003. Decomposition in Test 004 was complete between 1.0 and 1.2 in. (Figure 34), and in Test 005, decomposition was complete between 0.75 and 0.9 in. (Figure 35). The exact point of complete decomposition is not known. Therefore, because Equation 1 is only an approximation, the location of the thermocouple reading maximum temperature was chosen as the point of complete decomposition for the calculation. Using the data from Tests 002 and 004, the predicted  $L$  for Test 004 is calculated to be 1.24 in., where  $L$  is in good agreement with that found experimentally. However, the predicted length for Test 005 was 3.8 in. and is in considerable error from that found experimentally. The following table gives the experimental data used in the calculations:

(C)	Test No.	$TP$ , psim	$P_c$ , psia	$\Delta P_{cp}$ , psi	$L$ , in.
	001	48.7	4426	32	0.7
	002	58.9	4534	34	0.7
	003	59.4	4454	27	0.7
	004	82.1	4400	52	1.2
	005	108.0	4209	298	0.9

## III, B, Technical Discussion (cont.)

(U) Two probable explanations for the discrepancy in Test 005 can be found by again reviewing the results obtained in the subscale catalyst program of Phase I: (1) When the length of the subscale catalyst was less or equal to 1.2 in., the pack-pressure drop was essentially constant between 30 and 70 psia; however, when the catalyst was longer or equal to 1.5 in., the pressure drop was 200 to 500 psi. This indicates a discontinuity in the relationship between catalyst length and pressure drop, that is, a catalyst pack can be too long. (2) When the subscale catalyst pack was recompressed after use, the "effective" compaction of the screens was much greater than intended, because of the softening of the screens with use. For example, a 3.1-in.-long pack decreased in length by 0.44 in. (14%) after one firing and after recompression to 4000 psi. The pressure drop of the catalyst increased twofold in this case.

(U) The similarity between the subscale tests and Test 004 lies in the fact that additional screens were added in Test 005 to lengthen the pack and that the used screens had been recompressed. Before Test 005 the screens were compressed to about 4000 psi. However, the effective compaction of the used screens, as indicated by subscale test results, was much higher. A definite discontinuity therefore existed in the catalyst bed of Test 005. The seven new catalyst screens upstream in the bed were at 4000-psi compaction, whereas the remaining 39 screens were at a much higher effective compaction. The resistance to flow of liquid and gas through the pack thus increased in the initial portion of the catalyst, possibly aiding in the chugging observed.

(U) The high pressure drop in Test 005 can, therefore, be explained by one or both of the following factors: (1) excessive number of catalyst screens, and/or (2) high pack compression. The inconsistency in the length calculations is thus explained as a result of excessive changes in pack geometry and does not reflect upon the validity of the equation.

## III, B, Technical Discussion (cont.)

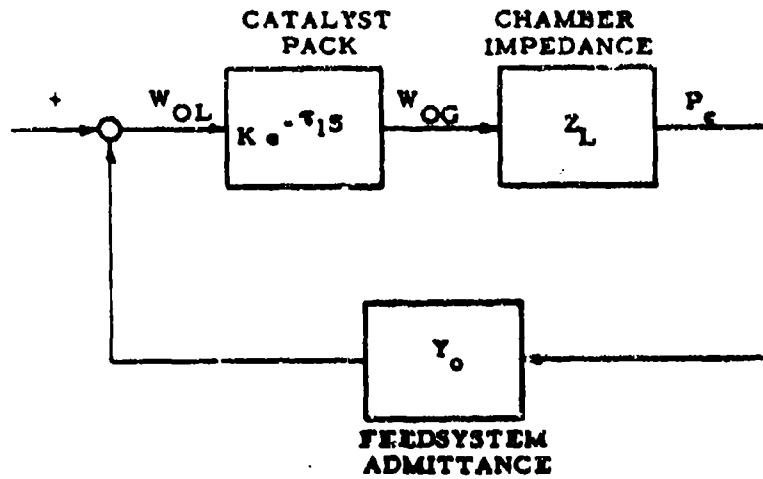
## c. Preburner Test Combustion Instability

(U) An analysis was conducted to investigate the cause of a low-frequency instability which occurred during Test 1.2-01-AAC-005. An examination of the oscillograph records indicated that the instability was coupled to the decomposition process and to the feed system. During starting at low flow and low chamber pressure, the observed instability frequency was 45 to 55 cps. After the main thrust chamber valve was opened and a higher steady-state chamber pressure was achieved, the frequency increased to 100 cps. The source of system excitation appeared to be located in or near the catalyst pack where both parameters POJ-PB and POCF-7, located on the upstream and downstream end of the pack, respectively, showed the highest amplitudes of oscillation. Both POJ-PB and POCF-7 were in-phase and led the other monitored feed-system pressures (POPC-2, POPC-8, POPN-3, POTCV, and POT) during the 100-cps oscillation. (See Figure 13 for parameter locations.)

(U) To gain some insight into the problem, a simplified analysis was performed assuming a low-frequency combustion stability model for the preburner. As shown in Figure 36,  $Z_L$  represents the distributed-parameter impedance properties of the chamber and nozzle just downstream of the catalyst pack and  $Y_0$  represents the distributed-parameter admittance properties of the feed-system upstream of the catalyst pack. The unknown block in the loop is assumed to be a catalyst-pack reaction gain and an associated transport time. The chamber impedance,  $Z_L$ , and the feed-system admittance,  $Y_0$ , were then evaluated at the observed instability frequency of 100 cps. The gain and the phase of the product  $Z_L Y_0$  were then obtained. The additional open-loop gain and the phase lag necessary to make the system unstable were assumed to be provided by the catalyst-pack reaction process, which is assumed to have the form  $Ke^{-T_1 S}$ . In this case,  $K$  is the gain,  $S$  is the Laplacian variable, and  $T_1$  is the transport-time delay required to yield a particular phase lag at

# UNCLASSIFIED

Report 10785-F, Phase II



ASSUMED SYSTEM BLOCK DIAGRAM

$$Z_L = 3.32 \cdot 10^{-3} / 93.3^\circ \quad \text{at 100 cps}$$

$$Y_o = 4.55 / -87.4^\circ$$

PARAMETER	LOCATION
PoT = 4790 psia	TANK PRESSURE
POJPB = 4470 psia	UPSTREAM OF CATALYST PACK
POCP7 = 4230 psia	DOWNSTREAM OF CATALYST PACK
POPC2 = 2760 psia	DOWNSTREAM OF TURBINE ORIFICE
$\dot{W}_T = 30 \text{ lb/sec}$	

Figure 56. Combustion Dynamics Parameters

UNCLASSIFIED

# UNCLASSIFIED

Report 10785-F, Phase II

## III, B, Technical Discussion (cont.)

100 cps. The product  $Z_L Y_0$  was found to be  $(1/66.2) / 5.9^\circ$ , and thus the necessary gain,  $K$ , is 66.2 at 100 cps. Because the phase lag must be  $-180^\circ$ , the necessary phase shift is  $-185.9^\circ$ . The transport-time delay,  $\tau_1$ , corresponding to  $-185.9^\circ$  at 100 cps, can be computed from the ratio of the phase (in radians) to the observed frequency (in radians/second). This results in a value for  $\tau_1$  of  $5.15 \times 10^{-3}$  sec, which is not unreasonable since this corresponds roughly to the time required for the  $H_2O_2$  to traverse the catalyst pack at the observed steady-state flow rate.

(U) From the preceding calculations it is concluded that preburner chugging may be attributed to a mechanism similar to that which sustains low-frequency instability in conventional bipropellant engines. The necessary amplification of pressure perturbations may be a result of the decomposition process, whereas the transport-time delay was probably caused by phase-shifting. A brief literature search disclosed little about the dynamic behavior of decomposition in a catalytic pack. Further investigations into the dynamic response of catalytic reactions will therefore be required before the above concepts can be applied in a stability analysis. In general, however, increasing the chamber volume or increasing the feed system pressure drop would be helpful in reducing the probability of low-frequency instability.

UNCLASSIFIED



## SECTION IV

## STAGED-COMBUSTION EVALUATION

## A. PROGRAM OBJECTIVES AND APPROACH

(U) The principal objective of the staged-combustion portion of the program was to demonstrate (at 20,000 lbf thrust) the feasibility of the staged combustion of 98%  $H_2O_2$  and Alumizine-43 at a chamber pressure of 3000 psi. Secondary objectives included evaluation of two injector concepts, realization of at least 87% of theoretical specific impulse (this was a program goal), the gathering of transient-heat-flux data in critical combustion chamber areas, and comparison of performance at two characteristic chamber lengths, 40-in.  $L^*$  and 70-in.  $L^*$ . Late in the program, when it became evident that the scope of testing could be enlarged, an additional objective, the demonstration of the combustion of 90%  $H_2O_2$  with Alumizine-43, was also undertaken.

(U) Uncooled hardware was designed and fabricated for the staged-combustion evaluation because only short-duration (1 to 2 sec) tests were planned. This permitted the construction of rugged and dependable hardware. Ablative materials were used in the chamber section, in the entry section to the throat, and in the exit cone. The solid and segmented throat as well as the heat-flux transducer rings were made from silver-infiltrated tungsten.

(U) It was the intent of the program to evaluate propellant combustion performance and heat-flux characteristics, not hardware or materials. Therefore, materials selection was limited to those materials which had a proven history of service in similar metal-bearing and high-pressure combustion environments.

## IV, A, Program Objectives and Approach (cont.)

(U) However, when it became apparent, through theoretical investigation of the effect of mixture ratio upon performance, that higher MR's might cause excessive tungsten erosion, this phenomenon was thoroughly investigated. The investigation showed that the thrust chamber could be operated safely up to an MR = 1.0 without significant erosion of tungsten. The performance investigation showed higher performance was favored by mixture ratios in excess of the theoretical optimum, 0.5. These two investigations are discussed in the following section.

(U) Three injector configurations were designed, and two were subsequently selected for fabrication and evaluation. Each of the three concepts employed widely diverse injection modes that were evolved from previous metalized propellant and high-pressure staged-combustion programs conducted at Aerojet-General Corporation.

(U) Performance data derived from the tests (digitized by an analog-to-digital computer program, ADC) were compared to theoretical performance values ( $I_g$ ,  $c^*$ ,  $C_F$ ) by an Aerojet performance comparator program. These values were then further analyzed by the interaction theory method to identify the principal losses attributed to such parameters as friction, geometry, heat, energy release, mixture-ratio distribution, kinetics, gas particle flow, and mass distribution.

(U) Temperature data derived from the heat-flux transducers were also analyzed to identify the heat flux at critical locations in the chamber and nozzle.

## IV, Staged-Combustion Evaluation (cont.)

## B. TECHNICAL DISCUSSION

1. Hardware (Secondary Combustor)

(U) The same philosophy of design as that used for the preburner governed the design of the secondary combustor components. The same seals, bolts, bolt hole circles, etc., were used as much as possible to maintain a maximum in flexibility and interchangeability and to reduce the expense of procurement and fabrication to a minimum. The Conoseal joints used on the preburner were not necessary on the secondary combustor, since the secondary combustor operated at 3000 psia or less. O-ring joints were found to be satisfactory and resulted in a significant savings in seal cost.

(U) The hardware designed and fabricated during this portion of the program included injectors, steel housings and ablative liners for the chamber, throat entry section and exit cone, tungsten throats, and tungsten heat-flux transducers.

(U) Thrust chamber assembly design parameters are presented in Table IV.

a. Injector Design

(U) Three basic injector configurations were designed. Each design was unique within itself and embodied design features that were evolved from previous staged-combustion and Improved Titan technology (Ref. 7). Two designs were selected for evaluation during Phase II. The vane-type injector was the primary selection and the tubular injector the secondary selection. The multi-nozzle injector was a backup design.

TABLE IV

## 20,000-LBF STAGED-COMBUSTION ENGINE DESIGN PARAMETERS

 $H_2O_2$ /Alumizine-43

<u>Parameter</u>	<u>Symbol</u>	<u>Unit</u>	<u>Value</u>
Thrust	F	lb	20,000
Specific impulse	$I_s$	sec	302.8
Efficiency, specific impulse	$\eta_{Is}$	%	94
Weight flow total	$\dot{W}_T$	lb/sec	66.05
Mixture ratio	MR	---	0.5
Total oxidizer flow	$\dot{W}_o$	lb/sec	22.02
Total fuel flow	$\dot{W}_f$	lb/sec	44.03
Secondary chamber pressure	$P_{sc}$	psia	3000
Characteristic velocity	$c^*$	ft/sec	5755
Efficiency, combustion	$\eta_c$	%	96
Efficiency, nozzle	$\eta_{noz}$	%	98
Pressure ratio	$P_c/P_o$	---	65
Area ratio	---	---	10
Area, throat	$A_c$	in. <sup>2</sup>	3.94
Diameter, throat	$D_c$	in.	2.24
Thrust coefficient	$C_f$	---	1.69

UNCLASSIFIED

## 14. B, Technical Discussion (cont.)

(U) The injector housings were designed to permit the insertion of any number of injector configurations into the housing with a minimum of modification. The fuel manifold was designed to be removable to permit inspection after firings and to allow removal of any residual Alumizine deposits. Details of this arrangement are shown in Figure 37.

The injector fuel circuits were hydraulically calibrated with water to determine their flow coefficients. The relationship used was:

$$K_W = \frac{\dot{W}}{Sp.G \times \Delta P} \quad (Eq. 2)$$

where

$K_W$  = flow coefficient

$\Delta P$  = pressure drop, psi

SpG = specific gravity

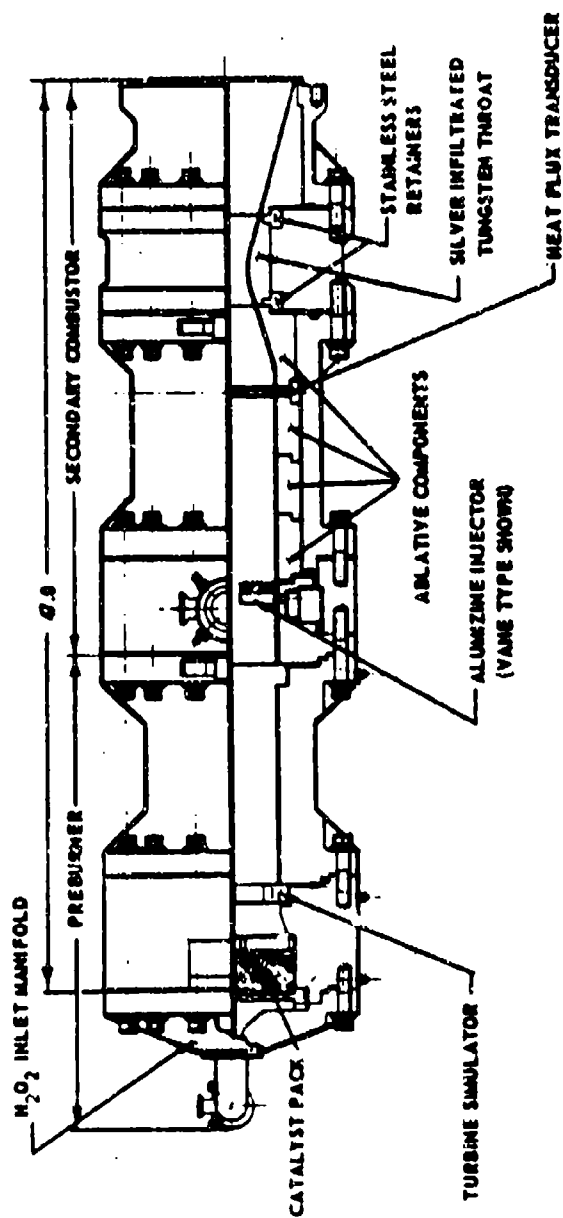
$\dot{W}$  = weight flow rate, lbm/sec

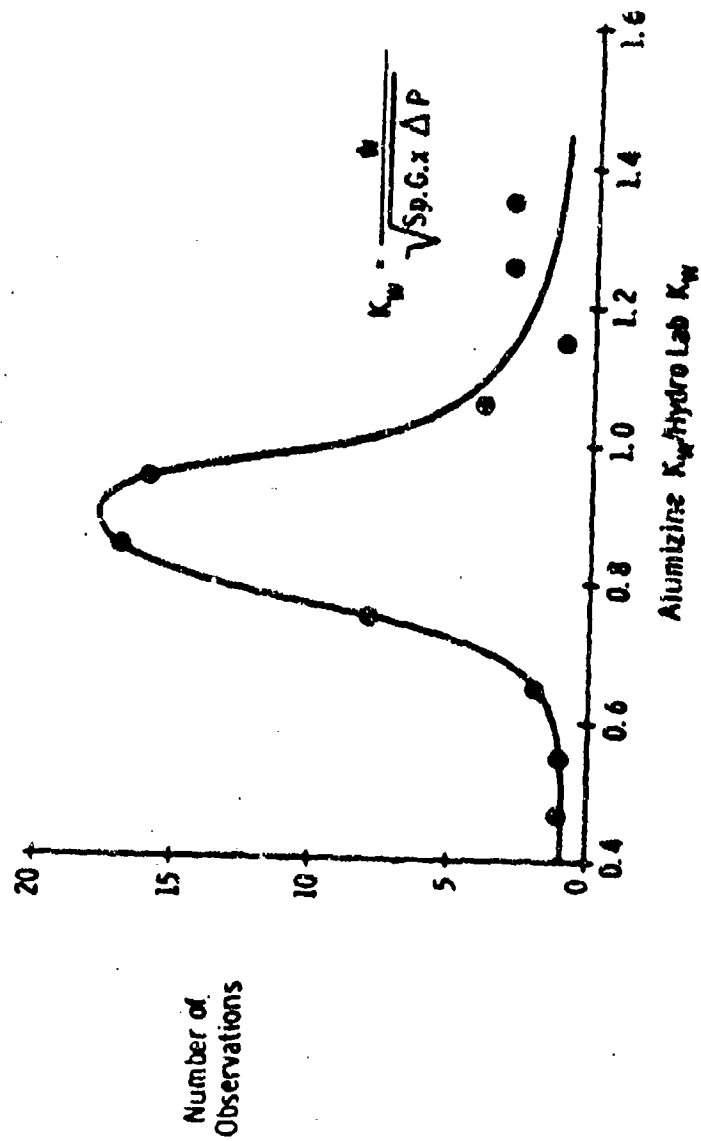
The  $K_W$  flow coefficient was then modified by multiplying by 0.9 to conform to results that were statistically determined for use with Alumizine during the Improved Titan Program (Ref. 7). These results are presented in Figure 38.

#### (1) Tubular Injector

(U) The tubular injector consisted of 44 constant-diameter tubes through which Alumizine was axially introduced into the combustion chamber. Each tube entered the chamber perpendicularly to the chamber axis and then turned 90° to form the desired axial pattern. The injector is shown in Figure 39.

(U) Fuel velocity through each tube was 60 ft/sec; this increased to 125 ft/sec at the injector face by using predrilled orifice plugs inserted in the tube ends. The total pressure drop was about 400 psi; thus the injector was adequately decoupled from the fuel feed system.

Figure 37. H<sub>2</sub>O<sub>2</sub>/Alumizine-43 Staged-Combustion TCA

Figure 38. Comparison of Alumazine-43  $K_v$  with Hydro Lab  $K_v$

UNCLASSIFIED

Report 10785-F, Phase II

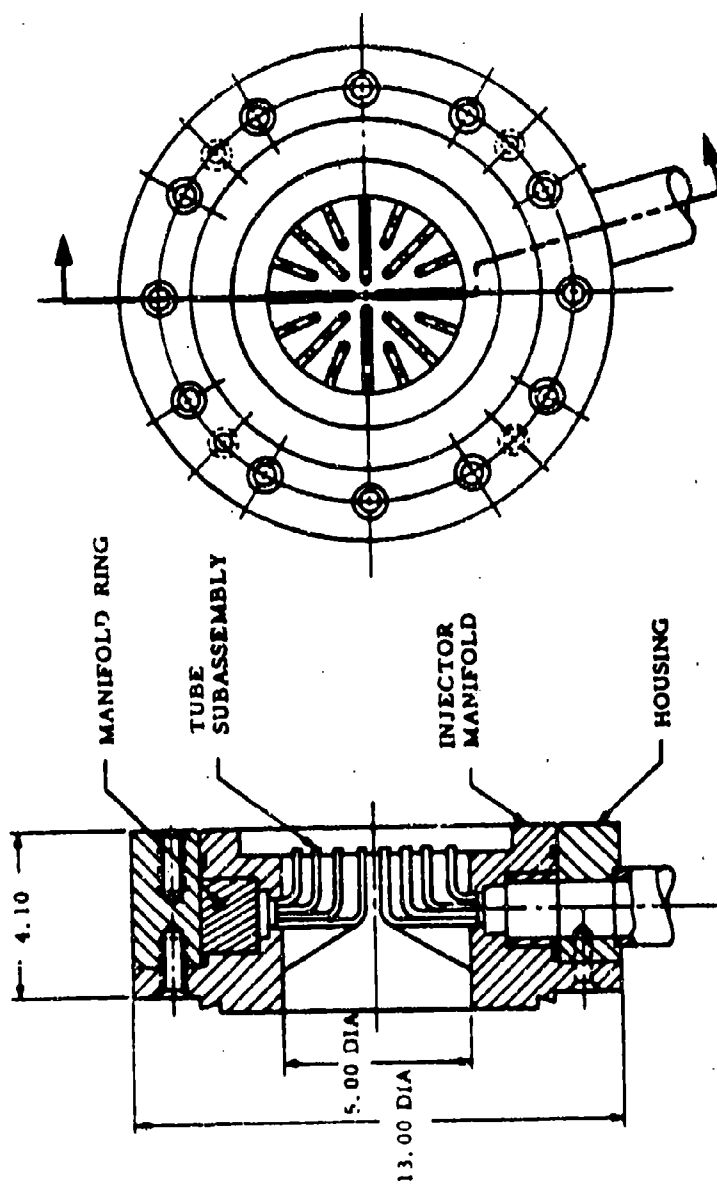


Figure 39. Tubular Injector

Page 10

UNCLASSIFIED



## IV, B, Technical Discussion (cont.)

(U) The fuel tubes were supported and attached to the outer structure to minimize thermal stresses during firing. These supports also protected the tubes from direct oxidizer impingement and resulting heating. As shown in Figure 39, the fuel tubes and their support structure offered low blockage to gaseous oxidizer flow. The flow area was 58.6% of the total available area.

(U) Mixture-ratio distribution across the face of this injector was designed to be uniform at an oxidizer-to-fuel weight flow ratio of 0.5.

## (2) Multi-Nozzle Injector

(U) The second injector design, a multi-nozzle concept, is shown in Figure 40. The basic philosophy, which influenced the selection of this concept, was to provide a high-velocity low-pressure-drop oxidizer circuit to obtain decoupling of the secondary combustor from the preburner. The face includes a convergent entrance section and a divergent exit section. The gas velocity increases from 47 to 760 ft/sec through the throat of the gas injection nozzles. Pressure recovery was anticipated to be 97% at injection because of favorable entry and exit conditions.

(U) The fuel side is decoupled by the pressure drop across the injector orifices. At the design fuel flow rate of 44 lb/sec, this pressure drop was calculated to be 400 psi. The fuel manifold velocity was estimated at 60 ft/sec. The fuel is manifolded by cross-drilling from the periphery. The fuel is injected in showerhead fashion through tubes extending 0.25 in. from the trailing edge of the gas nozzles. Four tubes are located around each oxidizer-injection nozzle.

UNCLASSIFIED

Report 10733-F, Phase II

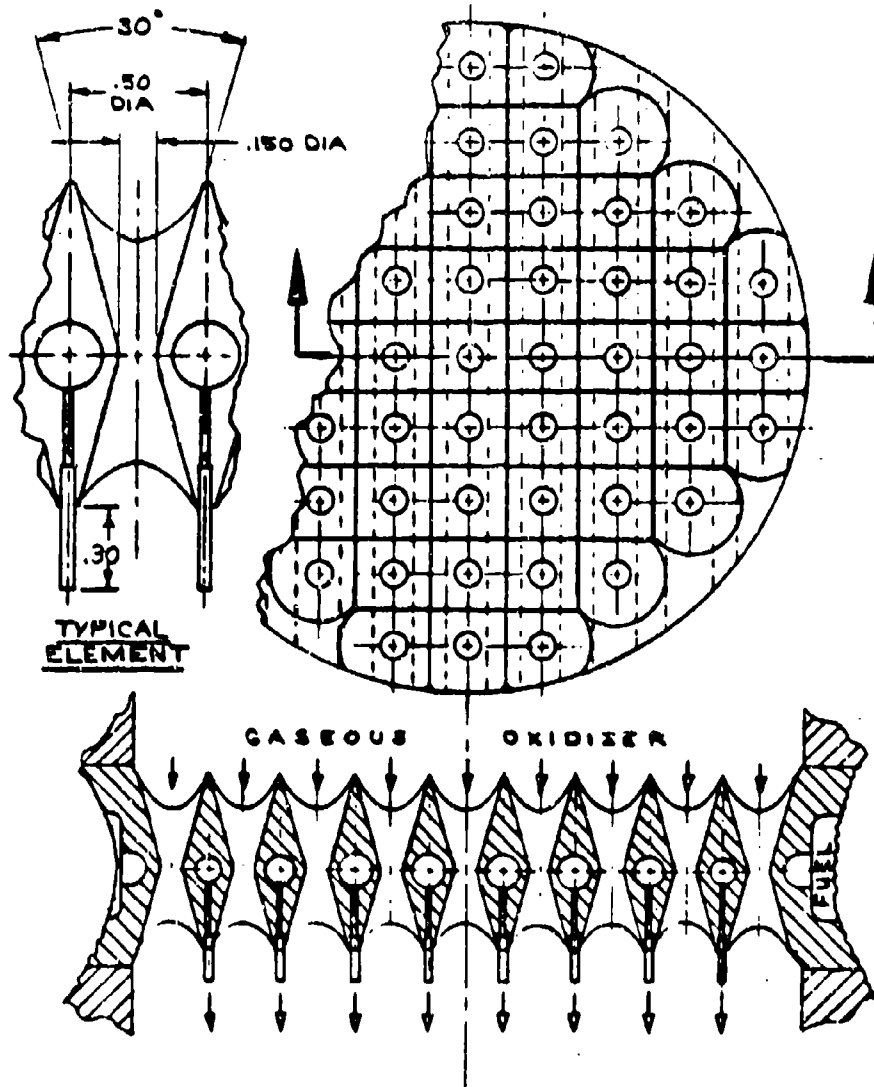


Figure 40, Multinozzle Injector

Page 93

UNCLASSIFIED

## 1.3, Technical Discussion (cont.)

(U) The cross section may appear to be quite complex for design and manufacturing. However, fabrication may easily be accomplished by conical milling of the nozzles. The overlap of adjacent cuts forms the configuration. The structure should not present any thermal-shock or thermal-expansion problems because of its geometric shape. Also, the structure is cooled by the fuel flow.

## (3) Vane-Type Injector

(U) A vane-type injector similar to that tested in another staged-combustion program was designed. This injector design was the primary configuration for Phase-II staged-combustion testing. The injector, shown in Figures 41 and 42, consisted of 36 cantilevered vanes with 11 small Alumizine-43 injection tubes located on the trailing edge of each vane. This gave a total of 396 Alumizine injection tubes. The vanes were sized and spaced carefully to obtain an open area of 33 to 40% through which the oxidizer flows. The actual calculated open area obtained was a nominal 36.5%. Oxidizer velocity through this area at 1750°F and 3000 psia was calculated to be about 150 ft/sec.

(U) The mixture ratio across the face of the injector, as originally designed, was constant. This was accomplished by first dividing the area across the injection plane into ten equal concentric areas. These areas were further divided geometrically into subareas. Fuel was distributed by orienting fuel tubes to the center of each geometric subarea. The tubes were, in turn, sized according to the percent of area at each respective location and bent where necessary to reach the geometric center.

(U) The vanes were produced from castings made of Type 347 stainless steel.

UNCLASSIFIED

Report 10735-F, Phase II

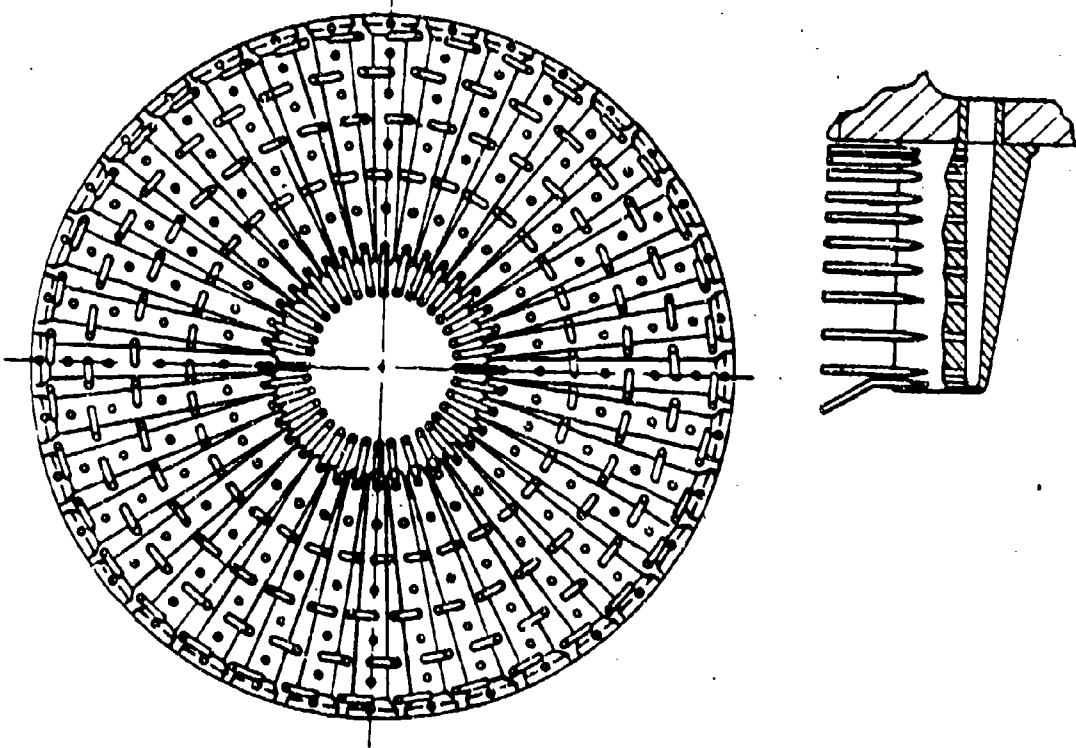


Figure 41. Valve-Type Injector--Mod I

Page 100

UNCLASSIFIED



# 2025-2026 Budget Request

UNCLASSIFIED

## IV. B. Technical Discussion (cont.)

(U) During hydraulic calibration of this injector, it was discovered that the fuel circuit had an excessively high pressure drop. The high L/D of the tubes had resulted in pressure drop that had not been considered during design. The pressure drop at the design flow rate of 44 lbm/sec, corresponding to a mixture ratio of 0.5, would have been 956 psi. To lower the pressure drop to a more acceptable value<sup>(13)</sup> about half the tubing length was removed by electrical discharge milling (Eloxing). This reduced the anticipated pressure drop for the above stated flow conditions to 735 psi, not as low as was desired, but acceptable. Thermochemical calculations and performance analysis conducted indicated the desirability of operating at a mixture ratio of 0.7 which would bring the pressure drop down further to 581 psi. This modified injector could thus be used with system pressure limitations and the available operating pressure.

(U) The pattern was compromised by the reduction in tube length as shown in Figure 43. Therefore, it was decided to use this injector only in the injector concept screening tests and initiate redesign to realize better distribution at a reduced pressure drop on later tests. Therefore, two modified designs were developed, subsequently called Mod II and Mod III to differentiate these injectors from the original injector, Mod I. The three designs are compared in Table V.

(U) The Mod II injector used surplus drilled vanes from the fabrication of the Mod I injector. The size of the innermost seven tubes was increased. This reduced pressure drop at a mixture ratio of 0.5 to 417 psi. However, mixture-ratio distribution in such a Mod II injector suffered accordingly.

(13) Note: On the fuel side, the maximum possible system feed pressure is 3600 psi because of tubing pressure capacity limitations.

UNCLASSIFIED

CONFIDENTIAL

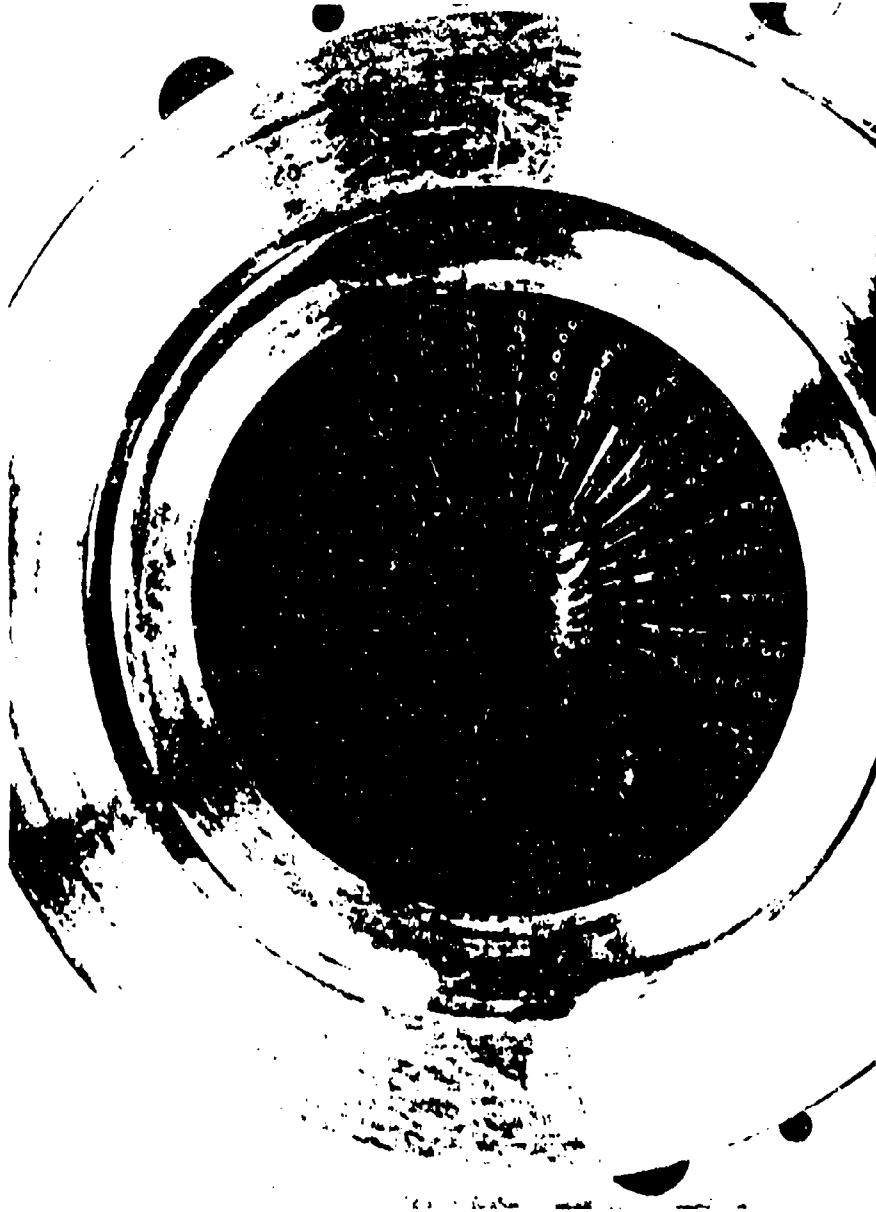


Figure 3. M-1 Valve Type Injector--after Modification

CONFIDENTIAL

TABLE V  
COMPARISON OF VANE-TYPE INJECTOR DESIGNS (u)

	Injector						
	Mod-I		Mod-II			Mod-III	
Number of tubes per vane	2	9	2	2	7	2	9
Outer diameter, in.	0.049	0.063	0.049	0.063	0.072	0.038	0.072
Wall thickness, in.	0.008	0.010	0.008	0.010	0.009	0.009	0.009
Distance from centerline of vane core to end of tubes, in.	1.20		0.90			0.90	
Injection angle, degrees	30		45			45	
Area of tubes, in. <sup>2</sup>	0.592		0.792			0.808	
ΔP at MR of 0.5, psi	738		417			400	
ΔP at MR of 1.00, psi	252		187			184	
Injection velocity, ft/sec	125		93.8			92.0	



## IV, B, Technical Discussion (cont.)

(U) The Mod III injector was designed to produce an even mixture-ratio distribution across the face and a reduction in pressure drop. The vane drill pattern was changed to permit tubes of larger diameter across the entire trailing edge of the vanes. The pressure drop through this model was 400 psi at a mixture ratio of 0.5. The injection angle was increased to 45° to shorten the tubes (which increases rigidity) and to reduce the L/D effect on pressure drop while keeping injection velocity reasonably high.

## b. Secondary Combustion Chamber and Nozzle

(U) Since the firing duration was short (2 to 3 sec), an uncooled approach was taken to the design of the secondary combustion chamber and nozzles. The assembly consisted of a series of three cylindrical steel vessels, stressed to at least a safety factor of 3:1. The vessels were lined with compression-molded silica-reinforced phenolic in the chamber and throat entry section, silver-infiltrated tungsten in the throat, and silica phenolic again in the exit cone (Figure 37).

(U) The 15° half-angle exit cone provided a maximum area ratio of 10:1. Analysis indicated that for this propellant combination, an area ratio in excess of 8:1 would produce good data.

(U) Two chamber sizes, 70 and 40 in. L\*, were designed. The 70 L\* chamber was the baseline size for this program and was selected on the basis of test results from ICP, HIF<sub>c</sub>, and the Improved Titan programs conducted at Aerojet-General. Improved Titan results at the 15,000-lbf-thrust level showed high-performance at an L\* of about 100 in., demonstrating that no more L\* than 100 in. is required with N<sub>2</sub>O<sub>4</sub>/Alumizine-43. Correlation of

## IV, B, Technical Discussion (cont.)

these and other  $H_{f,c}$  results indicated that the  $L^*$  required for efficient gas-liquid combustion was at least 30% less than that required for liquid-liquid combustion. Therefore, since the combustion mechanism is approximately the same for  $H_2O_2$ /Alumizine as for  $N_2O_4$ /Alumizine, a baseline  $L^*$  of 70 in. was selected. The purpose of designing and fabricating the 40  $L^*$  chambers was to determine the effect of  $L^*$  variation upon performance.

(U) A portion of the chambers and throats were also equipped with heat-flux transducers (Figure 44). The size of these rings was determined from heat-flux measurement requirements, and the thickness of the ablative-chamber wall was correspondingly adjusted. All of the rings were fabricated from silver-infiltrated tungsten. The location of each ring is shown in Figure 45.

(U) A secondary-combustor heat-flux-transducer study was conducted to size the rings and to estimate the temperature profiles that would be expected. These rings, which have a "T" cross section (Figure 44), have chromel-alumel thermocouples installed at precise depths from the inner surface exposed to the combustion gas. The resultant temperature/time curves are used to determine the boundary-layer transient and steady-state heat-flux rate from the gas to the walls.

(U) In the heat-transfer analysis, the temperatures predicted for the heat-transfer rings were calculated assuming a two-dimensional model of constant thermophysical properties. The method of calculation was based upon a finite difference method derived from the basic G. Duminbarre transient-conduction scheme. This method is in computer program form and is referred to as Aerojet's Thermal Analyzer Program (No. 278). Boundary conditions at the exposed hot-gas surface were predicted from the Dittus-Boelter correlation. Propellant combustion efficiencies of 80 and 95%,

Donnerstag, 10. April 1941, 10.00 Uhr

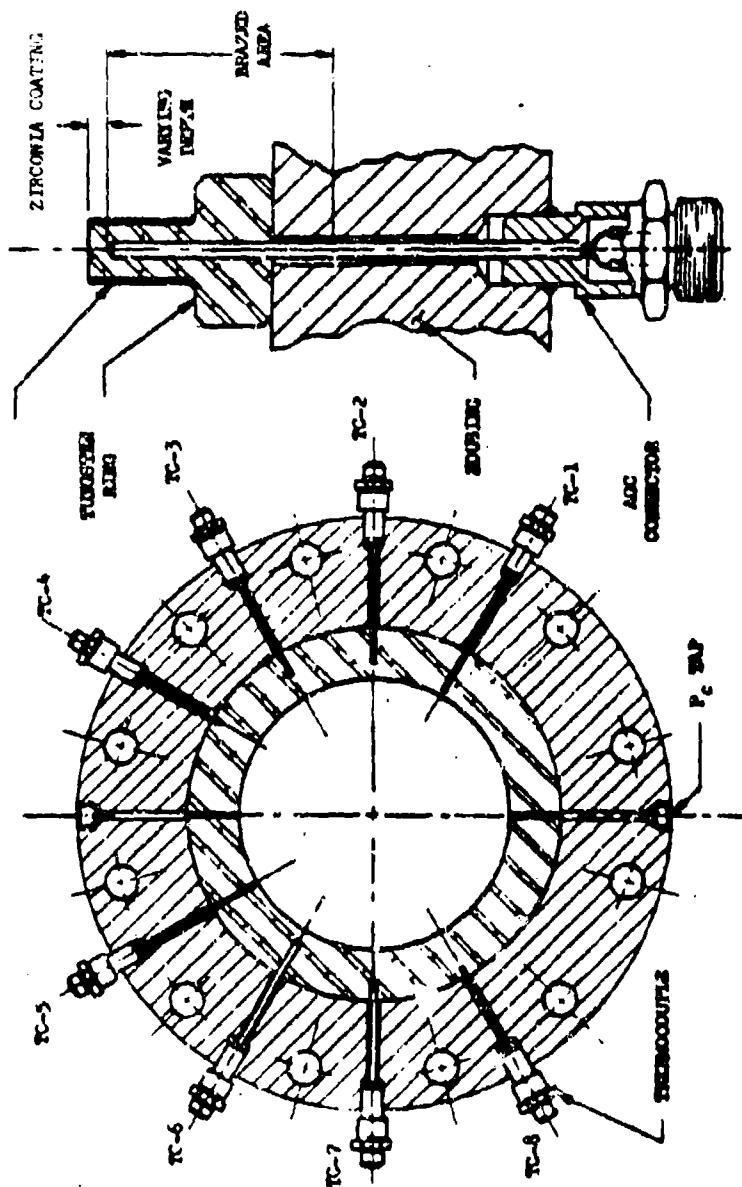


**Figure 44. Heat-Flux Transducer Installation**

**UNCLASSIFIED**

UNCLASSIFIED

FIGURE 45-2, PHASE IV

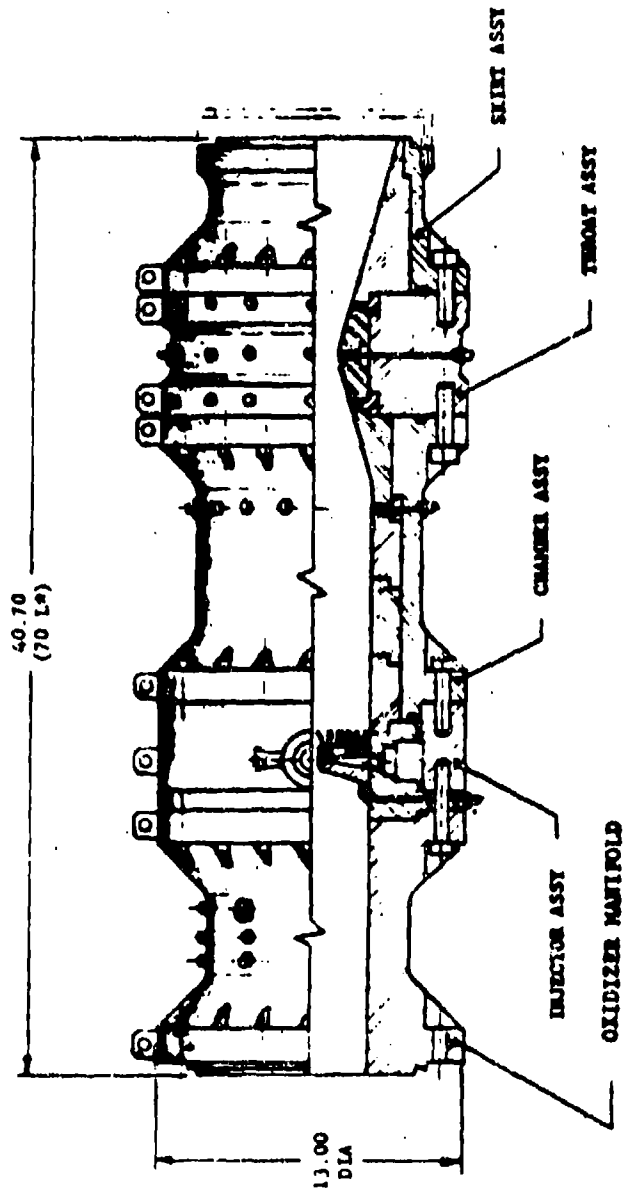


Figure 45. Secondary Combustor

UNCLASSIFIED

# UNCLASSIFIED

Report 10785-F, Phase II

## IV, B, Technical Discussion (cont.)

demonstrating gas temperatures of 4633 and 5588°F, respectively, were considered in the analysis. Results of this analysis are shown graphically in Figures 46 and 47. These curves show typical expected temperature rise rates for two locations in the combustion chamber.

(U) Ablative-material selection was based upon past experience with these materials in high-pressure and  $Al_2O_3$ -bearing combustion environments and upon recommendations by knowledgeable vendors and Aerojet material specialists. A building block approach to the insertion of the ablative liners into the chambers was taken, as shown in Figure 45. Bonding and sealing was accomplished with RTV-60,<sup>(14)</sup> a room temperature curing silicone rubber. The materials used included the following:

(1) "Astroquartz" (J. P. Stevens Co., New York, N. Y.) impregnated with SC-1008 phenolic (Monsanto Chemical Co., St. Louis, Mo.)

(2) MX-2600, a phenolic-impregnated high silica fabric (Fiberite Corp., Winona, Minnesota)

(3) MXO-83, a phenolic-impregnated silica-rayon fabric (Fiberite Corp., Winona, Minnesota)

(4) WBC-2230, silica phenolic high-strength char (Western Dacking Corp., Culver City, Calif.)

---

(14) RTV-60, a product of the General-Electric Co., Waterford, New York

# UNCLASSIFIED

UNCLASSIFIED

Report 10785-F, Phase II

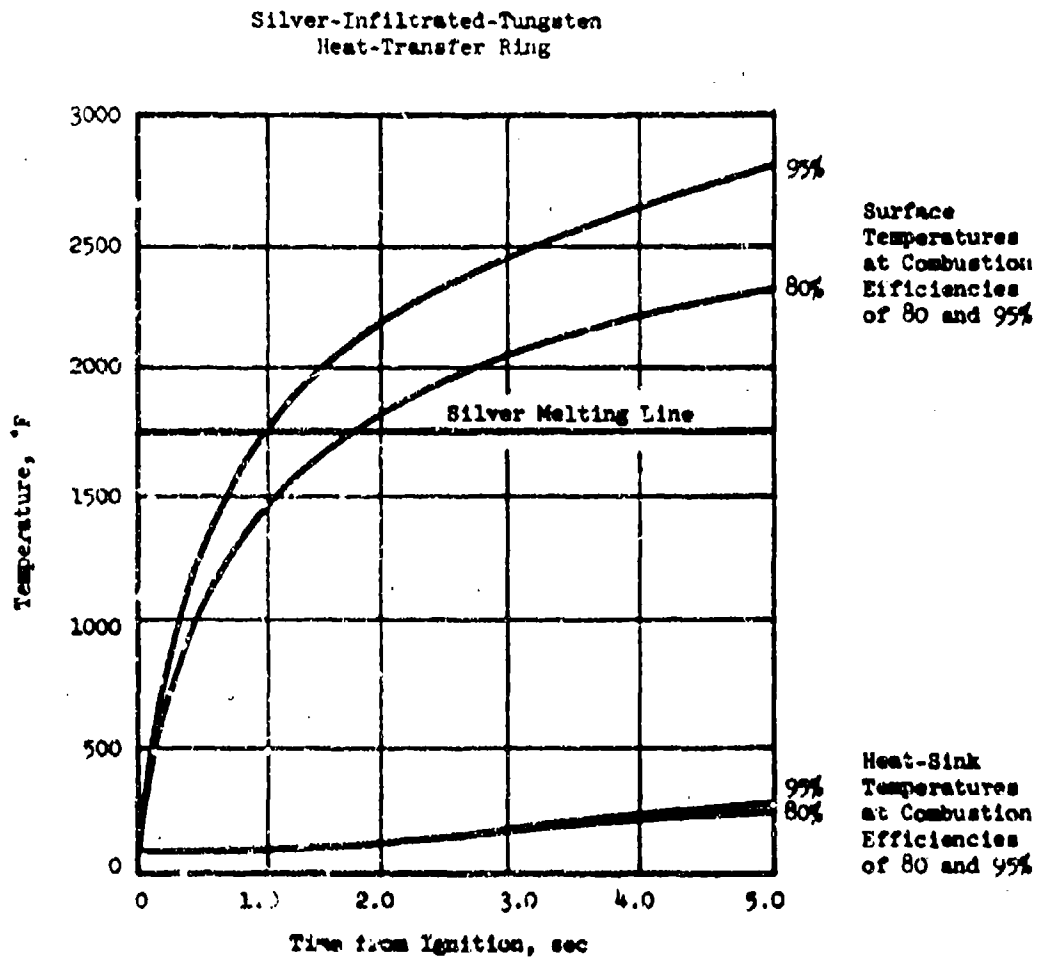


Figure 47. Predicted Chamber Heat-Flux Transducer Temperature Transient

UNCLASSIFIED

UNCLASSIFIED

Report 10785 E, Phase II

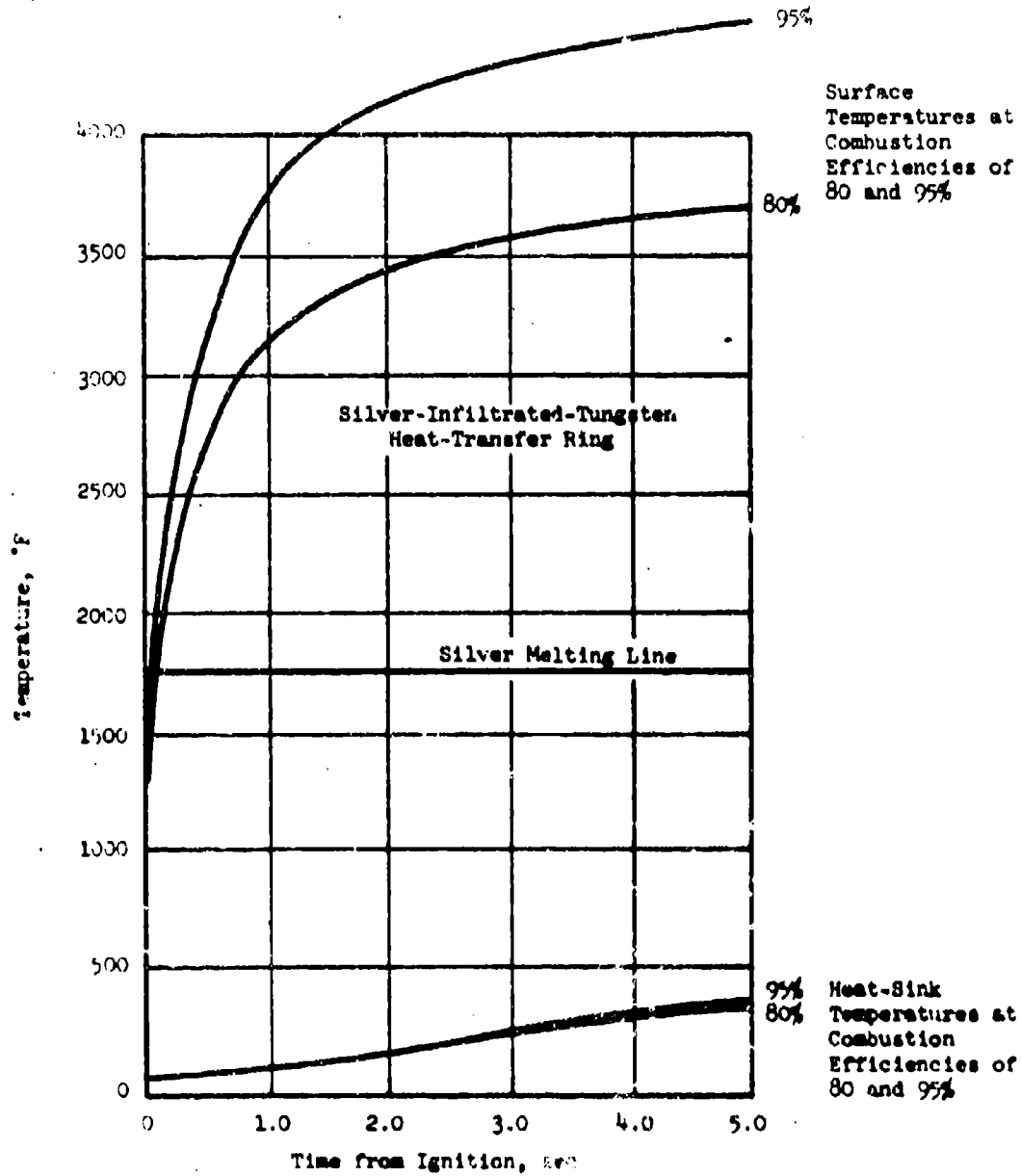


Figure 111. Surface Temperatures at Combustion Efficiencies of 80 and 95% and Heat-Sink Temperatures at Combustion Efficiencies of 80 and 95% versus Time from Ignition, sec.

Page 111

UNCLASSIFIED

UNCLASSIFIED

Report 10785-F, Phase II

IV, B, Technical Discussion (cont.)

c. Instrumentation

(1) Instability Monitoring

(U) The Photocon Model 307 water-cooled transducer was used to monitor the possible occurrence of high-frequency instability. The preburner (Figure 48) was instrumented with transducers at the following stations: (1)  $H_2O_2$  inlet manifold PQJPE(PN); (2) forward end of mixing chamber POFC1(PN); (3) aft end of mixing chamber POFC9(PN). A transducer was also installed at the injector fuel inlet PFJSC(PN). No attempt was made to install high-frequency transducers in the combustion chamber, because such installations through ablative materials have proved to be unsatisfactory. The transducer installed in the oxidizer manifold (POFC9(PN)) would be indicative of chamber conditions.

(2) Temperature Measurement

(U) Provisions were made to continue the measurement of temperature at strategic points in the preburner (Figure 48).

(3) Pressure Measurement

(U) Pressures were measured on the face of the injector at two locations, inlet manifold to the injector, and on each heat-flux transducer. Taber transducers were used.

UNCLASSIFIED





# UNCLASSIFIED

Report 10785-F, Phase II

## IV, B, Technical Discussion (cont.)

### 2. Method of Testing

#### a. Start Transient and Thrust-Chamber Operation Analysis

(U) A transient and steady-state analysis for the staged-combustion engine was conducted to determine the most favorable engine operating sequence. The selected sequence consisted of five events, each of which had to be satisfactorily completed before proceeding to the next.

(U) The analysis revealed that, during staging to operating pressure, the thrust-chamber valves could not be relied upon to control flow because of their poor resistance versus opening characteristics. It was shown that staging (or ramping) should start before opening the main thrust-chamber valves and that the valves should be opened as quickly as possible. In this way, by simultaneously staging and quickly opening the thrust-chamber valves, chamber-pressure oscillations and mixture-ratio excursions during the start transient could be avoided.

#### (1) Initiation

(U) During this event, the main oxidizer thrust-chamber valve was bypassed at about 3 lbm/sec and at an oxidizer manifold pressure of 900 psia. This condition was similar to that used during the last three pre-burner tests. A thrust-chamber pressure switch, set at about 240 psia, was used to sense peroxide decomposition and initiate the next event.

UNCLASSIFIED

# UNCLASSIFIED

Report 10785-F, Phase II

## IV, B, Technical Discussion (cont.)

### (2) Pack Preheat and Injector Cooling

(U) This event was timed for a duration of 2.5 sec to allow the pack to preheat to greater than 1600°F. The timing was experimentally determined during the preburner evaluation and provided assurance that the  $H_2O_2$  decomposition was near completion. As was also found during preburner testing, temperature conditioning of the turbine simulator was required to ensure a constant pressure drop during steady-state operation.

(U) In addition, water was passed through the secondary injector at 2 to 4 lbm/sec and at 200 psig to keep the vanes cool and prevent ingress of decomposed peroxide into the fuel circuit during the preheat event. Failure of the coolant water valve to open would initiate shutdown. The valve was closed at the end of this event.

### (3) Staging

(U) The completion of the preheat event initiated opening of the thrust-chamber fuel valve and the start of staging. The oxidizer valve opening was delayed 50 to 75 millisec to compensate for the difference in valve characteristics. The fuel flow was controlled by a Jamesbury<sup>(15)</sup> ball valve while the oxidizer side had used an Annin<sup>(16)</sup> globe valve. The oxidizer bypass valve was closed by a position switch on the main thrust-chamber oxidizer valve.

(15) Manufactured by the Jamesbury Corp., Worcester, Mass.

(16) Manufactured by the Annin Co., Montebello, Calif.

UNCLASSIFIED

# UNCLASSIFIED

Report 10785-F, Phase II

## IV. B. Technical Discussion (cont.)

(U) The staging rate, psi/sec, was controlled on both intensifiers to maintain a mixture ratio of 0.4 to 0.9 during staging. Staging occurred over a 1.5-sec period. The oxidizer pressure was ramped from a preset value of 900 to 5000 psig at the intensifier outlet. The fuel pressure was ramped from a value of 850 to 3500 psig.

### (4) Steady State

(U) The steady-state event was initiated during staging by a thrust-chamber pressure switch set at about 2500 psia. Steady-state pressure was 3000 psia, and the duration was set for about 1.2 to 1.4 sec. Failure of the thrust-chamber pressure switch to complete the malfunction detection circuit within a preset time initiated the shutdown sequence.

### (5) Shutdown

(U) The valves were sequenced to close in such a manner as to obtain a fuel lag of 50 to 75 millisecc and thus minimize flow of oxidizer over the hot tungsten surfaces. Initially, nitrogen at 1000 psig was passed through the secondary injector to purge residual Alumixine-43. Water was later used as the injector purge. The chamber downstream of the catalyst pack was also purged with nitrogen to prevent residual oxidizer from entering the secondary combustor and to prevent a backflow of combustion gas and water from the secondary combustion to the primary chamber and catalyst.

### b. Mixture-Ratio Analysis

(U) An analysis was conducted to evaluate the delivered performance of 98%  $H_2O_2$ /Alumixine-43 as a function of mixture ratio. Results of this analysis (conducted at the 100,000-lbf-thrust level), presented in

UNCLASSIFIED

UNCLASSIFIED

Report 10785-F, Phase II

IV, B, Technical Discussion (cont.)

Figure 49, indicate that even though maximum theoretical specific impulse occurs at a mixture ratio near 0.5, the estimated losses caused the desired operating point to move toward higher mixture ratios. A mixture ratio approaching 1.0 appears to be the desired operating point to deliver maximum specific impulse for a cooled engine. (A lower mixture ratio would be acceptable for an uncooled engine.) Therefore, the test plan was designed to evaluate and compare performance of 70-in. L\* chambers with 40-in. L\* chambers over a range of mixture ratios.

(U) An evaluation of the effect changes in mixture ratio would have upon flow dynamics of the system revealed that both the oxidizer and fuel circuit could handle the corresponding reduction in fuel flow and increase in oxidizer flow which would result from an increase in MR from 0.5 to 1.0.

c. Effect of Thermal Gradient and Oxidizer Upon Tungsten Components

(U) Because one of the major constituents in the combustion chamber, both for heat-flux transducers and throat sections, was silver-infiltrated tungsten, an analysis was performed to consider the effects of the thermal gradient and oxidizer-rich gases upon tungsten components.

(U) A thermochemical analysis was conducted to define the heat load imparted to these components during the start transient; i.e., to examine the heating characteristics and species of the gas as the engine starts with an oxidizer lead, passes through a stoichiometric mixture ratio, and steadies at the operating point. Gas molecular constituents, recovery temperature, and heat-transfer coefficients were examined as a function of mixture ratio.

UNCLASSIFIED

UNCLASSIFIED

Report 13785-4, Phase II

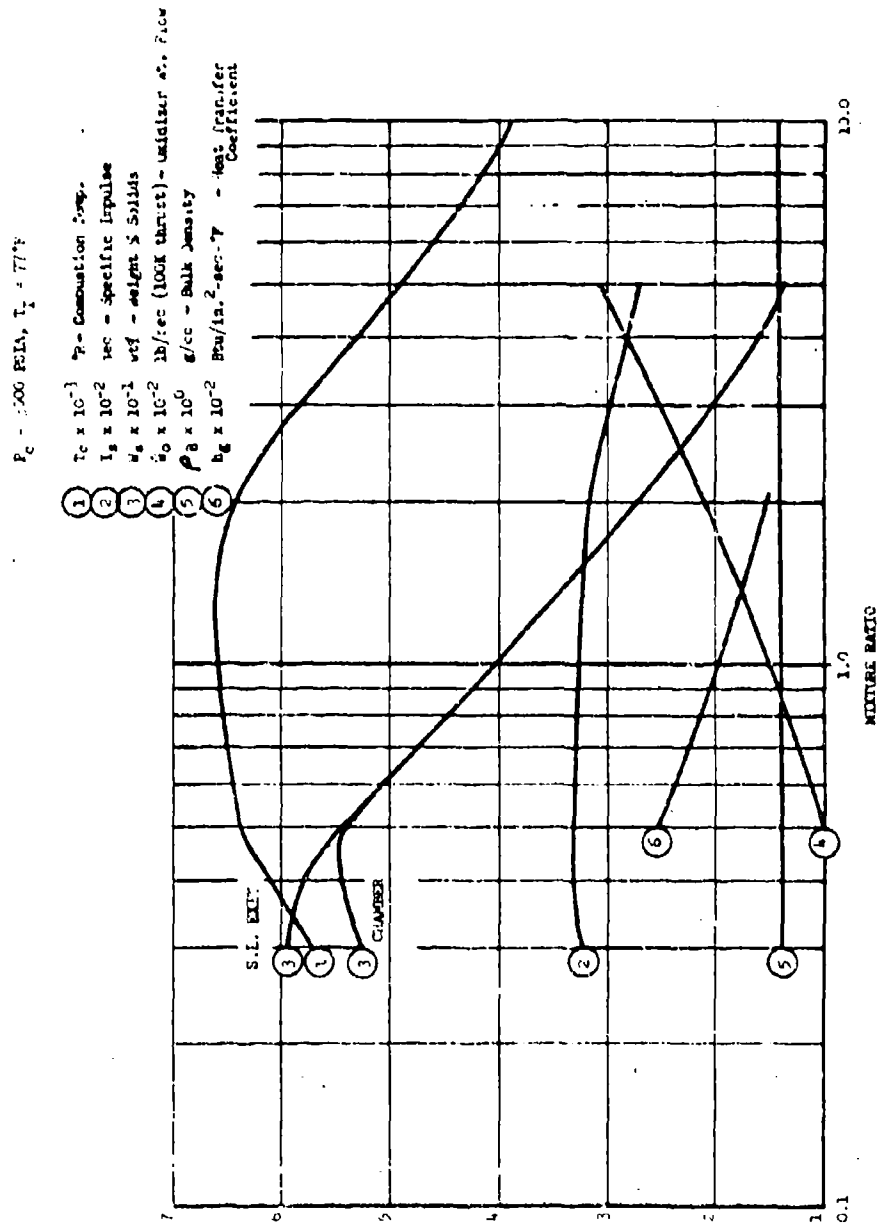


Figure 49. 98%  $\text{H}_2\text{O}_2$ /Alumizine-43 Performance Parameters vs Mixture Ratio

UNCLASSIFIED

## Report 10785-F, Phase II

## IV. B. Technical Discussion (cont.)

(U) This analysis indicated that the gas temperature at stoichiometric mixture ratio is about 200°F higher than at the operating point of 0.5. However, the thermochemical analysis shows a reduction in heat-transfer coefficient of the gas at the higher mixture ratio. It appears, therefore, that during the start transient the heat load increases as a function of decreased mixture ratio, and that the peak heating condition is achieved at a mixture ratio of 0.5.

(U) The literature was reviewed to evaluate the oxidation rate of the tungsten in the secondary chamber, and two excellent correlations were found. The correlation by Ong and Fassell (Ref. 8), for temperatures between 1300 and 2400°F and pressures between 0.02 and 306 psia, resulted in the following expression for the regression rate of tungsten,  $\frac{dx}{dt}$  (W):

$$\frac{dx}{dt} \text{ (W)} = 3.05 \times 10^2 \times 10^{-5290/T} P_{O_2}^{1/2} \text{ (cm/hr)} \quad (\text{Eq. 3})$$

where

T = °K

$P_{O_2}$  = partial pressure of oxygen in atmosphere

(U) An extrapolation of this relationship, shown in Figure 50, gives a regression rate of  $1.6 \times 10^{-5}$  in./sec for the primary chamber exhaust conditions.

P = 4000 psia

T = 1756°F

$P_{O_2}$  = 1300 psia

UNCLASSIFIED

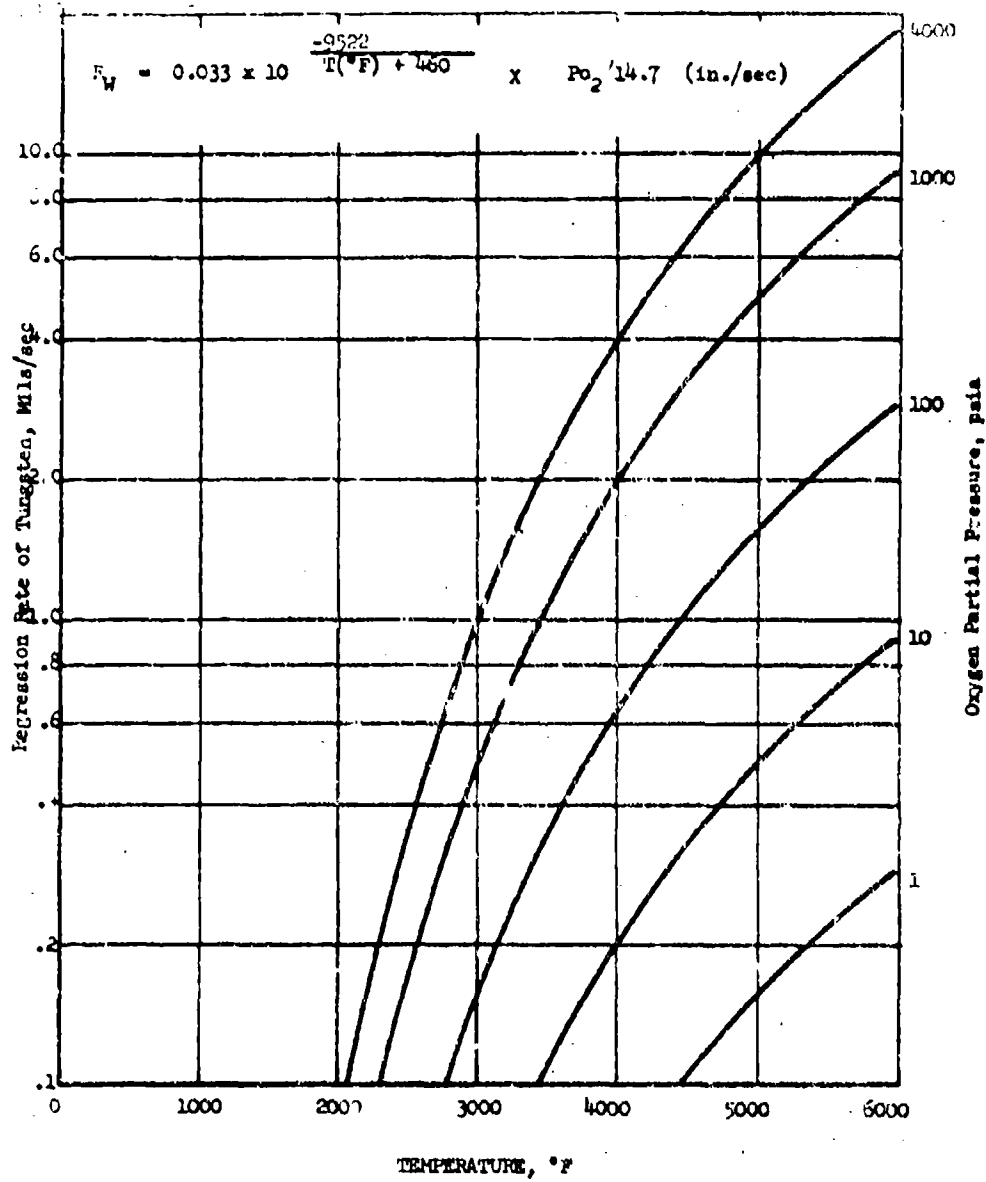


Figure 40. Regression Rate of Tungsten

UNCLASSIFIED



# UNCLASSIFIED

Report 10785-F, Phase II

## IV, B, Technical Discussion (cont.)

(U) The tungsten in the secondary chamber will, therefore, not be affected by a long start transient. The mechanism of tungsten oxidation in this temperature regime involves the rapid vaporization of tungsten oxide ( $WO_3$ ). An increase in pressure will tend to inhibit the vaporization of the oxide and thus reduce the amount of oxidation; the rate equation does not reflect this effect.

(U) The mechanism for oxidation under the secondary chamber conditions differs significantly from that just described. As the temperature is increased, the free energy of formation of the oxide becomes more positive until a temperature is reached at which tungsten oxidation is negligible. A correlation by Perkins, Price, and Crooks (Ref 9) resulted in the following expression:

$$R_w = 20 \times P_{O_2}^{0.84} e^{-24,500/RT} \text{ (gm/cm}^2\text{-min) (Eq 4)}$$

where

R = gas constant 1.987

T = °K

(U) The steady-state regression rate,  $R_w$ , calculated from this equation for the 20,000-lbf combustion throat, gives  $7.6 \times 10^{-5}$  in./sec at  $T = 5000^\circ\text{F}$ ,  $P = 3000$  psia, and  $P_{O_2} = 8.7$  psia ( $MR = 1.0$  for  $H_2O_2/Al-43$ ). This regression rate is completely satisfactory for operation of the 20,000-lbf-thrust engine. However, it is a pessimistic estimate because regression rate at high temperatures should decrease rather than increase with temperature, as shown by the equation that represents the rate at temperatures near  $3600^\circ\text{F}$ .

(U) Predictions based on the above cited Ong-Fassell equation and the empirical regression rate data compiled from Minuteman and Polaris solid-rocket firings correlated well.

# UNCLASSIFIED

UNCLASSIFIED

Report 10785-F, Phase II

IV. B. Technical Discussion (cont.)

(U) Chemical-composition calculations also were made to establish the threshold for erosion of tungsten versus 98%  $H_2O_2$ /Alumizine-43 mixture ratio. Standard equilibrium thermodynamics procedures were used for the system 98%  $H_2O_2$ /Alumizine-43/W (tungsten) at propellant mixture ratios from 0.5 to 1.2. The data are summarized in Figure 51 at a temperature of 6000°F. Note that the amount of oxidized tungsten is negligible below a mixture ratio of 0.65, and that the oxidation increases rapidly above a mixture ratio of 1.0.

(U) The variation of the oxidation process with temperature is illustrated in Figure 52. It can be seen that less tungsten trioxide ( $WO_3$ ) is formed as the temperature is reduced. The amount of tungstic acid ( $H_2WO_4$ ), however, does not decrease rapidly until temperatures below 5000°F are reached. Note that if the tungsten wall temperature is reduced to about 4500°F, as would be the case with a regeneratively cooled chamber, the operating mixture ratio can be increased slightly without increasing the amount of oxidation.

(U) On the basis of the material analysis, tungsten appears to be a satisfactory chamber material for use with 98%  $H_2O_2$ /Alumizine-43. The analysis, however, indicates that the regression rate may be excessive above a mixture ratio of 1.0 and at shutdown if there is a long oxidizer-rich tailoff.

d. Treatment of Test Data

(U) Several types of data were obtained from each staged-combustion test. These included:

UNCLASSIFIED

UNCLASSIFIED

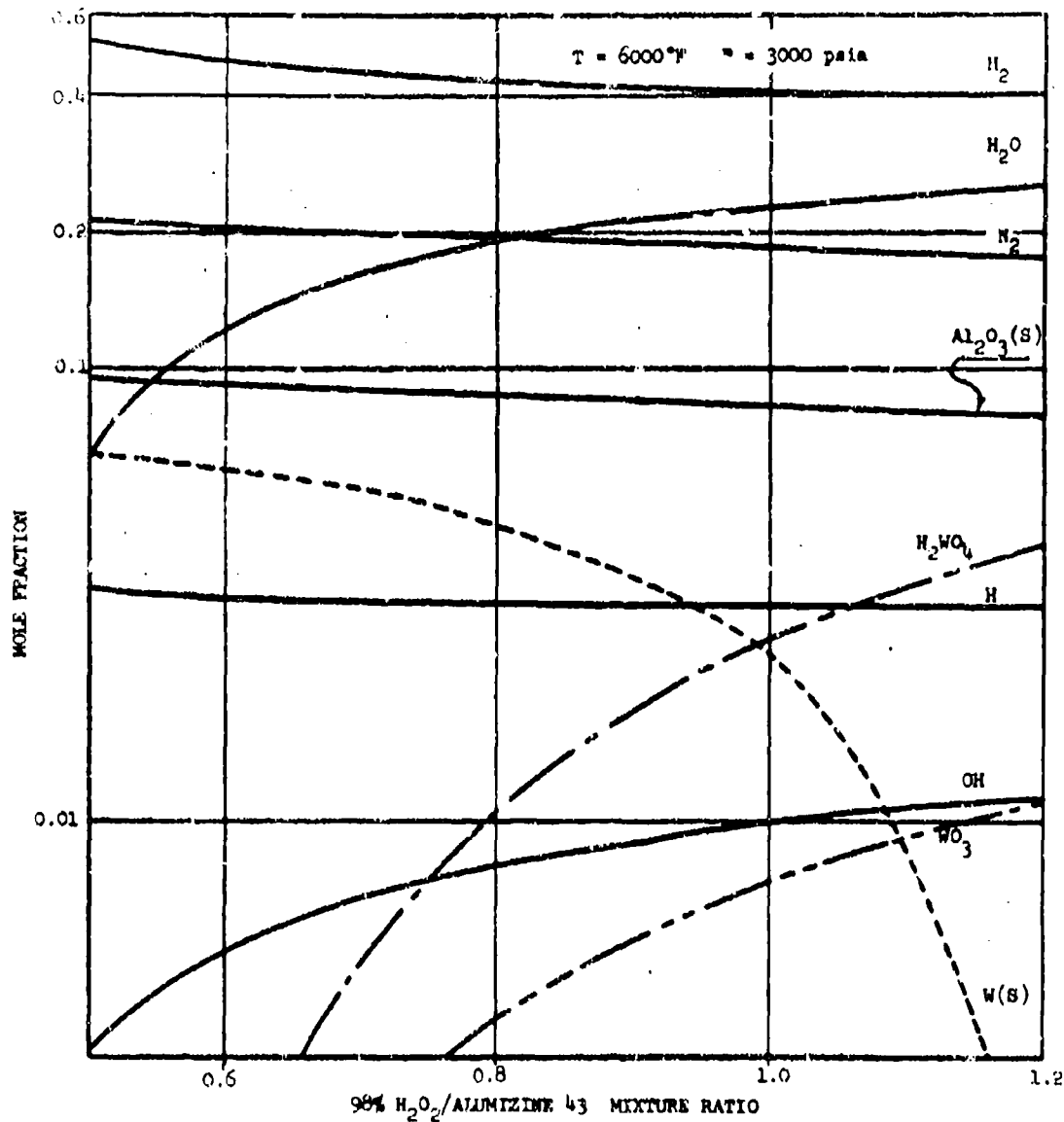


Figure 51. Thermochemistry of 98%  $H_2O_2$ /Alumizine-43 System  
in Presence of Tungsten at 6000°F

UNCLASSIFIED

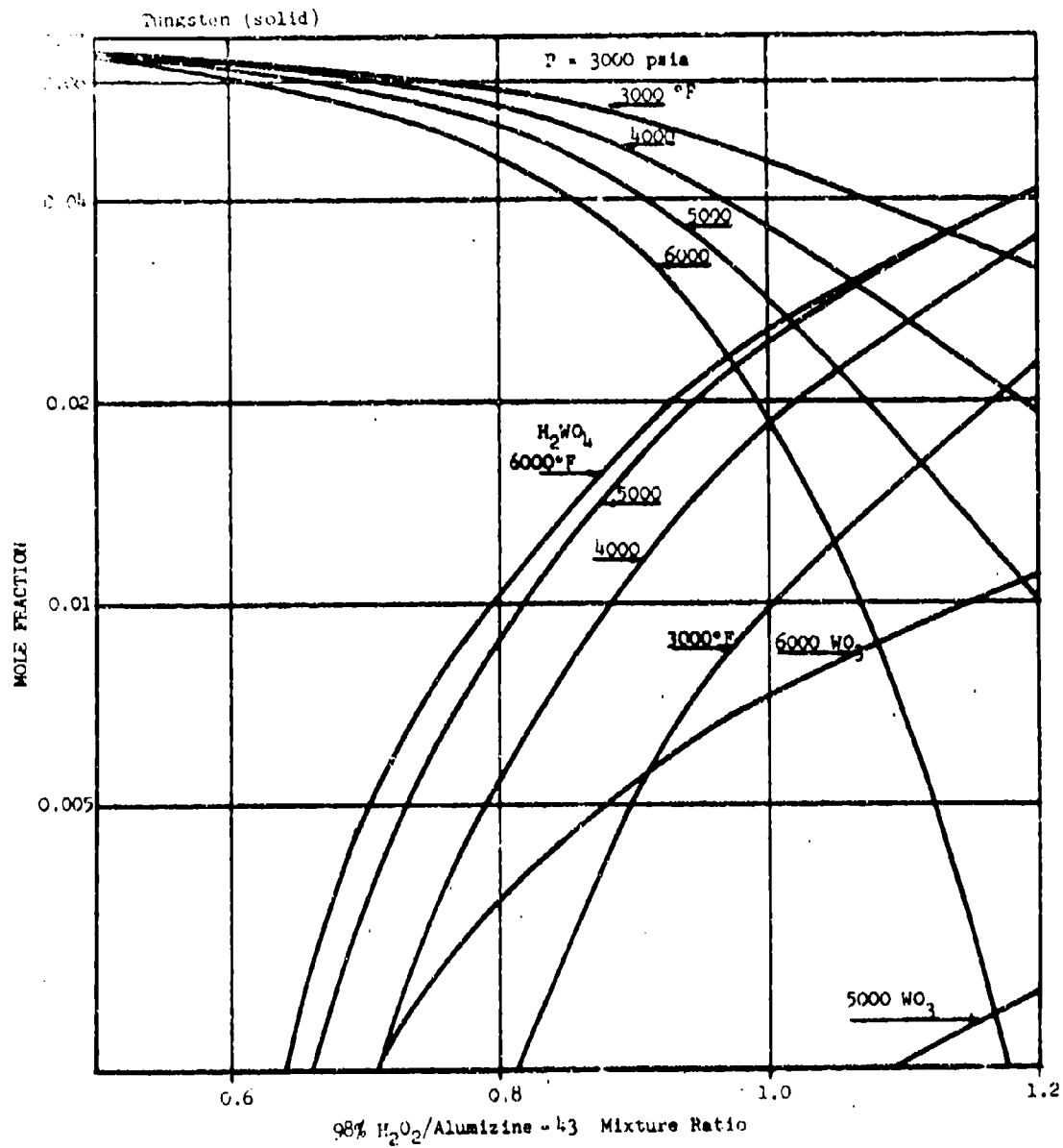


Figure 31. Variation of Oxidation of Tungsten with Temperature

UNCLASSIFIED

Report 10785-F, Phase II

IV, B, Technical Discussion (cont.)

(1) Slow-speed strip-charts which permitted a preliminary posttest evaluation of thrust, flow, pressures, and performance.

(2) Oscillographs which allowed examination and evaluation of such test parameters as valve phasing, low-frequency pressure perturbations; and pressure, flow and thrust transients. These data were used mainly in the qualitative sense.

(3) High-frequency tape recording--to monitor the possible occurrence of high-frequency pressure perturbations. Oscillograph-type records were produced from the magnetic tape for evaluation.

(4) Analog-to-digital conversion system (ADC). This system provided digital data, which became the main source of derived quantitative data and plots. It was also used in conjunction with a computer program to calculate performance parameters. The remainder of this discussion concerns itself mainly with the treatment of the ADC data.

(U) Initially, a plot of pertinent test parameters was prepared to make the selection of the time period over which data would be evaluated. The test parameters considered were oxidizer and fuel inlet manifold pressures (FOJ-FB and FFJ-BC), catalyst pack temperature (TOCP-2), decomposed  $H_2O_2$  temperature (TOPC-5), thrust (F), oxidizer and fuel flow rates (WO and WF), valve phasing (LOTCV and LFTCV) and chamber pressure (PCSC-1). Selection was made on the basis of constancy of these parameters during the period of nominal operating conditions (approximately 3000-psia chamber pressure and 20,000-lbf thrust). This is contrary to the period of time usually defined as steady state (time period greater than 90% of chamber pressure) which was used primarily as an indicator of test duration and not for data analysis. Selection of the steady-state period by the

UNCLASSIFIED

## IV, B, Technical Discussion (cont.)

method outlined was intended to rule out such phenomena as stand ringing (which gives large swings in thrust) and flow and pressure fluctuations during transients. Typical steady-state periods selected by this method ranged from 0.4 to 1.0 sec in duration.

(U) The data for the selected time periods were then averaged and used for calculation of both sea level and vacuum performance parameters. Vacuum performance parameters were used in the performance interaction evaluation discussed in Section IV,B,4. The use of vacuum performance parameters effectively rules out variations in chamber pressure for the range of pressures obtained (2650 to 3050 psia) and allows a realistic comparison of the data from test to test.

(U) Characteristic exhaust velocity was calculated from the following relationship:

$$c^* = \frac{P_c A_t g_c}{\dot{W}_T} \quad (\text{Eq 5})$$

where

$P_c$  = Plenum total pressure, psia  
 $A_t$  = Instantaneous throat area, in.<sup>2</sup>  
 $g_c$  = Acceleration of gravity = 32.174 ft/sec<sup>2</sup>  
 $\dot{W}_T$  = Total weight flow, lbm/sec

The instantaneous throat area was determined by assuming that any change in throat area that occurs during the firing is linear over the time period corresponding to greater than 90% of chamber pressure. The pretest area corresponds to the start 90% chamber pressure and the posttest area corresponds to the shutdown 90% chamber pressure. The plenum total pressure was obtained by averaging the two injector face static pressures recorded during the test.

## IV. B, Technical Discussion (cont.)

Weight flow rates were computed from booster (intensifier) travel measured by a capacitance probe, or secondarily (if the capacitance probe malfunctioned), by a linear potentiometer.

(U) Vacuum specific impulse was calculated as follows:

$$I_{sv} = \frac{F + P_a A_e}{\dot{W}_T} \quad (\text{Eq 6})$$

where:

$F$  = Thrust, lbf

$P_a$  = Atmospheric pressure, psia

$A_e$  = Exit area, in.<sup>2</sup>

$\dot{W}_T$  = Total weight flow, lbm/sec

(U) Thrust measurements were corrected to include a thrust cell correction bias determined during calibration. The exit area was calculated in the same manner as that used for the throat area for the  $c^*$  calculation.

(U) These values were then compared to theoretical values corresponding to the same chamber pressure, MR, and exit area ratio by the performance comparator program. Coefficient of thrust,  $C_F$ , was also calculated, but has been accorded less significance in this report.

#### e. Secondary Injector Cleaning

(U) Alumizine exposed to air will decompose and leave a residual solid material which can block small tubes and passageways and even coat line and manifold surfaces. It was necessary to remove the injector after each firing to eliminate the residual Alumizine. Past experience had

UNCLASSIFIED

Report 10785-F, Phase II

IV. B. Technical Discussion (cont.)

shown that postfire nitrogen and water purges, while helpful, were not totally effective. Consequently, the injector was removed after each firing and immersed in a hot 5% sodium hydroxide bath for a minimum of 4 hr. Following this immersion, it was placed in 20% nitric acid for 30 min. This procedure proved effective in removing decomposed Alumazine from the injectors throughout the program; drilling was required to remove decomposed Alumazine (not dissolved by the caustic and acid) from some of the small tubes.

UNCLASSIFIED



# CONFIDENTIAL

Report 10785-F, Phase II

## IV, B, Technical Discussion (cont.)

### 3. Staged-Combustion Test Description and Results

(U) Fourteen tests were conducted during the staged-combustion evaluation program. In general, the objectives of these tests were to evaluate two secondary injector configurations and select the better of the two for subsequent testing; to determine transient heat flux at strategic locations in the chamber; to compare the performance of 96%  $H_2O_2$ /Aluminine-43 at characteristic chamber lengths ( $L^*$ 's) of 40 and 70 in. (baseline) over a range of mixture ratios; and to determine the performance of 90%  $H_2O_2$ /Aluminine-43.

(C) All of the objectives of the test program were satisfactorily attained in three series of tests. In the first series of four tests (1.2-02-AAC-001 through 004) two injector configurations were evaluated. As a result of this series, the 396 tube-vane type secondary injector was selected to perform the subsequent two series of evaluations. This injector demonstrated greater than 89% of theoretical specific impulse on its first two firings (see Table VI), thus exceeding easily the program goal of 87% of theoretical  $I_g$ . The tubular injector, consisting of 44 axially directed tubes (a much coarser injection system), gave only 84.3% of theoretical  $I_g$ .

(U) The test program was temporarily discontinued at this point because of major damage sustained by the oxidizer intensifier and feed system due to a test stand malfunction. The affected components were restored to a Class 2 condition (see Section III, B, 3), and the test program was resumed.

(C) During the second series of seven tests, 1.2-03-AAC-001 through -007, the performance comparison and heat-flux determination were satisfactorily completed. Two of these tests did not produce useful data because of malfunctions. Results are presented in Table VI. The test results confirmed the theoretical analysis which predicted that higher performance was

CONFIDENTIAL

1  
2  
3  
4  
5  
6  
7  
8  
9  
10  
11  
12  
13  
14  
15  
16  
17  
18  
19  
20  
21  
22  
23  
24  
25  
26  
27  
28  
29  
30  
31  
32  
33  
34  
35  
36  
37  
38  
39  
40  
41  
42  
43  
44  
45  
46  
47  
48  
49  
50  
51  
52  
53  
54  
55  
56  
57  
58  
59  
60  
61  
62  
63  
64  
65  
66  
67  
68  
69  
70  
71  
72  
73  
74  
75  
76  
77  
78  
79  
80  
81  
82  
83  
84  
85  
86  
87  
88  
89  
90  
91  
92  
93  
94  
95  
96  
97  
98  
99  
100  
101  
102  
103  
104  
105  
106  
107  
108  
109  
110  
111  
112  
113  
114  
115  
116  
117  
118  
119  
120  
121  
122  
123  
124  
125  
126  
127  
128  
129  
130  
131  
132  
133  
134  
135  
136  
137  
138  
139  
140  
141  
142  
143  
144  
145  
146  
147  
148  
149  
150  
151  
152  
153  
154  
155  
156  
157  
158  
159  
160  
161  
162  
163  
164  
165  
166  
167  
168  
169  
170  
171  
172  
173  
174  
175  
176  
177  
178  
179  
180  
181  
182  
183  
184  
185  
186  
187  
188  
189  
190  
191  
192  
193  
194  
195  
196  
197  
198  
199  
200  
201  
202  
203  
204  
205  
206  
207  
208  
209  
210  
211  
212  
213  
214  
215  
216  
217  
218  
219  
220  
221  
222  
223  
224  
225  
226  
227  
228  
229  
230  
231  
232  
233  
234  
235  
236  
237  
238  
239  
240  
241  
242  
243  
244  
245  
246  
247  
248  
249  
250  
251  
252  
253  
254  
255  
256  
257  
258  
259  
260  
261  
262  
263  
264  
265  
266  
267  
268  
269  
270  
271  
272  
273  
274  
275  
276  
277  
278  
279  
280  
281  
282  
283  
284  
285  
286  
287  
288  
289  
290  
291  
292  
293  
294  
295  
296  
297  
298  
299  
300  
301  
302  
303  
304  
305  
306  
307  
308  
309  
310  
311  
312  
313  
314  
315  
316  
317  
318  
319  
320  
321  
322  
323  
324  
325  
326  
327  
328  
329  
330  
331  
332  
333  
334  
335  
336  
337  
338  
339  
340  
341  
342  
343  
344  
345  
346  
347  
348  
349  
350  
351  
352  
353  
354  
355  
356  
357  
358  
359  
360  
361  
362  
363  
364  
365  
366  
367  
368  
369  
370  
371  
372  
373  
374  
375  
376  
377  
378  
379  
380  
381  
382  
383  
384  
385  
386  
387  
388  
389  
390  
391  
392  
393  
394  
395  
396  
397  
398  
399  
400  
401  
402  
403  
404  
405  
406  
407  
408  
409  
410  
411  
412  
413  
414  
415  
416  
417  
418  
419  
420  
421  
422  
423  
424  
425  
426  
427  
428  
429  
430  
431  
432  
433  
434  
435  
436  
437  
438  
439  
440  
441  
442  
443  
444  
445  
446  
447  
448  
449  
450  
451  
452  
453  
454  
455  
456  
457  
458  
459  
460  
461  
462  
463  
464  
465  
466  
467  
468  
469  
470  
471  
472  
473  
474  
475  
476  
477  
478  
479  
480  
481  
482  
483  
484  
485  
486  
487  
488  
489  
490  
491  
492  
493  
494  
495  
496  
497  
498  
499  
500  
501  
502  
503  
504  
505  
506  
507  
508  
509  
510  
511  
512  
513  
514  
515  
516  
517  
518  
519  
520  
521  
522  
523  
524  
525  
526  
527  
528  
529  
530  
531  
532  
533  
534  
535  
536  
537  
538  
539  
540  
541  
542  
543  
544  
545  
546  
547  
548  
549  
550  
551  
552  
553  
554  
555  
556  
557  
558  
559  
560  
561  
562  
563  
564  
565  
566  
567  
568  
569  
570  
571  
572  
573  
574  
575  
576  
577  
578  
579  
580  
581  
582  
583  
584  
585  
586  
587  
588  
589  
590  
591  
592  
593  
594  
595  
596  
597  
598  
599  
600  
601  
602  
603  
604  
605  
606  
607  
608  
609  
610  
611  
612  
613  
614  
615  
616  
617  
618  
619  
620  
621  
622  
623  
624  
625  
626  
627  
628  
629  
630  
631  
632  
633  
634  
635  
636  
637  
638  
639  
640  
641  
642  
643  
644  
645  
646  
647  
648  
649  
650  
651  
652  
653  
654  
655  
656  
657  
658  
659  
660  
661  
662  
663  
664  
665  
666  
667  
668  
669  
670  
671  
672  
673  
674  
675  
676  
677  
678  
679  
680  
681  
682  
683  
684  
685  
686  
687  
688  
689  
690  
691  
692  
693  
694  
695  
696  
697  
698  
699  
700  
701  
702  
703  
704  
705  
706  
707  
708  
709  
710  
711  
712  
713  
714  
715  
716  
717  
718  
719  
720  
721  
722  
723  
724  
725  
726  
727  
728  
729  
730  
731  
732  
733  
734  
735  
736  
737  
738  
739  
740  
741  
742  
743  
744  
745  
746  
747  
748  
749  
750  
751  
752  
753  
754  
755  
756  
757  
758  
759  
760  
761  
762  
763  
764  
765  
766  
767  
768  
769  
770  
771  
772  
773  
774  
775  
776  
777  
778  
779  
780  
781  
782  
783  
784  
785  
786  
787  
788  
789  
790  
791  
792  
793  
794  
795  
796  
797  
798  
799  
800  
801  
802  
803  
804  
805  
806  
807  
808  
809  
810  
811  
812  
813  
814  
815  
816  
817  
818  
819  
820  
821  
822  
823  
824  
825  
826  
827  
828  
829  
830  
831  
832  
833  
834  
835  
836  
837  
838  
839  
840  
84

TABLE VI

1. RESEARCH (a) RESEARCH (b) RESEARCH

101	102	103	104	105	106	107	108	109	110	111	112	113	114	115	116	117	118	119	120	121	122	123	124	125	126	127	128	129	130	131	132	133	134	135	136	137	138	139	140	141	142	143	144	145	146	147	148	149	150	151	152	153	154	155	156	157	158	159	160	161	162	163	164	165	166	167	168	169	170	171	172	173	174	175	176	177	178	179	180	181	182	183	184	185	186	187	188	189	190	191	192	193	194	195	196	197	198	199	200
-----	-----	-----	-----	-----	-----	-----	-----	-----	-----	-----	-----	-----	-----	-----	-----	-----	-----	-----	-----	-----	-----	-----	-----	-----	-----	-----	-----	-----	-----	-----	-----	-----	-----	-----	-----	-----	-----	-----	-----	-----	-----	-----	-----	-----	-----	-----	-----	-----	-----	-----	-----	-----	-----	-----	-----	-----	-----	-----	-----	-----	-----	-----	-----	-----	-----	-----	-----	-----	-----	-----	-----	-----	-----	-----	-----	-----	-----	-----	-----	-----	-----	-----	-----	-----	-----	-----	-----	-----	-----	-----	-----	-----	-----	-----	-----	-----	-----	-----	-----

# CONFIDENTIAL

Report 10785-F, Phase II

## IV, B, Technical Discussion (cont.)

favorable by higher mixture ratios. Figure 53 shows the delivered specific impulse at sea level for the baseline 70-in. L\* chamber and vane injector plotted against mixture ratio. Area ratio was constant at 10/1. For comparison purposes, the theoretical specific impulse against mixture ratio is shown in Figure 54. At 0.5 MR, about 91%  $I_{sp}$  is realized and increases to about 93%  $I_{sp}$  at 0.8 MR. These plots show the need to optimize the operating point for an engine using this propellant combination. The relationship of L\* to performance is discussed under Section IV,B,4, Performance Analysis. The heat-flux data obtained during this test series are discussed in detail in Section IV,B,5.

(C) The third series of three tests, 1.2-03-AAC-008 through -010, demonstrated the 90%  $H_2O_2$ /Alumixine-43 staged-combustion cycle. Two of these tests produced useful data (see Table VI). The performance levels, in terms of the percentage of theoretical specific impulse, were lower than those achieved with 98%  $H_2O_2$ /Alumixine-43, largely because a modified Mod II vane injector and a modified tubular injector were used to perform the tests. The modification to the vane injector is explained in detail below in the discussion of Test 1.2-03-AAC-008. However, the tubular injector, modified by incorporating three to four weld beads in each tube outlet to increase Alumixine-43 dispersion, e.g., surface exposure, produced a radical increase of 6% in performance over the original version evaluated on Test 1.2-02-AAC-004. This is extremely valuable data in that it shows the significance of fuel surface exposure area. The injector pressure drop was also increased resulting in a higher injection velocity; however, past staged-combustion experience has indicated that injection velocity per se has little or no effect on performance.

(U) Figure 55 shows the flow schematic for the system. The staged-combustion TCA is shown in Figure 37, and the location and identification of instrumentation parameters are shown in Figure 48. The tests are summarized in the following paragraphs:

CONFIDENTIAL

CONFIDENTIAL

Report 10785-F, Phase II

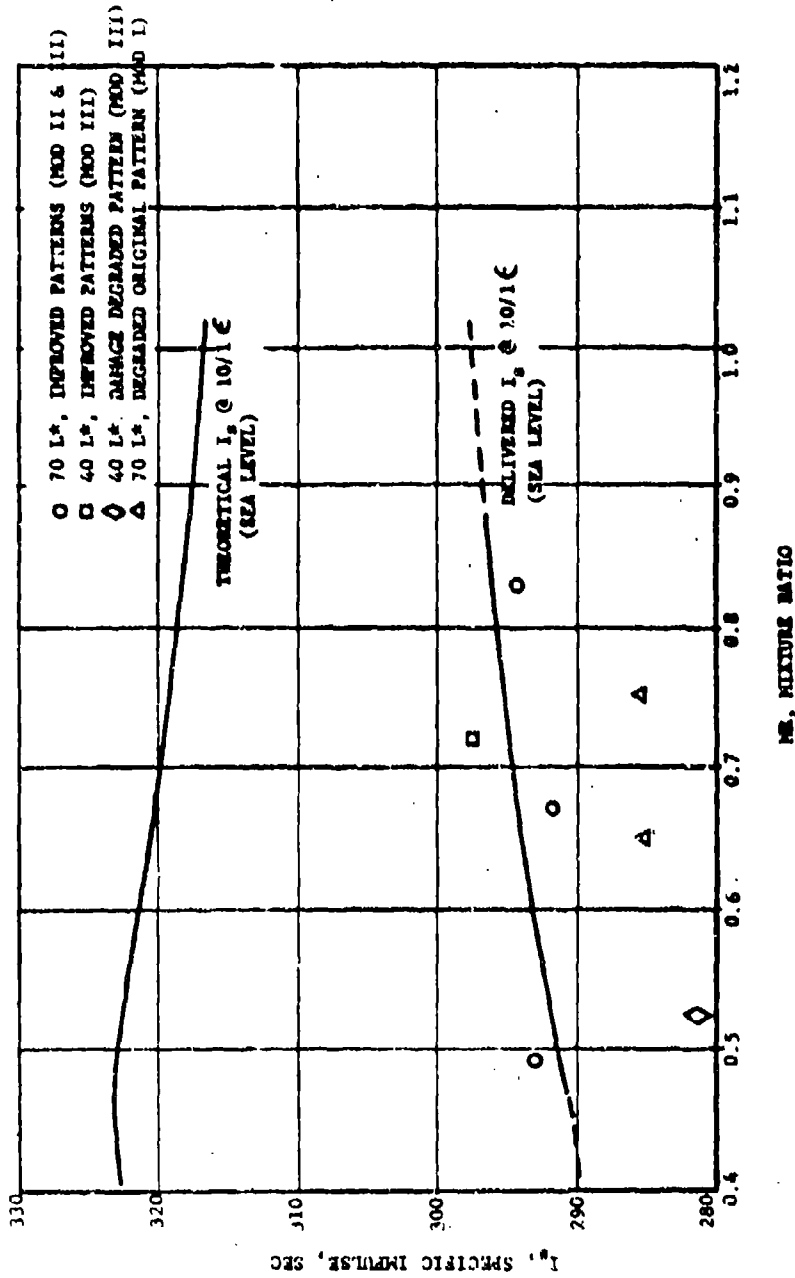


Figure 53. Comparison of Delivered  $I_s$  vs Theoretical  $I_s$ , 98%  $F_2O_2$ /Alumizine-43 (Vane Injector Only) (u)

CONFIDENTIAL

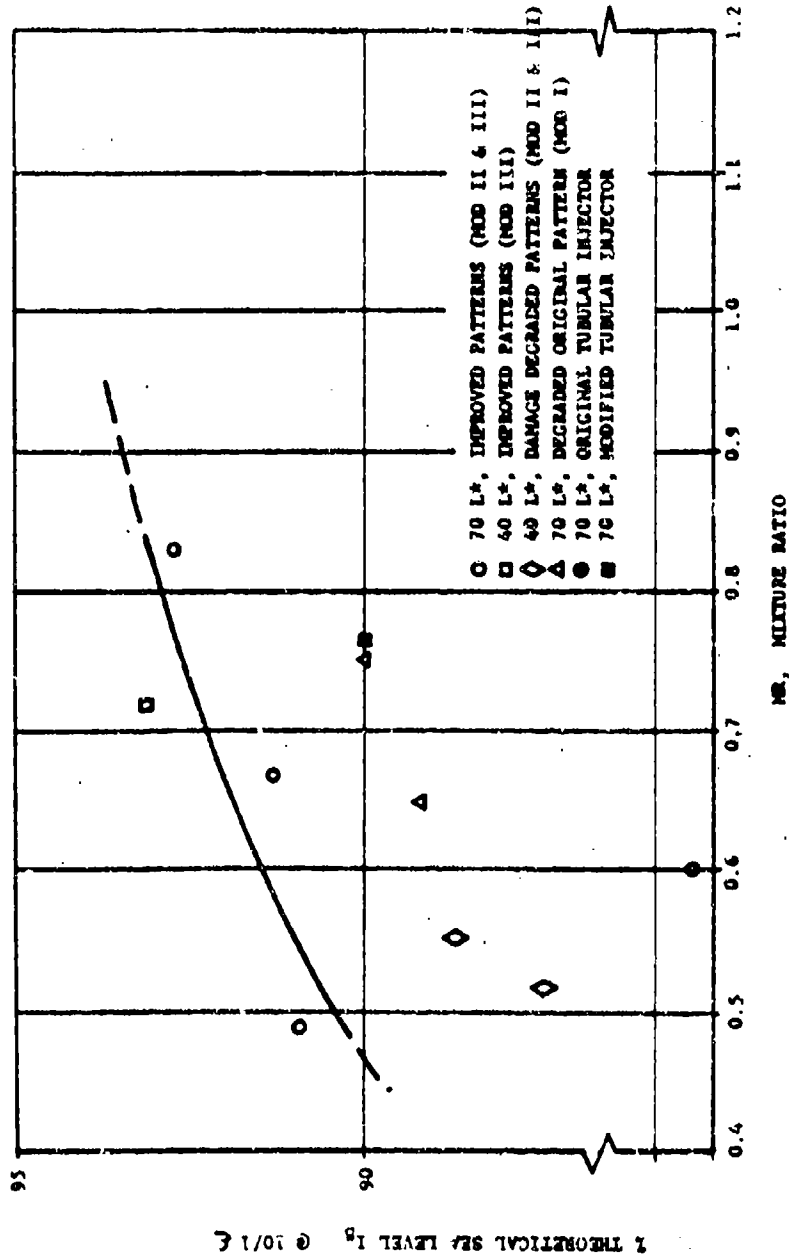


Figure 54. Percent Theoretical  $I_2$  vs MR for 90 and 98%  $H_2O_2$ /Aluzine-43 (u)

CONFIDENTIAL

Report 10785-F, Phase II

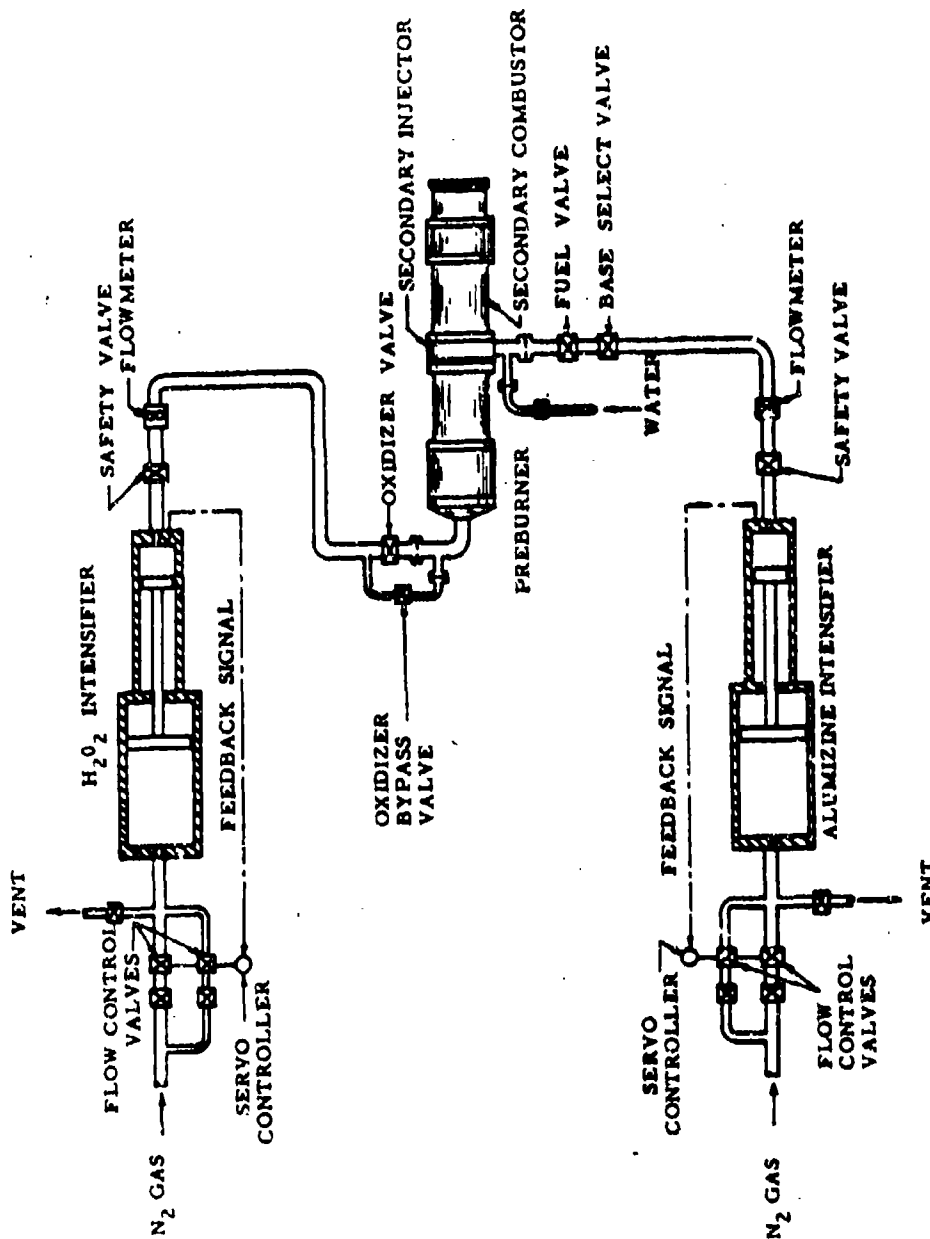


Figure 55. Staged-Combustion Flow Schematic

Page 134

CONFIDENTIAL

(This Page is Unclassified)

CONFIDENTIAL

Report 10785-F, Phase II

IV, B, Technical Discussion (cont.)

a. Test 1.2-02-AAC-001

(U) The objectives of this test, conducted with water flowing through the fuel circuit instead of Aluminine-43, were to check out preburner operation and the staged-combustion firing and shutdown sequences. The flow sequence used is described in Section IV,B,2. The water exhausted to ambient pressure through orifices sized to reproduce the pressure schedule in the injector of the secondary chamber. Secondary chamber hardware was not used in this simulation test. Oxidizer and fuel sequencing was satisfactory (Figure 56). Preburner catalyst performance is summarized in Table VI and in Figure 57.

(U) The catalyst performed satisfactorily in this test as well as in subsequent tests. The catalyst pack had been repacked by using eight Ageite-225 screens from the original low-throughput pack. New silver screens and ten new Ageite-220 screens were incorporated, as shown schematically in Figure 57.

b. Test 1.2-02-AAC-002

(U) The objectives of this test were to evaluate the first of two injector concepts and to determine staged-combustion performance at a chamber pressure of 2800 psia and a mixture ratio of 0.7 with a chamber  $L^*$  of 70 in. This mixture ratio was chosen because (1) the performance analysis had indicated that at least this mixture ratio is required to ensure ignition of aluminum if the hydrazine ( $N_2H_4$ ) is assumed to burn with the peroxide and the resulting flame temperature exceeds the melting point of aluminum oxide ( $Al_2O_3$ ), and (2) the oxidation of the tungsten in the silver-infiltrated-tungsten throat insert would be minimal at a mixture ratio below 0.7.

CONFIDENTIAL

(This page is Unclassified)





# CONFIDENTIAL

Report 10785-F, Phase II

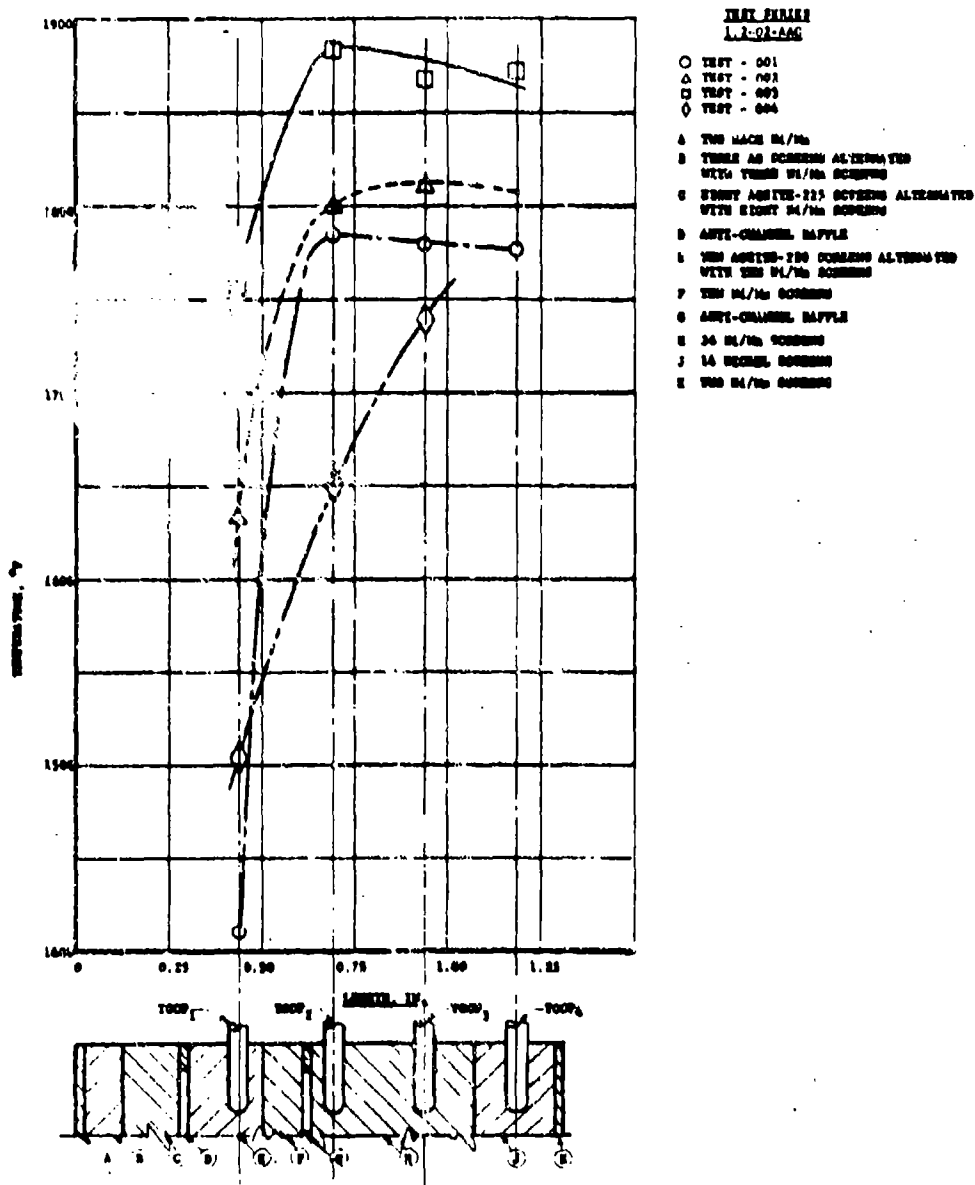


Figure 57. Staged-Combustion Catalyst Pack Temperature Profiles,  
Test Series 1.2-02-AAC (a)

CONFIDENTIAL

## IV, B, Technical Discussion (cont.)

(U) The chamber pressure was lowered from 3000 (nominal) to 2800 psia because of: (1) an excessively high pressure drop for design flow rates in the Mod I vane-type secondary injector, and (2) a facility limitation (maximum operating pressure of the fuel system, 3600 psia). When the high pressure drop was discovered during hydraulic calibration, the length of the tubes on the injector face was reduced from 1.0 to 0.65 in. through Elonging (electrical-discharge milling). Figure 43 shows a view of the modified injector face. The two larger tubes are pressure taps. Theoretically, shortening of the tubes degrades the flow-distribution pattern. However, with 396 tubes, this degradation was not considered to be appreciable.

(U) The start-transient sequence was modified to include a water purge to keep the injector vanes cool during preburner starting operation. Rather than use an injector fuel-fill event (through bypass of the main fuel valve), water flow of 4.2 lb/sec was initiated when the preburner reached 240 psia and was discontinued at the initiation of staging to full  $H_2O_2$  and Alumazine-43 flow rates. The event was incorporated into the sequence to prevent any possible failure of the injector vanes due to autodecomposition of Alumazine in contact with a hot surface and, also, to prevent decomposed  $H_2O_2$  from flowing back into the fuel injector.

(U) The TCA installation on the test stand is shown in Figure 58. Note thermocouple connectors protruding from chamber.

(U) The chamber heat-flux transducer did not respond during testing because the thermocouples were inadvertently sheared during assembly of ablative components into the chamber.

CONFIDENTIAL

Report 1.2-02-A-C-002

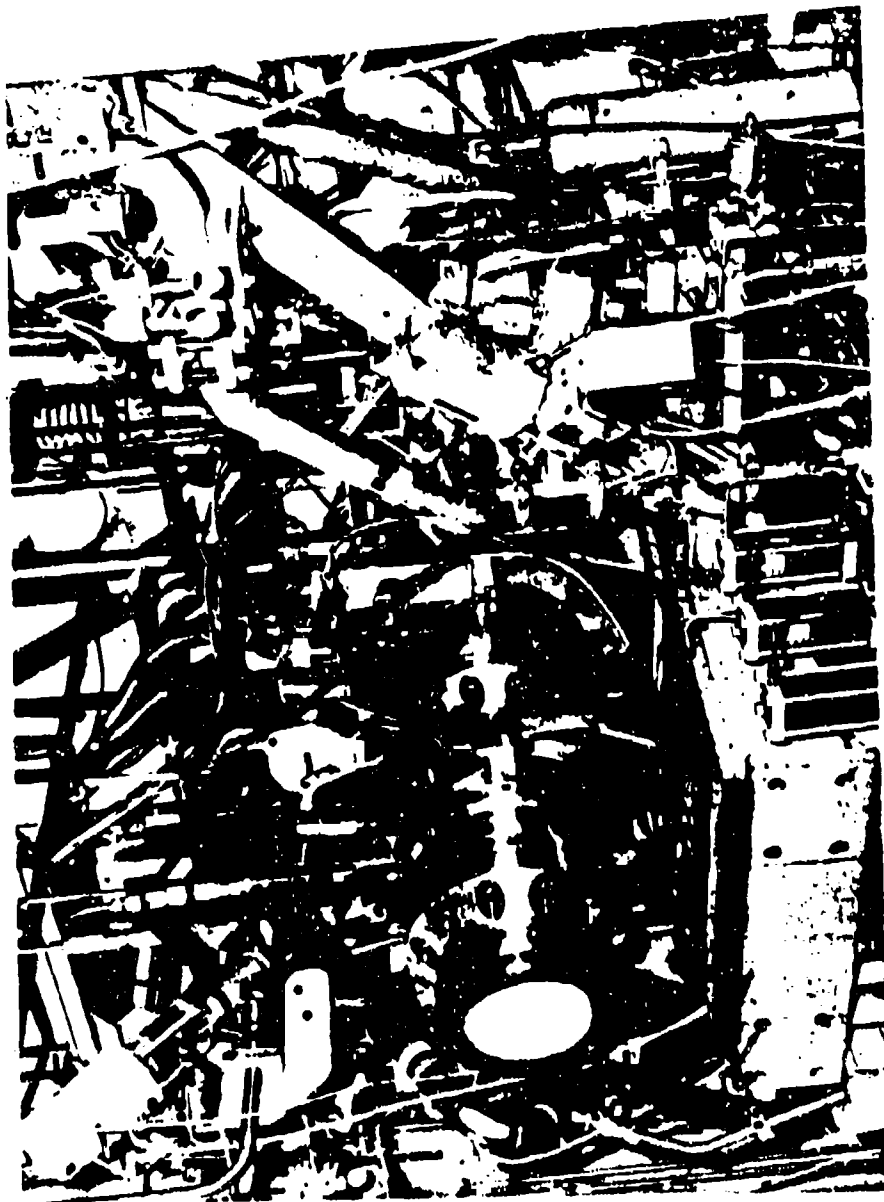


Figure 58. TCA Installation on Test Stand J-1, Test 1.2-02-A-C-002

Page 13

CONFIDENTIAL

Only use in the laboratory

IV, 3, Technical Discussion (cont.)

(C) The test was satisfactory. A specific-impulse efficiency of 89.3% at sea level was achieved at a mixture ratio of 0.65 and at a chamber pressure of 2750 psia (Table VI) thus exceeding the program goal of 87%. The injector face was undamaged and the tungsten throat showed no erosion. Steady-state duration was 1.57 sec (at greater than 90%  $P_c$ ).

(U) The fuel flowmeter readings were erratic (Figure 59), but fuel capacitance-probe measurements were steady. The catalyst pack heated up slowly and required about 9 sec for a significant temperature rise (Figure 60). During this test and during the preceding checkout test, the readings on the first thermocouple in the catalyst pack were appreciably lower than those recorded during tests with the original low-throughput pack in the preburner test series (Figure 57).

(U) After testing, the fuel injector was purged with 1500-psig nitrogen and deionized water. Four of the 396 tubes required drilling to remove residual decomposed Alumina. It should be noted that the fuel manifold has been designed to facilitate removal of residual Alumina; however, the bent tubes in the vaned injector are difficult to clean. The purge system was not successful in removing all the residual Alumina after shutdown.

(U) Upon disassembly it was noted that the chamber was coated with Alumina (Figure 61), indicating that the desired shutdown sequence had been achieved; i.e., the oxidizer and the fuel valve had closed simultaneously. Ablation of the chamber phenolic caused the chamber heat-flux transducer to protrude about 1/16 in. into the chamber. In addition, erosion just aft of the tungsten throat was also noted, as expected. This erosion was very similar to that observed on Polaris and Minuteman nozzles.

1.  $\frac{1}{2}$

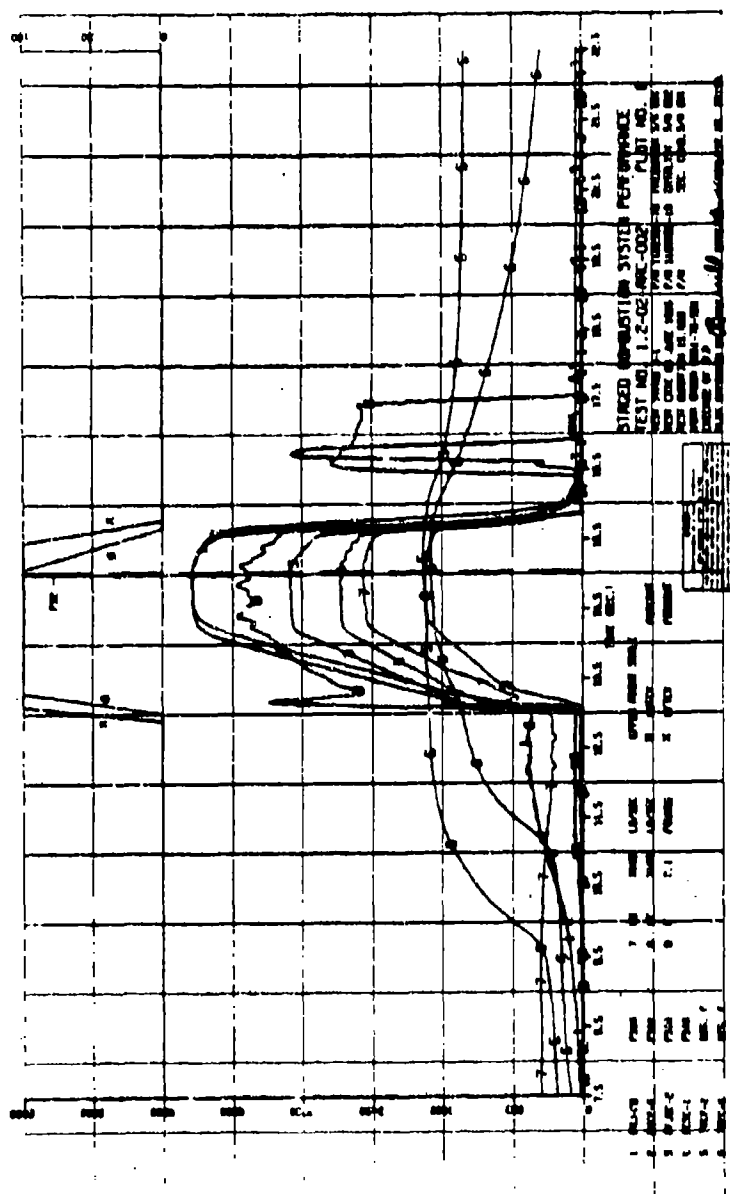


Figure 59. Staged-Combustion System Performance, Test 1.2-02-AAC-002 (Plot B) (u)

**CONFIDENTIAL**



1  
2  
3  
4  
5  
6  
7  
8  
9  
10  
11  
12  
13  
14  
15  
16  
17  
18  
19  
20  
21  
22  
23  
24  
25

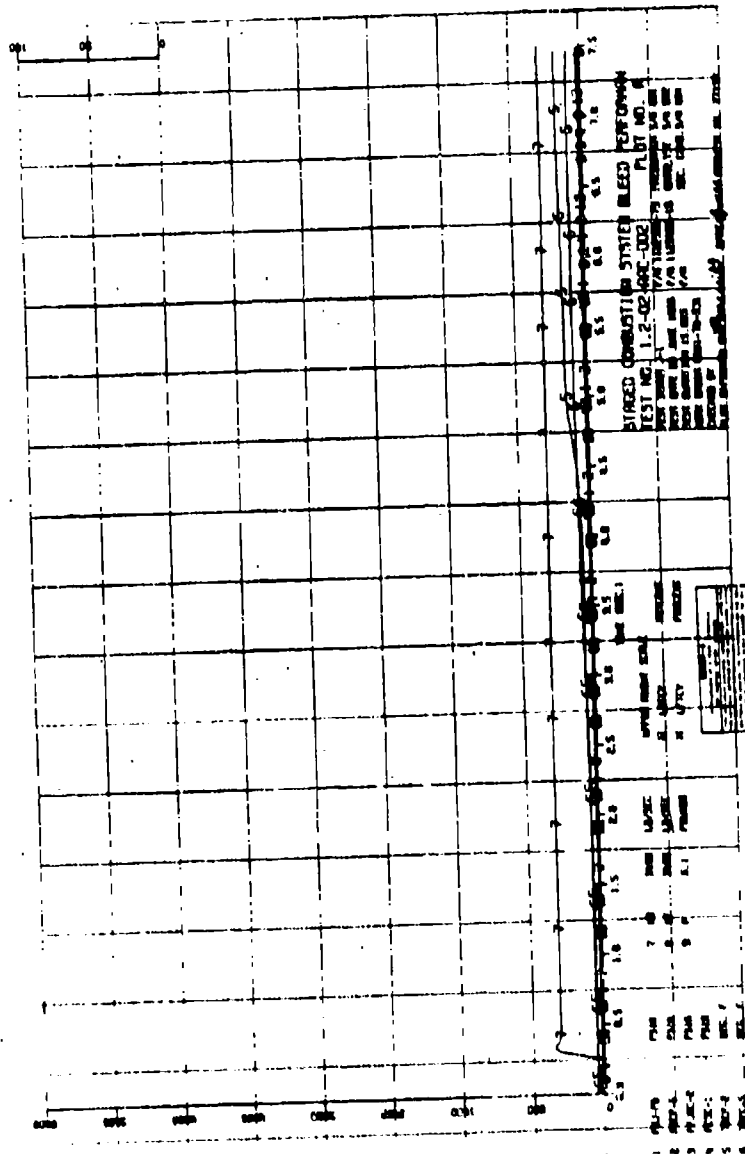


Figure 60. Stage1-Combustion System Performance, Test 1.2-02-AAC-002 (Plot A) (u)

**CONFIDENTIAL**

CONFIDENTIAL

1.2-02-002, Figure 61

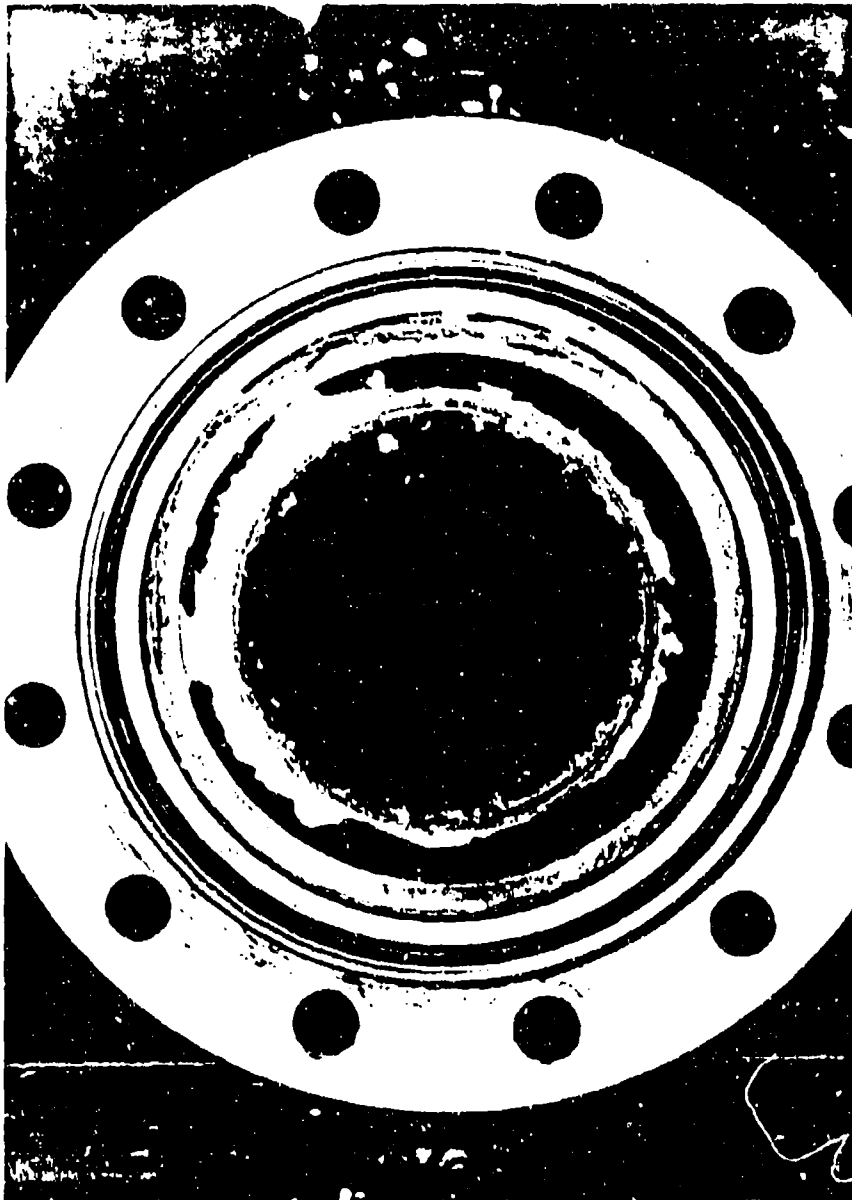


Figure 61. Ablative Chamber Viewed from Injector after Test 1.2-02-AAG-002

Page 145

CONFIDENTIAL

CONFIDENTIAL (When Released)

# CONFIDENTIAL

Report 10785-F, Phase II

## IV. B, Technical Discussion (cont.)

(U) The performance calculations, summarized in Table VI, are based upon oxidizer flow rate (measured with a 2-in. turbine-type flowmeter), fuel flow rate (measured by a capacitance probe), and thrust (measured with a calibrated load cell).

### c. Test 1.2-02-AAC-003

(U) The principal test objectives of this test were to verify the performance achieved on the first test and to determine the effect of mixture-ratio change on specific impulse efficiency. The test setup remained unchanged except that the target MI was increased to 0.8. The hardware was identical to that used for Test 002.

(C) The test was satisfactory and proceeded as programmed. Specific-impulse efficiency improved slightly to 89.9%, which confirmed that an efficiency exceeding 87.0% may be obtained reproducibly with this injector concept. Mixture ratio was 0.75 and chamber pressure was 2655 psia, both somewhat lower than desired because of the high pressure drop across the turbine simulator (2031 psi).

(U) As shown in Figure 62, the Alumisine-43 flowmeter again behaved erratically, but flow measurements by monitoring displacement of the intensifier piston were steady. All other traces were smooth, indicating stable and even combustion.

(U) A postfire inspection of the hardware indicated that eight injector tubes had been damaged; three tubes were split and five were burned back to the vane. Residual, decomposed Alumisine-43 from the manifold apparently plugged the tubes on startup and thus allowed stagnation and subsequent autodecomposition of the hydrazine. All tubes were free of obstructions

CONFIDENTIAL



CONFIDENTIAL

Report 10785-P, Phase II

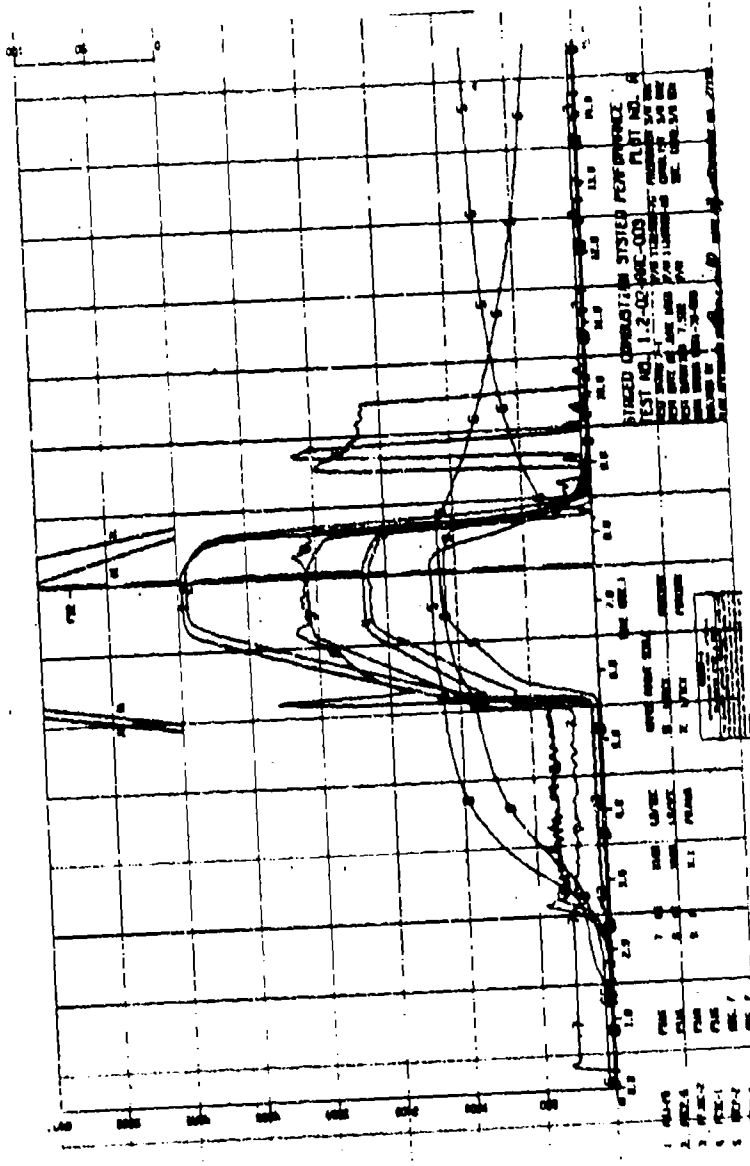


Figure 62. Staged-Combustion System Performance, Test 1.2-02-AAC-003 (u)

CONFIDENTIAL

## IV, B, Technical Discussion (cont.)

prior to firing. Figure 63 shows the postfire condition of the injector face and the damage to the tubes as observed after the two tests.

(U) The erosion of ablative components is diagrammatically shown in Figure 64. This erosion is typical of that which occurred on later tests. Appreciable erosion occurred in quartz-reinforced phenolic convergent chamber section. The forward stainless-steel retainer ring for the silver-infiltrated-tungsten throat was exposed by the loss of ablative material and had melted and burned in places. The burned and melted steel caused erosion of the forward section of the throat.

## d. Test 1.2-02-LAC-004

(U) The main objective of this test was to evaluate the second injector concept, i.e., the 44-tube injector. This injector, with its tubes directed axially in overhead fashion, is representative of technology developed during the Titan IIA program. However, fuel distribution is somewhat more coarse than with the final injector concept adopted on that program (Ref. 7).

(U) The ablative liner in the secondary chamber ( $L^* = 70$  in.), the tungsten throat, and the exit cone were replaced, and the chamber was instrumented with a heat-flux transducer at the location shown in Figures 37 and 43. The turbine simulator was replaced with one having a lower pressure drop to reduce the required supply pressure from the intensifier. (On the previous test, the outlet pressure of the intensifier was at its maximum and still the desired flow of  $H_2O_2$  was not obtained.) The catalyst pack and the preburner remained the same as in previous tests.

UNCLASSIFIED

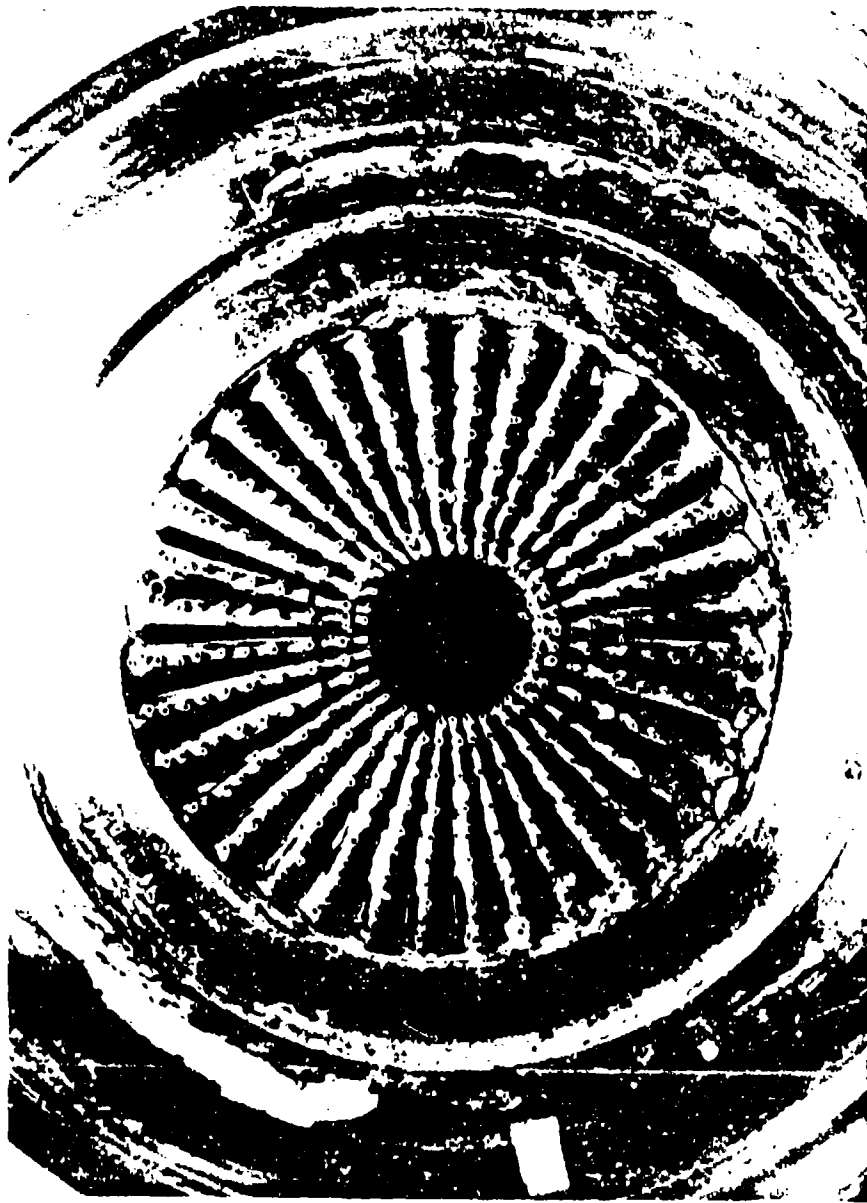


Figure 14. No. 1 Turbo-Injector Firing after Test: L-2-01-AAC-003 and -004

UNCLASSIFIED



UNCLASSIFIED

Report 10785-F, Phase II

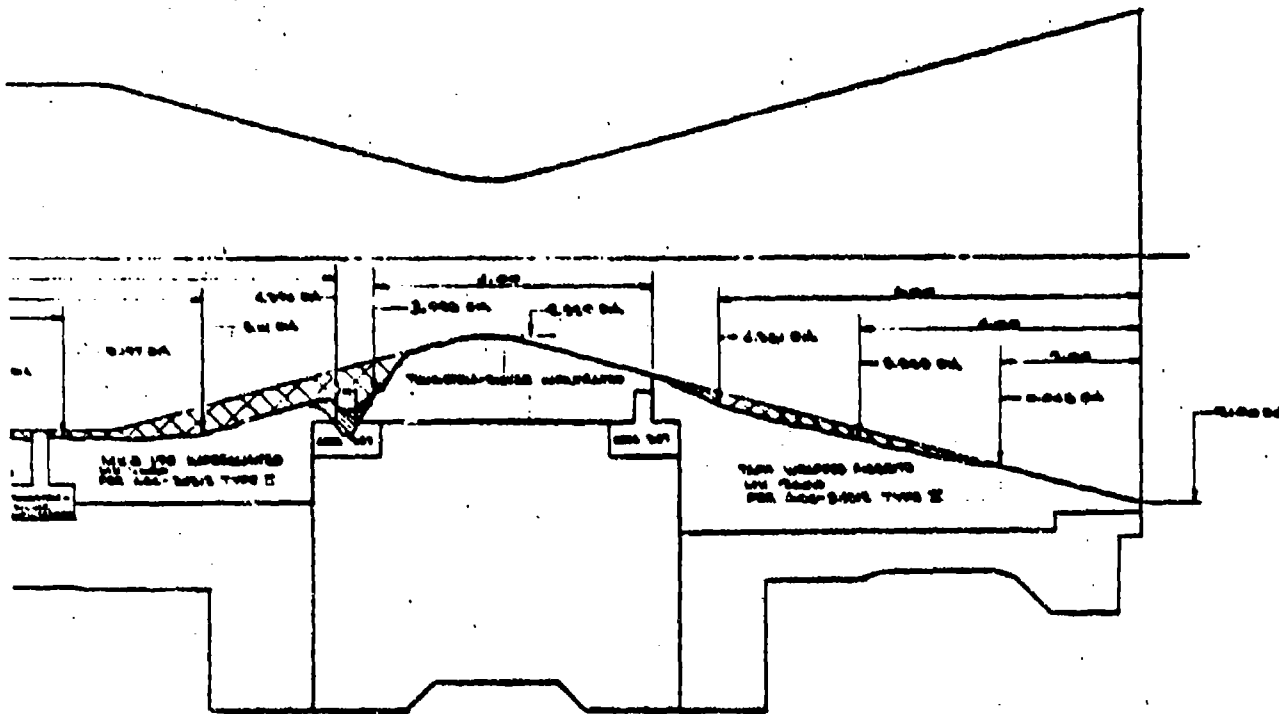


Figure 64. Postfire Contour after Tests 1.2-02-AAC-002 and -003

Page 148

UNCLASSIFIED

2

## IV, B, Technical Discussion (cont.)

(U) The fuel and oxidizer flow settings for the test were for a mixture ratio of 0.7 and a chamber pressure of 2800 psia. The test sequence and the timer settings were the same as for Tests 002 and 003.

(U) The test was characterized by low performance and rough combustion (pressure oscillations). These oscillations are discussed in Section IV,B,3.

(C) A specific-impulse efficiency of 84.3% at sea level was achieved at a mixture ratio of 0.60 and a chamber pressure of 2793 psia. This  $I_{sp}$  efficiency is less than the program goal of 87% and less than that achieved with the vane-type injector. The vanned injector was therefore chosen as the configuration for the remaining tests. Figures 65 and 66 summarize the pressures, flows, and temperatures obtained.

(U) Exhaust particles were collected on this test with the device shown in Figure 67. The device was placed 150 feet downstream in the exhaust plume. A shutter (not shown) opened the inlet of the device during the steady-state period and blocked it during the remainder of the firing sequence. This ensured that the particles collected were representative of particles produced during nominal operating conditions. The device was developed on the Investigation of Heterogeneous Propellant Two-Phase Flow Criteria Program (Ref. 10) recently completed at Aerojet-General Corp. The significance of particle size and distribution is discussed in Section IV,B,4.

(U) The injector was undamaged (Figure 68), but the tungsten throat and the ablative chamber material showed considerable grooving. Figure 69 shows the grooving sustained by the throat. This fact tends to verify the theoretical dependency of tungsten upon a homogeneous gas, since poor propellant distribution and mixing occurred and corresponded to the low specific impulse efficiency.

CONFIDENTIAL

Report 10785-F, Phase II

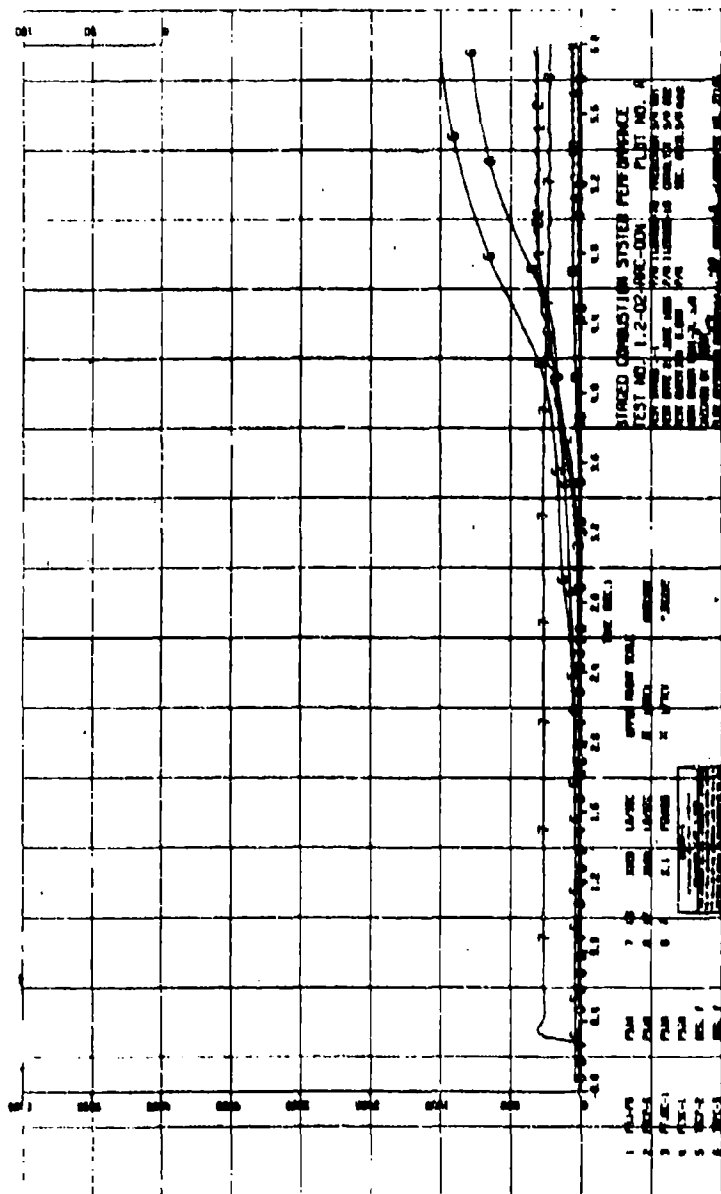


Figure 65. Staged-Combustion System Performance, Test 1.2-02-AAC-004  
(Plot A) (u)

CONFIDENTIAL

CONFIDENTIAL

Report 10785-F, Phase II

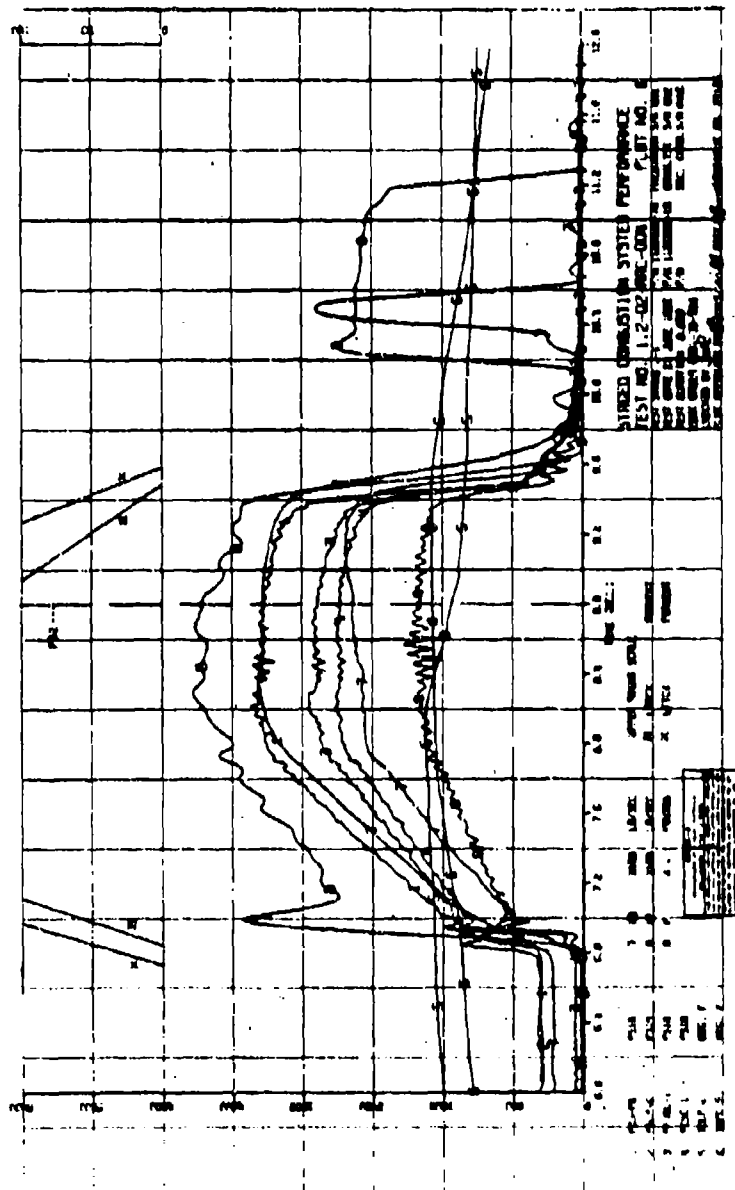


Figure 66. Staged-Combustion System Performance, Test 1.2-02-AAC-004  
(Plot B) (u)

CONFIDENTIAL



CONFIDENTIAL

Report 10785-F, Phase II

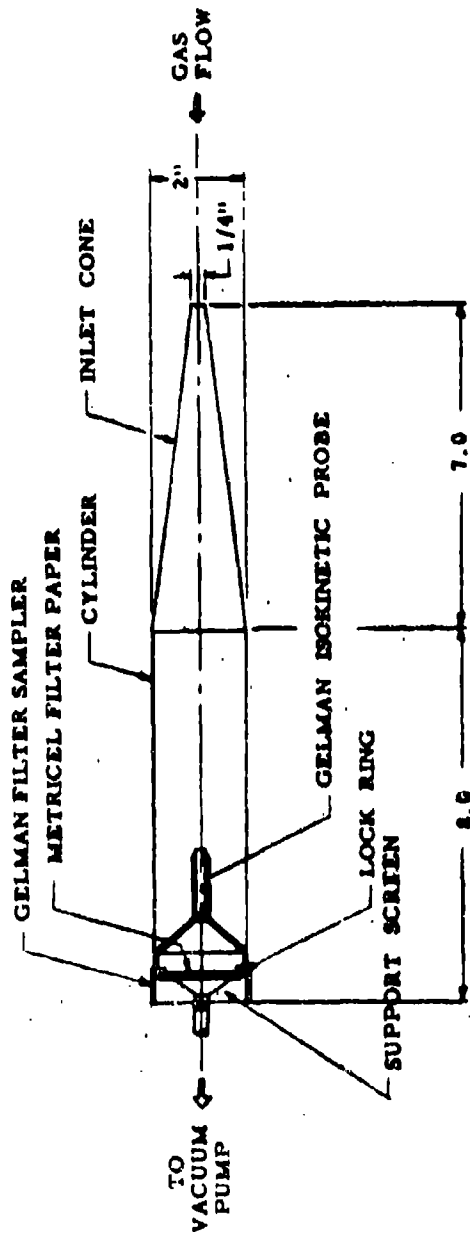


Figure 67. Filter Particle Sampler

CONFIDENTIAL

(This Page is Unclassified)

UNCLASSIFIED

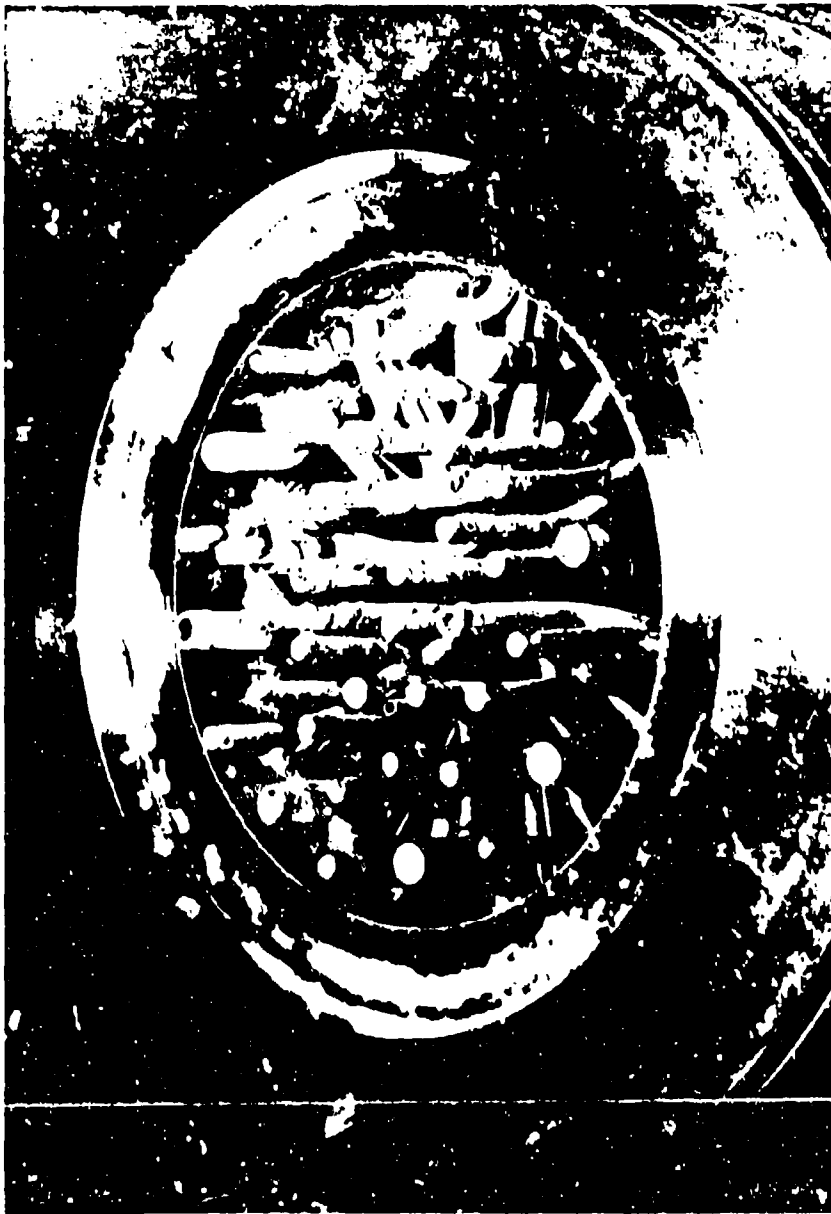


Figure 63. Tubular-Injector Face after Test 1.2-01-MC-004

UNCLASSIFIED

UNCLASSIFIED



Figure 69. Inlet Side of Tungsten Throat after Test 1.2-02-AC-04

UNCLASSIFIED

# CONFIDENTIAL

Report 10785-P, Phase II

## IV, B, Technical Discussion (cont.)

(U) It will be noted on Figure 68 that one side of the injector was more heavily coated with residual Alumizine than the other. The heavier coating was located on the tubes that were opposite the fuel inlet. The presence of the coating confirms that the shutdown sequence was fuel-rich. Purging with  $H_2$  was responsible for the nonsymmetric coating.

### a. Test 1.2-03-AAC-001

(U) The objectives of this test were (1) to determine performance (in terms of specific impulse efficiency) at 70 L\* with the improved Mod III vane-type injector design (see hardware section) at 0.7 MR and (2) to determine heat flux in the combustion chamber, throat entry section, and throat. The 0.7 mixture ratio was chosen as a starting point because it was representative of previous operation with the Mod I injector and would serve as a comparison between Mod III and Mod I injector performance.

(U) The engine sequence was essentially the same as that employed during the previous test series. Water was passed through the fuel injector during the 2.5-sec catalyst pack heating period as a coolant and purge. This flow was discontinued during staging to the full operating pressure. The catalyst heating period was controlled by a timer initiated by a pressure switch set to energize at 270 psia during the  $H_2O_2$  start sequence. The  $H_2O_2$  preheat flow rate was about 3.0 lbm/sec. Steady-state duration (time at  $P_c$  greater than 90% of desired) was established at 1.2 sec.

(U) The catalyst pack was similar to the pack employed on the previous test series except that five silver screens interleaved with five nickel-manganese screens were added to the front end of the pack to increase activity. This modification resulted from discussions with Mr. McCormick of FMC in which he indicated that their test results showed better pack starting

CONFIDENTIAL

(This page is Unclassified)

## IV, B, Technical Discussion (cont.)

characteristics with the higher silver loading. Ten nickel-manganese screens were removed from the downstream end of the pack to compensate for the additions to the front end. Pack dimensions and compression were identical.

(U) Only three of four heat-flux transducers were instrumented because of a limitation in the number of chromel-alumel instrumentation channels available in the test facility. Duplicate positions on each transducer (four pairs) were wired in parallel to obtain an average transient temperature profile for the corresponding depths.

(U) The thrust chamber is shown installed on the stand in Figure 70. Note the thermocouples emanating from heat-flux transducers.

(C) The test was satisfactory. A specific impulse efficiency of 91.3% at sea level was achieved at a mixture ratio of 0.67 and a chamber pressure of 3061 psia (Table VI). This represents an increase of 1.5 to 2.0% in performance over that previously achieved with the Mod I injector. Steady-state duration was 1.32 sec at greater than 90%  $P_c$ . Performance parameters are plotted in Figure 71.

(U) The injector face was damaged in the center and on the outer periphery. An examination of the records revealed that the fuel valve closing was delayed significantly beyond the time originally planned as indicated by the lag in LFTCV vs LOTCV in Figure 71. This caused a heavy surge of fuel through the chamber after the oxidizer valve had closed. The high-speed motion pictures of the test showed several pronounced pulses of flame from the chamber corresponding to the time period. It is probable that this uncontrolled burning was responsible for the damage to the injector. The vanes were subsequently removed from the injector, and the injector was converted to Mod II because of the immediate availability of Mod II-type vanes.

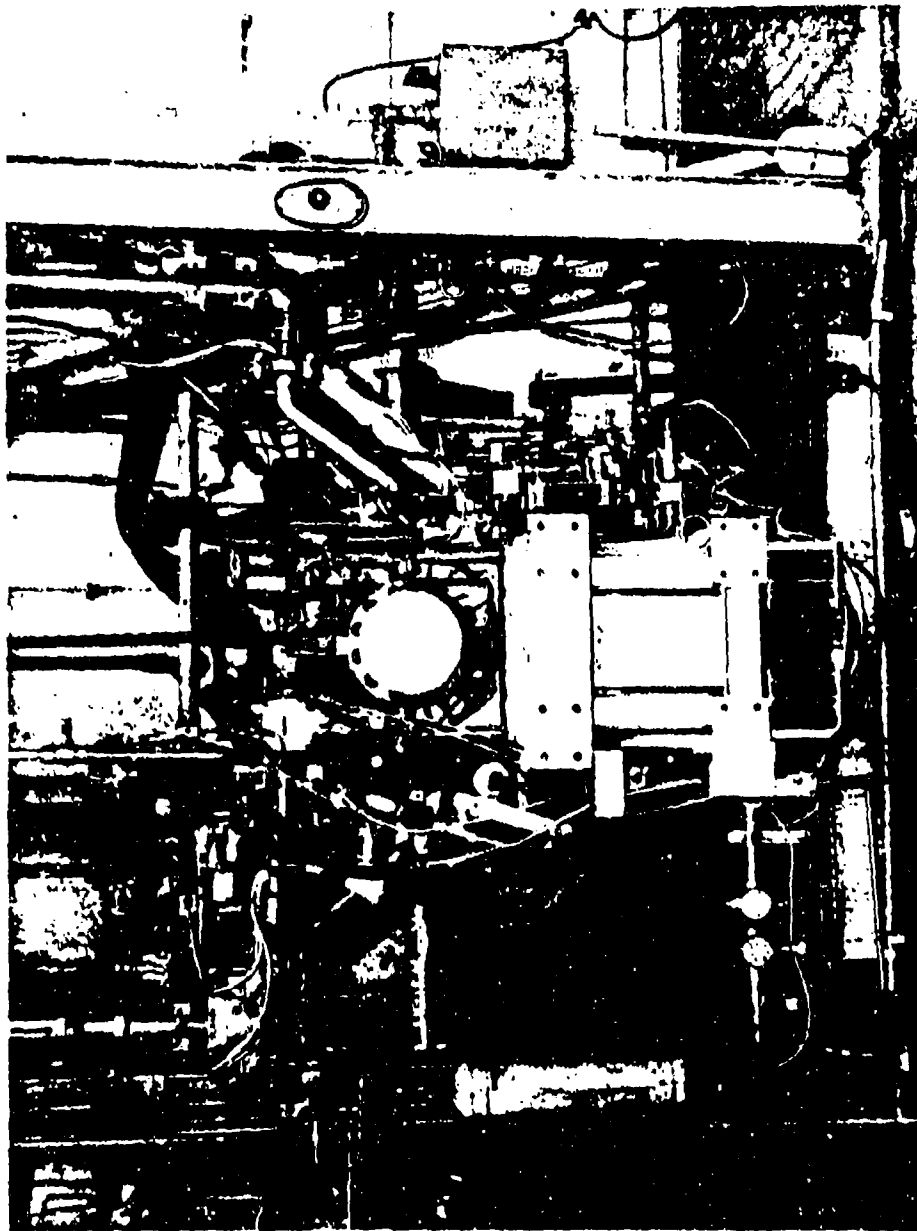
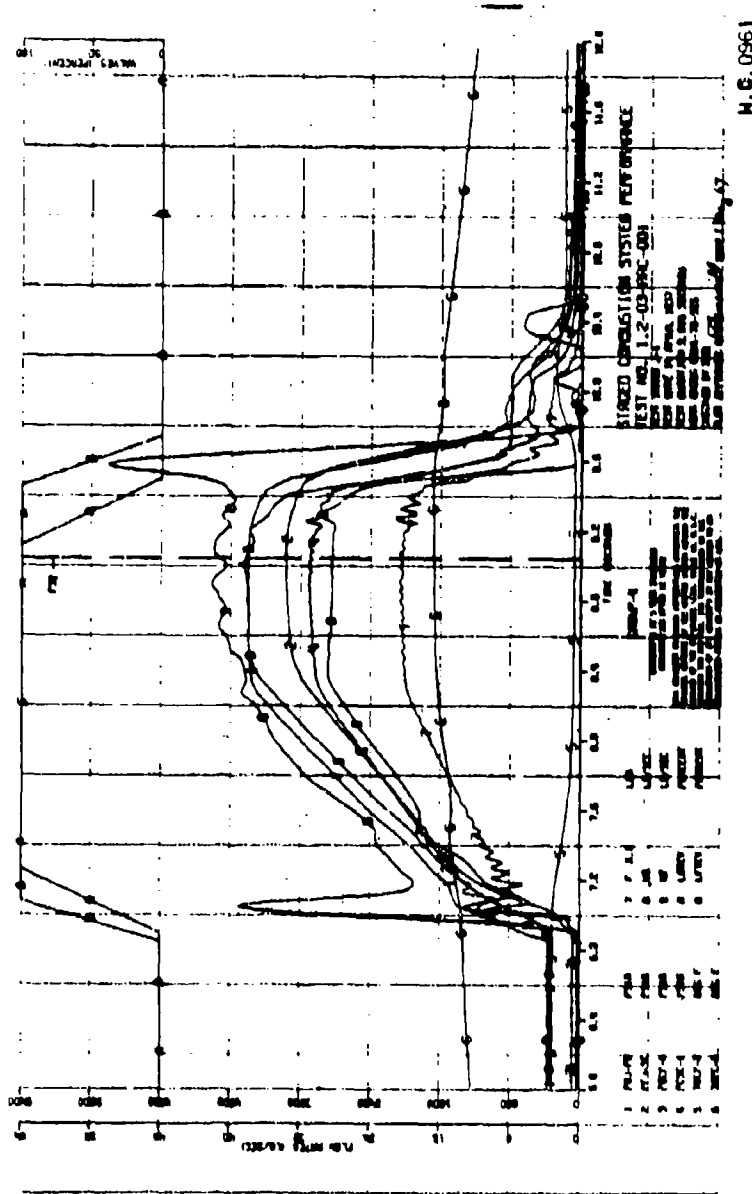


Figure 70. TCA Installation on Test Stand J-1, Test 1.2-03-AAC-001

PAGE 27

**CONFIDENTIAL**

(CLASSIFIED BY 210010100)



M.C. 0961

Figure 71. Staged-Combustion System Performance Test, Test 1.2-03-AAC-001 (u)

## IV, 3, Technical Discussion (cont.)

(U) Low-frequency oscillations at 70 cps occurred in the preburner. In addition, the temperature profile through the catalyst pack showed the highest temperature occurring deep in the pack at the No. 4 thermocouple position (TOCP-4 in Figure 72). Temperature at the No. 2 (TOCP-2) and 3 (TOCP-3) positions dropped during staging to full flow. Upon disassembly, it was discovered that the pack had been inverted during installation. The turbine simulator plate and preburner chamber were heavily coated with silver. It was concluded that the improper installation of the pack was responsible for the low-frequency oscillations. Fortunately, the oscillations were not reflected in the staged-combustion operation. The silver-bearing portion of the pack required subsequent replacement.

(U) The throat diameter did not change, but three fine-line longitudinal cracks were observed (see Figure 73). Cracking of tungsten throats is caused by recrystallization during cool-down and is normal based upon previous Polaris and Minuteman experience. Heavy deposits of Alumizine were found throughout the chamber, as shown in Figure 74, and some moderate grooving of the ablative material occurred. The exit cone was very smooth. The chamber, throat, and exit cone were considered to be refirable.

(U) All heat-flux transducer thermocouples, except one on the transducer located in the combustion chamber, functioned during the test. These data are presented and discussed in Section IV, B, 5.

## f. Test 1.2-03-AAC-002

(U) The objective of this test was to determine the performance of the 98%  $H_2O_2$ /Alumizine-43 system at 40-in. L\*. No heat-flux transducers were included on this test. A solid silver-infiltrated tungsten throat, with ablative chamber, entry section and exit cone was used. The injector

**CONFIDENTIAL**

(This page is Unclassified)



CONFIDENTIAL

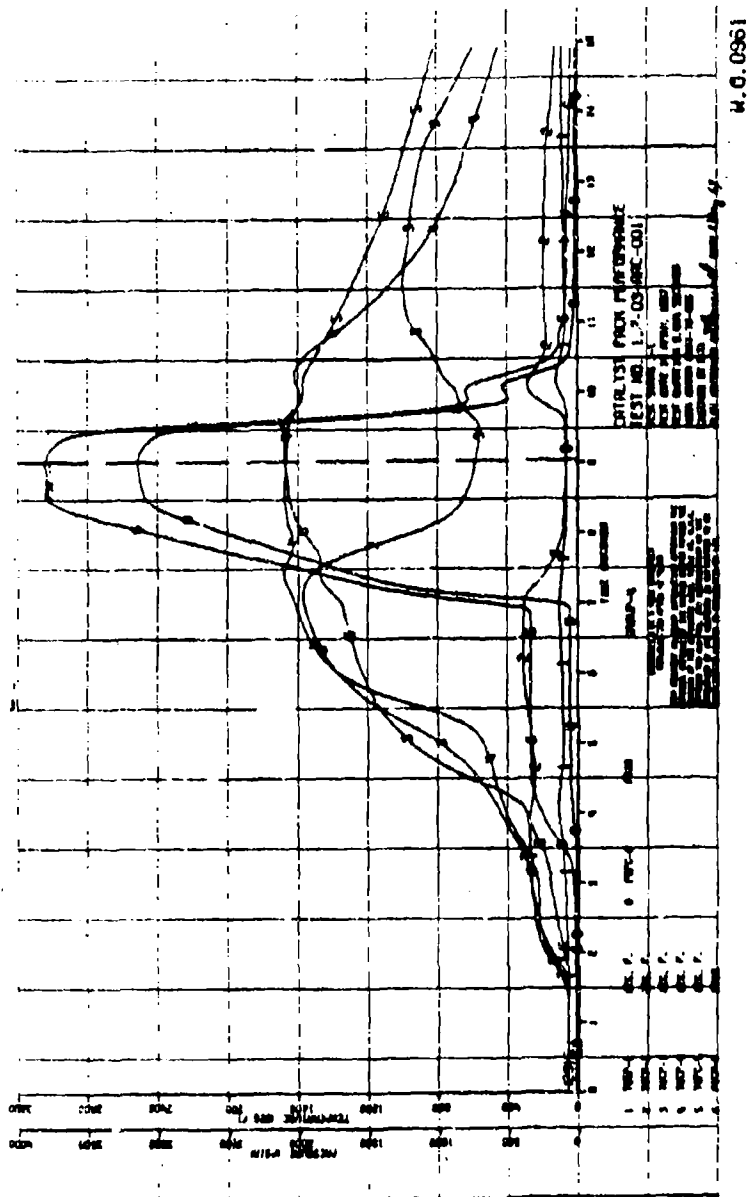


Figure 72. Catalyst Pack Performance, Test 1.2-03-AAC-001 (u)

CONFIDENTIAL

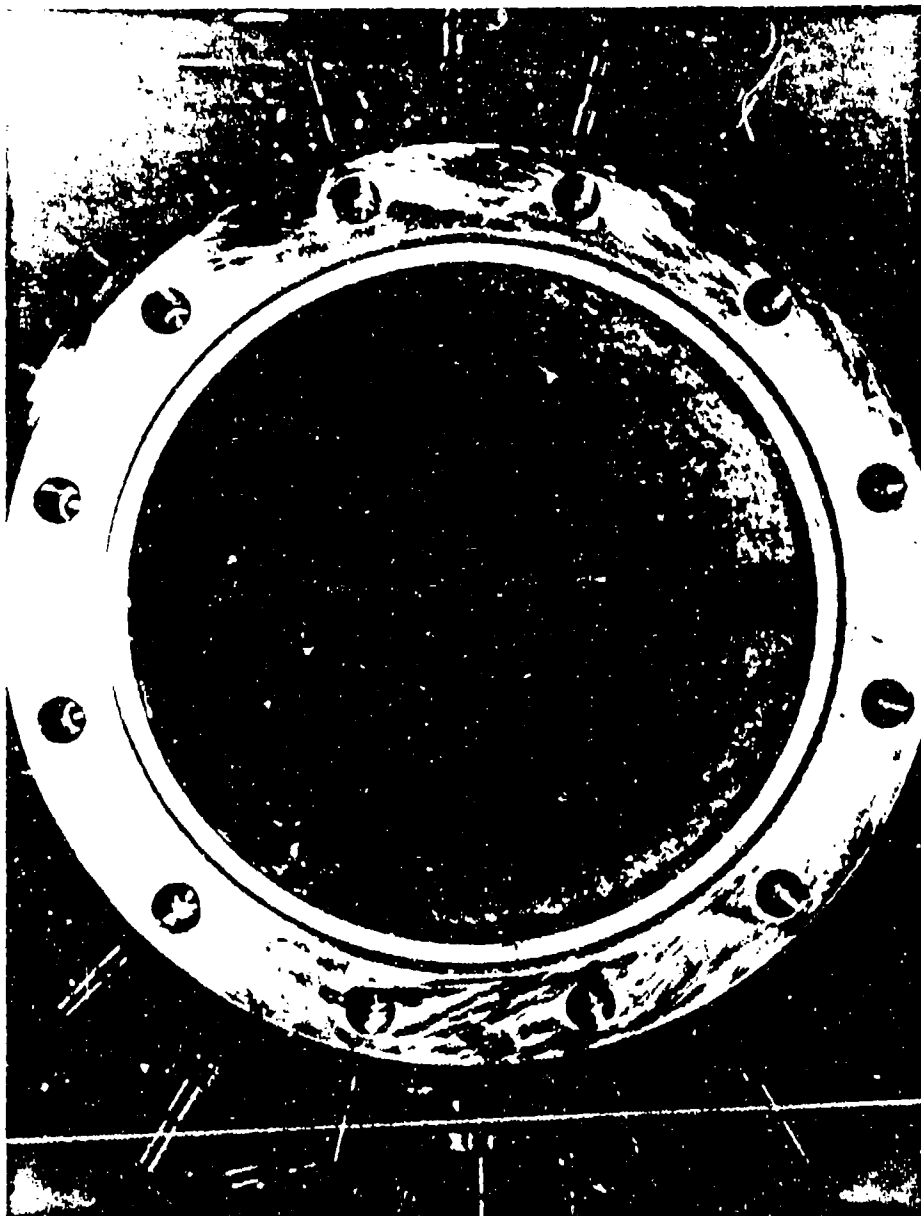
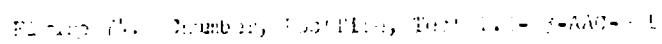


Figure 1. Thermal and Exit Cone, J. 10111111, Post 11-11-11-11-11

UNCLASSIFIED

$$x_0 = \frac{1}{\sqrt{2}}, \quad x_1 = \frac{1}{\sqrt{2}} e^{i\pi/4}, \quad x_2 = \frac{1}{\sqrt{2}} e^{i\pi/2} = i/\sqrt{2}$$


UNCLASSIFIED

# CONFIDENTIAL

Report 10785-P, Phase II

## IV, B, Technical Discussion (cont.)

used was the Mod III vane-type injector (SN 002). All other operating conditions were identical to Test 001. The catalyst pack from the initial test series was used in the preburner. The TCA is shown installed on the test stand in Figure 75.

(U) The sequence was altered to improve the valve phasing. The amount of fuel valve lead during the start transient and fuel valve lag during the shutdown were shortened. The fuel valve opening and closing times were also increased in an attempt to reduce the surge of fuel flow that had characteristically occurred on start transients in previous tests. In particular, see Trace 9 in F1, ire 71 on previous test.

(C) The test was satisfactory. A specific impulse efficiency of 93.1% at sea level was obtained at a mixture ratio of 0.72 and a chamber pressure of 3053 psia (Table VI). Performance parameters are plotted in Figure 76.

(U) The injector face received only minor tube damage and did not require extensive repair (Figure 77). However, because of delay in caustic cleaning the injector after the test, the Alumizine-43 residual material decomposed and plugged the tubes. The tubes were drilled to remove the hardened residue.

(U) Similar to Test -001, the throat dimensions did not change. Several hairline cracks appeared in the throat as in Test -001. The chamber ablative insert was moderately grooved. Alumizine deposits were considerably reduced compared with those resulting from Test -001, which indicated that the altered sequence was beneficial.

CONFIDENTIAL

CONFIDENTIAL

CONFIDENTIAL

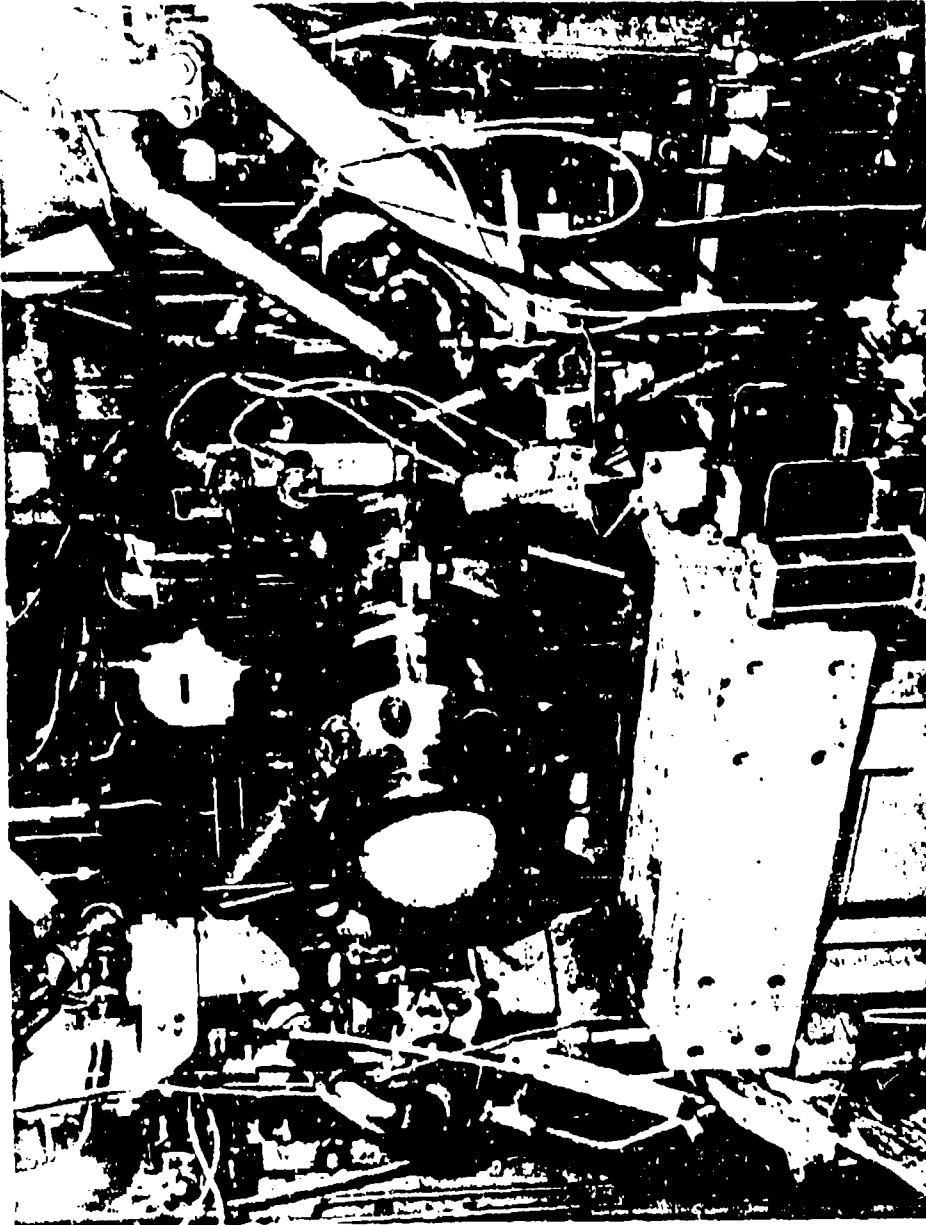


Figure 75. TCA Installation on Test Stand J-1, Test 1.2-03-AAC-002

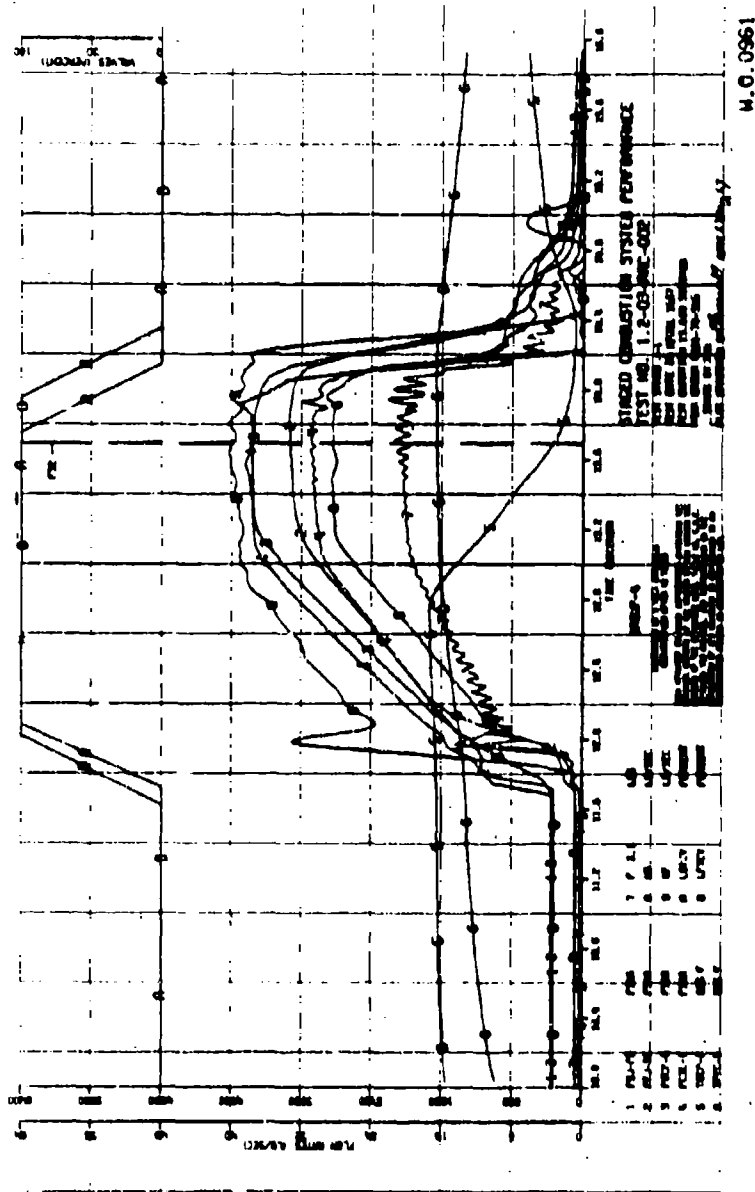
Page 104

CONFIDENTIAL

CONFIDENTIAL

CONFIDENTIAL

Report 10785-F, Phase II



M.O. 0961

Figure 76. Staged-Combustion System Performance Test 1.2-03-AAC-002 (u)

CONFIDENTIAL

CONFIDENTIAL

Report 1.2-03, Phase II

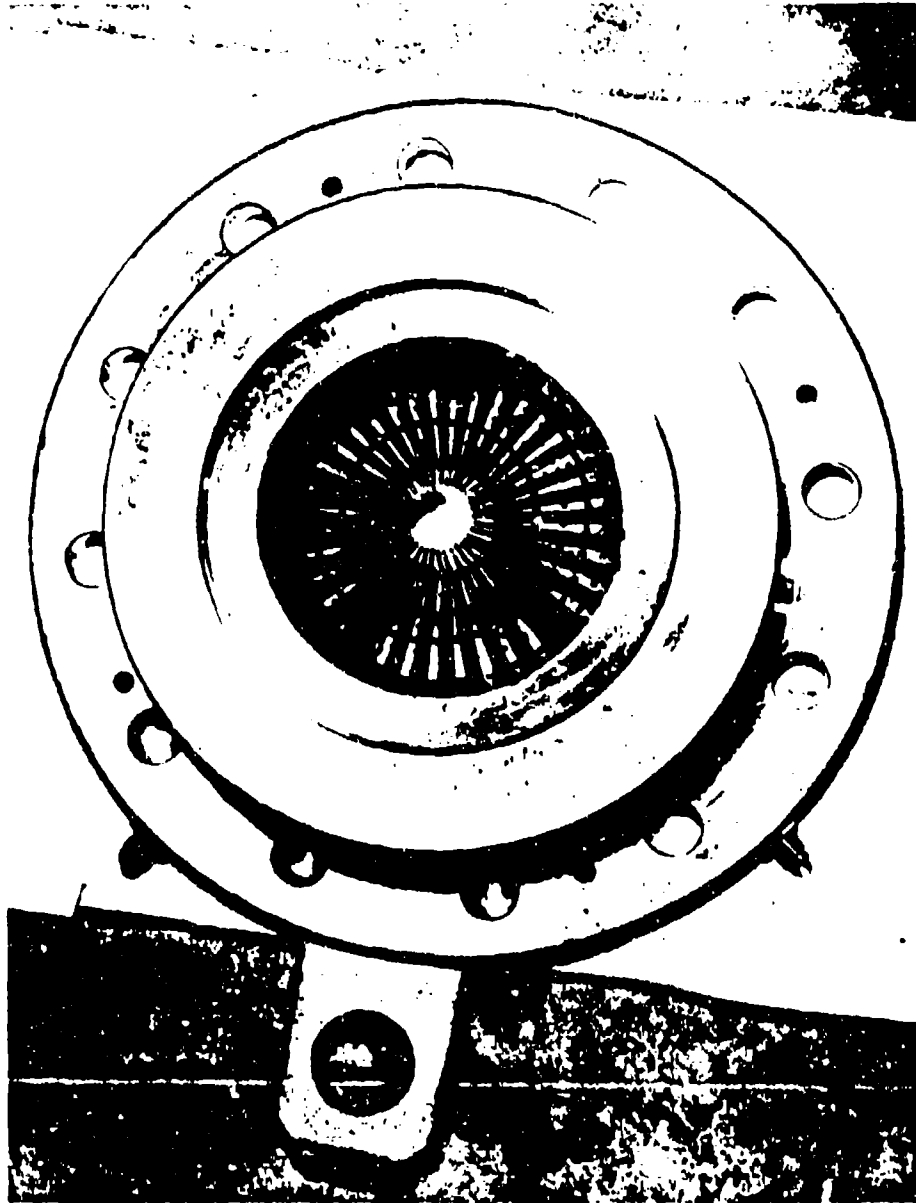


Figure 77. Mod III Vane Injector after Test 1.2-03-AAC-002

Page 106

CONFIDENTIAL

(This Page Is Unclassified)

# CONFIDENTIAL

Report 10785-F, Phase II

## IV. B. Technical Discussion (cont.)

(U) The preburner was slow in starting and dropped in pack temperature during steady state. This catalyst pack had been stored for 10 months and probably required rejuvenation. It contained three silver screens as opposed to eight screens in the pack used on Test -001. Figure 78 presents catalyst pack performance.

(U) Some low-frequency oscillations in the range of 800 to 1000 cps at amplitudes of less than 3% of steady state also occurred in the preburner on this test. These oscillations were random in nature, and an instability analysis did not indicate the existence of an organized low-frequency instability.

### g. Test 1.2-03-AAC-003

(U) The objectives of this test were (1) to determine performance at high MR with the 70 L\* configuration to further define the performance/MR map, and (2) to obtain transient heat-flux data. The chamber, throat, and exit cone had previously been fired on Test 1.2-03-AAC-001. The injector used was the Mod II vane injector, SN 001. The pretest setup appeared similar to that shown in Figure 70.

(U) The use of this injector on this test influenced the choice of the mixture ratio. The injector had been flow tested with water, and the data revealed that the injector had a higher pressure drop than the Mod III injector. Therefore, a low MR was selected for this test condition. Also, it should be noted that the injector was operated with only 26 of the 36 center tubes. The other ten had been removed and sealed, because they had become filled with brase material during the furnace brazing cycle.

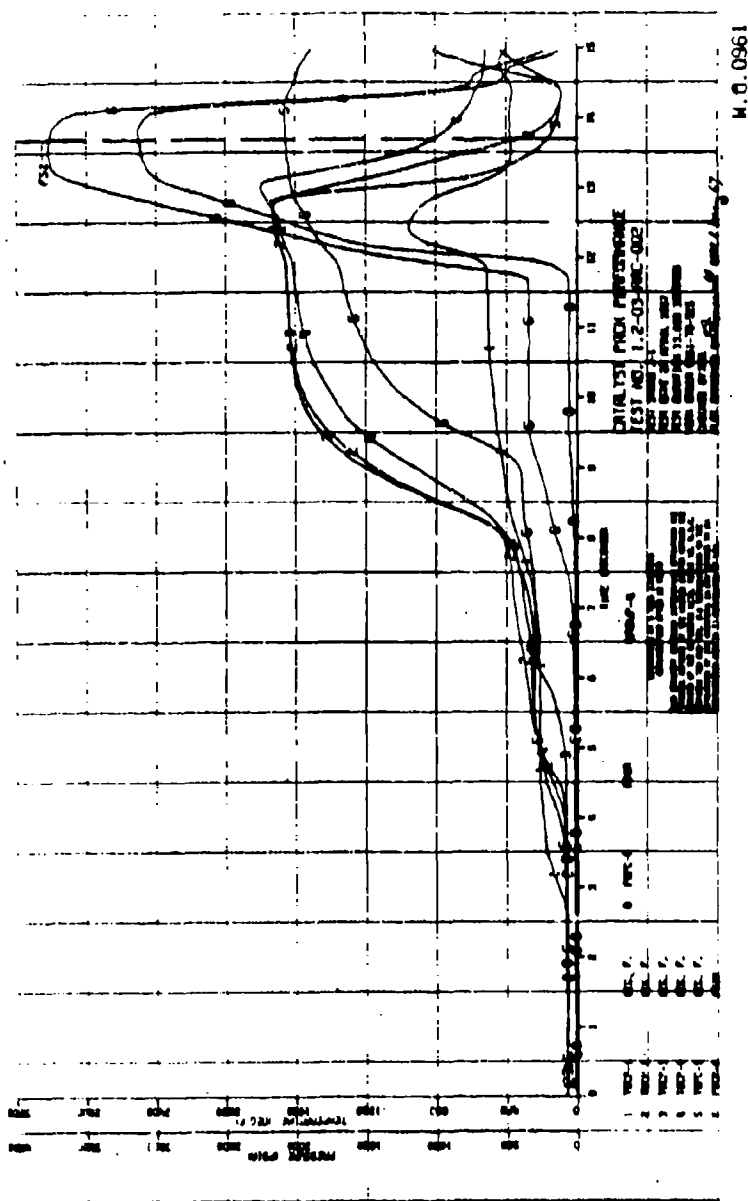
CONFIDENTIAL

(This page is Unclassified)



CONFIDENTIAL

Report 10785-F, Phase II



M. O. 0961

Figure 78. Catalyst Pack Performance, Test 1.2-03-AAC-002 (u)

CONFIDENTIAL

## 11. B, Technical Discussion (cont.)

(U) The catalyst pack, used on Test 1.2-03-AAC-001, was rebuilt, and the silver screens were replaced with one 6.50-in.-dia silver screen and seven 4.58-in.-dia silver screens. (Additional 6.50-in.-dia silver screens were not available.) The latter screens were sized for use in the high-throughput pack; however, they were usable in this pack by placing them in the pack in a clover-leaf pattern. All of the silver screens were interleaved with 12-mesh nickel-manganese screens.

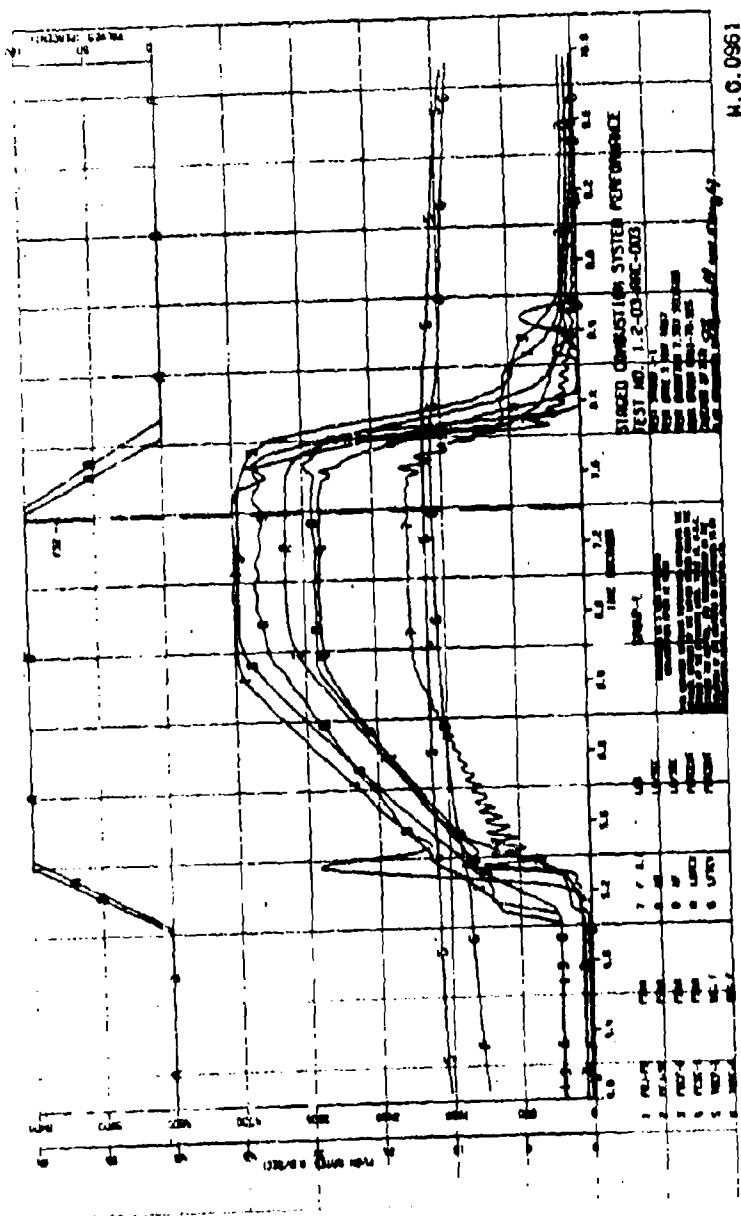
(U) Adjustments to further reduce fuel valve opening lead and fuel valve closing lag on startup and shutdown, respectively, were again made in the engine sequence. The planned fuel valve lead on startup for this test was 30 millisecc compared to 100 millisecc on the previous test. Changes were desirable in this sequence to reduce the surge of fuel flow during staging. The fuel valve lag on shutdown was reduced from 200 millisecc experienced on the previous test to 100 millisecc on this test--again, for the same reasons as mentioned on Test 1.2-03-AAC-002. The thrust chamber pressure switch setting, which starts the steady-state timer, was increased from 2270 to 2500 to obtain a longer steady-state period. This had the net effect of increasing the steady-state period by about 200 millisecc. In addition, the fuel injector water-coolant purge flow was increased from about 1.25 lbm/sec to 4.2 lbm/sec during start and was substituted for the 1500-psig nitrogen purge of the injector during shutdown. This was done to cool the injector vanes and tubes more effectively.

(C) The test was satisfactory. A specific impulse efficiency of 92.7% at sea level was obtained at a mixture ratio of 0.83 and a chamber pressure of 3007 psia. Performance parameters are shown in Figure 79.

(U) Examination of oscillograph and high-frequency tape records revealed that all pressures were smooth and stable with no evidence

CONFIDENTIAL

Report 10785-F, Phase II



M. G. 0961

Figure 79. Staged-Combustion System Performance, Test 1.2-03-AAC-003 (u)

CONFIDENTIAL

UNCLASSIFIED

Report 10701-7, Phase II

IV, B, Technical Discussion (cont.)

of oscillatory behavior. This is significant because it shows that high performance may be achieved with this propellant system under extremely stable steady-state conditions.

(U) The injector received minor erosion on its periphery at a location between 6 and 9 o'clock (with respect to the handling lug at 12 o'clock). See Figure 80. Four small peripheral tubes adjacent to the wall, three center tubes, and three tubes in various other locations were eroded. These were subsequently intentionally sealed. The remaining tubes were found to be generally free of residue. Thus, the water purge on shutdown was found to be beneficial and was used for the remaining tests.

(U) The ablative liner in the chamber in addition to ablative loss of material was also grooved over the first 4-1/2 in. just below the injector. The heat-flux transducer in the combustion chamber was exposed from 1/8 to 3/16 in. because of the loss of phenolic adjacent to it. Some grooving of the throat also occurred in the cracked areas which were observed after the first firing (see Figure 81). The exit cone eroded to a depth of 1/8 to 1/4 in. just downstream of the throat. This behavior is typical of what has also been observed in solid motor firings.

(U) The catalyst pack started about one sec after initiation of start and functioned smoothly throughout the test. A maximum steady-state temperature of 1805°F was recorded by the TOCP-2 thermocouple position. Figure 82 shows the temperature profiles.

(U) The four temperature profiles recorded in the throat heat-flux transducer appeared to be valid and are presented below. Only two apparently valid temperature profiles were obtained in the nozzle entry and nozzle exit transducers, respectively.

UNCLASSIFIED

UNCLASSIFIED

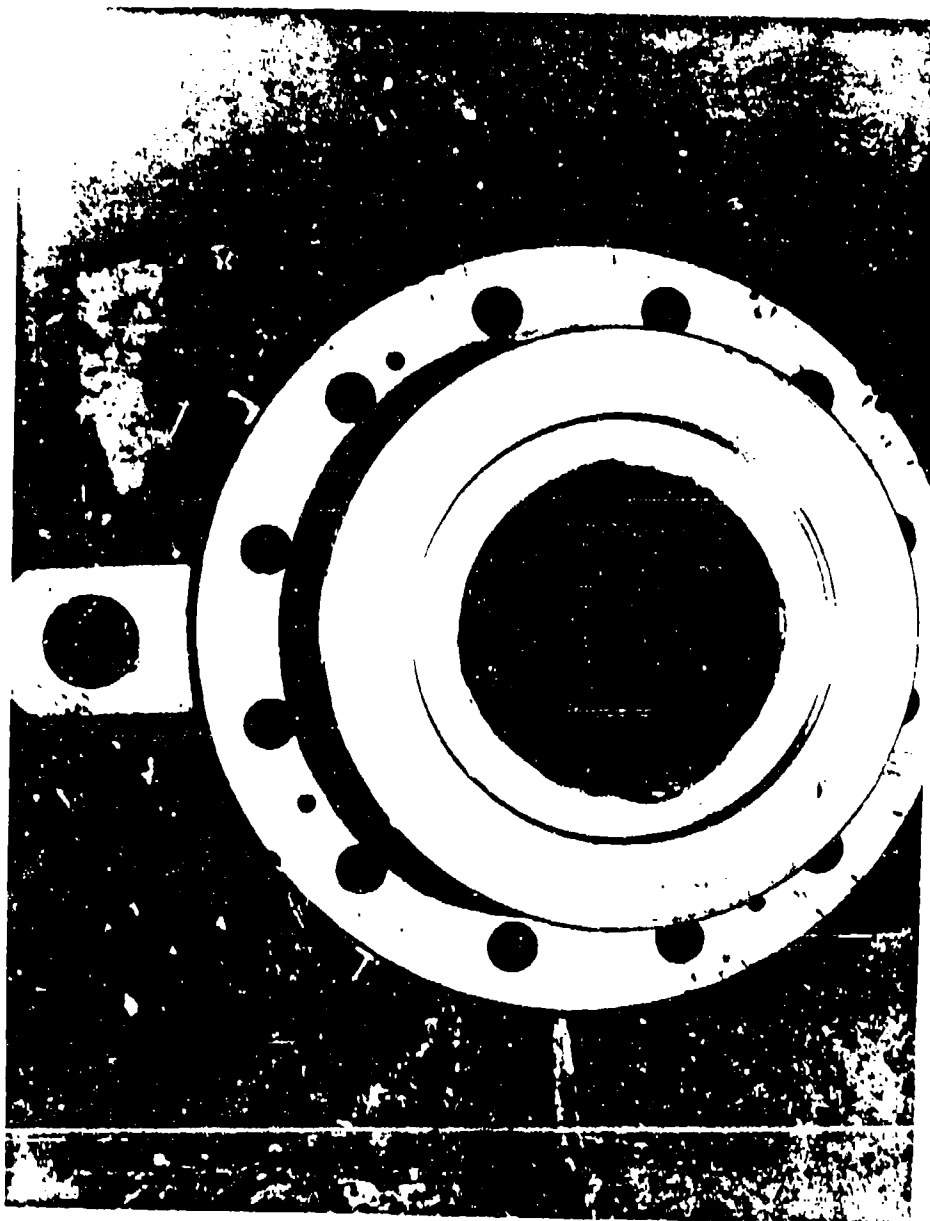


Figure 1. M-11 Case Subject to other Test 100-0-000000

UNCLASSIFIED

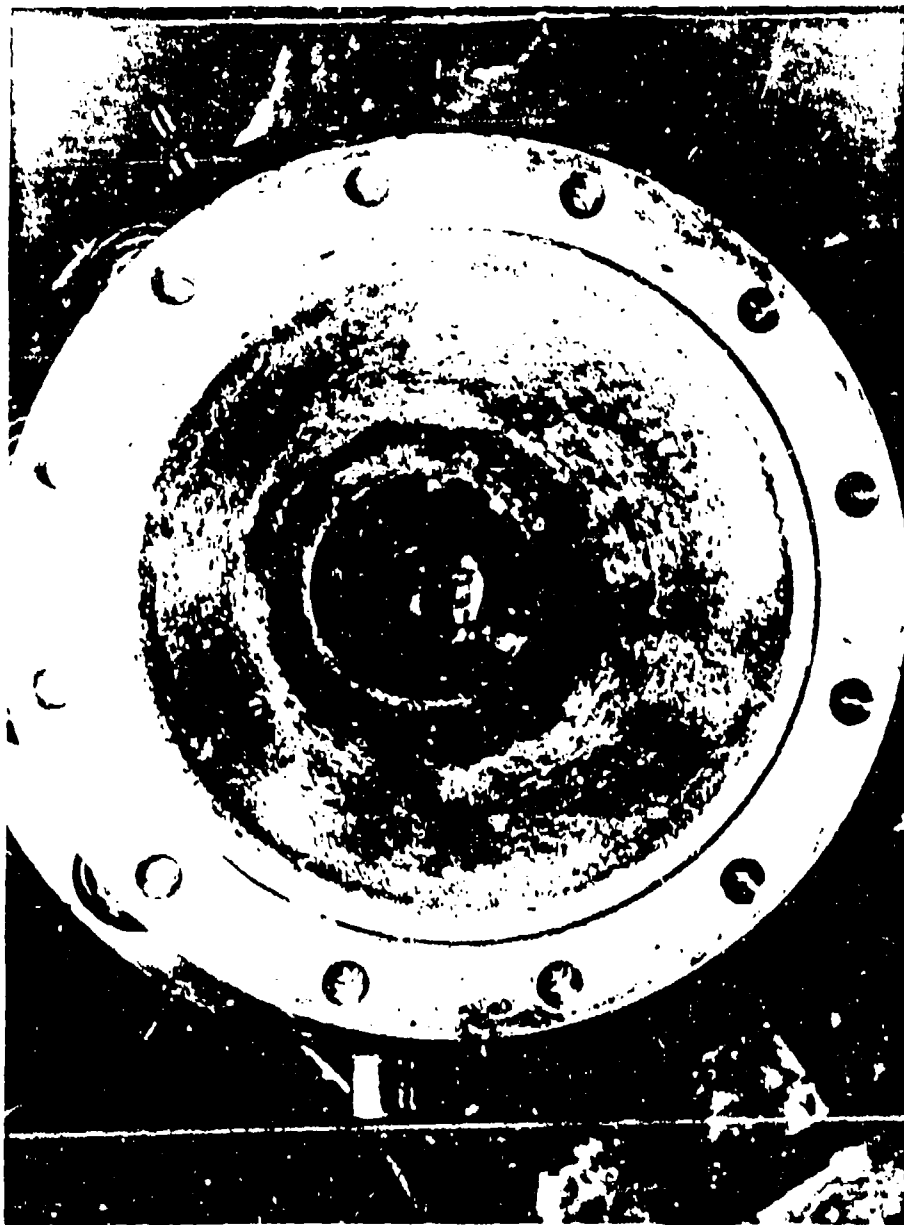


Figure 41. Throat and Exit Cone, F stub, Test 1-2-03-AAC-003

CONFIDENTIAL



## IV, B, Technical Discussion (cont.)

## h. Tests 1.2-03-AAC-004 and -005

(U) The objective of these tests was to determine performance at or near 0.5 MR with the 40-in. L<sup>2</sup> chamber. The chamber, entry section, throat, exit cone, and injector were the same hardware as that used on Test 1.2-03-AAC-002. During repair of the injector three tubes were intentionally sealed, because drills were broken off in them during a drilling operation to remove residual, decomposed Alumizine. However, it is felt this would not significantly affect performance. The test setup was similar to that shown in Figure 75.

(U) Test 1.2-03-AAC-004 was terminated during the start transient by a malfunction detection circuit. The fuel valve failed to open beyond 20%. The sequence requires that a valve switch on the fuel valve make contact before a valve switch on the main oxidizer valve. (Note: Prior to this test, during the sequence check, the fuel valve was inadvertently opened with Alumizine-43 present under pressure just upstream of the valve. Alumizine-43 passed into the injector and the injector had to be removed and cleaned.)

(U) The malfunctioning fuel valve was replaced, and Test 1.2-03-AAC-005 conducted. No changes in sequence were made.

(U) Injector operation on this test was unsatisfactory and produced questionable performance data. The two vanes at a location of 6 o'clock clogged with residual, decomposed Alumizine and eroded during the firing. The clogging caused a nonsymmetrical distribution of the flame front and resulted in erosion of several adjacent vanes, as well. The unbalance in the oxidizer flow had resulted in a significant mixture ratio distribution loss. For this injector design, under normal injector operation, this loss is considered negligible.



# UNCLASSIFIED

Report 10735-F, Phase II

## IV, B, Technical Discussion (cont.)

(U) The performance data were, however, analyzed by the performance interaction technique and are discussed in a succeeding section. Test parameters are shown in Figure 83 and Table VI.

(U) There are two possible causes for this occurrence. Either or both of the causes could have been responsible for plugging of the vanes, and subsequently, the burnout. They were:

(U) (1) A leak was found in the fuel select valve, (17) a 2-in. ball valve about 2 feet upstream of the fuel valve; this was evidenced by a thick (1/8 in.) coating of decomposed Alumizine that was found on the inner surface of the line between the two valves. It is considered that the select valve began leaking prior to Test 1.2-03-AAC-003. A system hydraulic analysis was made and tended to verify this hypothesis. It was found on Test 1.2-03-AAC-003 that pressure drop in the fuel system between the intensifier outlet and the fuel manifold increased slightly, from that observed in Test 002. This indicated that decomposed Alumizine had reduced the line area. During the start transient, chips of dried Alumizine could have been carried into the injector and caused the blocking of the two vanes. Note: The line between the two valves is normally purged with nitrogen during prefire check of fuel valve sequencing.

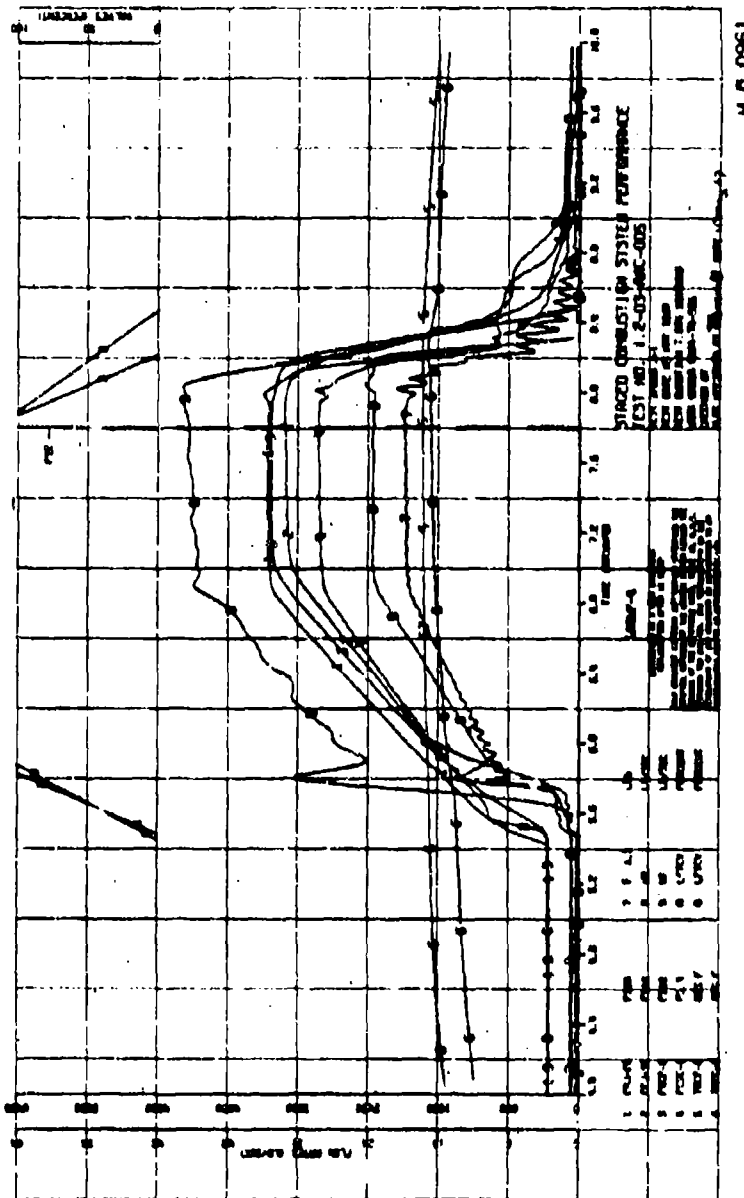
(U) (2) Alumizine could have entered the injector manifold during the partial opening of the fuel valve during Test 1.2-03-AAC-004 and flowed to the bottom of the manifold (6 o'clock). There it may have remained and dried through evaporation of the hydrazine component while preparations were being made to conduct Test 1.2-03-AAC-005. This test was conducted about 4 hr after Test 1.2-03-AAC-004.

(17) The purpose of the fuel select valve is to keep the line from the intensifier to the valve filled with Alumizine, thus minimizing cleaning between tests and permitting prefire sequencing of the fuel valve.

UNCLASSIFIED

CONFIDENTIAL

Report 10785-F, Phase II



M.O. 0961

Figure 83. Staged-Combustion System Performance, Test 1.2-03-MAC-005 (u)

CONFIDENTIAL

# CONFIDENTIAL

Report 10785-F, Phase II

## IV, 8, Technical Discussion (cont.)

(U) The catalyst pack functioned satisfactorily on both tests. Catalyst pack performance for Test 1.2-03-AAC-005 is shown in Figure 84.

(U) The injector was removed, and all the vanes were replaced.

### 1. Tests 1.2-03-AAC-006 and -007

(U) The objective of these tests was to determine performance of 98%  $H_2O_2$ /Aluminate-43 at or near a 0.5 MR with a chamber characteristic length ( $L^*$ ) of 70 in. The chamber, entry section, throat, and exit cone had not been previously tested. The throat assembly was instrumented with three heat-flux transducers. These data were supplementary to those collected during Tests 1.2-03-AAC-001 and -003. These data would be used to calculate heat flux if the data from those tests were found to be inadequate.

(U) A new (rebuilt) Mod III injector was used for the tests.

(U) The sequences were the same as those used for Test 1.2-03-AAC-005. The test setup was similar to that shown in Figure 70.

(U) Test 1.2-03-AAC-006 was discontinued after about 20 sec of  $H_2O_2$  bleed (preheat) when the engine failed to stage to operating flows and pressure. A postfire inspection indicated that the thrust chamber pressure switch, which initiates the catalyst preheat timer, had not actuated. The test records indicated that the switch was set to actuate at a pressure above that achieved during the preheat flow condition.

(C) The thrust chamber pressure switch was reset, and Test 1.2-03-AAC-007 was then conducted. This test was satisfactory, and a specific impulse efficiency of 91.1% was obtained at a 0.49 MR and a chamber pressure of 2977 psia. Performance data are plotted on Figure 85.

CONFIDENTIAL

CONFIDENTIAL

Report 10785-F, Phase II

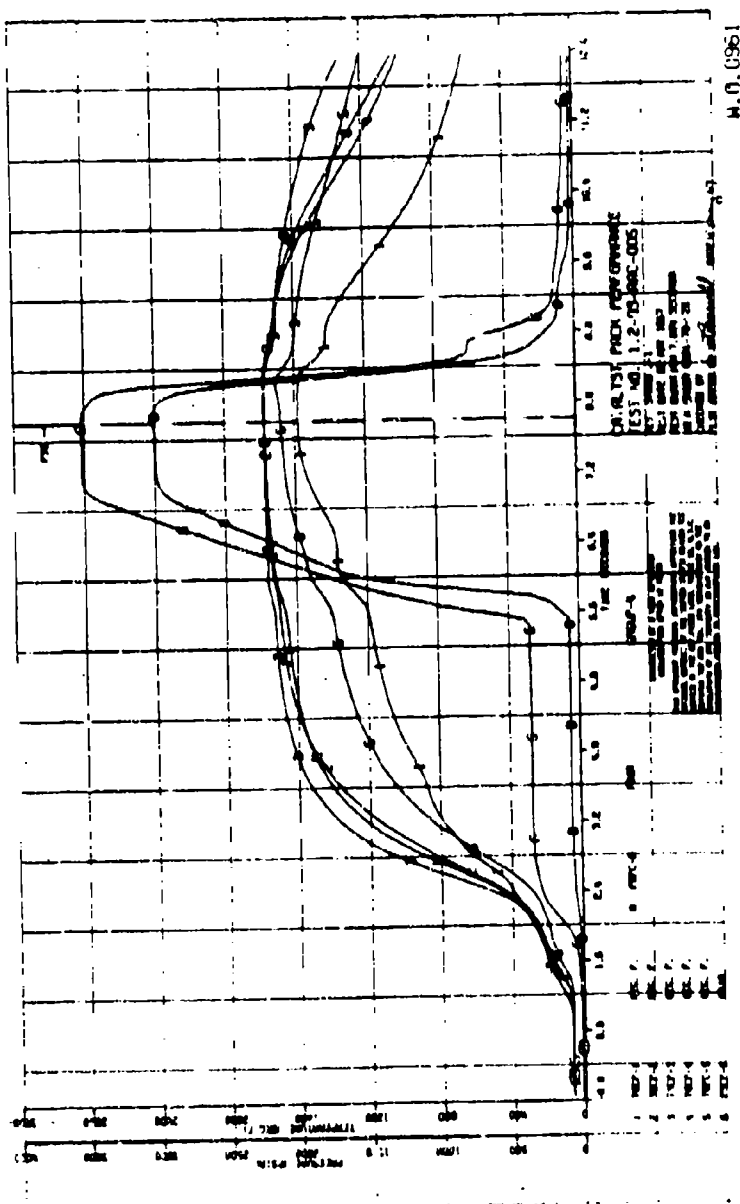


Figure 34. Catalyst Pack Performance Test 1.2-03-AMC-005 (u)

CONFIDENTIAL

**CONFIDENTIAL**

Report 10785-F, Phase II

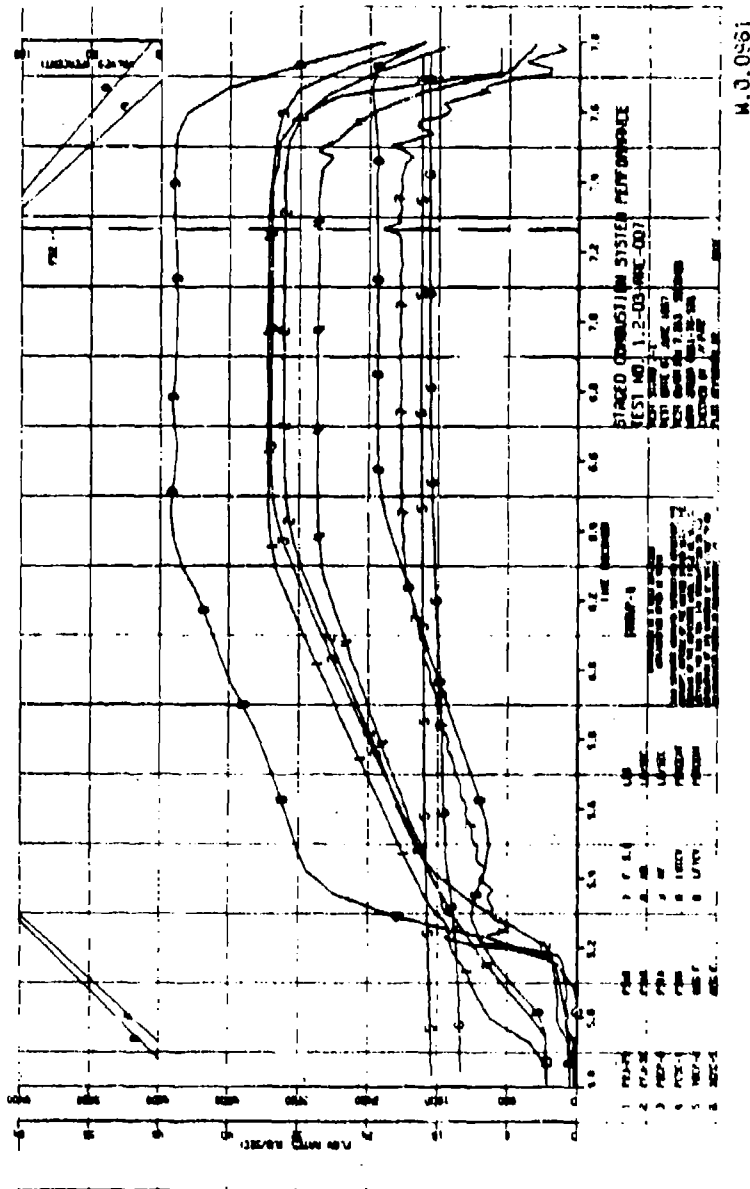


Figure 85. Staged-Combustion System Performance, Test 1.2-03-fac-007, (u)

**CONFIDENTIAL**

# CONFIDENTIAL

Report 10785-F, Phase II

## IV, B, Technical Discussion (cont.)

(U) Exhaust particles were collected on this test with the same device used on Test 1.2-02-AAC-004. Analysis of these particles is reported in Section IV,B,4.

(U) A postfire inspection of the hardware indicated that the outer periphery of the injector was eroded over about 60% of its circumference and 14 of the outer tubes at the wall were burned. Several other tubes on the main face of the injector were damaged. Some plugging was also evident. It was determined that 16 of the 36 vanes would have to be replaced to restore the injector to refirable condition.

(U) The ablative liner material on the chamber, exit cone, and throat entry section were in excellent condition, similar to Figures 73 and 74. The throat retained its original dimensions, but again showed some hairline cracks. Such cracks have been observed after each test with a new throat. In general, the ablative and tungsten hardware was in excellent condition after the first exposure to the combustion environment.

(U) Again, as in the previous valid tests, all oscillograph pressure traces were smooth and stable, and no abnormal oscillatory behavior was evident.

(U) The catalyst pack started quickly and functioned smoothly throughout the test. A peak steady-state temperature of 1812°F was achieved at the No. 3 thermocouple position. The pack parameters are shown in Figure 86.

(U) Three valid temperature profiles were obtained on each of the heat-flux transducers. These data were held for possible calculation of heat flux. The temperature profiles are shown in Figures 87, 88 and 89.

CONFIDENTIAL

(This page is Unclassified)

CONFIDENTIAL

Report 10,39-4, Phase II

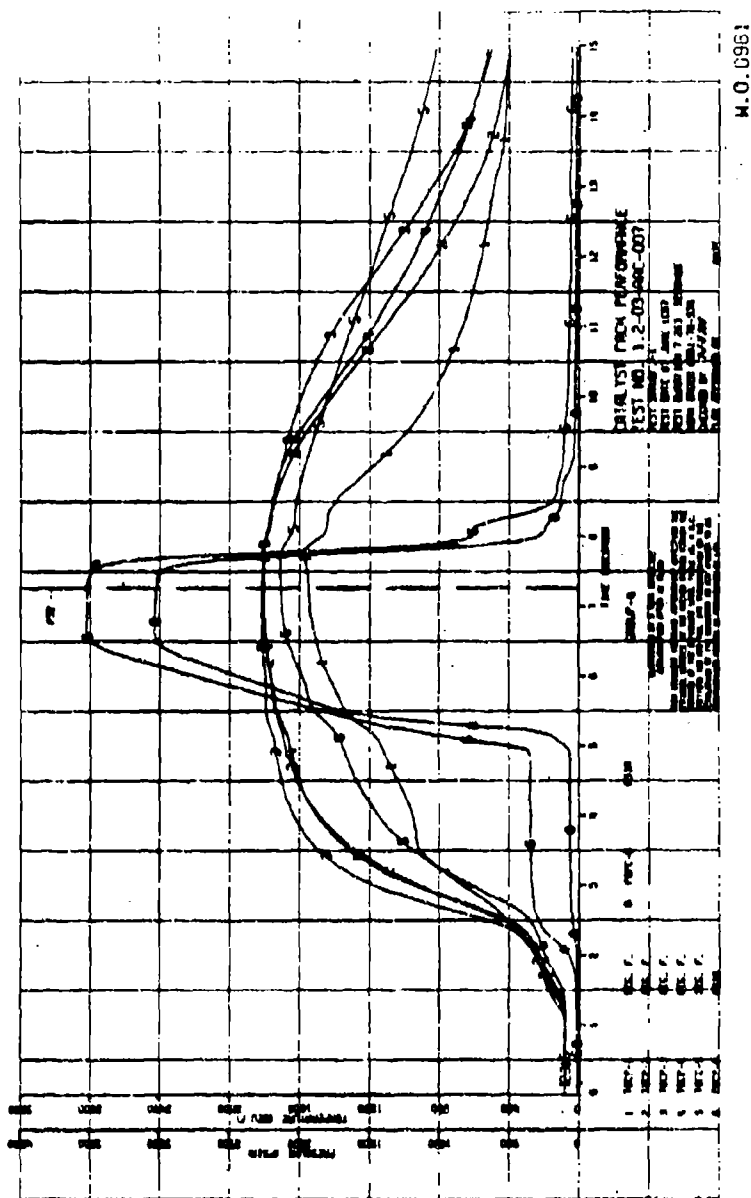


Figure 56. Catalyst Pack Performance, Test 1.2-03-AAC-007 (u)

CONFIDENTIAL

CONFIDENTIAL

Report 10785-F, Phase II

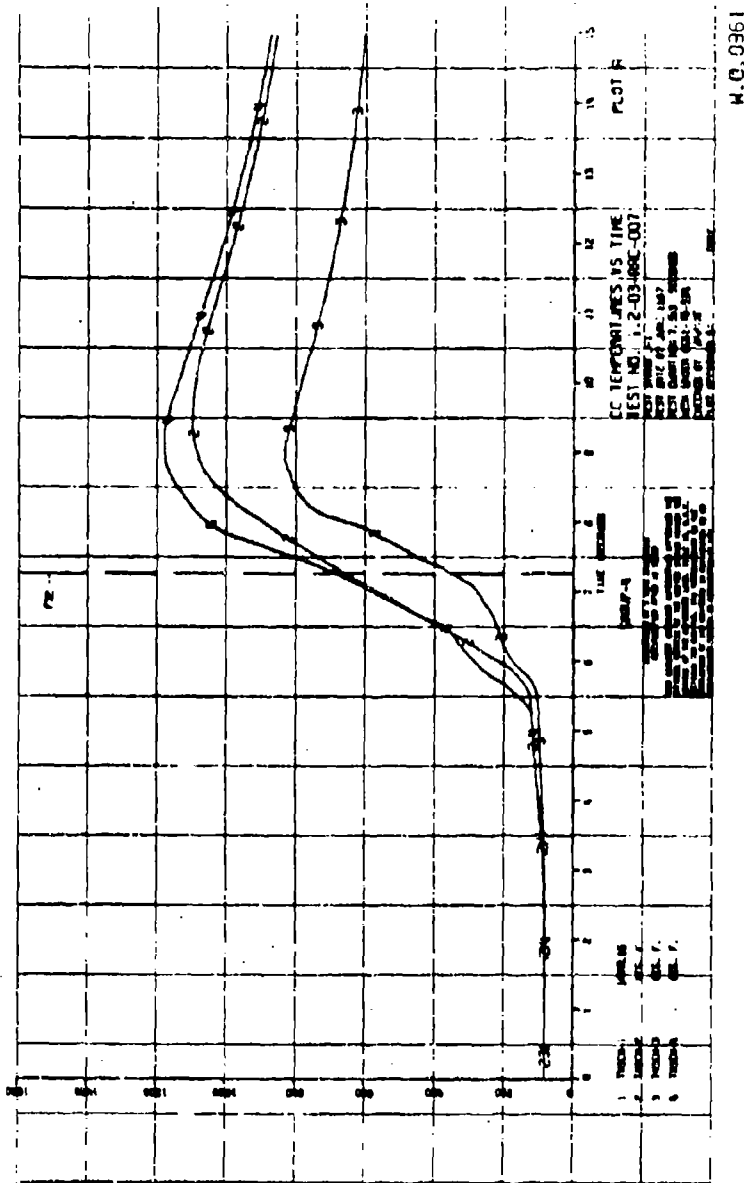


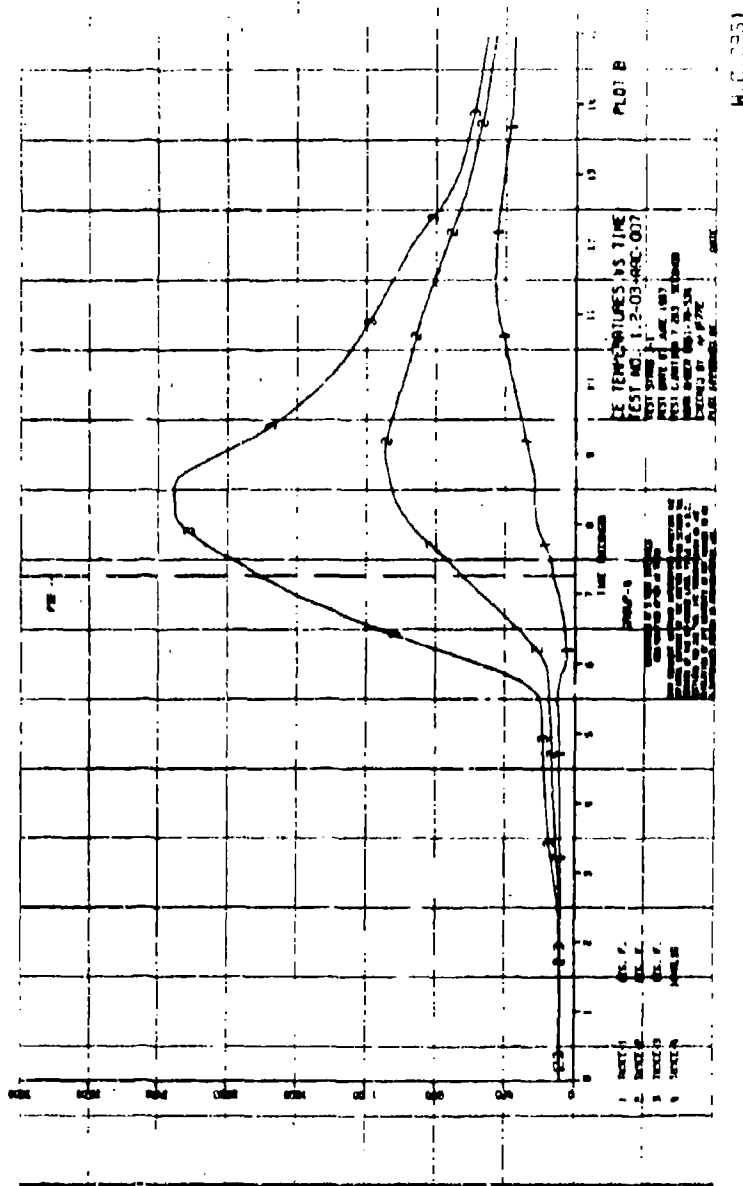
Figure 87. CC (Combustion Chamber) Heat-Flux Transducer Temperature, Test 1.2-03-AAC-007 (u)

CONFIDENTIAL



CONFIDENTIAL

Report 10755-P, Phase II



W.C. 0351

Figure 88. CE (Throat Entry Section) Heat-Flux Transducer Temperatures, Test 1.2-03-49C-007 (u)

CONFIDENTIAL

CONFIDENTIAL

Report 10785-F, Phase II

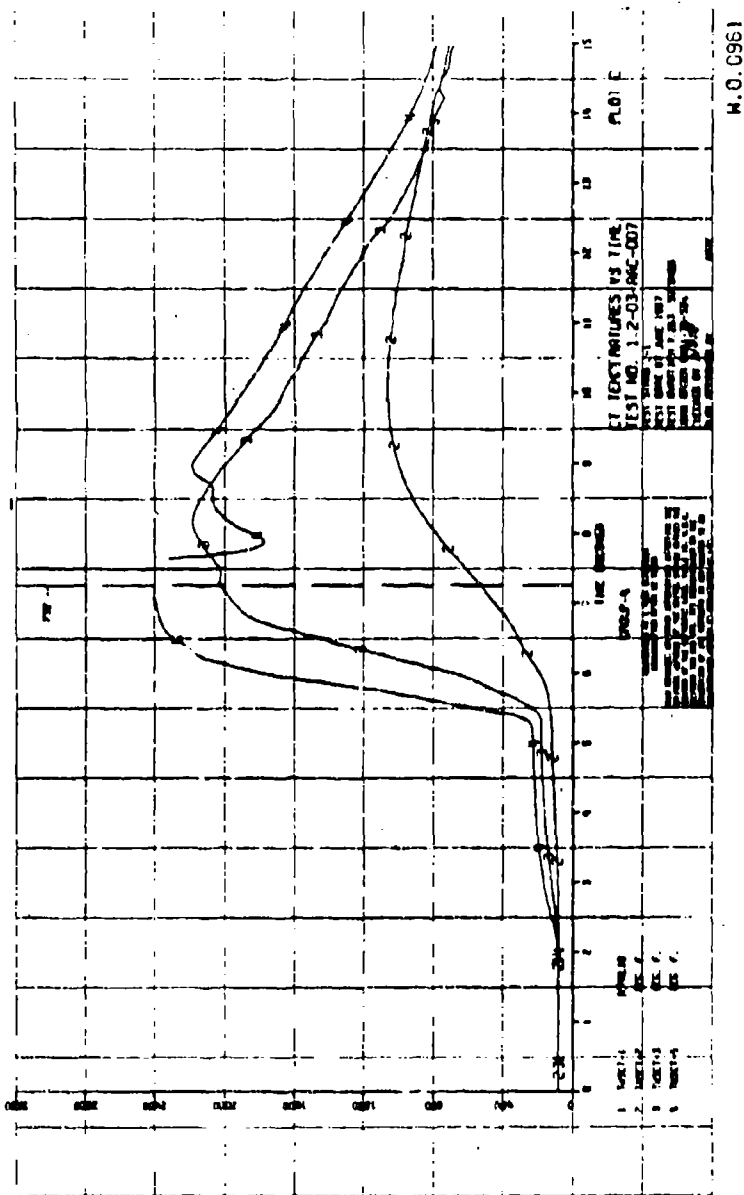


Figure 89. CT (Throat) Heat-Flux Transducer Temperatures, Test 1.2-03-AAC-007 (u)

CONFIDENTIAL

CONFIDENTIAL

Report 10785-7, Phase II

IV. D. Technical Discussion (cont.)

J. Test 1.2-03-AAC-008

(U) The objective of this test was to determine the performance of 90%  $H_2O_2$  with Alumizine-43 at a mixture ratio of about 0.5. The chamber (40 L\*), entry cone, throat, and exit cone were new. The injector used was the modified Mod II vaned injector previously used on Test 1.2-03-AAC-003. Twenty of the 36 small center tubes and 7 of the other injector face tubes had been plugged. It was realized that these modifications might reduce performance; however, this injector was the only vaned unit remaining for test. No heat-flux transducers were instrumented; and the engine sequence was the same as that used for Test 007. The catalyst pack was the same as that used during all tests since Test 1.2-03-AAC-003.

(C) The test was satisfactory, and a specific impulse efficiency of 88.8% at an MR of 0.55 and chamber pressure of 3,068 psia was achieved. The relatively low  $I_p$  efficiency, compared to results with 98%  $H_2O_2$ , was probably a result of unbalanced MR distribution across the injector face caused by the elimination of some of the injector tubes. Performance parameters are shown in Figure 90.

(U) The injector eroded on the periphery at a location of 9 o'clock (with respect to the handling lug). The injector was immersed in hot caustic immediately following the test, and the procedure cleaned virtually all the tubes. Only two tubes required drilling to remove decomposed Alumizine. Several eroded tubes were intentionally sealed prior to Test 1.2-03-AAC-009.

(U) Minor erosion of the throat occurred, on this test, as a result of unequal MR distribution and oxidizer-rich zones occurring across the face of the injector. However, it was difficult to measure the extent of throat erosion, since there was a heavy deposit of  $Al_2O_3$  and residual Alumizine

CONFIDENTIAL

CONFIDENTIAL

Report 10737-F, Phase II

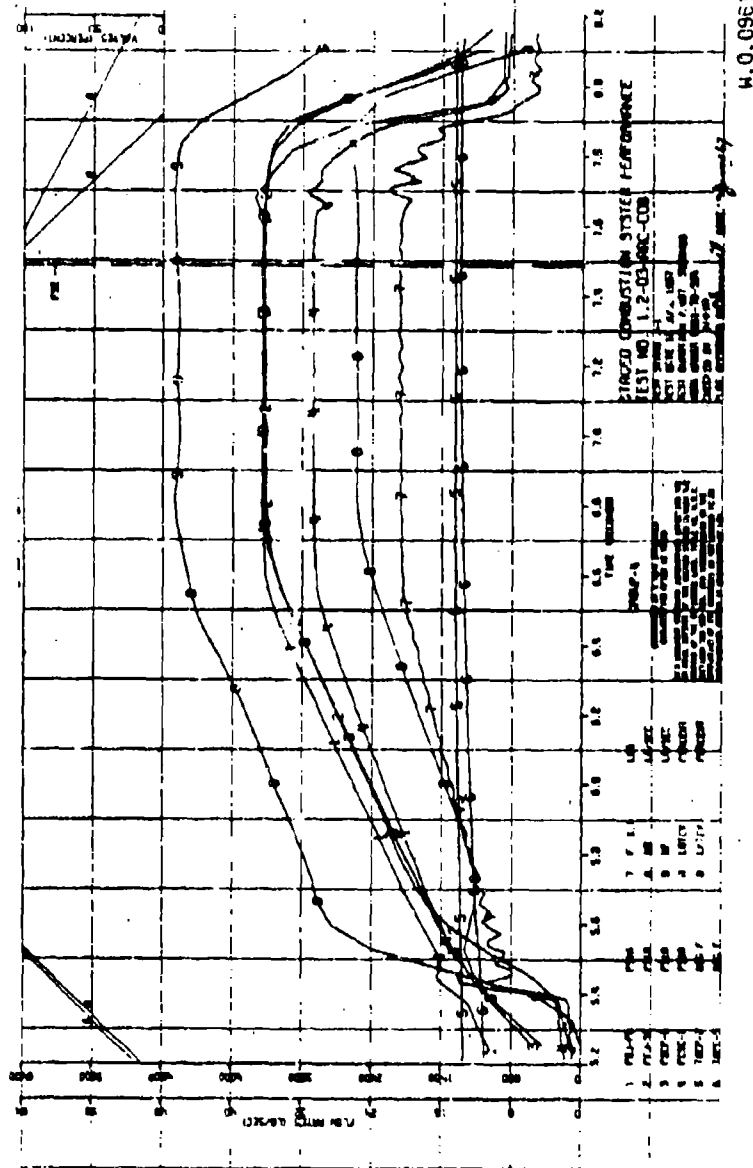


Figure 90. Staged-Combustion System Performance, Test 1.2-03-AAC-003 (u)

CONFIDENTIAL

**CONFIDENTIAL**

Report 10785-F, Phase II

IV, B, Technical Discussion (cont.)

on the throat after the test. All the ablative components were in good condition.

(U) All pressure traces were smooth and there was no evidence of unstable behavior. The catalyst pack started easily (Figure 1) with the lower concentration peroxide. The maximum decomposition temperature in the pack was 1450°F.

k. Test 1.2-03-AAC-009

(U) This test had the objective of determining performance of 90%  $H_2O_2$  with Alumizine-43 at or near an MR of 0.7. The hardware used on this test was the same as that used on Test 1.2-03-AAC-008.

(U) The test was terminated during the start transient by a malfunction detection circuit. Thus, no steady-state data were obtained. A thrust chamber pressure switch preset to initiate the steady-state period at about 2600 psia chamber pressure failed to actuate within the prescribed time limitation of 1.4 sec after staging began. In all other respects, the test appeared to proceed as programmed.

(U) The injector eroded more extensively on the periphery, and tubes and vanes were badly plugged. Repeated exposure to the hot caustic solution was unsuccessful in cleaning the injector. Major repair would have been required to permit retesting of this injector.

l. Test 1.2-03-AAC-010

(U) This test had the same objectives as the previous test, i.e., performance of 90%  $H_2O_2$ /Alumizine-43 at about 0.7 MR. The 70 L\* chamber

**CONFIDENTIAL**

(This page is Unclassified)

CONFIDENTIAL

Report 10785-F, Phase II

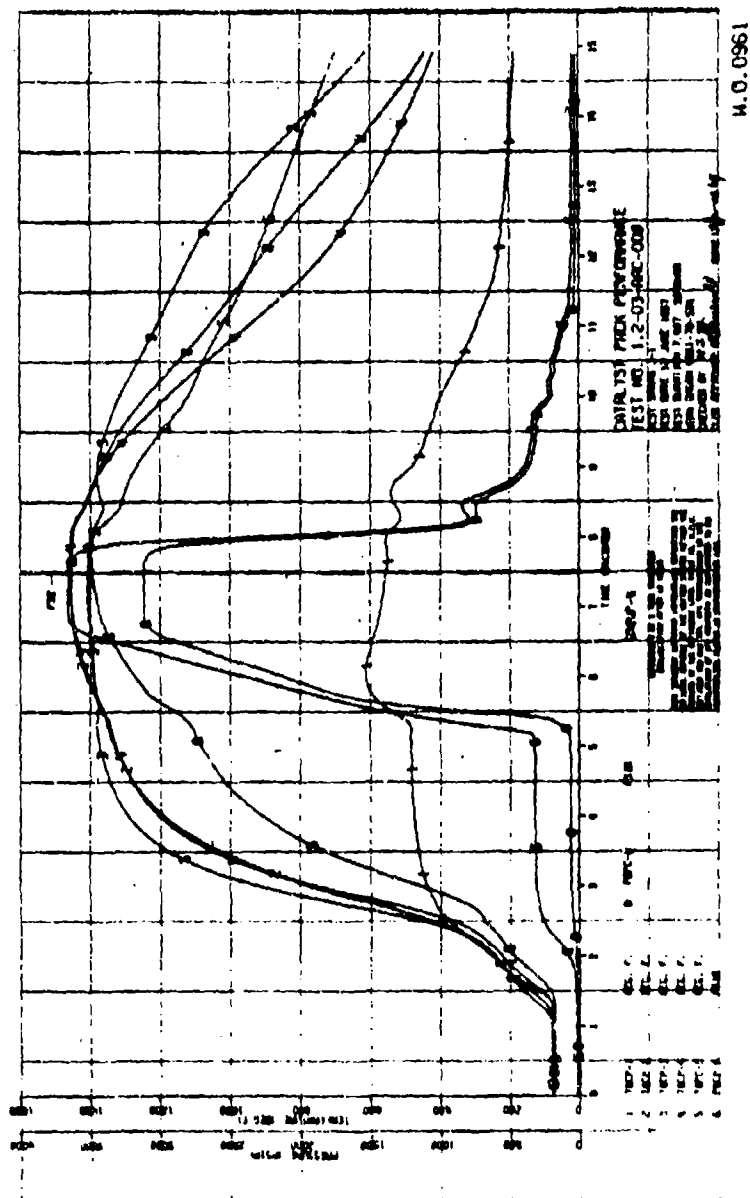


Figure 91. Catalyst Pack Performance, Test 1.2-03-AAC-008 (u)

CONFIDENTIAL

# CONFIDENTIAL

Report 10785-F, Phase I.

## IV, B, Technical Discussion (cont.)

and the tungsten throat remaining from Test 1.2-03-AAC-007 were used. The injector was a modification of the tubular injector (44 tubes) which had been used on Test 1.2-02-AAC-004. Three to four weld beads had been added to the outlet of each tube to obtain greater Alumizine-43 surface exposure and dispersion as it is injected into the chamber.

(U) The thrust chamber pressure switch was reset to a lower actuation pressure of 2,350 psia to ensure initiation of the steady-state period (reset to a value of 1.4 sec).

(C) The test was satisfactory and a specific impulse efficiency of 90.0% was achieved at MR of 0.76 and a chamber pressure of 2,737 psia. The chamber pressure was somewhat lower (Figure 92) on this test because the pressure drops across the fuel injector and the turbine simulator were higher than anticipated.

(C) A postfire inspection of the hardware indicated that the injector was in perfect condition (Figure 93). However, the throat was severely eroded in a manner similar to that experienced during the first test of the injector. It should be noted, though, that performance of this injector increased dramatically from 84.3% on Test 1.2-02-AAC-004 to 90.0% on this test simply by increasing Alumizine dispersion. The throat damage further substantiates the need for fine injection and the elimination of streaks to operate with tungsten.

(U) The catalyst pack started smoothly and functioned perfectly, and produced a maximum decomposition temperature of 1489°F. The gas temperature downstream of the pack was 1433°F (Figure 94).

CONFIDENTIAL

CONFIDENTIAL

Report 10785-F, Phase II

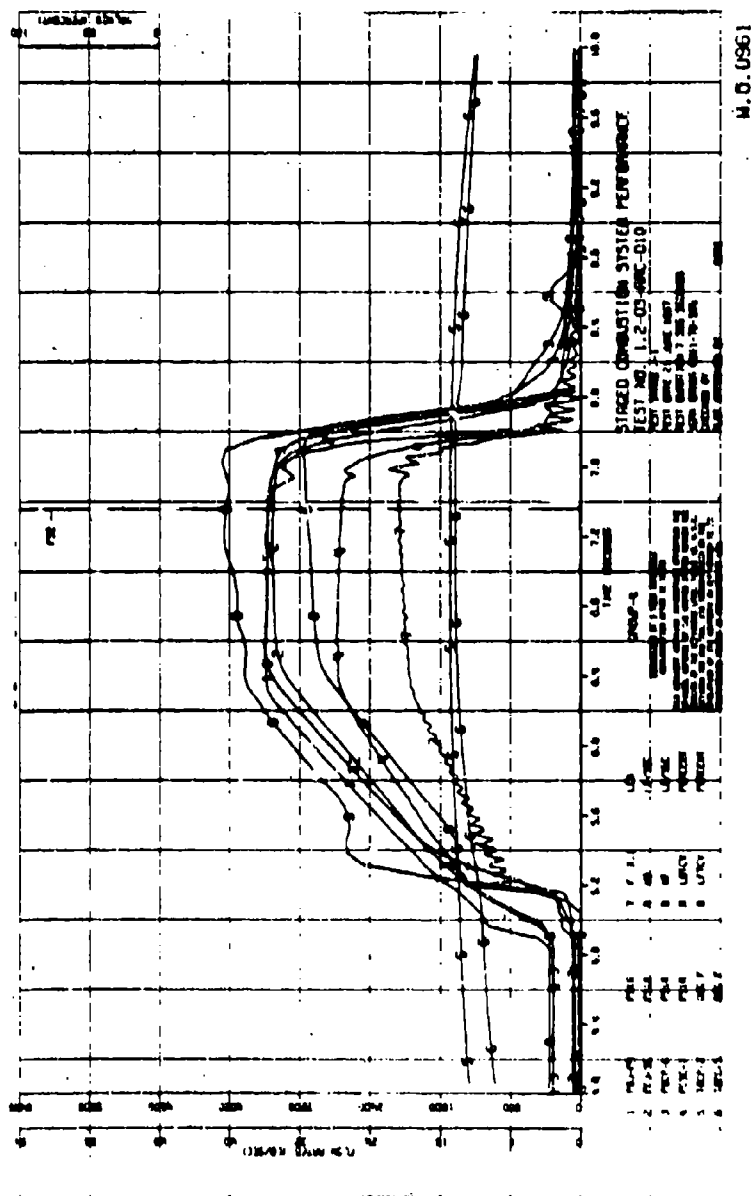


Figure 92. Staged-Combustion System Performance, Test 1.2-03-AAC-010 (u)

CONFIDENTIAL



CONFIDENTIAL

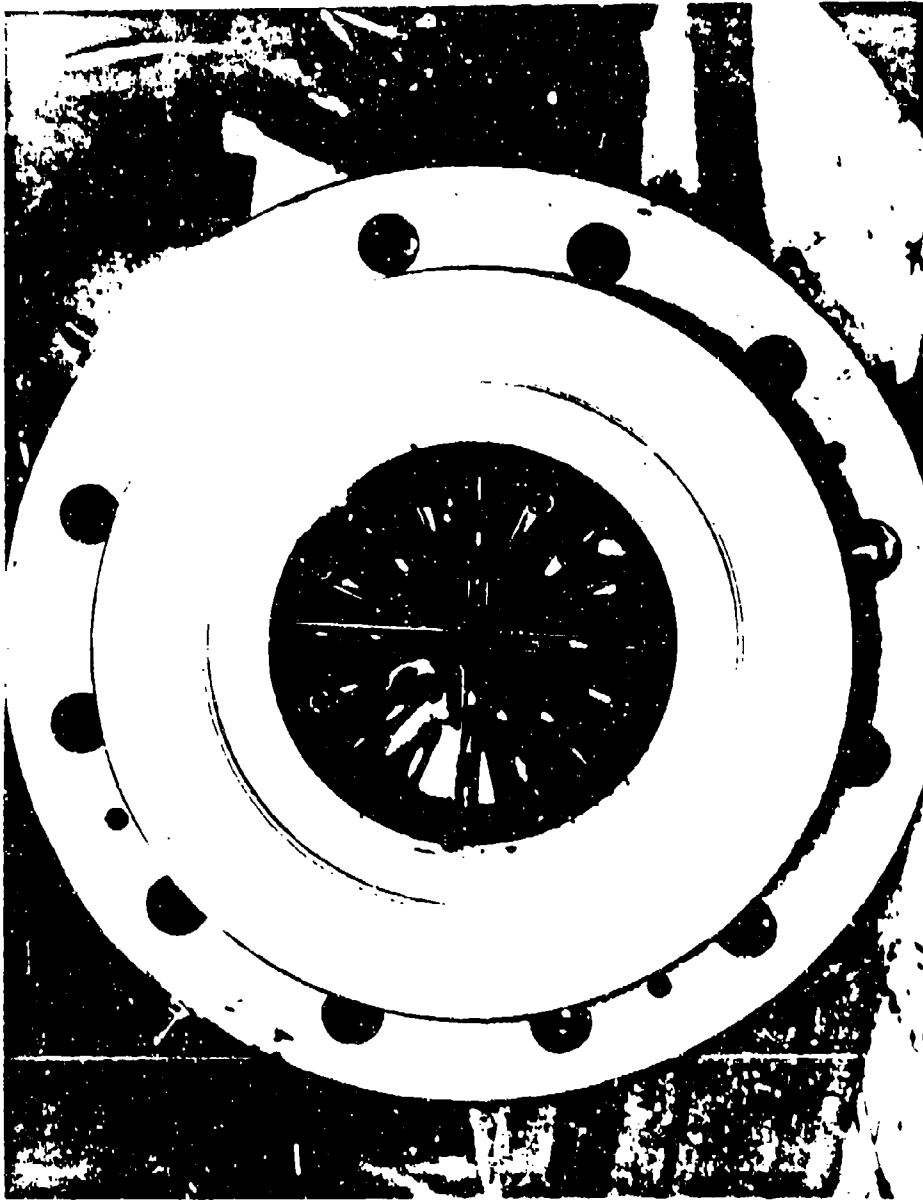


Figure 25. Modified Tubular Injector, Fostfire, Test 1.2-03-AAC-010

CONFIDENTIAL

CONFIDENTIAL

Report 10785-F, Phase II

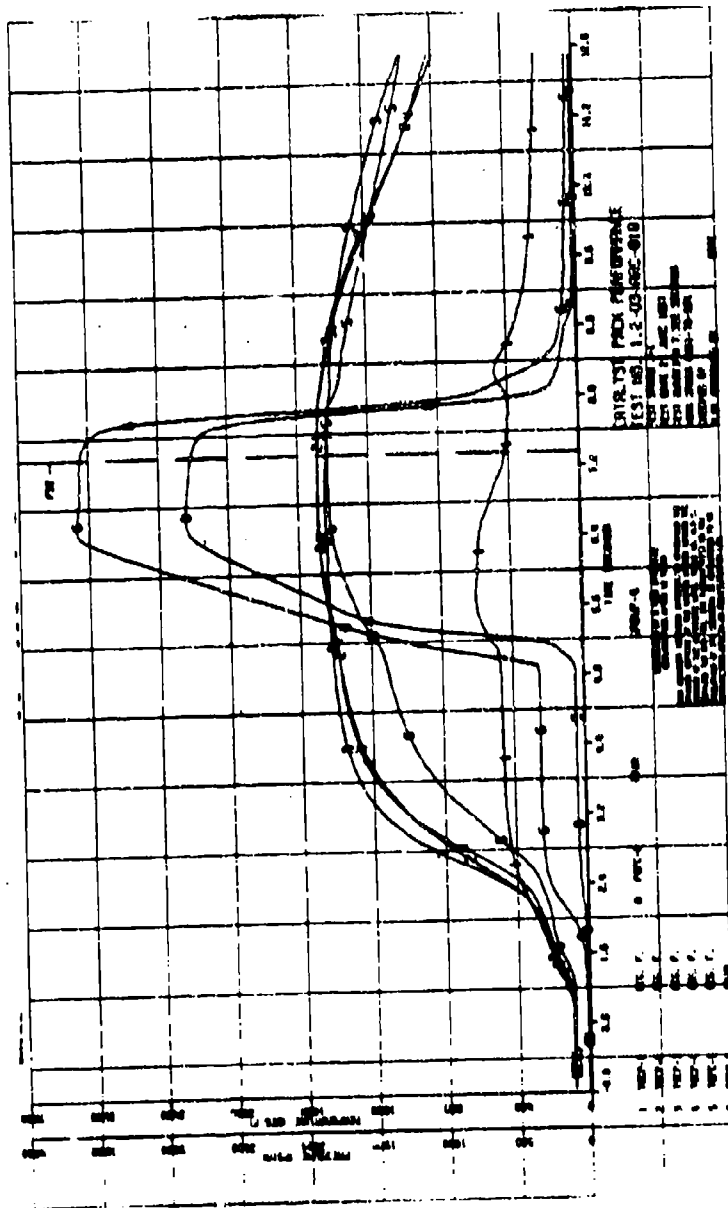


Figure 94. Catalyst Pack Performance, Test 1.2-03-AAC-010 (u)

CONFIDENTIAL

IV. B. Technical Discussion (cont.)

4. Performance Analysis

a. General

(U) The performance technique used for this program was the Interaction Theory method as described in Appendix II. In order to apply the Interaction Theory, the sea-level test data were corrected to vacuum conditions and magnitudes of individual performance losses were established. Separation of the total engine performance losses into individual losses allows the sources of performance degradation to be isolated and minimized. A more accurate extrapolation of the sea-level test data to altitude conditions or to another thrust level can be achieved by using the interaction theory.

(U) Two basic configurations of secondary injectors were tested. The 36-vane injector consisted of 396 fuel injection tubes which were designed to uniformly disperse the fuel across the injector face for maximum performance. Three fuel injection tube modifications of the vane injector concept were tested with their major differences as described in Section IV.D.1. Two variations of the 44-tube injector assembly were also tested. The original design consisted of 44 tubular orifices; whereas, the modified injector orifices included a pattern of weld beads to improve atomization characteristics. The injectors were tested with chambers having characteristic chamber lengths ( $L^*$ ) of 40 and 70 in. with 5:1 contraction ratio and 10:1 nozzle exit area ratio.

b. Overall Engine Performance Efficiency

(U) The summarized test performance data are tabulated in Table VII. Engine efficiency is plotted versus mixture ratio in Figure 95. Ten tests were conducted during this program over a mixture ratio range of

CONFIDENTIAL

Report 10705-F, Phase II

TABLE VII

PERFORMANCE SUMMARY--ADVANCED PROPELLANT PROGRAM (U)

Test Series No.		1.2-02-AAC				1.2-03-AAC				1.2-04-AAC			
Test No.	Inj. Type	002	003	004	001	002	003	005	007	008	010	Mod. 44 Tube	
		Mod I	Mod I	Orig. 44 Tube	Mod III	Mod III	Mod II	Mod III	Mod III	Mod II	Mod. 44 Tube		
$P_c$	p.s.i.a.	2750	2655	2800	3061	3053	3007	2953	2977	3068	2755		
$C/F$	-	.658	.749	.597	.671	.716	.827	.519	.487	.553	.760		
$\dot{W}_t$	lb <sub>m</sub> /sec	62.78	60.41	69.48	69.46	68.10	57.79	70.13	69.63	73.25	73.34		
$L^*$	in.	70	70	70	70	40	70	40	70	40	70		
$\epsilon$	-	10.0	10.0	10.0	9.78	9.82	9.78	9.82	9.84	9.78	8.60		
$P_v$	lb <sub>f</sub>	18,945	17,800	19,261	20,894	20,846	20,577	20,275	20,958	21,252	21,121		
$I_{sp}$ , v theo	sec.	329.5	328.4	330.3	328.6	328.2	326.8	330.7	331.4	326.8	319.3		
$I_{sp}$ , v, meas	sec.	295.4	294.6	277.2	299.9	305.8	303.5	289.1	301.0	290.0	288.0		
$I_{sp}$ , v	-	89.65	89.71	83.92	91.27	93.17	92.88	87.42	90.83	88.74	90.20		
$\Delta I_s$ , noz. fric.	sec.	3.1	3.1	3.1	3.1	3.1	3.1	3.1	3.1	3.1	3.0		
$\Delta I_s$ , noz. geom.	sec.	5.1	5.1	4.8	5.2	5.3	5.2	5.0	5.2	5.0	5.0		
$\Delta I_s$ , WEC	sec.	0.0	0.0	0.0	0.0	0.0	0.0	2.6	0.0	0.0	0.0		
$\Delta I_s$ , stem HT	sec.	0.5	0.5	0.4	0.5	0.5	0.5	0.5	0.5	0.5	0.5		
$\Delta I_s$ , stem, fric	sec.	0.5	0.5	0.4	0.5	0.4	0.5	0.4	0.5	0.4	0.5		
$\Delta I_s$ , II Phase	sec.	4.6	4.4	7.6	4.6	4.4	5.1	5.3	5.5	4.9	6.4		
$\Delta I_s$ , ERL	sec.	20.3	20.2	36.8	14.8	8.7	9.9	24.7	15.6	22.9	15.9		
$\Delta I_s$	-	6.16	6.14	11.12	4.50	2.65	3.03	7.46	4.71	7.01	4.96		
$I_{sp}$ , v $I_{sp}$ (Inferred)	-	90.40	90.00	83.0	92.88	95.72	94.80	89.6	93.66	85.5	91.72		

CONFIDENTIAL

CONFIDENTIAL

Report 10735-F, Phase II

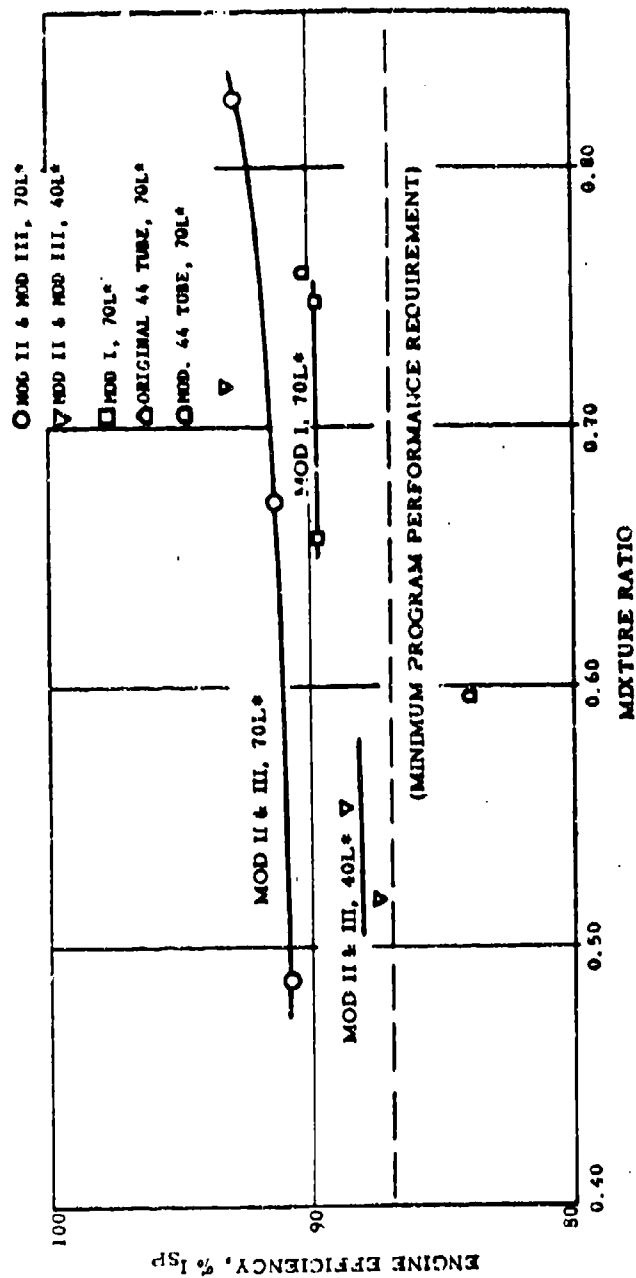


Figure 95. Effect of Mixture Ratio vs Efficiency (u)

CONFIDENTIAL

## IV, B, Technical Discussion (cont.)

from 0.49 to 0.83. Eight tests were conducted with 98%  $H_2O_2$  and the last two tests were with 90%  $H_2O_2$ . No discernible difference in engine efficiency could be noted with the change in  $H_2O_2$  concentrations.

(C) Nine of the ten tests exceeded the 87% minimum program performance goal. It was determined that energy release loss was the major performance loss of the Advanced Propellant Staged-Combustion System and that the loss could be influenced by injector design and to a lesser extent by  $L^*$ . Only the overall results will be presented in this section with further discussion of individual losses to be followed in Section 4, c, below.

(C) Initially, two 70  $L^*$  tests were conducted with the Mod I vane injector. An engine efficiency performance of 89.7% of theoretical was obtained and exceeded the minimum program performance requirement. However, the Mod I injector had been modified to reduce its pressure drop at the expense of its potential performance. Changes were made to the Mod II and Mod III configurations to obtain more uniform fuel distribution and the engine performance efficiency improved to approximately 91.7% of theoretical. Three additional tests of the Mod II and III injectors were conducted with the 40-in.  $L^*$  chamber. Two tests indicated approximately 2.5% decrease in efficiency. However, one test indicated a 93.2% efficiency (1.5% increase) which was the highest indicated efficiency achieved in all the staged-combustion tests. This high performance was unexpected with the reduced  $L^*$  (40 in.), and the test data were subjected to an extensive analysis. No errors could be found. It is felt, therefore, that the data point is correct, and the high performance can be attributed to the increased mixture ratio and the improved fuel distribution.

(C) Only one of the ten valid tests did not achieve the 87% minimum performance goal. This test was conducted with the original 44-tube injector. Because of the coarse fuel injection distribution, the fuel

## IV. B. Technical Discussion (cont.)

Atomization and dispersion were not as fine as that achieved by the 396-tube vane injector and only 83.9% of theoretical specific impulse was obtained. To improve the atomization characteristics of the tubular injector, the fuel injection tips were modified by a pattern of weld beads and 90.2% engine efficiency was obtained with the modified 44-tube injector. The injector was operated with 90%  $H_2O_2$  and Alumizine; however, the performance efficiencies of the 90%  $H_2O_2$  and 98%  $H_2O_2$  are comparable.

## c. Detail Performance Loss Analysis

(U) Not all of the ten possible performance losses considered by the Interaction Theory method of analysis were significant enough to warrant consideration in the 98%  $H_2O_2$ /Alumizine-43 system. The magnitude of the nozzle heat loss was estimated to be only about 0.1% or less of vacuum specific impulse and was therefore neglected. Kinetic losses were also negligible at the high chamber pressures and moderate exit-area ratios considered for the advanced propellant system. Mass-distribution effects were likewise neglected because mass distribution at the face of the secondary injector was essentially uniform. Thus, only nozzle-friction and nozzle-geometry losses; chamber heat and friction losses; and energy-release, mixture-ratio-distribution, and gas-particle performance losses were considered potentially significant for this analysis and a discussion of the resulting detail analysis follows.

## (1) Nozzle Friction Loss

(U) Nozzle friction loss was calculated by using Aerojet-General's Computing Services Division Program P-133, which is based upon the extended Frankl-Voishel expression for average skin friction. Nozzle friction loss is primarily determined by nozzle length. Friction loss for the smooth-walled nozzle of the Advanced Propellant Staged-Combustion engine with an

CONFIDENTIAL

## IV, B, Technical Discussion (cont.)

exit-area ratio of 10:1 and an exit half-angle of 15 degrees was found to be less than 1% of theoretical vacuum specific impulse. A slight roughening of the nozzle surface, caused by minor ablation of the nozzle wall during testing, was not considered significant enough to require correction for rough wall nozzle friction loss.

## (2) Nozzle Geometry Loss

(U) The nozzle geometry loss was calculated on Aerojet-General's Computer Program 10036 to be about 1.7% of the sum of delivered specific impulse and nozzle geometry loss.

$$I_{sp,N.G.} = 1.7\% \left( I_{sp,DEL} + I_{sp,N.G.} \right)$$

## (3) Chamber Heat and Friction Loss

(U) The effect of chamber boundary layer (heat and friction) losses on the performance of a large rocket engine is insignificant because the chamber surface area per unit of propellant flow rate is low; therefore, these losses are usually combined with the energy release loss. However, in smaller rocket engines these losses become significant; if summed with the energy release loss and then scaled to the losses of a large engine, the error in this extrapolation may become quite large, predicting higher-than-actual performance losses for larger engines, and conversely, lower-than-actual losses for smaller engines. Since the Advanced Propellant Staged-Combustion engine is of intermediate size (20,000 lbf thrust) these losses were identified separately.

(U) The heat transfer to the ablative chamber liner was found to be minor due to the low thermal conductivity of the ablative material.



# UNCLASSIFIED

Report 10785-F, Phase II

## IV, B, Technical Discussion (cont.)

However, the heat transfer to the silver-infiltrated-tungsten throat insert was significant. The mean bulk temperature within the thermal boundary layer was calculated to be reduced by about 1% because of chamber heat loss. The effect of this heat loss upon engine performance was to decrease overall specific impulse by about 0.3 sec. Of this performance loss, about 75% occurred upstream of the throat and the remainder (an interaction loss) occurred within the nozzle expansion cone. Viscous effects in the chamber resulted in a drag of about 39 lbf, corresponding to a performance loss of about 0.5 sec with the 70-in. L<sup>4</sup> chamber.

(U) The methods used to calculate chamber heat and friction losses are presented in Appendixes II and III, respectively.

### (4) Mixture-Ratio Distribution Loss

(U) The theoretical specific impulse of H<sub>2</sub>O<sub>2</sub>/Alumizine-43 decreases almost linearly with increasing mixture ratio over the range of from 0.5 to 1.0. Therefore, for small perturbations in local mixture ratio the decreased theoretical performance in a stream tube with a higher-than-nominal mixture ratio is almost exactly offset by the increase in theoretical performance in an adjacent stream tube with a lower-than-nominal mixture ratio. Thus the performance loss attributed to mixture-ratio distribution was zero for all tests listed in Table VII with the exception of Test 1.2-03-AAC-005. On this test, two adjacent vanes of the 36 available vanes were completely plugged and restricted to fuel flow prior to testing. A pure oxidizer sector resulted with the remainder of the injector face being fuel rich. The resultant maldistribution in local mixture ratio was responsible for the 2.6-sec performance loss noted. Only with such gross deviations are mixture-ratio distribution losses possible with H<sub>2</sub>O<sub>2</sub>/Alumizine-43. Several tests were conducted with the vane injector in which several fuel injection tubes at the injector axis were removed and sealed without additional loss.

UNCLASSIFIED

## IV, B, Technical Discussion (cont.)

## (5) Gas-Particle Two-Phase Flow Losses

(C) Particle samples were collected in the exhaust plume and analyzed for both the vane and tubular injectors. Only particles having diameters of 0.1 micron ( $\mu$ ) and larger were considered. The cumulative sample weight is plotted versus particle diameter in Figure 96 for both injectors. The following statistical averages were computed with the two samples:

<u>Injector</u>	<u>396-Tube Vane</u>	<u>44 Tubular</u>
Number of Particles Counted	972	1551
Test No.	1.2-03-AAC-007	1.2-02-AAC-004
Mass Median Diameter, microns	1.83	2.59
Mass Mean Diameter, microns	1.21	1.33
Number Mean Diameter, microns	0.93	0.74

It was noted that the 396-tube vane injector yielded a finer particle size and a more uniform distribution with fewer small and fewer large particles. This was attributed to the finer and more uniform secondary Alumizine injection distribution.

(C) It was shown that representative gas-particle performance losses can be calculated by using the measured mass median particle diameter instead of the actual particle-size distribution. Figure 97 shows the effect of particle diameter upon two-phase flow losses for the mixture-ratio range of 0.5 to 1.0. The performance loss increases with increasing particle diameter because of the greater thermal and velocity lags for larger particles. The loss also increases with decreasing mixture ratio because of increasing mass fraction of particles at the lower mixture ratio. The two-phase flow losses presented in Table VII are based upon the measured 1.83 $\mu$  mass median particle diameter for the vane injector and 2.56 $\mu$  diameter for the 44 tubular injector. The resultant two-phase flow losses ranged between 1.25 to 2.3% of theoretical specific impulse.

CONFIDENTIAL

Report 10705-F, Phase II

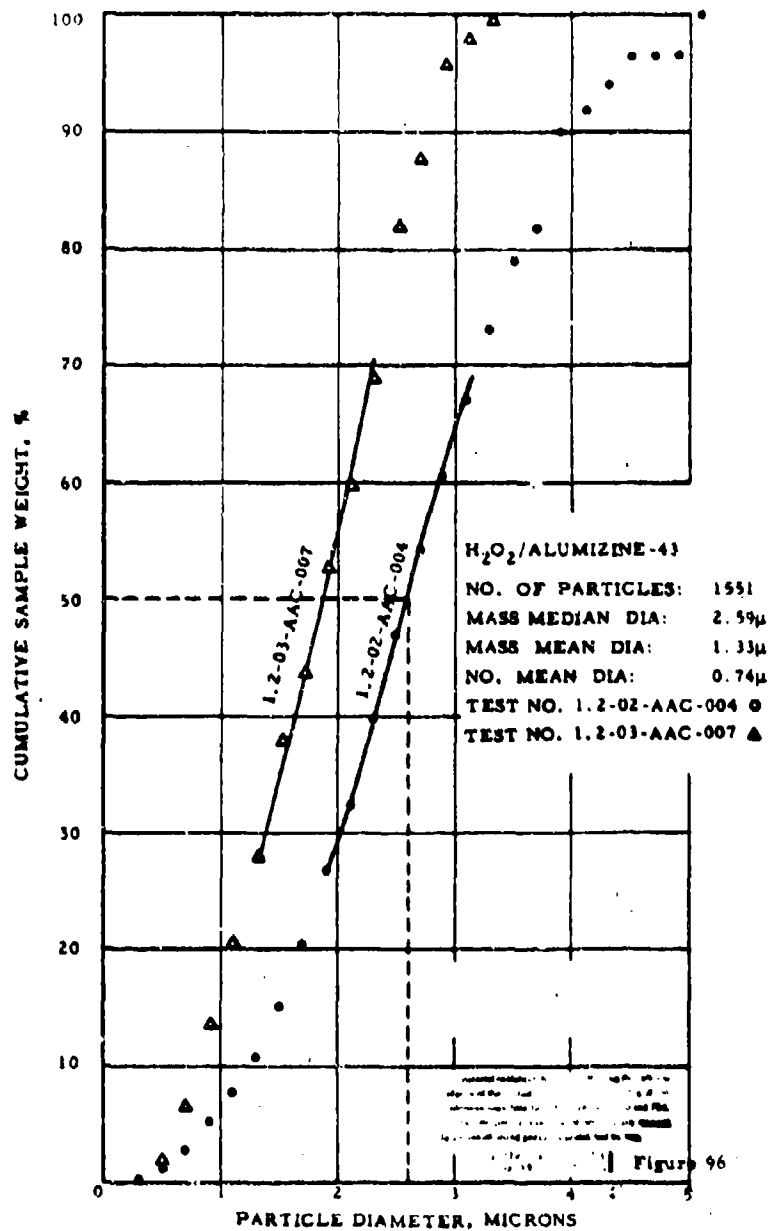


Figure 96. Particle Mass Distribution vs Particle Diameter (u)

CONFIDENTIAL

UNCLASSIFIED

Report 10785-F, Phase II

98%  $H_2O_2$ /ALUMIZINE-43

$P_c = 3000$  PSIA

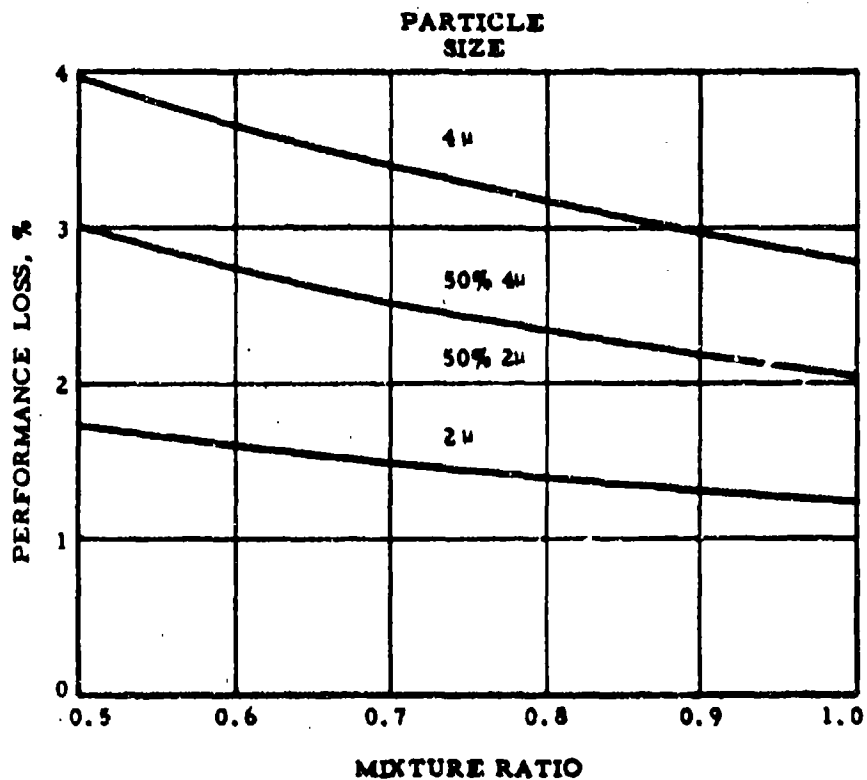


Figure 97. Effect of Mixture Ratio on Gas-Particle Loss

UNCLASSIFIED

## IV, B, Technical Discussion (cont.)

## (6) Energy Release Loss

(U) The performance degradation attributed to energy release loss was the single most significant performance loss of the Advanced Propellant Staged-Combustion System. There are two possible sources for energy release loss in the  $H_2O_2$ /Alumizine-43 propellant system. The first loss is caused by reduced availability of aluminum, which occurs when the temperature of the combustion flame is too low to melt the aluminum-oxide coating on the aluminum fuel particle. The other source of loss is attributed to vaporization and reaction rate limitations in attaining complete combustion and energy release efficiency.

## (a) Reduced Aluminum Availability

(U) The energy release loss attributed to reduced combustion enthalpy of unreacted aluminum may occur either because of insufficient chemical reaction time or because of reduced aluminum availability. If the loss occurs because of insufficient chemical reaction time, an increase in residence time (increased  $L^*$ ) will eventually eliminate this loss and will be discussed in the following section. However, if the loss occurs because of reduced aluminum availability, i.e., the aluminum contained in the Alumizine-43 is not heated sufficiently to combust, a performance loss as great as 10% can occur even with an infinitely long chamber. It has been found that the combustion of aluminum is influenced by the melting of a protective oxide coating. The melting point of aluminum oxide is 4172°R (JANAF data), which is approximately the observed ignition temperature of aluminum. Thus, if the temperature of the  $H_2O_2/N_2H_4$  reaction is not above 4200°R, it is quite possible that the aluminum will not ignite. The theoretical combustion flame temperatures for both the  $H_2O_2/N_2H_4$  and  $H_2O_2/Al-43$  reactions are shown in Figure 98 as a function of the metalized propellant mixture ratio from 0.5 to 1.0. Pretest analysis

UNCLASSIFIED

Report 10785-F, Phase II

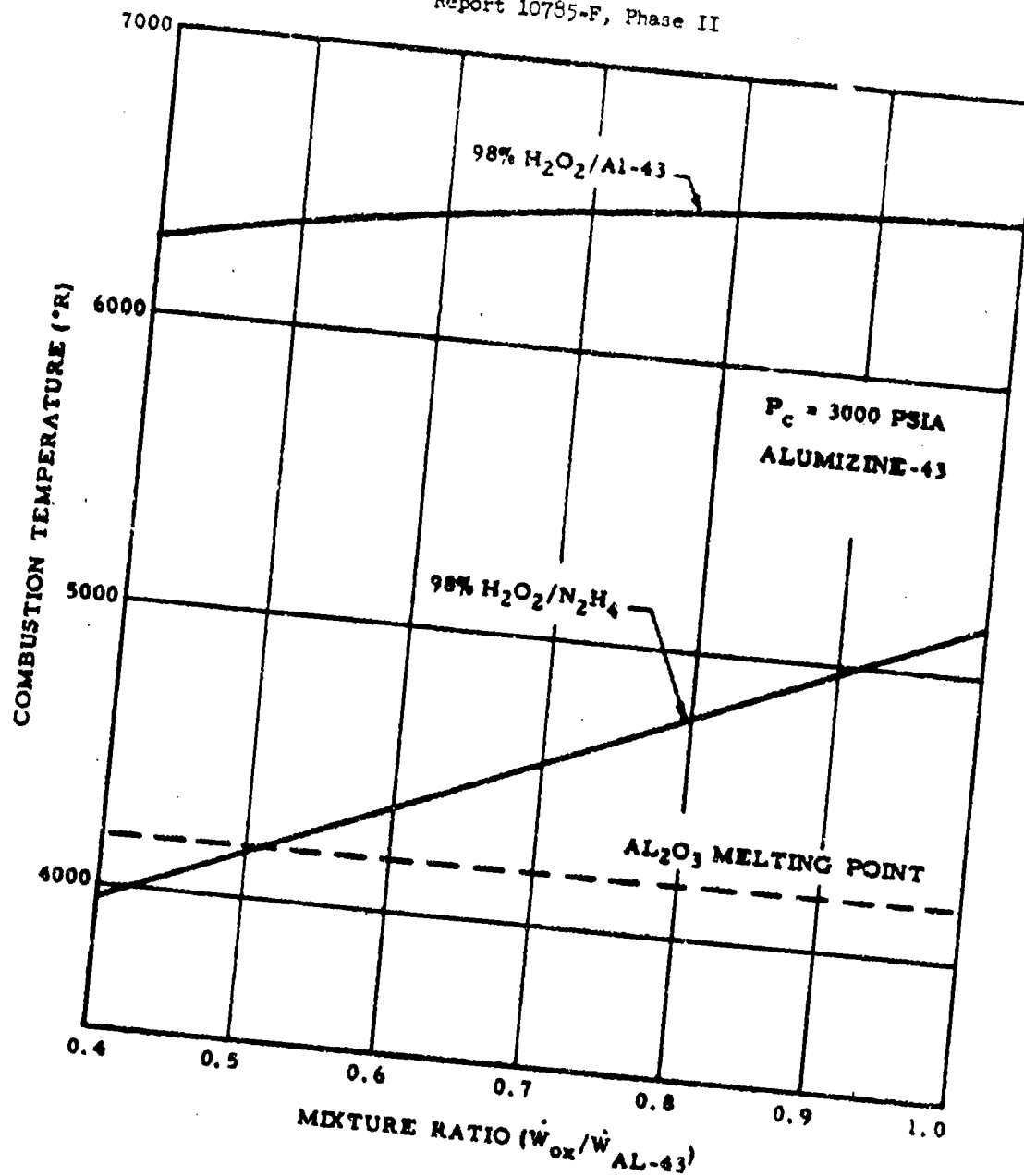


Figure 98. Effect of Operating Mixture Ratio on the Theoretical Combustion Temperature with and without Aluminum Combustion

UNCLASSIFIED

## IV. B. Technical Discussion (cont.)

indicated that at the lower end of mixture ratios, the  $H_2O_2/N_2H_4$  flame temperature (which neglects heat loss to the aluminum) was marginal for assurance of  $Al_2O_3$  melting based on the  $N_2H_4$  combustion theory. However, analysis of the test data indicated that no perceptible increase in performance loss could be attributed to reduced aluminum availability down as low as 0.487 mixture ratio. Therefore, it must be concluded that even with marginal  $H_2O_2/N_2H_4$  flame temperatures, local ignition of the aluminum occurs and provides sufficient heat to permit complete aluminum availability. However, it is also realized that some lower mixture-ratio limit must exist where the aluminum will no longer become available for combustion.

## (b) Vaporization and Reaction Rate Limited Energy Release Loss

(U) Propellant vaporization rates have been calculated analytically for conventional propellant systems on the basis of injector design parameters which influence atomization, from propellant transport properties which determine propellant volatility and from chamber design criteria which determine propellant residence time within the chamber. The energy release efficiency of such engines can often be predicted from vaporization criteria within an accuracy of  $\pm 1\%$ . The oxidizer ( $H_2O_2$ ) for the Advanced Propellant Staged-Combustion System is decomposed in the primary combustor and therefore its resultant energy release loss in the secondary combustor due to unvaporized oxidizer is nil. On the other hand, the transport properties (surface tension, viscosity, and heat of vaporization) of Alumazine are not known with sufficient accuracy nor are the characteristics of non-Newtonian propellant atomization adequately known to permit calculation of Alumazine atomization and vaporization rates. Therefore, the energy release efficiency of the Advanced Propellant Staged-Combustion Engine cannot be analytically calculated and was determined as the difference between the theoretical and experimentally measured specific impulse less all other calculable performance losses.

IV, B, Technical Discussion (cont.)

(U) The energy release loss determined by difference in this manner is listed in Table VII and plotted versus mixture ratio in Figure 99. Although the precise magnitude of the vaporization rates cannot be analytically calculated, the vaporization model can, nevertheless, be used to explain the observed experimental trends of engine efficiency as parameters are varied.

(U) For example, the energy release efficiency (ERE) can be defined by:

$$\bar{x}_{ERE} = \frac{[(\bar{x}_{Oxid. Vap.}) \times \dot{W}_O + (\bar{x}_{Fuel Vap.}) \times \dot{W}_F] \times I_{sv, O/F}}{[(100\% \times \dot{W}_O) + (100\% \times \dot{W}_F)] \times I_{sv, O/F}}$$

Where:  $O/F$  = Engine Mixture Ratio,  $\dot{W}_O/\dot{W}_F$

And:  $O/F$  = Effective Vaporized Mixture Ratio,  $\frac{(\bar{x}_{Oxid. Vap.})}{(\bar{x}_{Fuel Vap.})} \times O/F$

However, because the  $H_2O_2$  is completely vaporized within the primary combustor the energy release loss can be attributed solely to the unvaporized fuel. The energy release efficiencies for various engine mixture ratios are shown as a function of fuel vaporized in Figure 100. The resultant fuel vaporization rates which were inferred from the measured energy release losses were then plotted versus mixture ratio in Figure 101. The only significant influences observed to affect fuel vaporization rates were injector design (which influences atomization) and chamber length (which determines propellant stay time).

(C) The original (Mod I) 396-tube secondary injector consisted of about 1-in.-long tubes which were bent to achieve a uniform fuel distribution between the vanes as well as downstream of each vane.



CONFIDENTIAL

Report 10785-F, Phase II

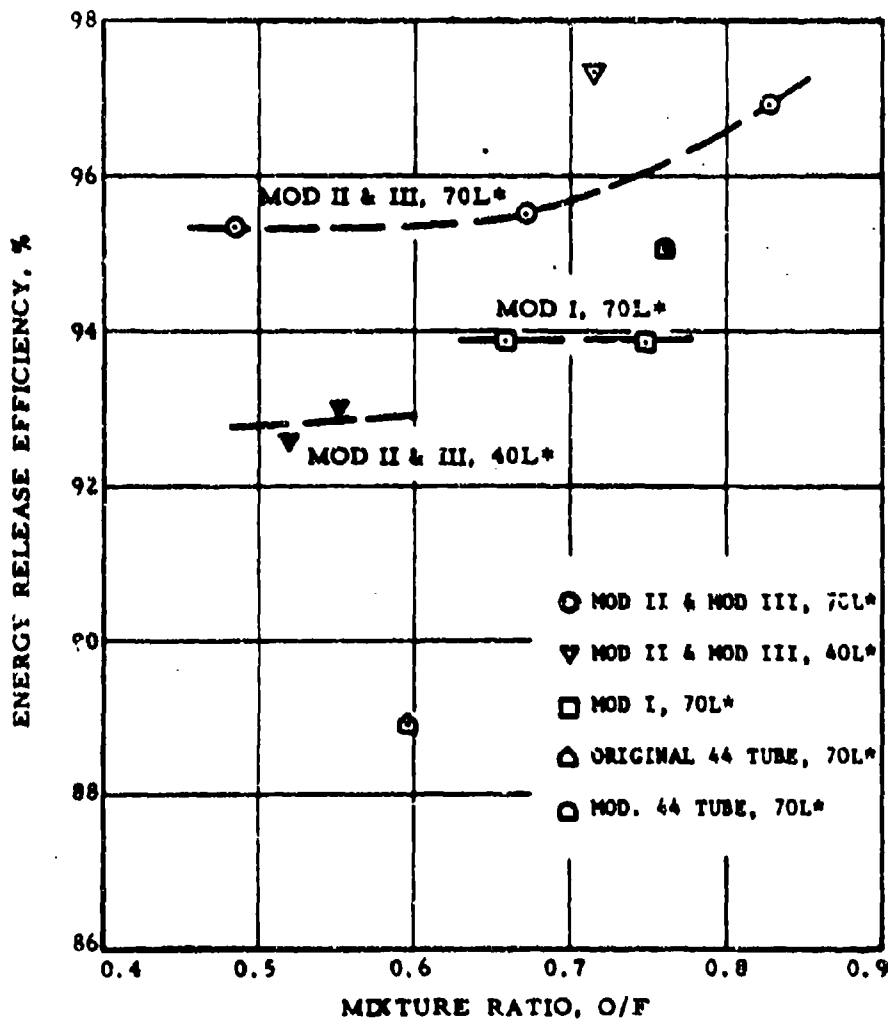


Figure 10. Effect of Mixture Ratio upon Energy Release Efficiency (a)

CONFIDENTIAL

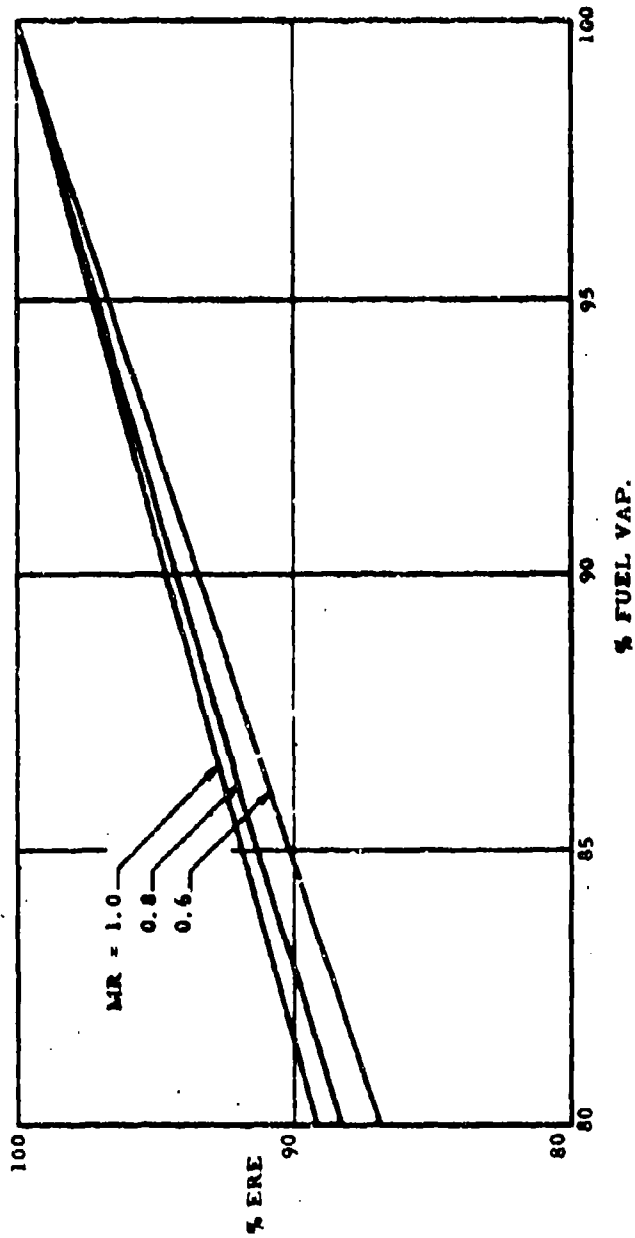


Figure 100. Effect of Fuel Vaporization Rate upon Energy Release Efficiency

**CONFIDENTIAL**

(This page is Unclassified)

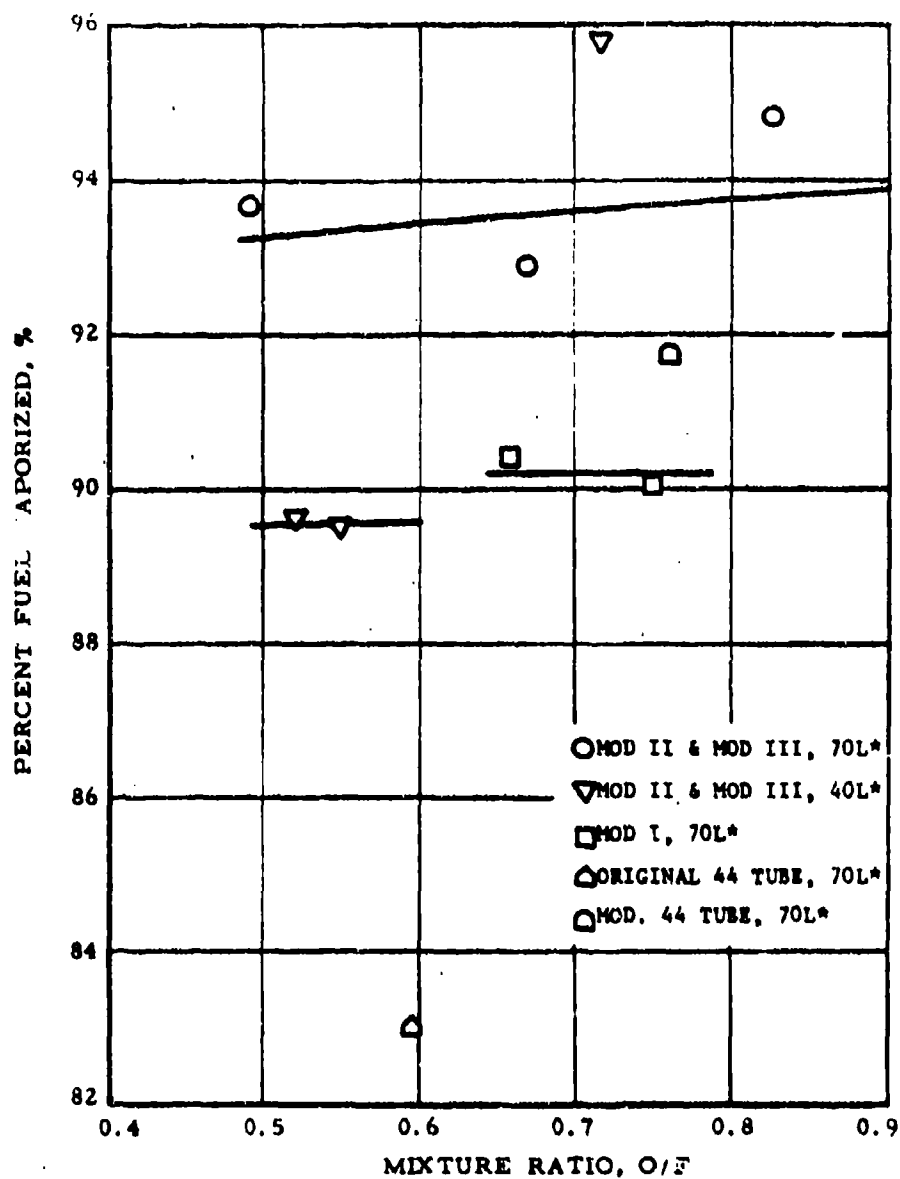


Figure 101. Effect of Mixture Ratio upon Fuel Vaporization Rate (u)

**CONFIDENTIAL**

## IV, B, Technical Discussion (cont.)

However, because of an excessive hydraulic pressure drop through the secondary injector vanes and tubes, the injection tubes had to be reduced in length to 0.65 in. to attain the required fuel flow rate with the available system pressure drop. However, when the tubes were shortened, the bent portions of the tubes were cut off; this produced a configuration resembling that of a showerhead, with fuel concentration directly downstream of each vane and oxidizer concentration between each vane and at the injector axis. Thus, the nonuniform injection distribution of oxidizer and fuel resulted in a fuel vaporization rate of  $90.2 \pm 0.2\%$  and a corresponding 6.13% energy release loss for the 70-in. L\* chamber. To decrease the energy release loss, the fuel injection tubes of the Mod II and Mod III variations of the 396-tube injector were replaced by tubes of larger diameter. The larger tubes reduced injector pressure drop permitting longer tubes which could then be bent to retain the uniform fuel distribution. Furthermore, the larger tubes reduced the fuel injection velocity and thus the fuel residence time within the chamber was increased. The above modification increased fuel vaporization rate by approximately 3%, which improves the energy release efficiency 2%.

(C) When the Mod II and Mod III injectors were tested with the 40-in. L\* chamber instead of the 70-in. L\* chamber, two tests indicated a 2.5% decrease in energy release efficiency in agreement with the greater loss which would be predicted by the propellant vaporization model if atomization is assumed constant. However, Test Number 1.2-03-AAC-002 with the Mod III injector also at 40-in. L\* indicated approximately 1.5% performance improvement which, if real, is contrary to what would logically be expected. It is possible that there are factors other than those considered in the vaporization model that influence this performance.

(U) In addition to the effect of chamber length (or L\*) upon energy release loss, the vaporization model also predicts that contraction ratio has an effect. For example, the Advanced Propellant

**CONFIDENTIAL**

## IV, B, Technical Discussion (cont.)

Staged-Combustion chamber has a 5:1 contraction ratio. If chamber characteristic length were maintained constant and the contraction ratio were reduced to approximately 2.0, the vaporization model would predict approximately 1.6% increase in energy release efficiency for the same injector atomization characteristics. This performance improvement is predicted because as contraction ratio decreases, combustion gas velocities at every comparable point within the chamber will be higher and uniform, thus resulting in increased heat transfer and mass transfer (vaporization) rates for the propellant within a given axial chamber length. However, other considerations besides performance may determine selection of design contraction ratio. For example, contraction ratios of four to five are normal for a high-pressure combustion chamber because of other considerations, such as injector geometry, pressure drop, and packaging.

(C) Overall engine efficiency for the original 44-tube secondary injector on Test 1.2-002-AAC-004 was 83.9%. This low engine efficiency resulted from 11.1% energy release loss and 83% fuel vaporization rate. The high energy release loss (in a 70-in. L\* chamber) was due to the poor atomization characteristics of the reduced number of injection elements. However, by modifying the element tips with weld beads the atomization characteristics were substantially improved. The modification resulted in noncircular orifice exits, which improved atomization by the following mechanisms:

(1) Decreased orifice area which increased injection velocity. (This assumes that the performance gain through increased atomization outweighs the loss resulting from reduced stay time.)

(2) Increased dispersion through nonuniform exit velocity profile across orifice.

IV, B, Technical Discussion (cont.)

(3) Increased effective orifice surface area per unit flow area.

By thus improving the atomisation efficiency, 90.2% engine efficiency was obtained with the modified 44 tubular injector. It should be noted that the latter test was conducted with 90%  $H_2O_2$  instead of 98%  $H_2O_2$ ; however, the performance improvement cannot be attributed to the  $H_2O_2$  concentration because there was no perceptible change in efficiency between Tests 1.2-03-AAC-003 and -008, which were basically similar except for  $H_2O_2$  concentration. Furthermore, the  $H_2O_2$  is decomposed in the primary combustor and cannot influence energy release efficiency.

(U) d. Experimental Observations

There were three tests conducted with 40-in.  $L^*$  combustion chambers that produced data. Two of these tests were made using 98%  $H_2O_2$  while one was conducted with 90%  $H_2O_2$ . Two tests produced performance below that anticipated for the mixture-ratio condition, while one test produced the highest performance achieved in the program.

(U) The ablative liners used in the high-performance 40-in.  $L^*$  test and a corresponding 70-in.  $L^*$  test were compared in an attempt to determine the distance from the injector face at which complete combustion occurred. It was evident that the maximum material loss was at a station approximately 4 in. from the injector face for both  $L^*$ 's. The chamber wall was smooth from this station to the throat, thus indicating that the combustion gas was homogeneous. It is hypothesized from the ablation experienced and high performance that the 40-in.  $L^*$  chamber had sufficient volume to permit complete combustion when tested with a high quality injector. The low performance tests with the 40-in.  $L^*$  chambers, however, indicated unsymmetrical ablation and erosion of the

# CONFIDENTIAL

Report 10785-F, Phase II

## IV, B, Technical Discussion (cont.)

liners down to and through the throat. This pattern seems to correlate to the measured low performance and may have been caused by injector deficiency. On one of these tests, two vanes were severely damaged, and on the other, the majority of the injector face tubes in the center were not used.

(U) From these observations, it is concluded that 40-in. L\* is sufficient chamber volume to obtain high combustion performance if a high quality injector is used.

### e. Correlation with Other Metallized Systems

(U) The combustion of heterogeneous and metal bearing fuels differs from that of "neat" propellants, and significant differences have been noted between the predicted and actual performance. A comparison was made between the data obtained in the program and combustion data of other metallized fuels. The performance of the 20K lbf thrust chamber was predicted by correlating test data from a number of metallized propellants. The correlation parameter was the equivalence ratio (ratio of the stoichiometric mixture ratio to the mixture ratio under consideration). This parameter allows the comparison of all propellant combinations in relation to the oxidizer balance. For example: (1) an equivalence ratio (ER) of 1.0 refers to complete oxidation of all available fuel ( $H_2 \rightarrow H_2O$ ,  $Al \rightarrow Al_2O_3$ , etc) assuming no dissociation of the products; (2) an ER greater than 1.0 indicates a fuel-rich combustion; and (3) an ER less than 1.0 indicates an excess of oxidizer in the combustion products.

(U) A correlation of the combustion efficiency of several representative metallized propellant combinations (98%  $H_2O_2$ /Alumizine-20,  $N_2O_4$ /Alumizine-43 emulsion, and air/propylpentaborane) with ER is shown in Figure 102. It can be seen that high combustion efficiencies are attained in a slightly

Page 214

CONFIDENTIAL

(This page is Unclassified)

# CONFIDENTIAL

Report 10785-F, Phase II

- Laboratory Combustion  
98%  $H_2O_2$ /Alumisine-20  
AF 04(611)-8529  
MR (Stoich) = 2.12
- △  $N_2O_4$ /Alumisine-43 Emulsion  
RPL: MacGregor, Hobbs, Randolph  
Bull. 7th Liq. Prop. Symposium  
MR (Stoich) = 1.37
- ⊙ Air/ $(C_2H_5)_3Al$   
○ Air/ $C_3H_7-B_5H_8$   
Marquardt Corporation  
Test 2796  
● MR (Stoich) = 12.66  
○ MR (Stoich) = 13.8

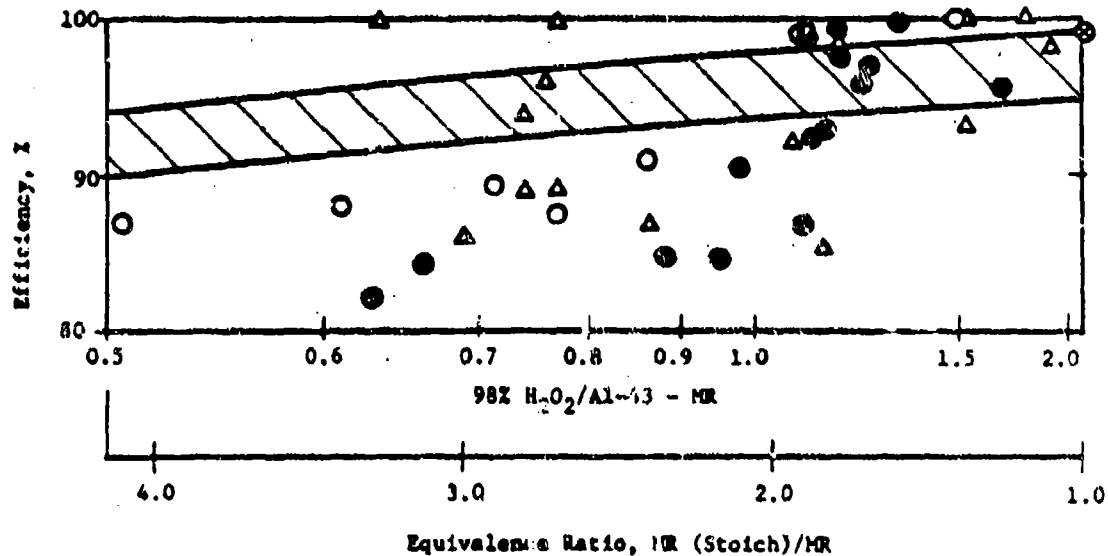


Figure 102. Estimated and Experimental Combustion Efficiency (%)

CONFIDENTIAL



CONFIDENTIAL

Report 10735-F, Phase I

IV. , Technical Discussion (cont.)

fuel-rich condition, corresponding to an ER of from 1.0 to 2.0. Combustion efficiency begins to decline at an ER greater than 2.0.

(U) The band shown in Figure 102 represents the estimate of combustion efficiency for the 98%  $H_2O_2$ /Alumizine-43 propellant combination. The band was drawn above the majority of experimental data at the higher ER's because combustion efficiency is strongly dependent upon injector configuration and  $L^*$ , and therefore, might be raised by applying unique design techniques.

(U) The specific impulse efficiency of the uncooled thrust chamber was estimated by incorporating empirical, two-phase flow losses into the combustion efficiency correlation. The result of the correlation, shown in Figure 103 as the cross-hatched band, can thus be represented by:

$$\eta_{Is} = \eta(\text{combustion}) \times \eta(\text{two-phase flow}).$$

Measured performance data for  $N_2O_4$ /Alumizine-43 (gel and emulsion) are plotted for comparison in Figure 103. Lowering of the band (dashed line band) by 2% to account for nozzle geometry losses provides an excellent agreement with the majority of the experimental data. Note that the specific impulse efficiency shows a gradual rise as the mixture ratio approaches stoichiometric (ER from 3.3 to 1.1). This rise corresponds to the rise in combustion efficiency shown in Figure 102 and might indicate a higher delivered specific impulse at higher than theoretically optimum mixture ratios for 98%  $H_2O_2$ /Alumizine engines.

(U) To examine the possibility that the uncooled thrust chamber might deliver higher performance at a higher mixture ratio than the theoretical optimum, a plot of normalized specific impulse was made. The specific impulse efficiency of Figure 103 was multiplied by the ratio

$$\frac{\text{theoretical } I_s \text{ @ mixture ratio}}{\text{theoretical } I_s \text{ @ ER 0.5} = 331.2 \text{ sec}}$$

CONFIDENTIAL

(This page is hereby cleared)

# CONFIDENTIAL

Report 10785-F, Phase II

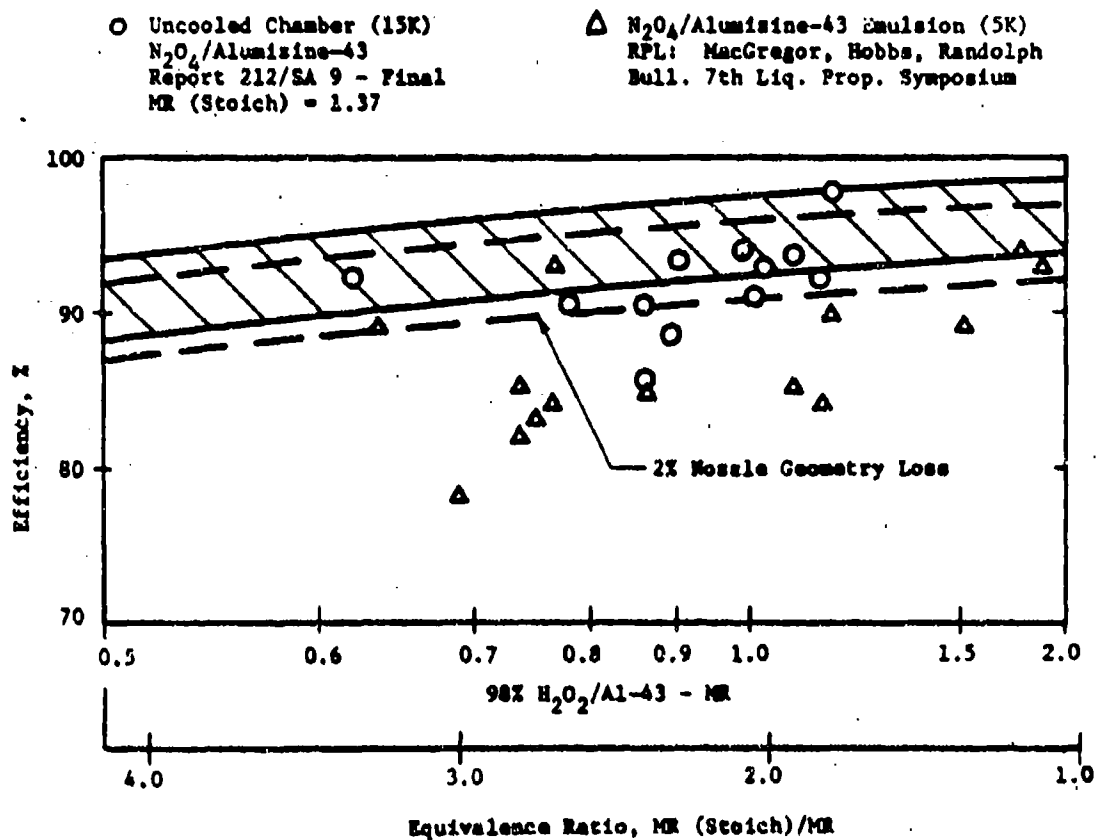


Figure 103. Estimated and Experimental Specific Impulse Efficiency ( $\eta$ )

CONFIDENTIAL

# CONFIDENTIAL

Report 10785-F, Phase II

## IV. B. Technical Discussion (cont.)

to obtain the normalized efficiency shown by the cross-hatched band in Figure 104. The benefit of correlating the specific impulse efficiency in the normalized form is that the maximum in the curve represents the maximum delivered specific impulse.

(U) The performance data obtained in the present program are also shown in Figure 104. Note the excellent representation of the data if the cross-hatched band is lowered by 2% to account for nozzle geometry losses. Also note that there appears to be no difference within experimental accuracy in performance between the 40-in.  $L^*$  and 70-in.  $L^*$  chambers.

(U) The conclusion to be reached from both the analytical and experimental studies is that the delivered  $I_p$  is practically constant from a mixture ratio from 0.5 to 1.0 (with the possibility of being highest around  $MR=1.0$  and not at the theoretically highest  $MR=0.5$ ). This unique characteristic provides wide flexibility in engine design and also permits variations in mixture ratio (because of propellant loading, propellant density variation) without a resultant change in engine performance.

### f. Extrapolated Performance of 100,000 lbf Thrust Engine

(U) Based upon the demonstrated performance of the 20K (20,000 lbf thrust) Advanced Propellant Staged-Combustion Engine, the performance was extrapolated for a 100K (100,000 lbf thrust) altitude engine. By separately calculating the individual performance losses and by using the Interaction Theory model, to extrapolate to altitude conditions, performance can be extrapolated to any other thrust level within  $\pm 1\%$  accuracy. The study has shown that the 100K uncooled engine can achieve 93.8 to 95.2% of theoretical vacuum specific impulse.

Page 218

CONFIDENTIAL

(This page is Unclassified)

CONFIDENTIAL

Report 10785-F, Phase II

Contract AF 04(611)-10785  
Uncooled Hardware  
(Numbers Indicate L\*)  
H<sub>2</sub>O<sub>2</sub>/Aluminine-43

○ 98% H<sub>2</sub>O<sub>2</sub> MR (Stoich) = 2.06

● 90% H<sub>2</sub>O<sub>2</sub> MR (Stoich) = 2.25

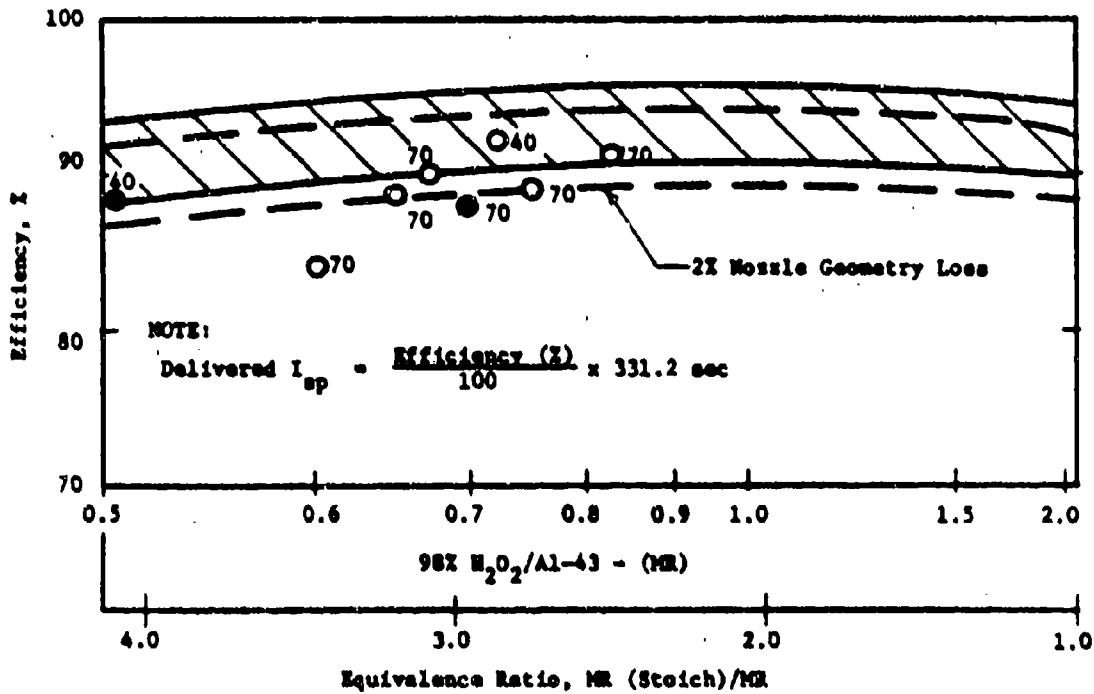


Figure 104. Estimated and Experimental Specific Impulse Normalized Efficiency (u)

CONFIDENTIAL

# CONFIDENTIAL

Report 10785-F, Phase II

## IV, B, Technical Discussion (cont.)

(U) The assumed engine operating conditions are as follows:

Propellants	98% $H_2O_2$ /Al-43
Chamber Pressure	3000 psia
Mixture Ratio	0.6 through 1.0
Thrust	100,000 lbf (100K)
Nozzle Exit Area Ratio	23:1
Chamber Length	16 in. (comparable to 20K, 70-in. L*, test)

Furthermore, scaling the 396-fuel-tube injector at 20K would indicate a minimum of 2000 equivalent fuel injection tubes are needed on the 100K injector to obtain comparable energy release efficiency. A decreased chamber contraction ratio between 2 and 3 may further improve Alumina combustion characteristics.

(U) As explained for the 20K engine, the nozzle heat loss, kinetic loss, and performance loss due to mass distribution effects were again neglected for the 100K engine analysis. The remaining applicable performance losses are summarized in Table VIII at engine mixture ratios of 0.6, 0.8, and 1.0.

(C) A nozzle contour having an exit area ratio ( $A_e/A_t$ ) of 23:1 was designed using Computer Program Job 447 for the 100K engine application. Nozzle friction loss for this design was evaluated using Aerojet Computing Program 48099. Nozzle performance losses due to frictional and geometry effects amounted to approximately 1.3 and 0.1%, respectively, as shown in Table VIII.

(C) Chamber friction and heat loss were evaluated by the methods described in Appendixes III and IV for both ablative and regeneratively cooled combustion chambers. Because of the low ratio of chamber surface area per unit weight flow rate of high-thrust engines, chamber performance losses

CONFIDENTIAL

# CONFIDENTIAL

Report 10785-F, Phase II

TABLE VIII

PREDICTED 100K ENGINE PERFORMANCE  
ADVANCED PROPELLANT STAGED COMBUSTION PROGRAM (U)

$P_c$ , psia	3000	3000	3000
MR	0.60	0.80	1.00
$F$ , lbf	100K	100K	100K
$A_o/A_c$	23	23	23
Chamber length, in.	16	16	16
$I_{sv}$ , theo, sec	350.7	348.6	346.4
$\Delta I_s$ , chamber friction + heat loss, sec	0.3 (0.2)	0.3 (0.2)	0.3 (0.2)
$\Delta I_s$ , MRD, sec	0	0	0
$\Delta I_s$ , nozzle friction, sec	4.6	4.6	4.6
$\Delta I_s$ , nozzle geometry, sec	0.4	0.3	0.3
$\Delta I_s$ , 2 phase, sec	1.9(a)	1.7(a)	1.6(a)
$\Delta I_s$ , ERL, sec	14.4(b)	11.9(b)	9.9(b)
$I_{sv}$ , prod., sec	329.1	329.8	329.7
$Xi_s$ , vac	93.84	94.61	95.18
$Z$ ERL	4.1	3.4	2.85
$Z$ Fuel vaporisation	93.7	94.2	94.7

- ( ) Regeneratively cooled chamber loss.  
(a) Assumed 2-micron particle size.  
(b) Determined from extrapolated 20K engine data.

CONFIDENTIAL

# CONFIDENTIAL

Report 10785-F, Phase II

## IV. B. Technical Discussion (cont.)

For the 100K engine will be small. Chamber friction loss was calculated to be 0.2 sec of vacuum specific impulse for both ablative and regeneratively cooled chambers and heat loss was found to be 0.1 sec for the ablative chamber only. No performance loss occurs with the regeneratively cooled chamber because the heat from the combustion gases is only transferred to the regenerative coolant resulting in a higher propellant injection temperature, and thus no decrease results in overall chamber enthalpy from the engine system. Combined chamber friction and heat losses result in less than 0.1% performance loss.

(C) Two-phase flow (gas-particle) performance losses will be smaller for the proposed 100K engine having a 23:1 exit area ratio nozzle than for the previously tested 10:1 area ratio 20K  $H_2O_2$ /Alumazine engine. This occurs because the two-phase flow loss is almost at a maximum near the nozzle throat and decreases with increasing exit area ratio as shown in Figure 105. Effects of mixture ratio and particle size on the two-phase flow performance loss is shown in Figure 106. Performance loss, due to the particles, increases for larger particle sizes because of the greater heat retention (thermal lag) and drag (velocity lag) effects. Two-phase flow loss also increased with decreasing mixture ratio because of the higher mass fraction of particle flow rate. The losses were calculated from Aerojet Computing Services Division Program 48067. At the 20K engine thrust level, analysis of the particle samples indicated a 2.59-micron ( $\mu$ ) mass median particle diameter for the 44-tube injector and a 1.83 $\mu$  diameter for the 396-tube injector. This indicates smaller particles are produced with a finer fuel injection distribution. A survey of the current literature also suggests that slightly larger particles have been observed for either increased engine thrust or larger throat diameters. Since no quantitative conclusions could be derived from the literature; a 2 $\mu$  mass particle diameter was assumed for this prediction. The performance loss due to the assumed particle size is approximately 0.5% but may ultimately prove to be as much as 1%.

CONFIDENTIAL

UNCLASSIFIED

Report 10/85-F, Phase II

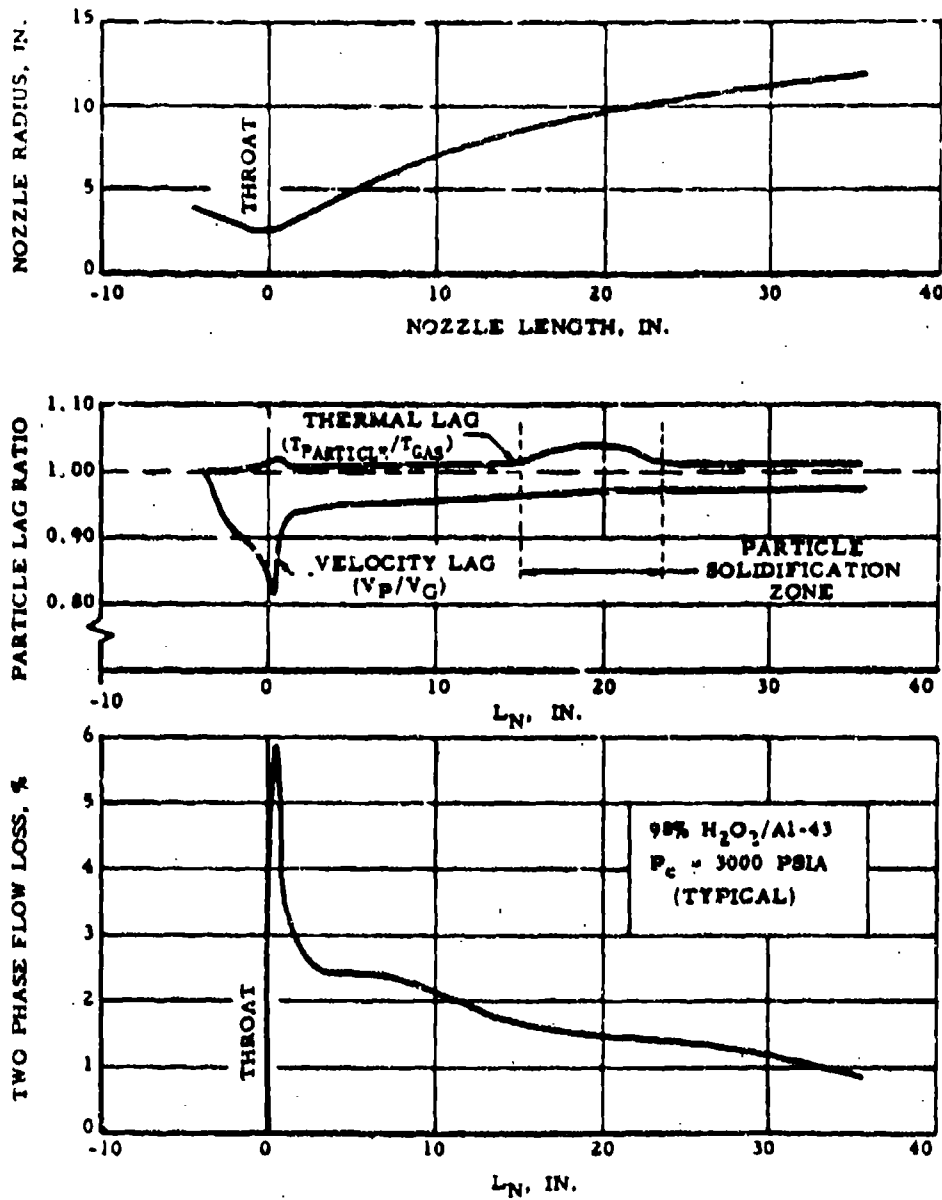


Figure 105. Effect of Nozzle Position on Two-Phase Flow Performance Loss

UNCLASSIFIED



UNCLASSIFIED

Report 10780-F, Phase II

98%  $H_2O_2$ /Al-43

$P_c = 3000$  PSIA

$D_t = 4.954$  IN.

$c = 23:1$

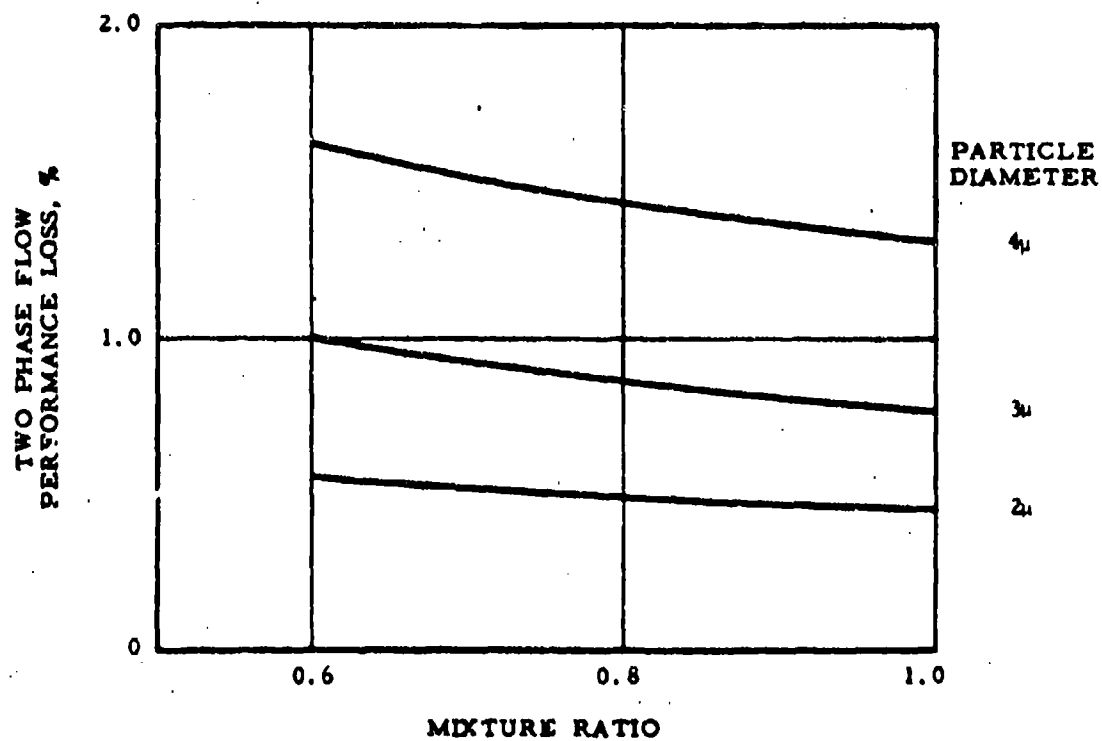


Figure 186. Effect of Mixture Ratio and Particle Size on Two-Phase Flow Performance Loss

UNCLASSIFIED

UNCLASSIFIED

Report 10785-F, Phase II

IV, E, Technical Discussion (cont.)

(U) It has been assumed that the secondary fuel injector for a 100K lbf engine would be designed to provide a uniform fuel injection distribution across the injector face. This precaution would eliminate performance losses due to mixture ratio distribution effects.

(U) The energy release loss is the greatest potential performance loss of the 100K Advanced Propellant Staged-Combustion Engine. It is assumed that the 100K injector will be designed to emulate the energy release efficiency of the Mod II and Mod III 396-tube injector. It will be necessary to provide an injection technique equivalent to 2000 fuel injection tubes to achieve this performance. This energy release loss has been derived from Figures 99 and 100.

UNCLASSIFIED

## IV, B, Technical Discussion (cont.)

5. Heat-Flux Analysis

## a. Introduction

(U) Thermochemical calculations have indicated that the heat capacity of 98%  $H_2O_2$ /Alumizine combustion system is significant. Little or no data exist for this propellant combination for which a reasonable heat-transfer coefficient can be derived. It was the intent of this program to obtain heat-flux data in the combustion chamber and throat of the 20,000-lbf-thrust 3000-psi combustion chamber.

(U) Heat-flux transducers were designed and fabricated from silver-infiltrated tungsten rings in which thermocouples had been buried to measure the material temperature at various distances from the gas-side (inside diameter) surface of the transducer. The design of these transducers can be seen in Figure 44, and a detailed discussion of their design can be found in Section IV,B,1.

(U) Temperature histories were obtained from these transducers during four staged-combustion tests, and the data were correlated with existing thermal models for determination of the heat-transfer coefficient. The location of the thermocouples for the two different heat-flux transducers can be seen in Tables IX and X. The transducers were installed in the combustion chamber and throat as can be seen in Figures 44 and 48. Combustion chamber heat-flux data were obtained in Tests 1.2-02-AAC-004 and 1.2-03-AAC-001, 003, and 007. The data obtained in Test 004 were previously analyzed by a technique which attempted to match the entire operation of the combustion chamber, i.e., start, steady state, and shutdown. It became apparent that the variations existing in mixture ratio, pressure, and combustion efficiency during the start transient made computer simulation of this transient very difficult. Also, Test 004 resulted in very low performance efficiency, because of gross fuel injection, as previously discussed.

TABLE IX

POSITION OF THERMOCOUPLE TIPS FOR HEAT FLUX TRANSDUCERS  
TESTS 1.2-03-AAC-001, 003, AND 007

<u>Station</u>	<u>Area Ratio</u>	<u>Thermocouple Identification</u>	<u>Depth From Surface, in.</u>
Throat	1.0	4	0.101
		3	0.251
		2	0.501
		1	0.751
Chamber	5.0	4	0.092
		3	0.242
		2	0.492
		1	0.742

TABLE X

POSITION OF THERMOCOUPLE TIPS FOR HEAT FLUX TRANSDUCER (CHAMBER)  
TEST 1.2-02-AAC-004

<u>Station</u>	<u>Area Ratio</u>	<u>Thermocouple Identification</u>	<u>Depth from Surface, in.</u>
Chamber	5.0	TWSCC3	0.086
		TWSCC3A	0.210
		TWSCC1	0.219
		TWSCC2	0.468
		TWSCC4	0.763

## 1.3, Technical Discussion (cont.)

(U) The data obtained during Tests 001 and 003 showed excellent correlation, and both tests achieved high combustion efficiency. Data from Test 007 have been included in the report but were not subjected to further analysis, since the data from Tests 001 and 003 were considered to be characteristic of the propellant system.

(U) Table XI shows the observed and calculated parameters representative of the steady-state conditions that existed during Tests 001 and 003. These parameters included combustion chamber pressure, oxidizer and fuel flow rates, and temperature of the oxidizer stream. Only the steady-state portion of the thrust chamber operation was used to correlate the test data.

(U) The thermodynamic properties of silver-infiltrated tungsten are shown in Figure 107 and were used as the basis for determining the heat input corresponding to the temperature history obtained during the tests. The temperature histories obtained during all tests are shown in Figures 108, 109, 110, 111, and 112.

## b. Method of Analysis and Assumptions

(U) In the thermal analysis, particular emphasis was placed upon correlating the data obtained at the chamber and throat sections of Tests 1.2-03-AAC-001 and 003, since this data was representative of the system. The temperature transients of the three operative thermocouples (taken at the throat section) of Tests 001 and 003 are plotted together in Figure 113. Since the firing sequences of the two tests were identical, the respective test temperature transients can be plotted together, by adjusting the time to Fire Switch 2 (FS-2) so that both tests start their steady-state rise together. The transient temperature data, as indicated by the thermocouples, are in excellent agreement for the two tests. In addition, the temperature results

CONFIDENTIAL

Report 10783-F, Phase II

TABLE XI

ENGINE OPERATION PARAMETERS  
(STEADY-STATE VALUES) (U)

	<u>TEST 1.2-G3-AAC</u>	
	<u>001</u>	<u>003</u>
Combustion temperature, °R	6000	5900
Molecular weight, lb/mole	11.7	14.0
Prandtl number	0.4	0.41
Viscosity, lb/ft/sec	$5.8 \times 10^{-5}$	$6.1 \times 10^{-5}$
Specific heat, Btu/lb-°F	0.84	0.775
Chamber pressure, psia	3000	3000
Oxidizer flow rate, lb/sec	29	30.5
Fuel flow rate, lb/sec	41	37.5
Mixture ratio,	0.71	0.82

CONFIDENTIAL

CONFIDENTIAL

CONFIDENTIAL

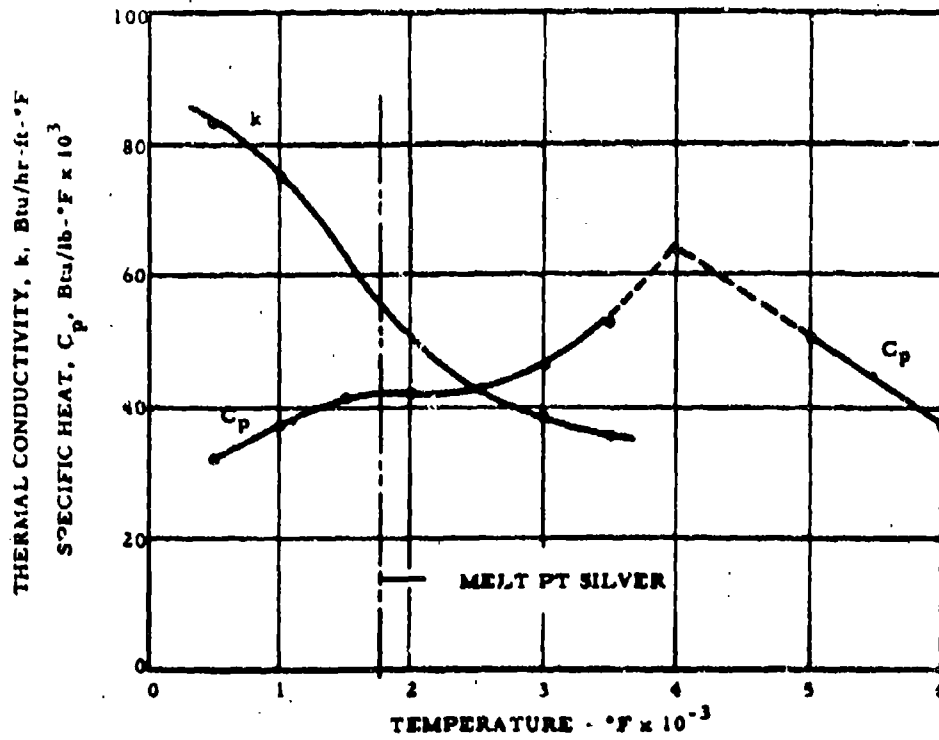


Figure 107. Thermodynamic Properties of Silver-Infiltrated Tungsten

Page 230

CONFIDENTIAL

(2010-1990 to Unclassified)

CONFIDENTIAL

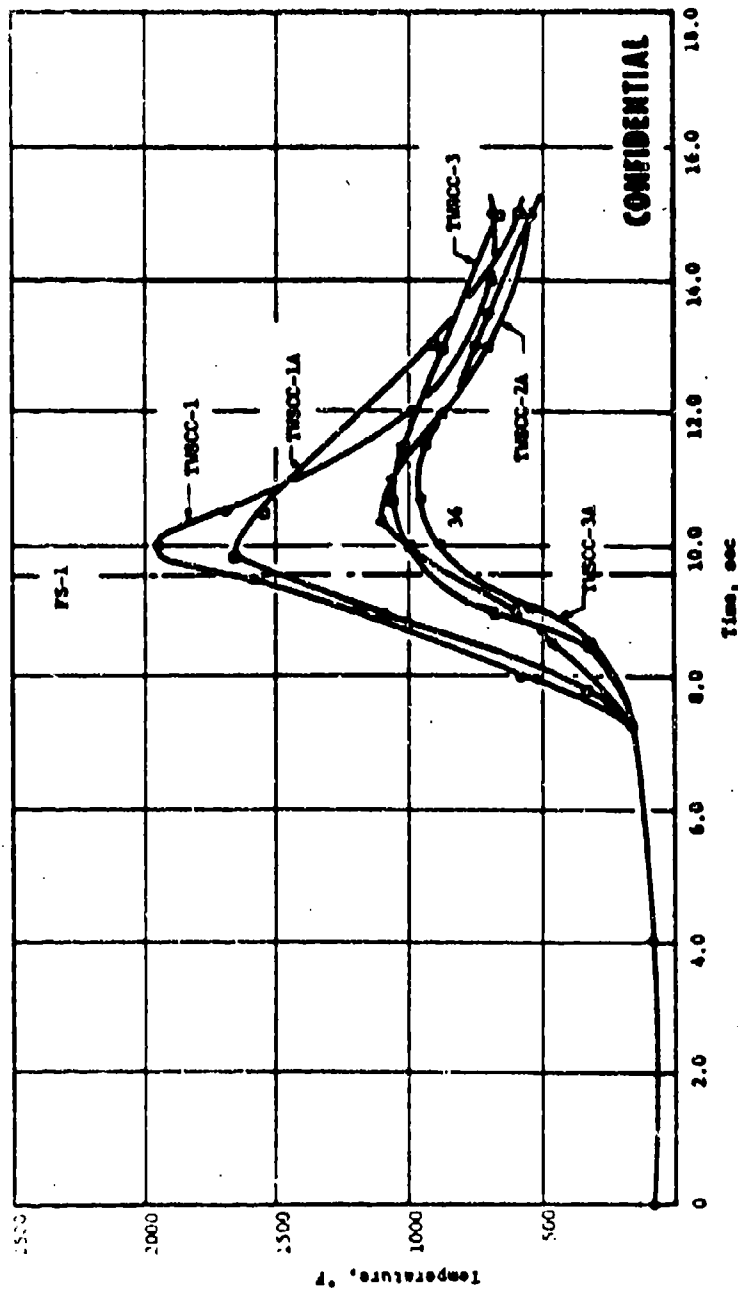
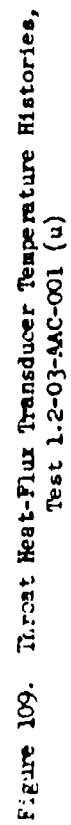


Figure 108. Combustion Chamber Heat-Flux Transducer Temperature Histories, Test 1.2-02-AAC-004 (u)

CONFIDENTIAL



1975-76, Class II



Page 232

**CONFIDENTIAL**

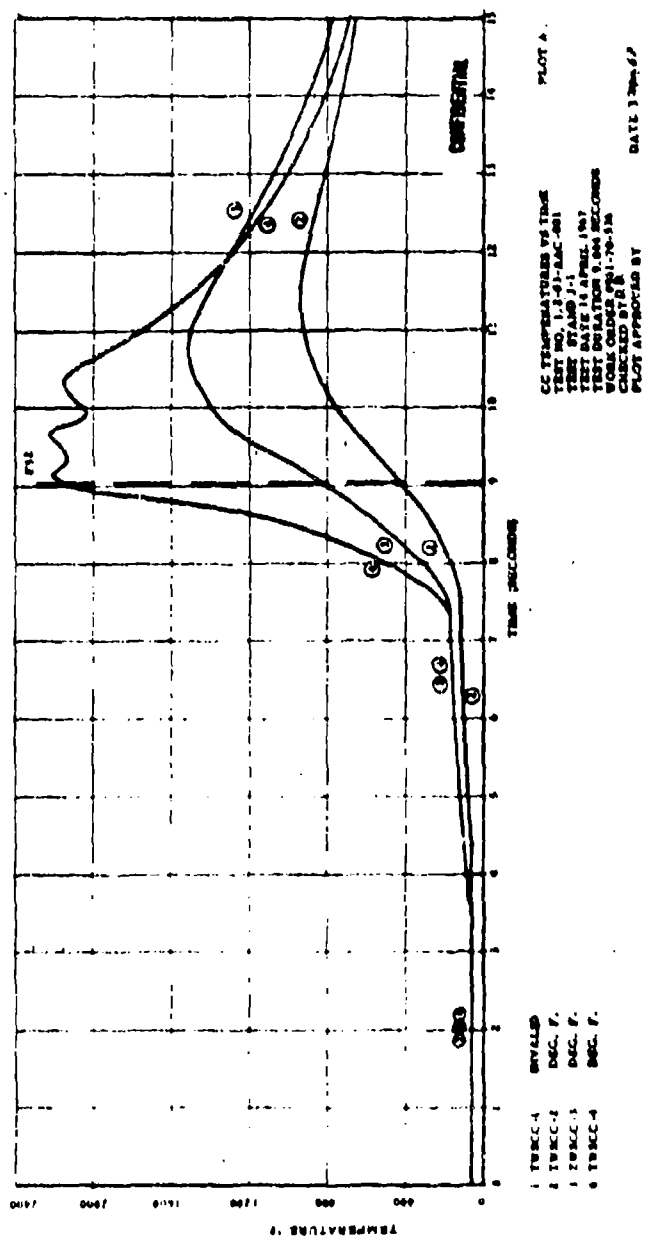


Figure 110. Combustion Chamber Heat-Flux Transducer Temperature Histories, Test L2-03-AAC-001 (u)

**CONFIDENTIAL**

CONFIDENTIAL

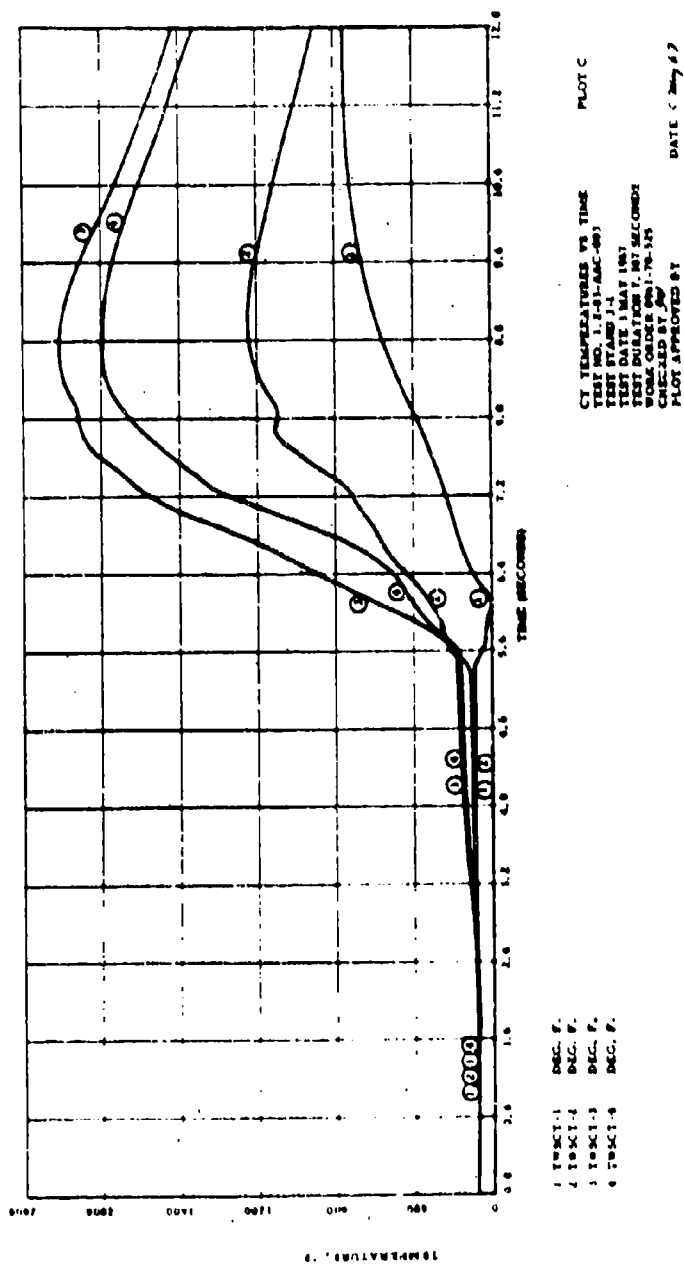


Figure 111. Throat Heat-Flux Transducer Temperature Histories,  
Test 1.2-03-FAC-003 (u)

Page 2 of 4

CONFIDENTIAL

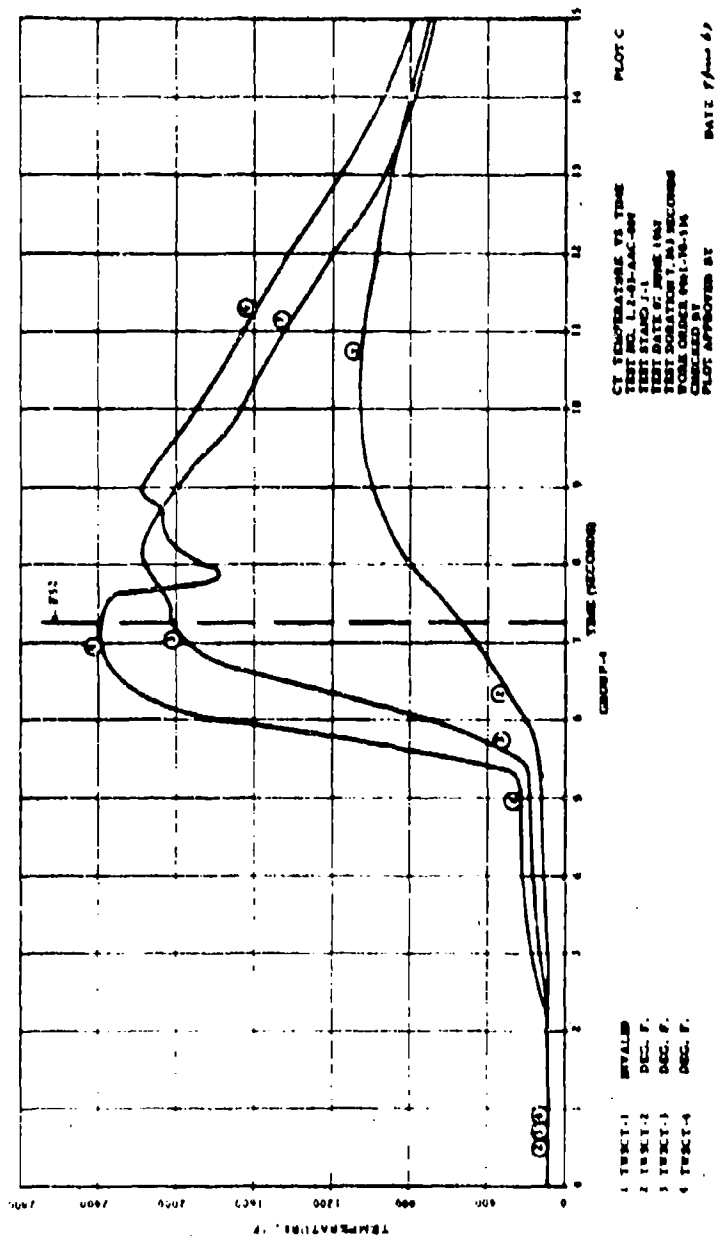


Figure 112. Throat Heat-Flux Transducer Temperature Histories,  
Test 1.2-03-AAC-007 (u)

**CONFIDENTIAL**

CONFIDENTIAL

Report 10789-E, Phase II

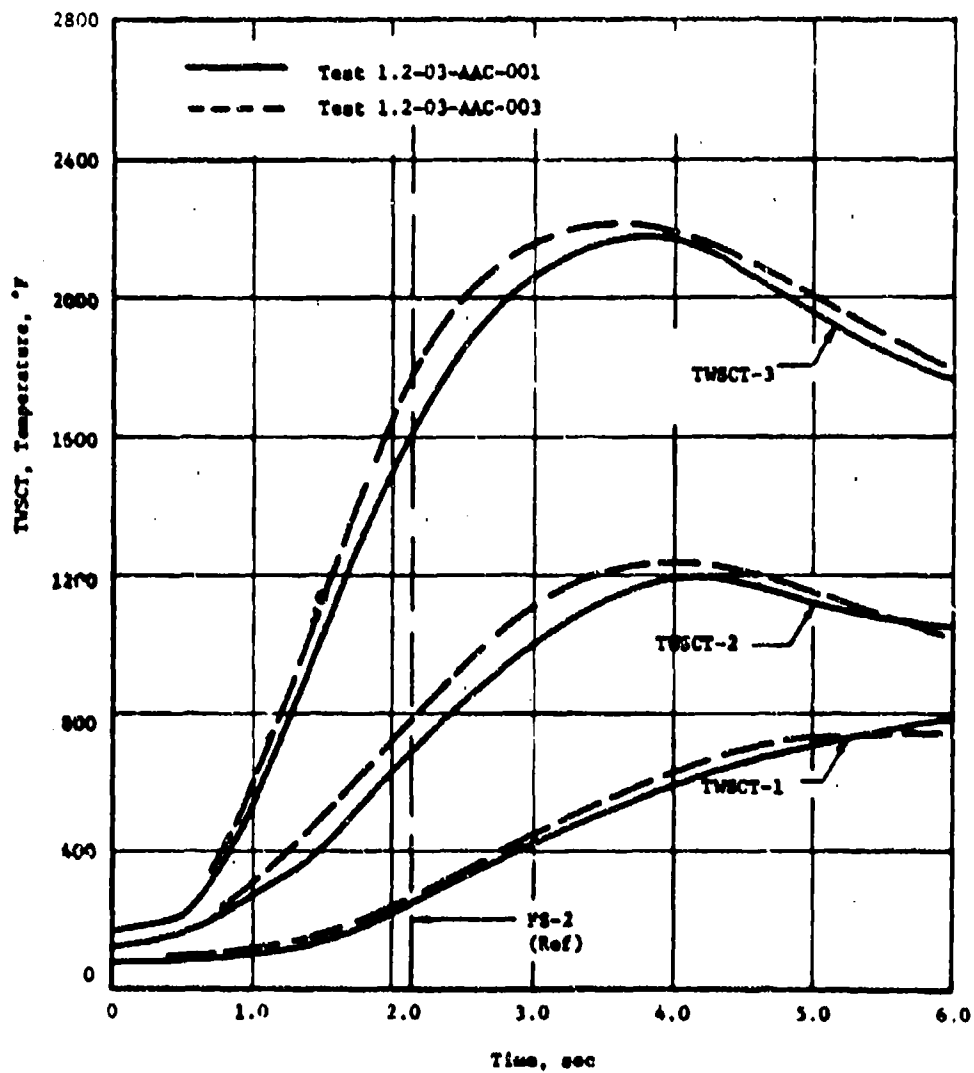


Figure 1. Comparison of Temperature for Three Tests.  
Data for Test 1.2-03-AAC-001 and 003 (i)

Page 10

CONFIDENTIAL

UNCLASSIFIED

Report 10785-F, Phase II

IV, B, Technical Discussion (cont.)

from Test 007 (Figure 112) are in fair agreement with 001 and 003. Therefore, the analysis applying to Tests 001 and 003 would apply to Test 007.

(U) During correlation of the data from the above tests, it became apparent that considerable tailoring of the theoretical conditions for the start and shutdown transients would be necessary in order to match the experimental results. The correlation of theoretical conditions to actual conditions conducted during the start and shutdown period for Test 1.2-02-AAC-004 was inadequate and not sufficiently accurate to determine the heat-transfer coefficient. Therefore, the analysis for Tests 001 and 003 was based on the establishment of steady-state heat-transfer coefficients and fluxes and did not consider the start and shutdown portions of the data.

(U) The experimental results of Tests 1.2-03-AAC-001 and 003 were quite reproducible (throat section; see Figure 113). The data from Test 001 were analysed for the throat and chamber section during the time period corresponding to the steady-state portion of the test run. The technique employed was to accept the temperature distribution that existed within the thermocouple ring at the start of the steady-state portion of the firing. Heat-transfer calculations were then made using various heat-transfer coefficients, and calculated actual combustion temperatures in an effort to match the transient portion of the temperature curves corresponding to the steady-state time period.

(U) Temperature profiles were predicted within the thermocouple ring by using existing computer programs which are based on a finite-difference solution of the heat-conduction equation. The variation of thermal conductivity and heat capacity with temperature was included in the analysis. Heat of fusion of the silver component in the thermocouple ring was also assumed to influence the temperature gradient; however, the effect of vaporization of silver was neglected. The validity of the latter assumption is

UNCLASSIFIED

## IV, B, Technical Discussion (cont.)

justified since the ring surface temperature is well below the saturation temperature of silver at the operating pressure for the entire firing duration.

(U) Figures 114 and 115 indicate the degree of correlation obtained over the steady-state portion of the test runs for the chamber and throat sections, respectively. For example, steady-state conditions for Test 1.2-03-AAC-001 commence at a time of about 8.3 sec. The theoretical flame temperature during stable operation was calculated to be about 6000°R.

(U) The steady-state gas temperature and heat-transfer-coefficient predictions are based on the mixture ratio, total flow rate, and transport properties as shown in Table XI. The transport properties of the chamber gases are based on the Eucken correction method as predicted by the Aerojet 287D Computer Program. These values were then used to determine the heat-transfer coefficients based upon the Colburn relationship:

$$h = \frac{0.023k}{D} Re^{0.8} Pr^{1/3} = \frac{0.023k}{D^{1.8}} \frac{\dot{w}_T}{u}^{0.8} Pr^{1/3} \quad (\text{Eq 7})$$

where:

- D = diameter of chamber bore, ft
- h = heat-transfer coefficient at chamber wall, Btu/hr-ft<sup>2</sup>-°F
- k = thermal conductivity of gas, Btu/hr-ft-°F
- Pr = Prandtl number of gas
- Re = Reynolds number
- $\dot{w}_T$  = mass flow rate of propellant, lb/sec
- $\mu$  = viscosity of chamber, gas, lb/ft-sec

The gas temperature was evaluated at a percentage of the theoretical value, consistent with the  $\eta^*$  efficiency obtained in the tests during steady-state operation.

CONFIDENTIAL

Report 10705-F, Phase II

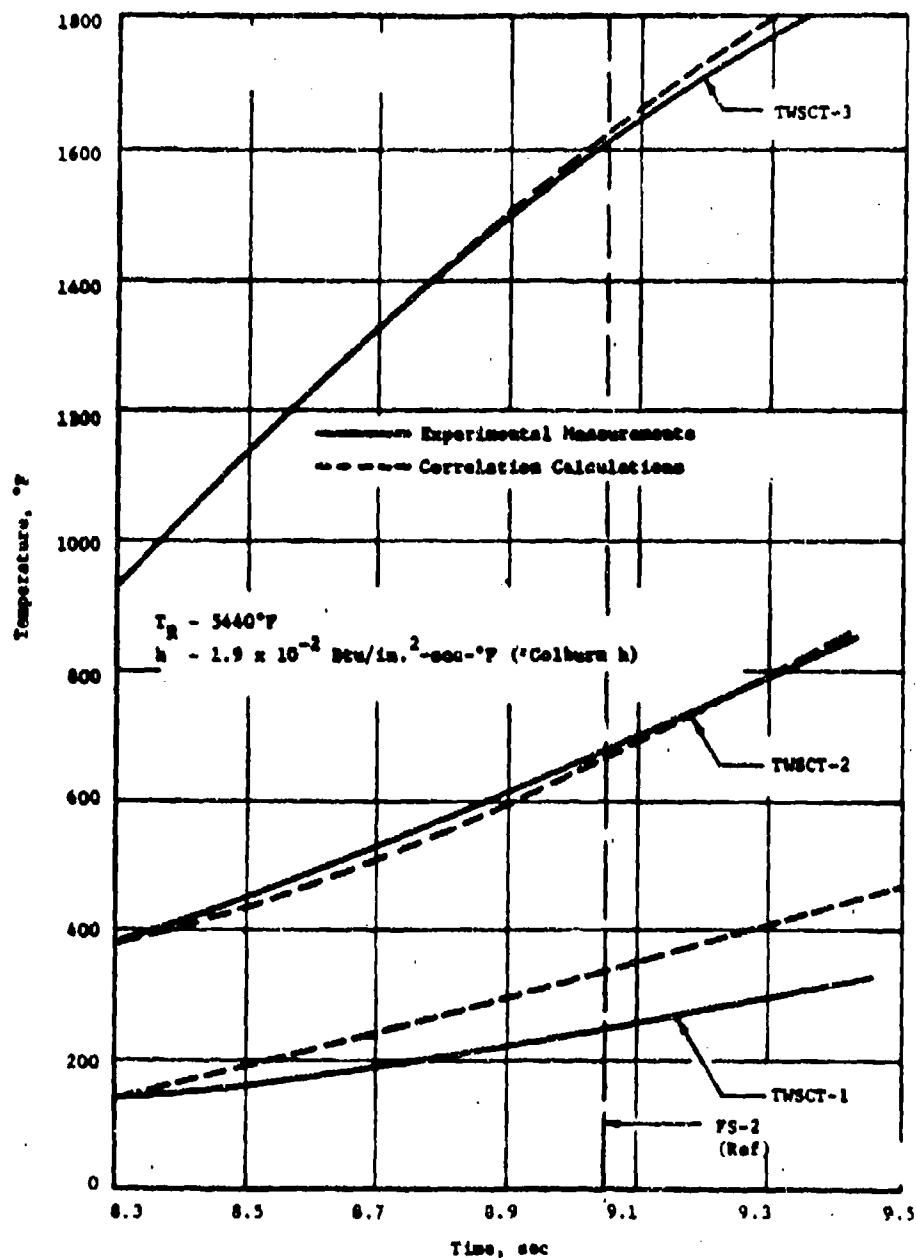


Figure 114. Temperature Transient During Steady State--Throat Section, Test 1.2-03-AAC-001 (u)

Page 239

CONFIDENTIAL



CONFIDENTIAL

Report 10789-1, Phase II

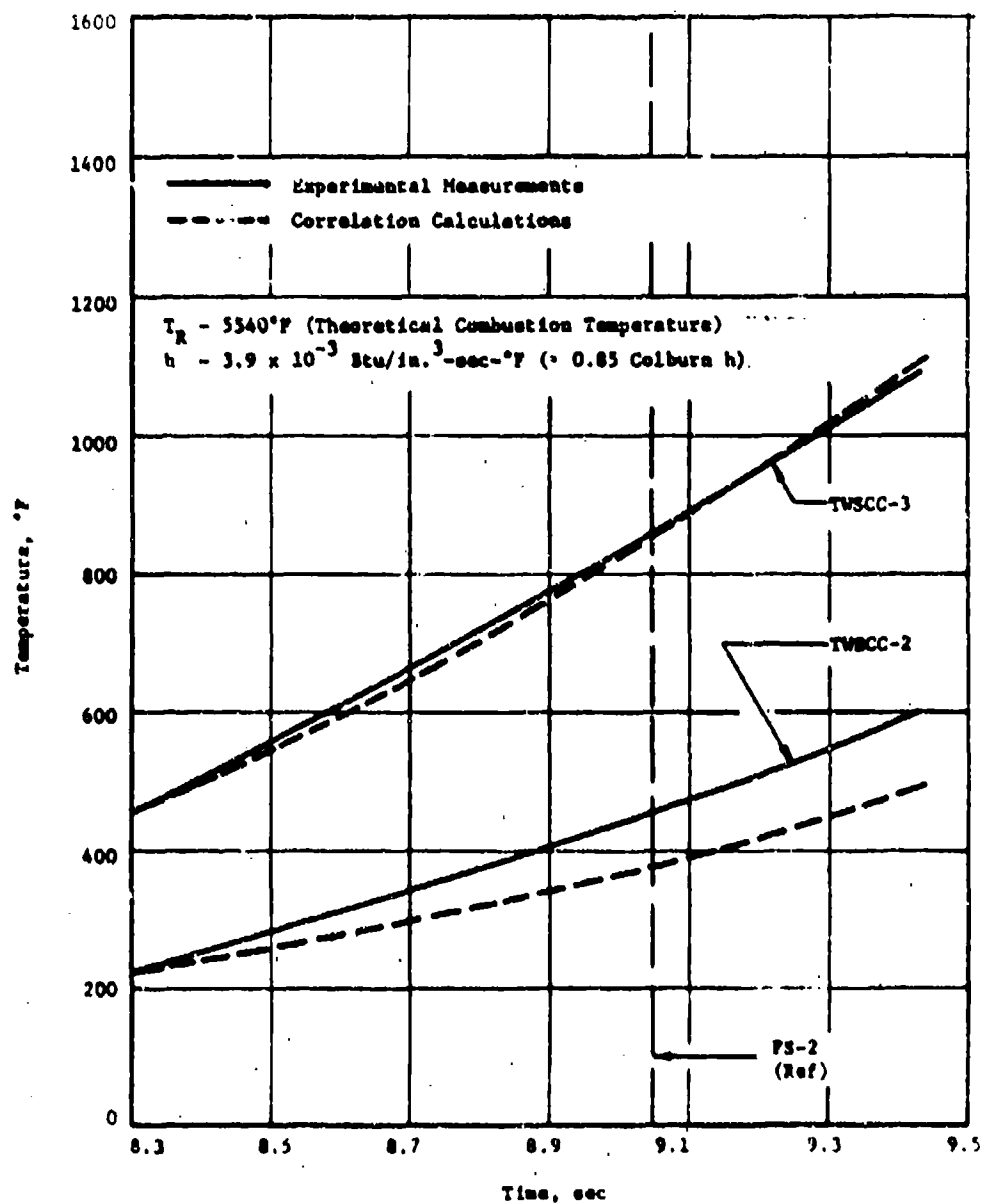


Figure 11. Temperature Transients During Steady State Collection Location, Post 1.2-03-AAC-001 (a)

Page 10

CONFIDENTIAL

## IV, B, Technical Discussion (cont.)

## c. Interpretation of Results

(U) In the early portions of this program, results from the first test, 12-02-AAC-004, indicated a poor correlation between experimental and analytical heat-transfer coefficients. From this work, it was later determined that there was lack of sufficient data (e.g., flow characteristics) to correlate the start and shutdown transients to a meaningful heat-transfer coefficient. In addition to the method of correlation, the low performance and off-design operation of the thrust chamber during the test firing contributed to the poor correlation obtained. Therefore, the present analysis places major emphasis on obtaining only the steady-state heat-transfer coefficient and does so by ignoring the start and shutdown transients. The heat-transfer coefficient existing during steady state is the most meaningful, from the standpoint of future thrust chamber design.

(U) The experimental thermocouple data for the steady-state portions of the tests (1.2-03-AAC-001 and 003) are shown in Figures 114 and 115. Superimposed on their respective graphs are the values of calculated thermocouple temperature which were determined by making conduction-program computer runs using various values of thermal resistance at the gas-wall interface and selecting the run whose calculated thermocouple temperature best matched the measured thermocouple temperature. The thermal resistance at the wall,  $R_w = 1/h_{obs} A$  (where  $A$  is the heat-transfer area), determines the heat-transfer coefficient,  $h_{obs}$ , which was assumed to be of the Colburn form except that a "prefix" coefficient is applied as shown below

$$h_{obs} = (1/\bar{a}) \frac{(.023)k}{D} Re^{0.8} Pr^{1/3}$$

UNCLASSIFIED

## B. Technical Discussion (cont.)

where:

- $\bar{a}$  = the prefix coefficient
- D = diameter of the gas port, ft
- h = heat-transfer coefficient at chamber wall, Btu/hr  $\cdot$  ft<sup>2</sup>  $\cdot$  °F
- k = thermal conductivity of gas, Btu/hr-ft  $\cdot$  °F
- Pr = Prandtl number of gas
- Re = Reynolds number

(U) The value of  $\bar{a}$  reflects the deviation from the theoretical Colburn result. The calculations indicate that the experimental heat-transfer coefficients were about the same as the analytically determined values.

(U) For this analysis, it was assumed that the data were free of any anomalies. In reality, there were various effects which could have influenced the results. These were: (1) poor thermocouple response (at some test locations) because of fabrication of instrumentation; (2) Al<sub>2</sub>O<sub>3</sub> deposits on the transducer ring surface; (3) and variable boundary effects existing during the assumed steady-state period because of ablation of the silica phenolic liner that composed the chamber. These effects should be analyzed in depth to find their separate influences upon the data; however, such a detailed analysis is beyond the scope of the program.

(U) The steady-state correlations show some deviation for the innermost buried thermocouples. This is probably due to side conduction effects, since the analysis performed was one-dimensional in nature and, therefore, did not consider the heat input or rejection to surrounding material. At the throat section it is quite likely that heat was transferred to the adjacent silver-infiltrated-tungsten throat insert, since the inner thermocouples indicate a lower temperature experimentally than was estimated by analytical calculation.

## IV, B, Technical Discussion (cont.)

(C) The heat-transfer characteristics for the  $H_2O_2$ /Alumizine propellant combination can be summarized concisely in tabular form as:

Section	$T_R, ^\circ R$	$h_g, \text{Btu/in.}^2\text{-sec.-}^\circ F$	% of Colburn, $\frac{h_g}{h_g}$	$\bar{a}$
Chamber	5540 (theoretical combustion temperature)	$3.9 \times 10^{-3}$	65	1.18
Throat	5440 (theoretical recovery temperature)	$1.9 \times 10^{-2}$	100	1

From the above data (a), it is clear that the Colburn equation predicts reasonably well the chamber and throat heat-transfer coefficients for the  $H_2O_2$ /Alumizine-43 system. For conservative preliminary designs utilizing these propellants, use of the Colburn equation as explained in this report is recommended for the thrust chamber heat-transfer evaluation and sizing of all regenerative, transpiration, and/or uncooled chambers.

6. Test Data Analysis

## a. Combustion Stability Analysis--Test 1.2-02-AAC-004

(U) Oscillations of 800 and 2400 cps occurred on Test 1.2-02-AAC-004 between  $FS_1 + 6.98$  and  $FS_1 + 7.40$  sec, both in the primary chamber and in the fuel feed system. Oscillations also occurred in the oxidizer manifold but were insignificant. During this time period, the TCA was in its start transient, with pressures in the secondary chamber ranging from 50 to 70% of steady-state chamber pressures. The oscillations developed

... 2, Technical Discussion (cont.)

and subsided very gradually, with no evidence of a pop or detonation to initiate or propagate them. The oscillations in the fuel manifold had a pre-dominant frequency of 800 cps at a peak-to-peak pressure of 110 psi, whereas the two transducers on the preburner indicated pressure oscillations of 2400-cps, with some 800-cps oscillations at amplitudes of 125 psi (peak-to-peak).

(U) Test -004 differed from the first two staged-combustion tests as follows:

(1) The fuel injector pressure drop was reduced 50% by substituting the tubular injector for the vane-type injector;

(2) Thrust per element of the tubular injector was increased ten-fold;

(3) Oscillations were present on Test -004, but did not occur on previous tests;

(4) Pressure drop through the turbine simulator was reduced significantly (Table VI).

(U) Estimation of longitudinal acoustic modes for the combination of the two chambers (preburner and secondary combustor) indicated the existence of such modes at oscillations of about 800 and 2400 cps. These modes are difficult to calculate because of the complex interaction between the resonance phenomena in the preburner and secondary chamber. The long feed lines to the TCA were capable of resonance at a large number of frequencies in these two ranges. Since increasing pressure drop in such a system can damp oscillations, the lowering of the pressure drop both through the turbine simulator and the fuel injector (as in Test -004) tended to increase the probability of oscillations (Ref. 11).

## IV, B, Technical Discussion (cont.)

(U) The frequency at which the tubular injector would be expected to reinforce acoustic oscillations was estimated by using empirical correlations compiled by Aerojet-General. These correlations show the sensitive time lag,  $\tau$ , as a function of chamber pressure and injector orifice diameter. The resonant frequency is related to  $\tau$  by

$$f = \frac{1}{2\tau}$$

This frequency, which is a function of mean pressure and of the diameter of the injector elements, was estimated to be 2500 cps at the pressure at which the oscillations occurred in Test -004. This explains the occurrence of the 2400-cps oscillations. As the chamber pressure continued to rise, the resonant frequency during the combustion process also increased until coupling with the chamber resonance was no longer possible. Therefore, the oscillations damped out. The 800-cps oscillations may have been caused by a feed-system mode coupled with a chamber mode, since they preceded the 2400-cps oscillations and existed during preburner operation only.

(U) Oscillations in the feed system can be reduced or eliminated, without increasing pressure drop, by installing a side-branch resonator one-quarter wave length upstream of the injector (Ref. 12). However, such a resonator would be effective only in its design frequency range. Other means of controlling the occurrence of oscillations are through the variation in pressure drop and in chamber dimensions. However, more analytical work would have been required to successfully predict the effect of design changes on system stability.

(U) Since the pressure drop in the vane-type injector was lowered in the Mod III injector design, this injector was also examined to determine if combustion instability would occur. The stability estimates were

## IV. B. Technical Discussion (cont.)

Based upon a more recent correlation similar to that given by Reardon (Ref. 12). It was assumed that the injection elements with a diameter of 0.054 in. would dominate since they carried about 90% of the flow. The following results were obtained:

<u>Chamber Pressure</u>	<u>Combustion Resonant Frequency, cps</u>
50% of steady state	3700
75% of steady state	4200
100% of steady state	4600

It was concluded that in the pressure range considered, resonant interaction with the 2400-cps longitudinal mode would not occur and that interaction with the 5600-cps first tangential mode of the secondary chamber was not probable.

UNCLASSIFIED

Report 10785-F, Phase II

SECTION V

CONCLUSIONS

(U) The analytical and experimental programs conducted under this contract have resulted in the development of a technology base from which an advanced rocket engine system using  $H_2O_2$  and Alumizine, or other heterogeneous fuels, could be developed. The conclusions drawn from these studies are categorized according to the major tasks in the contract.

A. TRANSIENT COOLING ANALYSIS

(U) 1. A regeneratively cooled thrust chamber assembly for an engine using  $H_2O_2$  and Alumizine can be safely started, shut down, and restarted with proper control of propellant phasing in the coolant jacket and turbine.

(U) 2. Thin thermal barrier coatings composed of mixtures of metals and oxides and having low thermal conductivity show significant advantages over thick tungsten coatings for coolant tubes, because the heat soak back from the thin coating is less pronounced.

(U) 3. The start and shutdown transients of a cooled  $H_2O_2$ /Alumizine engine must be oxidizer rich to satisfy transient cooling requirements.

B. PREBURNER

(U) 1. A 98%  $H_2O_2$  preburner can be operated satisfactorily with throughputs up to 110 psia and pressures in excess of 4500 psi. Significant reduction in catalyst length is possible through the operation of the catalyst pack at high pressure.

(U) 2. The experimental catalyst, developed by the FMC Corporation and the Age Catalyst Company, has both the activity and the high-temperature resistance required for decomposition of high-concentration  $H_2O_2$ .

UNCLASSIFIED



UNCLASSIFIED

Report 10785-F, Phase II

V. B. Preburner (cont.)

(U) 3. The decomposition temperature of 90 and 98%  $H_2O_2$  is only slightly affected by pressure.

(U) 4. Pure silver may be used as an active catalyst for 98%  $H_2O_2$  provided it is included only in the entrance portion of the catalyst pack where decomposition is initiated and pack temperature is low.

(U) 5. The unique pack construction, in which nickel-manganese screens are interspersed between the active catalyst screens, prevents the pack from losing its precompaction.

(U) 6. The catalyst developed for use with 98%  $H_2O_2$  is also satisfactory for the decomposition of 90%  $H_2O_2$ .

C. STAGED COMBUSTION

(U) 1. High specific impulse efficiency can be obtained with staged combustion of  $H_2O_2$  and Alumizine.

(U) 2. High performance with staged combustion using  $H_2O_2$  and Alumizine is obtained through the maximum dispersion of Alumizine into the gaseous oxidizer stream.

(U) 3. Tungsten resists erosion satisfactorily when exposed to the products of combustion of  $H_2O_2$  and Alumizine at mixture ratios up to 1.0. Therefore, tungsten is applicable to an advanced  $H_2O_2$ /Alumizine combustion chamber provided that a high performance, nonstreaking injector is used.

(U) 4. High-pressure staged combustion of  $H_2O_2$  and Alumizine has no inherent combustion instability.

# UNCLASSIFIED

Report 10785-F, Phase II

## V, C, Staged Combustion (cont.)

(U) 5. The staged-combustion cycle is applicable for use with this propellant combination.

(U) 6. A performance level in excess of 93% of theoretical  $I_p$  for a 100,000-lbf-thrust engine is predicted on the basis of the performance obtained in the 20,000-lbf-thrust tests.

(U) 7. The combustion efficiency of  $H_2O_2$  and Alumina is independent of the  $H_2O_2$  concentration over the concentration range from 90 to 98%.

UNCLASSIFIED

# UNCLASSIFIED

Report 10785-F, Phase II

## SECTION VI

### RECOMMENDATIONS

(U) This section contains recommendations for further study that would be required to obtain the technology for a high-pressure staged-combustion  $H_2O_2$ /Alumizine engine (or an engine based upon a related heterogeneous propellant system). This discussion has been organized according to areas of technology.

#### A. PERFORMANCE

(U) 1. The effects of mixture ratio, studied on a limited basis in this contract, should be further evaluated to optimize the operating mixture ratio and obtain the maximum delivered  $I_p$  for a candidate rocket engine system.

(U) 2. The effect of change in characteristic length ( $L^*$ ) has been investigated in this contract. The investigation of the effect of  $L^*$  on performance should be extended to investigate  $L^*$ 's less than 40.

(U) 3. An objective of this contract was to determine the feasibility of high-pressure staged combustion of  $H_2O_2$ /Alumizine-43. This propellant combination should also be considered for low-pressure (pressure-fed) systems. Consequently, an evaluation of the effect of combustion chamber pressure on performance is recommended.

(U) 4. Past analytical studies have indicated that the aluminum loading in hydrazine should be optimized for a particular engine system. Combustion experiments should be conducted to determine the proper aluminum loading for an  $H_2O_2$  and Alumizine system to obtain the maximum delivered  $I_p$  with the maximum propellant density.

UNCLASSIFIED

# UNCLASSIFIED

Report 10785-F, Phase II

## VI. Recommendations (cont.)

### B. COOLING

(U) 1. The major objective of this program, in the area of cooling, was to investigate the regenerative cooling characteristics of 98%  $H_2O_2$ . These studies indicated that a high-pressure regeneratively cooled TCA will require a 4500°F thermal barrier. To further evaluate this cooling technique, thermal barriers capable of operating at 4500°F should be developed.

(U) Other cooling techniques are promising and feasible but require further investigation. Transpiration cooling with liquid  $H_2O_2$  and decomposed  $H_2O_2$  should be investigated.

(U) 2. The most near-term application of this propellant combination to a rocket engine system would be through the use of an uncooled (heat sink) type combustion chamber. This type chamber would utilize tungsten and silver-infiltrated tungsten as the flame barrier. Long-duration testing of a tungsten-lined heat-sink type combustion chamber should be conducted to demonstrate the feasibility of this approach.

(U) 3. A high-pressure staged-combustion  $H_2O_2$ /Aluminine engine has available large quantities of high-pressure gas. Consequently, the film cooling characteristics of high-pressure, decomposed  $H_2O_2$  should be investigated.

(U) 4. The cooling characteristics of  $H_2O_2$  with rolling contact bearings should be investigated, because an engine system using this propellant combination, or  $H_2O_2$  in combination with another fuel, would use the  $H_2O_2$  as a bearing coolant.

UNCLASSIFIED

# UNCLASSIFIED

Report 10785-F, Phase II

## VI, B, Cooling (cont.)

(U) 5. The most near-term application of this propellant combination should consider the use of 90%  $H_2O_2$  instead of 98%  $H_2O_2$ , since the decomposition temperature is less than 1400°F; current turbine and catalyst technology is directly applicable. The lower  $H_2O_2$  concentration, however, reduces the specific impulse by approximately 1%. Therefore, higher performance can be achieved with 98%  $H_2O_2$  as the oxidizer. The decomposition temperature of 98%  $H_2O_2$  is approximately 1800°F, which will therefore require the use of high-temperature or cooled turbine blade technology. Turbine cooling techniques and oxidizer-resistant high-temperature materials should be investigated.

## C. CATALYST

(U) 1. The decomposition of 90 and 98%  $H_2O_2$  at high pressure has been accomplished with an advanced catalyst material. This new catalyst material has a high melting temperature and good activity. However, indications are that the activity of the catalyst was reduced as a function of exposure to the  $H_2O_2$ . Further investigation of this alloy and coatings for the alloy material is required to ensure long duration and restart capability for  $H_2O_2$  monopropellant gas generators.

(U) 2. The catalyst pack construction, although unique, was based on the design requirements for small monopropellant reaction motors. A high-pressure  $H_2O_2$ /Alumina staged-combustion engine would require a unique catalyst housing volume. Consequently, further investigation of catalyst construction, in particular the radial flow catalyst packs, is required.

UNCLASSIFIED

## VI, Recommendations (cont.)

## D. DESIGN

(U) Special design techniques are required for the Aluminine components in an advanced rocket engine system. Any heterogeneous fuel has the potential of deteriorating in an open system after use and thus producing a solid residual material which must be considered in the system design. Design techniques should be developed for the injectors and controls of a rocket engine system using heterogeneous propellants. Design of components having the capability of reuse without disassembly for cleaning should be investigated.

## E. MISSIONS AND APPLICATIONS

(U) This propellant combination should be investigated for its application to advanced booster engine systems, upper stage, and in-space propulsion. Specifications should be developed for these applications that would be used as a basis for the design of systems and components for any future candidate rocket engine.

UNCLASSIFIED

Report 10785-F, Phase II

REFERENCES

1. Final Report, Advanced Propellant Staged-Combustion Feasibility Program, (Phase I), Report AFRPL-TR-66-6, Contract AF 04(611)-10785, Aerojet-General Corporation.
2. Kousar, D. C. and Van Huff, N. E., Heat Transfer Characteristics of 98%  $H_2O_2$  at High Pressure and High Velocity, Report AFRPL-TR-66-263, Contract AF 04(611)-10785, Aerojet-General Corporation, August 1966.
3. Baumeister, Theodore, Marks Mechanical Engineers' Handbook, Sixth Edition McGraw Hill Book Company, New York, N. Y., p. 4-61.
4. Mason, S. J., "Feedback Theory, Further Properties of Signal Flow Graphs," Proceedings of the IRE, Vol 41, pp. 1144-1156, 1953.
5. Mason, S. J., "Feedback Theory, Further Properties of Signal Flow Graphs," Proceedings of the IRE, Vol 44, pp 920-926, 1956.
6. Materials of Construction for Equipment in Use with Hydrogen Peroxide, Bulletin No. 104, Food Machinery and Chemical Corporation, 1966 Revision.
7. Final Report, Improved Titan Predevelopment, Subscale TCA Testing, Volume II, BSD-TR-65-455, February 1966.
8. Ong, J. N. and Passel, W. M., Corrosion, No. 18, 382t, (1962).
9. Perkins, R. A., Price, W. L. and Crooks, D. D. Oxidation of Tungsten at Ultra-High Temperatures, NASA, N63-18738 (1962).
10. Final Report, Investigation of Heterogeneous Propellant Two-Phase Flow Criteria, Report AFRPL-TR-67-62, Contract AF 04(611)-11205, Aerojet-General Corporation.
11. Reardon, F. H., "Application of Crocco Theory," LCRPG 2nd Combustion Conference, CPIA Publication 103, May 1966.
12. Lewis, Blade, Dorsch, "Study of the Effect of a Closed-End Side Branch on Sinusoidally Perturbed Flow of Liquid in a Line," NASA TND-1876, September 1963.

UNCLASSIFIED

APPENDIX I

SHUTDOWN TRANSIENT EQUATIONS AND COMPUTER PROGRAMS



# UNCLASSIFIED

Report 10785-F, Phase II, Appendix I

## A. ENGINE FLOW MODEL

The objective of this portion of the analysis was to develop an analytical model of a prototype engine capable of predicting fuel and oxidizer flow rates during a variety of possible shutdown transients.

To keep this model as simple as possible, a number of simplifying assumptions were made. These assumptions and their justification are:

(1) Pump cavitation is neglected and inducer-pump performance is included in the main-pump performance. Cavitation is seldom a problem on shutdowns because of decreasing speeds and flow rates. Similarly, inducer performance on shutdown, starting from a steady-state operating point, should follow the main pumps closely.

(2) Fluid inertias are neglected. This is justified because the main error introduced will be in pressures upstream of the valves. The effect on flow rates for reasonable line lengths will be small.

(3) Primary combustor gas properties are assumed to be constant. This is justified by the nature of the decomposition process in the catalyst bed. Although temperature will vary with cooling-jacket exit temperature, this effect was neglected because one of the objectives of the thermal analysis is to keep the exit temperature nearly constant.

(4) Propellant fluid densities are assumed to be constant with time throughout the system. The justification for this assumption is the same as above.

With these assumptions, it is possible to represent engine performance by only three differential equations in three unknowns:  $P_{pc}$ , primary combustor pressure;  $P_{sc}$ , secondary combustor pressure; and  $N$ , turbopump speed.

# UNCLASSIFIED

Report 10785-F, Phase II, Appendix I

Additional auxiliary equations, required to relate these three parameters, are listed below in their usual form; for computer solution there will be a further combination of terms. The control parameters are  $C_{ov}$  and  $C_{fv}$ , oxidizer- and fuel-valve resistance, respectively, which are input as functions of time.

## 1. Oxidizer Line and Pump

$$P_{oD} = P_{pc} + [C_{oT} + C_{ov}(t)] \frac{W_o^2}{\rho_o} \quad (\text{Line})$$

$$P_{oD} = P_{os} + \rho_o N^2 \left[ C_{op1} + C_{op2} \left( \frac{W_o}{\rho_o N} \right) + C_{op3} \left( \frac{W_o}{\rho_o N} \right)^2 \right] \quad (\text{Pump})$$

These equations will be combined to give a quadratic and  $W_o$ . Valve resistances are to be input as functions of time. It is reasonable to assume that admittance ( $1/\sqrt{C}$ ) varies linearly with time, thus:

$$C_{ov}(t) = \frac{C_{ovs}}{\left( 1 - \frac{t - \tau_{ov1}}{\tau_{ov2} - \tau_{ov1}} \right)^2} \quad \tau_{ov1} < t < \tau_{ov2}$$

$$C_{fv}(t) = \frac{C_{fvs}}{\left( 1 - \frac{t - \tau_{fv1}}{\tau_{fv2} - \tau_{fv1}} \right)^2} \quad \tau_{fv1} < t < \tau_{fv2}$$

Subscripts:

- S = Steady-state
- 1 = Closing starts
- 2 = Closing ends

# UNCLASSIFIED

Report 10785-F, Phase II, Appendix I

## 2. Fuel Line and Pump

$$P_{fd} = P_{sc} + \left[ C_{fT} + C_{fv}(z) \right] \frac{W_f^2}{\rho_f} \quad (\text{Line})$$

$$P_{fd} = P_{fs} + \rho_f N^2 \left[ C_{fP1} + C_{fP2} \left( \frac{W_f}{\rho_f N} \right) + C_{fP3} \left( \frac{W_f}{\rho_f N} \right)^2 \right] \quad (\text{Pump})$$

These equations will be combined to give a quadratic in  $W_f$ .

## 3. Gas-System Pressure Drops

It is assumed that the ratio of the individual pressure drops to the total ( $P_{pc} - P_{sc}$ ) remains constant. Two pressure ratios are required ( $P_{R1}$  for computing turbine weight flow, and  $P_{R2}$  for computing turbine work). A reaction turbine is assumed.

$$P_{R1} = \frac{P_{ps} - C_{T1} (P_{pc} - P_{sc})}{P_{pc} - C_{T3} (P_{pc} - P_{sc})} \quad i = 1, 2$$

## 4. Turbine Weight Flow

Test for choked flow:

$$\text{If } P_{R1} < C_{T4},$$

$$P_{R1} = C_{T4}, \quad P_{R2} = C_{T5}$$

$$\text{If } P_{R1} \geq C_{T4},$$

(Use values from Section A, 3)

$$W_T = C_{T6} \left[ P_{pc} - C_{T3} (P_{pc} - P_{sc}) \right] P_{R1}^{n_1} \sqrt{1 - P_{R1}^{n_2}}$$

5. Turbine Output

Isentropic Spouting Velocity:

$$V_1 = C_{T7} \sqrt{1 - P_{R2}^{a_2}}$$

Turbine Efficiency:

$$\eta_T = C_{T8} \frac{N}{V_1} + C_{T9} \left( \frac{N}{V_1} \right)^2$$

Turbine Torque:

$$\mu_T = \frac{60 \eta_T W_T V_1^2}{4 \pi g N}$$

6. Pump Torques

$$\mu_o = \rho_o N^2 \left[ C_{oP4} + C_{oP5} \left( \frac{W_o}{\rho_o N} \right) + C_{oP6} \left( \frac{W_o}{\rho_o N} \right)^2 \right]$$

$$\mu_f = \rho_f N^2 \left[ C_{fP4} + C_{fP5} \left( \frac{W_f}{\rho_f N} \right) + C_{fP6} \left( \frac{W_f}{\rho_f N} \right)^2 \right]$$

7. Secondary Combustor

$$MR = W_T / W_f$$

$$c^* = C_{s1} + C_{s2} (MR) + C_{s3} (MR)^2 + C_{s4} P_{sc}$$

# UNCLASSIFIED

Report 10785-F, Phase II, Appendix I

Flow at Nozzle Throat:

$$W_{sc} = \frac{g A_c P_{sc}}{c^*}$$

## 8. Force Balance on Turbine

$$I \frac{d\Omega}{dt} = \tau_T - \tau_D - \tau_f$$

## 9. Continuity Equation for Primary Combustor

$$C_{P1} \frac{dP_{P1}}{dt} = W_D - W_T$$

## 10. Continuity Equation for Secondary Combustor

$$\frac{C_{S2}}{(c^*)^2} \frac{dP_{S2}}{dt} = W_T + W_f - W_{sc}$$

## B. ENGINE FLOW COMPUTER PROGRAM

An implicit numerical method using backward time differences has been programmed to solve the above engine system model. The inherent stability features of an implicit method, coupled with the relatively small inertial effects of the present system, allow the use of large time steps. This advantage is gained at the cost of solving the system difference equations simultaneously at each time step. However, a relatively simple iterative procedure has been developed for this solution, and it appears to have good convergence characteristics.

The primary or outer iterations adjust the primary and secondary combustor pressures simultaneously; an inner iteration loop determines the fuel flow  $W_f$  for each outer iteration. Therefore, the iteration equations given below for time  $t$  are written in terms of assumed pressures  $X_p$  and  $X_s$ , calculated pressures  $Y_p$  and  $Y_s$ , an assumed fuel flow rate  $X_f$ , and a calculated fuel flow rate  $Y_f$ .

### 1. Iteration Procedure and Equations

With assumed primary and secondary combustor pressures, the pressure ratios  $P_{R1}$  are known and the turbine weight flow  $W_T$  may be calculated from Section A.4. The oxidizer flow rate is then determined from

$$W_o = W_T + \frac{C_{p1}}{\Delta t} (X_p - P'_{pc})$$

in which  $P'_{pc}$  is the known primary pressure at the previous time step, i.e., at time  $t - \Delta t$ . In the inner iterations for  $W_f$ , the assumed flow  $X_f$  is used to evaluate the secondary combustor mixture ratio  $MR$  and thus  $c^*$ ; the calculated fuel flow is then given by

$$Y_f = \frac{g A_f X_s}{c^*} - W_T + \frac{C_{s2}}{(c^*)^2 \Delta t} (X_s - P'_{sc})$$

in which  $P'_{sc}$  is the secondary pressure at time  $t - \Delta t$ .

After the inner iteration converges to  $W_f$ , the turbine speed  $N$  is determined from the turbine force balance; the latter yields the following quadratic in  $N$ :

$$(\rho_o C_{OP4} + \rho_f C_{FP4}) N^2 + (C_{OP5} W_o + C_{FP5} W_f + \frac{1}{\Delta t} - \frac{15}{78} C_{TP9} W_T) N$$

$$- (\frac{1}{\Delta t} N' + \frac{15}{78} C_{TP8} V_1 W_T - \frac{C_{OP6}}{\rho_o} W_o^2 - \frac{C_{FP6}}{\rho_f} W_f^2) = 0$$

in which  $N'$  is the turbine speed at time  $t - \Delta t$ . Each outer or pressure iteration is completed by obtaining calculated pressures from the line and pump equations in Sections A.1 and A.2. Thus,

$$Y_p = P_{os} + \rho_o C_{OP1} N^2 + C_{OP2} W_o$$

$$= [C_{OT} - C_{OP3} + C_{OV}(t)] \frac{W_o^2}{\rho_o}$$

$$Y_f = P_{fs} + \rho_f C_{FP1} N^2 + C_{FP2} W_f$$

$$= [C_{FT} - C_{FP3} + C_{FV}(t)] \frac{W_f^2}{\rho_f}$$

## 2. Inner Iterations

Newton's method is used to modify  $X_f$  in the inner iterations; thus, for the  $(m+1)$ st iteration

$$X_{f,m+1} = X_{f,m} + \frac{Y_{f,m} - X_{f,m}}{1 - \left( \frac{d Y_f}{d X_f} \right)_m}$$

with

$$\frac{d Y_f}{d X_f} = \left[ \frac{8A_t X_m}{(c^*)^2} + \frac{2C_{P5}}{(c^*)^3 \Delta t} (X_m - P') \right] \left( \frac{C_{P2} W_T}{X_f^2} + \frac{2C_{P3} W_T^2}{X_f^3} \right)$$

These iterations are started using the fuel flow  $W_f$  from the previous outer iteration, or from the previous time step in the first outer iteration, and are terminated based on the convergence criterion

$$\left| \frac{Y_f - X_f}{X_f} \right| \leq \epsilon_f$$

### 3. Outer Iterations

A two-dimensional version of Newton's method is used to modify the assumed pressures in the outer iterations. Thus, for the  $(m+1)$ st iteration

$$X_{p,m+1} = X_{p,m} + \Delta_p$$

$$X_{s,m+1} = X_{s,m} + \Delta_s$$

with  $\Delta_p$  and  $\Delta_s$  from the simultaneous solution of

$$X_{p,m} - Y_{p,m} = \left[ \frac{Y_p(X_{p,m} + \delta X_p, X_{s,m}) - Y_p}{\delta X_p} - 1 \right] \Delta_p + \frac{Y_p(X_{p,m}, X_{s,m} + \delta X_s) - Y_p}{\delta X_s} \Delta_s$$

$$X_{s,m} - Y_{s,m} = - \frac{Y_s(X_{p,m} + \delta X_p, X_{s,m}) - Y_s}{\delta X_p} \Delta_p + \left[ \frac{Y_s(X_{p,m}, X_{s,m} + \delta X_s) - Y_s}{\delta X_s} - 1 \right] \Delta_s$$

in which  $Y_p = Y_p(X_{p,m}, X_{s,m})$

$$Y_s = Y_s(X_{p,m}, X_{s,m})$$



The perturbation increments  $\delta X_p$  and  $\delta X_s$  are selected as

$$\delta X_p = Y_{p,m} - X_{p,m}$$

$$\delta X_s = Y_{s,m} - X_{s,m}$$

with the restriction that

$$Y_p \leq |\delta X_p| \leq \lambda_p X_{p,m}$$

$$Y_s \leq |\delta X_s| \leq \lambda_s X_{s,m}$$

These iterations are started using the pressures from the previous time step, i.e.,  $X_p = P'_{pc}$  and  $X_s = P'_{sc}$ , and are terminated based on the simultaneous convergence criteria

$$\left| \frac{Y_p - X_p}{X_p} \right| \leq \epsilon_p$$

$$\left| \frac{Y_s - X_s}{X_s} \right| \leq \epsilon_p$$

### C. LOCAL CHAMBER-WALL ANALYSIS

#### 1. Coating

The equation for conduction in the coating, assuming constant thermal conductivity, is

$$(\rho C)_c \frac{\partial T}{\partial t} = K_c \frac{1}{r} \frac{\partial}{\partial r} \left( r \frac{\partial T}{\partial r} \right) \quad (\text{Eq 1})$$

which is subject to the boundary condition

$$K_c \frac{\partial T}{\partial r} = h_g (T_r - T_c), \quad r = r_g \quad (\text{Eq 2})$$

at the hot-gas surface and to heat-flux and temperature-continuity requirements at the tube-wall interface.

An approximate solution of the coating conduction equation will be used to simplify the analysis. Instead of solving the partial differential equation pointwise, i.e., at each radial position  $r$ , an integral form will be solved using an assumed temperature distribution. In this way, the conduction equation is reduced to an ordinary differential equation in time. This technique is analogous to the well established integral methods of boundary-layer theory. Its application to heat conduction is widely reported in the literature and has proved to be surprisingly accurate using simple temperature distributions.

Integrating Equation 1 over the thickness of the coating yields

$$(\rho C)_c r_c \delta_c \frac{d\bar{T}_c}{dt} = K_c r_g \left. \frac{\partial T_c}{\partial r} \right|_{r=r_g} - K_c r_i \left. \frac{\partial T_c}{\partial r} \right|_{r=r_i}$$

in which  $\bar{T}_c$  is the area-weighted average temperature of the coating. The temperature distribution in the coating is assumed to be of the form

$$T_c(r, t) = T_i(t) + a(t) \xi + b(t) \xi^2$$

in which

$$\xi = \frac{r - r_i}{\delta_c}$$

## Report 10785-F, Phase II, Appendix I

Substituting in the above integral or energy-balance equation gives

$$\frac{r_c}{a_c} \frac{d\bar{T}_c}{dt} = a + \frac{2r_c}{\delta_c} b \quad (\text{Eq 3})$$

The gas-side boundary condition (Equation 2) requires

$$B_g (a + 2b) = T_r - T_1 - a - b \quad (\text{Eq 4})$$

in which

$$B_g = \frac{K}{h_g \delta_c} \quad (\text{inverse gas-side Biot number})$$

The definition of  $\bar{T}_c$  yields

$$\bar{T}_c = T_1 + \beta_1 a + \beta_2 b \quad (\text{Eq 5})$$

in which

$$\beta_1 = \frac{r_1 + \frac{2}{3} \delta_c}{2r_c}$$

$$\beta_2 = \frac{r_1 + \frac{4}{3} \delta_c}{3r_c} \quad (\text{Eq 6})$$

Combining Equations 4 and 5 gives

$$b = \frac{T_r - \bar{T}_c - (B_g + 1 - \beta_1) a}{2B_g + 1 - \beta_2}$$

2. Tube Wall

The tube wall will be treated in the same way as the coating.  
The integrated conduction equation or energy balance is

$$(\rho C)_W r_W \delta_W \frac{d\bar{T}_W}{dt} = K_W r_i \left. \frac{\partial T_W}{\partial r} \right|_{r=r_i} - K_W r_L \left. \frac{\partial T_W}{\partial r} \right|_{r=r_L}$$

The tube-wall temperature distribution is assumed to be

$$T_W(r, t) = T_L(t) + c(t) \eta + d(t) \eta^2$$

in which

$$\eta = \frac{r - r_L}{\delta_W}$$

Substituting in the energy-balance equation gives

$$\frac{r_W \delta_W}{\rho_W} \frac{d\bar{T}_W}{dt} = c + \frac{2r_i}{\delta_W} d \quad (\text{Eq 7})$$

The coolant-side boundary condition requires

$$K_W \left. \frac{\partial T_W}{\partial r} \right|_{r=r_L} = h_L (T_W - T_b), \quad r = r_L$$

from which

$$B_L c = T_L - T_b \quad (\text{Eq 8})$$

in which

$$B_L = \frac{K_W}{h_L \delta_W} \quad (\text{inverse coolant-side Biot number})$$

The definition of  $\bar{T}_W$  gives

$$\bar{T}_W = T_L + \sigma_1 c + \sigma_2 d \quad (\text{Eq 9})$$

in which

$$\sigma_1 = \frac{r_L + \frac{2}{3} \delta_W}{3r_W}$$

$$\sigma_2 = \frac{r_L + \frac{1}{4} \delta_W}{3r_W}$$

Combining Equations 8 and 9 yields

$$d = \frac{1}{\sigma_2} \left[ \bar{T}_W - T_b - (\sigma_1 + B_L) c \right] \quad (\text{Eq 10})$$

### 3. Interface Conditions

At the interface of coating and tube wall, continuity of temperature and heat flux require

$$T_i = T_L + c + d \quad (\text{Eq 11})$$

and

$$\kappa a = c + 2d \quad (\text{Eq 12})$$

respectively, in which  $\kappa = K_C \delta_W / K_W \delta_C$ .

From Equations 10 and 12

$$c = \frac{2(\bar{T}_W - T_b) - \kappa\sigma_2 a}{2(\sigma_1 + B_L) - \sigma_2} \quad (\text{Eq 13})$$

$$d = \frac{(\sigma_1 + B_L) \kappa a - (\bar{T}_W - T_b)}{2(\sigma_1 + B_L) - \sigma_2} \quad (\text{Eq 14})$$

Expressing Equation 11 in terms of  $\bar{T}_c$  and  $\bar{T}_w$ ,

$$\bar{T}_c - B_1 a - B_2 b = \bar{T}_w + (1 - \sigma_1) c + (1 - \sigma_2) d$$

Substituting Equations 6, 13, and 14 for b, c, and d gives

$$\begin{aligned} T_r - T_b - \frac{2B_g + 1}{2B_g + 1 - B_2} (T_r - \bar{T}_c) - \frac{2B_g + 1}{2(\sigma_1 + B_L) - \sigma_2} (\bar{T}_w - T_b) \\ a = \frac{\sigma_1 - \sigma_2 + (1 - \sigma_2) B_1}{2(\sigma_1 + B_L) - \sigma_2} \kappa + \frac{B_1 (2B_g + 1) - B_2 (B_g + 1)}{2B_g + 1 - B_2} \end{aligned} \quad (\text{Eq 15})$$

Use of Equations 6, 13, 14, and 15 in the energy balances (Equations 3 and 7) eliminates the auxiliary parameters a, b, c, and d and defines  $\bar{T}_c$  and  $\bar{T}_w$  in terms of the boundary-condition variables  $T_r$ ,  $h_g$ ,  $h_L$ , and  $T_b$ .

#### 4. Boundary Conditions

The gas-side boundary-condition variables are related to the flow-system variables as follows:

$$T_r = C_{r0} + C_{r1} (MR) + C_{r2} (MR)^2 + C_{r3} (MR)^3 + C_{r4} (MR)^4$$

$$-C_{r5} \left[ \frac{3000 - P_{sc}}{1000} \right]^{n_3}$$

$$h_s = C_s \frac{W_{sc}^{0.8}}{D^{1.8}} z \left( \frac{T_{cs}}{T_r} \right) \left[ C_{h0} + C_{h1} (MR) + C_{h2} (MR)^2 + C_{h3} (MR)^3 \right]$$

in which the function  $z (T_{cs}/T_r)$  is table-input and is evaluated at the beginning of a time step so that Equations 6 and 15 may be solved explicitly for  $a$  and  $b$ . Note that

$$T_{cs} = \bar{T}_c + (1 - \beta_1) a + (1 - \beta_2) b$$

The coolant-side boundary conditions are:

$$h_L = C_L W_o^{n_4} \quad (\text{based on electrically heated laboratory tests})$$

$$T_b = T_{bs}, \text{ as a first approximation, or}$$

$T_b = T_b(t)$  from a coolant temperature-rise analysis (described in Section 2) if a more accurate solution is needed.

#### D. CHAMBER-WALL COMPUTER PROGRAM

Backward time differences are also used to solve the chamber-wall energy balances (Equations 3 and 7). Therefore, in difference form these equations become

$$\frac{r_c \delta_c}{\alpha_c \Delta t} (\bar{T}_c - \bar{T}_c') = a + \frac{2r_c}{\delta_c} b$$

$$\frac{r_w \delta_w}{\alpha_w \Delta t} (\bar{T}_w - \bar{T}_w') = c + \frac{2r_w}{\delta_w} d$$

in which  $\bar{T}_c'$  and  $\bar{T}_w'$  are the coating and wall average temperatures at time  $t - \Delta t$ ; the quantities  $a$ ,  $b$ ,  $c$ , and  $d$  are defined by Equations 6, 13, 14, and 15.

For given wall boundary conditions the above energy balance difference equations represent a pair of linear simultaneous equations in  $\bar{T}_c$  and  $\bar{T}_w$ . However, the gas-side convective coefficient  $h_g$  is dependent on the coating surface temperature  $T_{cg}$  and thus on  $\bar{T}_c$  and  $\bar{T}_w$ . Therefore, iteration on  $T_{cg}$  is necessary in solving the energy balance difference equations. Each iteration is accomplished using a trial  $T_{cg}$ , designated  $X_{cg}$ , solving for  $\bar{T}_c$  and  $\bar{T}_w$  and the difference equations and then calculating the resultant coating surface temperature  $Y_{cg}$  from

$$Y_{cg} = \bar{T}_c + (1 - \beta_1) a + (1 - \beta_2) b$$

Newton's method is used to modify  $X_{cg}$  for the next iteration; thus, for the  $(m + 1)$ st iteration

$$X_{cg, m+1} = X_{cg, m} + \frac{Y_{cg, m} - X_{cg, m}}{1 - \left( \frac{dY_{cg}}{dX_{cg}} \right)_m}$$



The derivative is calculated by perturbing  $X_{cg}$ , i.e.,

$$\left( \frac{dY}{dX} \right)_{cg} = \frac{Y_{cg}(X_{cg,m} + \delta X_{cg}) - Y_{cg,m}}{\delta X_{cg}}$$

with

$$\delta X_{cg} = Y_{cg,m} - X_{cg,m}$$

except for the requirement

$$Y_{cg} \leq |\delta X_{cg}| \leq \lambda_{cg} X_{cg,m}$$

The iterations are started using  $T_{cg}$  from the previous time step, and are terminated based on the convergence criterion

$$\left| \frac{Y_{cg} - X_{cg}}{X_{cg}} \right| \leq \epsilon_{cg}$$

### E. COOLANT-TEMPERATURE ANALYSIS

The coolant energy equation may be approximated as

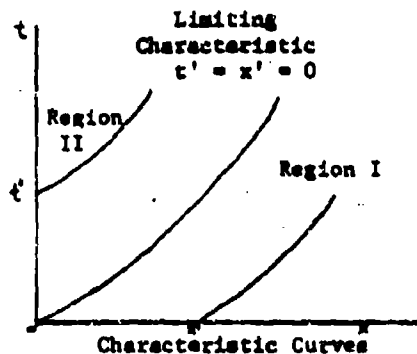
$$\rho_o c_p A_f \frac{\partial T_b}{\partial t} + W_o c_p \frac{\partial T_b}{\partial x} = q(x, t) \quad (\text{Eq 16})$$

The heat-input rate  $q$  is assumed to be space-time separable over large sections of the tube bundle; thus, in section  $j$

$$q(x, t) = q_j(x) \frac{c_j(t)}{c_{j0}}$$

with  $c_j(t)$  defined by Equations 13 and 15 from the local chamber-wall analysis of a point in the section.

Because the transient temperature increase of the coolant must be limited as one of the shutdown criteria, a quasi-steady solution may suffice for most of the analysis. In that case, the energy storage term involving the time derivative can be dropped from Equation 16. However, this assumption should be checked by comparison of the quasi-steady solution and the exact solution of Equation 16, as determined by the method of characteristics.



Solution of Equation 16 along characteristic curves, as illustrated above, yields the following:

Region I ( $x' > 0$ )

$$\int_0^x W_o dt = \int_{x'}^x \rho_o A_f dx \quad (\text{Eq 17})$$

$$T_b - T_{bs}(x') = \frac{1}{c_p} \int_{x'}^x \frac{q_s(x) c_j(t)}{c_{js} W_o(t)} dx$$

UNCLASSIFIED

Report 10785-8, Phase II, Appendix 1

In which  $t(x)$  is given by Equation 17.

Region II ( $t' > 0$ )

$$\int_{t'}^t w_0 dt = \int_0^x \rho_0 A_z dx \quad (\text{Eq 18})$$

$$T_b - T_{in} = \frac{1}{c_p} \int_0^x \frac{q}{c_{js} w_0(t)} c_p(t) dx$$

in which  $t(x)$  is given by Equation 18.

Note that  $x'$  and  $t'$  are dummy parameters which merely serve to define the starting point of any characteristic curve. Thus, for a given  $x$  and  $t$  of interest in Region I, Equation 17 defines  $x'$ ; similarly, Equation 18 defines  $t'$ .

UNCLASSIFIED

## F. NOMENCLATURE

1. English Letters

a(t)	Coefficient in coating temperature distribution
$A_c$	Secondary combustor throat area
$A_f$	Coolant flow area
b(t)	Coefficient in coating-temperature distribution
B	Inverse Biot number, $K/h\delta$
c(t)	Coefficient in tube-wall temperature distribution
$c^*$	Secondary combustor characteristic velocity
$C_{ov}, C_{fv}$	Oxidizer- and fuel-valve resistances
$C_{OT}, C_{FT}$	Oxidizer- and fuel-system resistances
$C_{OP1-6}$	Oxidizer-pump constants
$C_{fpl-6}$	Fuel-pump constants
$C_{T1-9}$	Turbine constants
$C_{S1-5}$	Secondary combustor constants
$C_{P1}$	Primary combustor or preburner constant
$C_p$	Oxidizer specific heat
$C_g, C_L$	Heat-transfer-coefficient multipliers
$C_{ro-5}$	Recovery temperature constants
$C_{ho-3}$	Heat-transfer-coefficient constants for mixture-ratio dependence
d(t)	Coefficient in tube-wall temperature distribution
D	Secondary combustor diameter
g	Gravitational constant
h	Convective-heat-transfer coefficient
I	Total turbopump inertia
K	Thermal conductivity
MR	Secondary combustor mixture ratio
N	Turbopump speed
$n_{1-4}$	Exponents
P	Pressure

# UNCLASSIFIED

Report 10735-F, Phase II, Appendix I

## English Letters (cont.)

$P_{R1,2}$	Turbine pressure ratios
$q$	Coolant heat-input rate per unit length (product of $\dot{q}_c$ and heated perimeter)
$r$	Radius
$t$	Time
$T$	Local coating or tube-wall temperature
$\bar{T}$	Average coating or tube-wall temperature
$T_r$	Secondary combustor recovery temperature
$T_b$	Coolant bulk temperature
$V$	Coolant velocity
$V_1$	Turbine spouting velocity
$W$	Flow rate
$x$	Axial coolant-flow coordinate
$X$	Assumed or trial values of iteration variables
$Y$	Calculated values of iteration variables
$Z$	Film-temperature correction factor for $h_g$

## 2. Greek Letters

$\alpha$	Thermal diffusivity
$\beta_{1,2}$	Coating geometric constants
$\gamma$	Lower limit on absolute perturbation increment magnitudes
$\delta$	Coating or tube-wall thickness
$\delta X$	Perturbation increments for calculating Newton's method derivatives
$\Delta$	Iteration increments on system pressure trial values
$\Delta t$	Time step increment
$\epsilon$	Convergence parameters
$\eta$	Dimensionless radial coordinate $(r-r_L)/\delta_w$

UNCLASSIFIED

Greek Letters (cont.)

$\eta_T$	Turbine efficiency
$A'$	Chamber-wall parameter $K_c \delta_w / K_w \delta_c$
$\lambda$	Upper limit on relative perturbation increment magnitudes
$\mu$	Torque
$\xi$	Dimensionless radial coordinate $(r-r_1)/\delta_c$
$\rho$	Density
$(\rho C)$	Volumetric heat capacity
$\sigma_{1,2}$	Tube-wall geometric constants
$\tau$	Valve-closing characteristic times
$q_c$	Heat flux to coolant

3. Subscripts

c	Coating
f	Fuel (fS-fuel suction, fD-fuel discharge)
g	Gas-side coating surface
i	Coating-tube wall interface
L	Coolant side of tube wall
m	Iteration index
O	Oxidizer (OS-oxidizer suction, OD-oxidizer discharge)
pc	Primary combustor or preburner
sc	Secondary combustor
S	Steady state
T	Turbine
W	Tube wall

4. Superscript

Value at previous time step, time  $t - \Delta t$

UNCLASSIFIED

Report 19785-F, Phase II

APPENDIX II

DESCRIPTION OF THE INTERACTION THEORY METHOD OF  
PERFORMANCE ANALYSIS

Page 278

UNCLASSIFIED

(U) Interaction theory (Ref. 1)\* was used for analysis of injector performance for the Advanced Propellant Staged-Combustion Evaluation Program. This method is unique in that interactions between the injector/chamber performance and the nozzle expansion process are considered. Interaction losses include the effect of the level-of-energy-release efficiency (injector/chamber performance) on nozzle efficiency, the interaction between injector mixture-ratio distribution and nozzle performance independent of the overall level-of-energy-release efficiency, and the interaction between mixture-ratio distribution and kinetic losses.

(U) The method involves determination of the actual performance potential of a specific injector/chamber based on the local mixture distribution at the injector face. The degree to which the potential will be achieved is determined by estimating the magnitude of various thrust-chamber performance losses. The following ten performance losses are the losses which are important in describing the performance of a given liquid rocket engine:

1. Nozzle Friction Loss
2. Nozzle Geometry Loss
3. Nozzle Heat Loss
4. Chamber Heat Loss
5. Chamber Friction Loss
6. Energy Release Loss (ERL Loss)
7. Mixture-Ratio-Distribution Loss (MRD Loss)
8. Kinetic Losses
9. Gas-Particle Flow Effects
10. Mass Distribution Effects

---

\*A list of references is given at the end of this appendix.



It may be noted that the first three of these losses are specific to the nozzle expansion section, whereas the other seven losses have both a chamber and nozzle component. Thus, it can be seen that nozzle performance is not independent of chamber performance. Therefore, any separation of chamber and nozzle performance which assumes that one is independent of the other (e.g., the  $c^* - C_F$  method) will not only lead to incorrect inference of the possible source of low performance but will also result in significant errors when extrapolating performance from the low-area-ratio test configuration to the high-area-ratio flight configuration.

#### B. PERFORMANCE LOSSES FOR THE 98% $H_2O_2$ /ALUMIZINE-43 STAGED-COMBUSTION SYSTEM

(U) Not all the performance losses listed in the previous section are germane to the Advanced Propellant Staged-Combustion System. The magnitude of the nozzle heat loss is estimated to be only about 0.1% or less of vacuum specific impulse and is neglected. Because of the high chamber pressure, kinetic losses are negligible. Mass-distribution effects are also considered negligible since an approximately even mass distribution exists at the secondary injector. Thus, only nozzle friction and geometry, chamber heat and friction, mixture ratio distribution, gas-particle, and energy release performance losses are considered potentially significant for this analysis.

##### 1. Nozzle Friction Loss

(U) The viscous effects between the gaseous boundary layer and the nozzle wall will result in a shear force which degrades nozzle thrust. Viscous effects may also be considered as slowing the velocity of the mainstream gases in the boundary layer, thereby lowering the total exit momentum from the nozzle. The effect of frictional drag on nozzle performance is calculated by use of the Aerojet Computing Services Division Program P-133, which is based upon the extended Frankel-Voishel Expression (Ref. 2) for average skin friction. Friction loss calculated by this method will be valid for the case of a smooth nozzle wall.

## 2. Nozzle Geometry Loss

(U) Nozzle geometry loss may be attributed to the loss in thrust due to the discharge coefficient of the throat and the loss in thrust resulting from the fact that part of the gases leaving the nozzle exit plane are not parallel to the nozzle axis. The geometric performance loss is determined from AGC Computer Program 10036 by comparing the performance of the three-dimensional axisymmetric nozzle with a one-dimensional configuration.

## 3. Chamber Heat Loss

(U) Heat loss from the combustion products to the chamber wall results in a loss in total combustion gas enthalpy. This loss in enthalpy reduces the available nozzle expansion work performed by the combustion gases. Chamber heat loss is one of the interaction losses. The method used to calculate chamber heat flux is described in Appendix III.

## 4. Chamber Friction Loss

(U) Viscous shear drag on the chamber wall results in a loss in thrust for the total engine system. On most high-thrust engines having practical utility the chamber friction loss can justifiably be neglected because of the low subsonic gas velocities in the chamber and the low ratio of chamber surface area/engine weight flow rate. However, for the 20,000-lbf-thrust hardware of the Advanced Propellant Staged-Combustion Evaluation Program this loss was separately identified because, if this loss is neglected and lumped together with the energy release loss and extrapolated to large thrust engine systems, excessive losses would be predicted. The method used to evaluate this loss is described in Appendix IV.

5. Mixture-Ratio-Distribution Loss

(U) Irregular mixture ratio distribution at the secondary injector face can result in a change in the performance potential of a thrust chamber when compared to the ideal performance calculated from the overall mixture ratio. The effect of the irregular mixture-ratio distribution on performance is determined by a stream-tube analysis. In this analysis, the flow is separated into regions of common mixture ratio. The fluid streams issuing from the injector in each region are presumed to mix, combust, and expand through the nozzle without mixing or interacting with any other stream from an adjacent region. Thus, although these stream tubes may change relative size during the expansion through the nozzle, they are assumed to retain their identity and specific mixture ratio. The stream tubes can take on any geometrical shape as required by the mixture-ratio distribution at the injector face. The number of stream tubes can vary from one--for the case of even mixture-ratio distribution--to as many as can be defined without any stream tube being smaller in width than the typical lateral dimension of turbulence. The minimum size is obviously that of the smallest mixing unit, or element. However, in the case of very small elements, or a high degree of turbulence, the smallest meaningful stream tube may cover many elements.

6. Gas-Particle Two-Phase Flow Loss

(U) Two-phase flow losses are associated with the presence of either liquid or solid particles in the gaseous flow stream of a rocket engine. The Chemical Composition Program (Ref. 3) considers the presence of the condensed phase and its inability to expand in the rocket nozzle, but it assumes kinetic and thermal equilibrium between the condensed/gaseous phases. In actuality, a thermal lag exists in which the particle temperature remains higher than that of the expanding combustion gases. Heat thus retained by the particle results in a decrease in the gas enthalpy available to accelerate the expanding gaseous phase in the assumed shifting equilibrium performance.

UNCLASSIFIED

Report 10785-F, Phase II, Appendix II

Furthermore, the slower moving particles create a drag on the accelerating gases and decrease the mainstream momentum. Therefore, the deviation from the assumed kinetic and thermal equilibrium condition is what constitutes the two-phase flow loss. The computer program used to determine the loss in specific impulse due to particles in the flow stream is Aerojet Computing Services Division Program 48067. This program computes the one-dimensional flow of a gas-particle system through a parabolic nozzle in both the subsonic and supersonic regions.

(U) The extent of the deviation from kinetic and thermal equilibrium is dictated by the absolute particle size. It is therefore mandatory that the particle-size distribution be known. As part of this evaluation program, particle samples were obtained for the two basic injector design concepts and their size distributions were determined.

7. Energy Release Loss

(U) The energy release loss of an engine represents the difference in performance between complete and incomplete energy release. For the Advanced Propellant Staged-Combustion System two mechanisms for energy release loss are possible. For most conventional propellant systems the propellant vaporization rate (Ref. 4) is the controlling mechanism of the combustion process and the energy release loss can be attributed to the combustion enthalpy reduction and gaseous phase mass reduction that results from the unvaporized propellant. However, with Alumizine-43 the basic assumption that vaporization is the rate-controlling mechanism may not be valid. That is, the degree of aluminum chemical reaction may also be responsible for energy release loss. This may occur either because insufficient aluminum reaction time was allowed or because the aluminum was not adequately heated to its ignition temperature (Ref. 5) resulting in reduced aluminum availability. Since neither of these losses was analytically calculable for the Alumizine-43, the energy release loss was determined as the difference between the theoretical and experimentally measured specific impulse less all other calculable performance losses.

UNCLASSIFIED

# UNCLASSIFIED

Report 10785-F, Phase II, Appendix II

## REFERENCES

1. Valentine, R. S., Deau, L. E., and Pieper, J. L., An Improved Method for Rocket Engine Performance Prediction, Aerojet-General Corporation Report PTDR 9642-034, 8 October 1965.
2. Rubesin, M. W., Maydew, R. C. and Varga, S. A., An Analytical and Experimental Investigation of the Skin Friction of the Turbulent Boundary Layer on a Flat Plate at Supersonic Speeds, NACA TN 2305, February 1951.
3. Crisman, P. A., Goldwasser, S. R., and Petrozzi, P. J., A General Computer Program for Calculation of Rocket Performance Parameters of Propellants Containing the Atomic Species C, H, O, N, F, and Cl, Proceedings of a Propellant Thermodynamics and Handling Conference, Special Report 12, June 1960.
4. Friem, R. J. and Heidmann, M. F., Propellant Vaporization as a Design Criterion for Rocket-Engine Combustion Chambers, NASA TR R-67, 1960.
5. Ignition and Combustion of Aluminum in Small-Scale Liquid Rocket Engines, AGC Report 9200-22-63, 15 December 1963.

UNCLASSIFIED

UNCLASSIFIED

Report 10785-F, Phase II.

APPENDIX III

A METHOD FOR EVALUATING CHAMBER HEAT LOSS

Page 285

UNCLASSIFIED

(U) The gas-side heat-transfer coefficient was determined from Bartz's equation

$$h_g = \frac{0.026}{1.644 d} 0.2 \left[ \frac{\mu^{0.2} C_p}{Pr^{0.6}} \right]_{am} \left[ \frac{W_T}{A} \frac{T_{fg}}{T_{am}} \right]^{0.8} \quad (\text{Eq 1})$$

where  $h_g$  = gas-side heat-transfer coefficient,  $\text{Btu/in}^2\text{-sec-}^\circ\text{R}$   
 $d$  = diameter, in.  
 $\mu$  = viscosity,  $\text{lbm/ft-sec}$   
 $C_p$  = specific heat,  $\text{Btu/lbm-}^\circ\text{R}$   
 $Pr$  = Prandtl number  
 $W_T$  = gas flow rate,  $\text{lbm/sec}$   
 $A$  = area,  $\text{in.}^2$   
 $T_{fg}$  = free-stream gas temperature,  $^\circ\text{R}$   
 $T_{am}$  = arithmetic mean temperature,  $^\circ\text{R} \left( \frac{T_r + T_{wg}}{2} \right)$   
 $T_r$  = gas recovery temperature,  $^\circ\text{R}$   
 $T_{wg}$  = gas-side wall temperature,  $^\circ\text{R}$

and where the transport properties are evaluated at the arithmetic mean temperature.

(U) Having calculated the heat-transfer coefficient by Equation 1, the coefficient was used to determine the dimensionless Biot number

$$Bi = (h_g r_2 / k) \quad (\text{Eq 2})$$

where:  $r_2$  = outer radius of chamber wall, in.  
 $k$  = wall thermal conductivity,  $\text{Btu/in.-sec-}^\circ\text{R}$

(U) The time variable is also made dimensionless by introducing the Fourier number

$$F_0 = \alpha t / r^2 \quad (\text{Eq 3})$$

where:  $\alpha$  = wall thermal diffusivity, in.<sup>2</sup>/sec  
 $t$  = time, sec

(U) One additional parameter, the ratio of inner wall radius to outer wall radius, is required to graphically determine the inner wall temperature using the Biot and Fourier numbers.\*

(U) If the wall temperature thus calculated does not agree with the assumed wall temperature used in Equation 1, further iterations may be required until convergence is achieved. It should be noted that all transport properties are temperature-dependent.

(U) The heat flux in the convergent nozzle section was calculated by dividing the zone into five segments, by calculating the heat flux at each section, and by multiplying the calculated flux by its corresponding surface area.

(U) The total chamber heat loss was then calculated by summing the local heat flux and the incremental chamber surface area.

$$Q_c = \sum h_{gi} (T_r - T_{wg})_i A_i$$

(U) To evaluate the effect of chamber heat loss upon engine specific impulse, the reduced temperature option of the Chemical Composition Program\*\*

\*Temperature Charts for Internally Heated Hollow Cylinders, Aerojet-General Technical Memorandum 165 SRP, July 1961.

\*\*Crisman, P. A., Goldwasser, S. R., and Petrozzi, P. J., A General Computer Program for Calculation of Rocket Performance Parameters of Propellants Containing the Atomic Species C, H, O, N, F, and Cl, Proceedings of a Propellant Thermodynamics and Handling Conference, Special Report 12, June 1960.



UNCLASSIFIED

Report 10745-W, Phase II, Appendix III

was used to determine the effect of enthalpy decrease in the chamber (at Mach number zero) to reduced flame temperature ( $\Delta H/\Delta T$ ).

$$\Delta T_{\text{Cham. Ht. Loss, b.l.}} = \frac{Q_c}{\dot{W}_{\text{b.l.}} (\Delta H/\Delta T)} \quad (\text{Eq 4})$$

where:  $\dot{W}_{\text{b.l.}}$  = propellant flow rate within the thermal boundary layer, lbm/sec

$\Delta T_{\text{Cham. Ht. Loss, b.l.}}$  = mean temperature reduction of flow within the thermal boundary layer, °R

(U) The engine performance loss resulting from chamber heat-transfer effects is proportional to the fractional mass flow rate of the thermal boundary layer and to the reduced specific impulse of the boundary layer corresponding to the temperature reduction of Equation 4. For purposes of this analysis, it was assumed that the boundary layer flow rate expanded to the exit-area ratio of the engine. Since the specific-impulse loss increases in the nozzle with increasing exit-area ratio for a given temperature reduction, chamber heat loss is one of the interaction losses.

(U) The approximation was made that the thickness of the thermal boundary layer was equal to the velocity boundary layer divided by the one-third power of the Prandtl number.

UNCLASSIFIED

UNCLASSIFIED

Report 10733-F, Phase 11

APPENDIX IV

A METHOD FOR EVALUATING CHAMBER FRICTION LOSS

Page 289

UNCLASSIFIED

(U) The velocity distribution of an incompressible fluid in a pipe for nonfully developed turbulent flow is

$$\frac{u(r)}{u_0} = \left[ \frac{R-r}{\delta} \right]^{\frac{1}{n}} \text{ when } R-\delta \leq r \leq R \quad (\text{Eq 1})$$

and  $\frac{u(r)}{u_0} = 1$  when  $0 < r < R - \delta$

where:  $u(r)$  = axial gas velocity at radius,  $r$   
 $u_0$  = free-stream velocity  
 $R$  = chamber radius  
 $\delta$  = velocity boundary layer thickness  
 $n^{-1}$  = velocity profile exponent

(U) The velocity profile exponent ( $n^{-1}$ ) is dependent upon Reynolds number as shown in the following tabulation:

#### HIGH REYNOLDS NUMBER FLOWS

	Reynolds Number			
	$2 \times 10^4$ to $4 \times 10^5$	$3 \times 10^5$ to $8 \times 10^5$	$8 \times 10^5$ to $2 \times 10^6$	$> 2 \times 10^6$
Velocity Profile Exponent, $n$	7	8	9	10

(U) The displacement boundary layer thickness,  $\delta_1$ , in an axisymmetric pipe is defined by

$$\delta_1 = \int_0^R \left( 1 - \frac{u(r)}{u} \right) \frac{r}{R} dr \quad (\text{Eq 2})$$

( ) Substitution of Equation 1 into Equation 2 yields

$$\delta_1 = \frac{\delta}{n+1} - \frac{\delta^2}{2R(2n+1)} \quad (\text{Eq 3})$$

(U) Similarly, the momentum boundary layer thickness,  $\theta$ , in axisymmetric pipe flow is defined by

$$\theta = \int_0^R \frac{u(r)}{u_0} \left[ 1 - \frac{u(r)}{u_0} \right] \frac{r}{R} dr \quad (\text{Eq 4})$$

(U) Solution of the integral using Equation 1 yields

$$\theta = \delta \left[ \frac{n}{(n+1)(n+2)} - \frac{\delta n}{2R(n+1)(2n+1)} \right] \quad (\text{Eq 5})$$

(U) The cumulative chamber wall drag,  $D$ , is taken to be equal and opposite to the drag upon the fluid in the cylinder so that

$$D = \int_0^R [u_0 - u(r)] \rho [u(r)] 2\pi r dr \quad (\text{Eq 6})$$

where  $\rho$  = fluid density

(U) Equation 6 can be rearranged to

$$D = (2\pi R) (\rho u_0^2) \int_0^R \left( \frac{u(r)}{u_0} \right) \left[ 1 - \frac{u(r)}{u_0} \right] \frac{r}{R} dr \quad (\text{Eq 7})$$

(U) But the integral in Equation 7 is simply the momentum boundary layer thickness. Therefore, the following relationship was used to calculate chamber drag:

$$D = (2\pi R) (\rho u_o^2) \theta \quad (\text{Eq 8})$$

(U) Equation 8 shows that the drag is only a function of chamber wetted perimeter, dynamic pressure, and momentum thickness. Furthermore, it should be noted that the free-stream velocity,  $u_o$ , varies in its relationship to the mean velocity,  $\bar{u}$ , with the velocity boundary layer thickness:

$$\frac{\bar{u}}{u_o} = \left[ 1 - \frac{\delta}{R} \left( \frac{2}{n+1} \right) + \left( \frac{\delta}{R} \right)^2 \frac{1}{(2n+1)} \right]$$

(U) For the purpose of this preliminary analysis, one additional simplifying assumption was made; i.e., that the velocity boundary layer grows at the same rate as for the velocity profile with the one-seventh power law (validity of this assumption requires further evaluation).

$$\delta(x) = 0.37 x R_{e_x}^{-0.2} \quad (\text{Eq 9})$$

where:

$$R_{e_x} = \frac{\rho \bar{u} x}{\mu}$$

$\mu$  = viscosity

and

$$\rho \bar{u} = \dot{W}_T / \pi R^2$$

(U) Equation 9 was therefore rearranged in the form

$$\frac{\delta(x)}{R} = 0.37 \left[ \frac{\pi \mu}{W_T} \right]^{0.2} R^{-0.6} x^{0.8} \quad (\text{Eq 10})$$

(U) The velocity boundary layer thickness calculated by Equation 10 was then substituted into Equation 5 to determine the momentum thickness for Equation 8. The boundary layer was assumed to start ( $x = 0$ ) at the injector face.

(U) Evaluation of the chamber gas-flow conditions for the 98%  $\text{H}_2\text{O}_2$ /Alumizine-43 system indicated a Reynolds number range corresponding to a one-tenth power-law ( $n = 10$ ) velocity profile.

(U) Frictional drag in the convergent portion of the nozzle was evaluated by dividing the convergent portion into five conical frustums. A mean diameter was selected for each frustum and treated as a cylindrical section. Mean gas densities and gas velocities were selected that corresponded to the mean contraction ratio of each section. Incremental drag due to each segment was then calculated in each convergent zone by determining a pseudo starting length so that the ratio of relative velocity boundary layer thickness to cylindrical radius at the start of the convergent zone was equal to the ratio at the trailing edge of the segment located immediately upstream. The pseudo drag was calculated at the leading edge and subtracted from the drag at the trailing edge to determine the drag increment of each convergent zone. The total chamber friction loss was calculated by summing the drag increments of all segments from the injector face to the nozzle throat and dividing the cumulative drag force by the total propellant flow rate to determine specific-impulse loss.

(U) Although incompressible-flow equations were used, the error is not expected to be significant if the densities in each of the convergent segments are adjusted.

UNCLASSIFIED

Unclassified

Security Classification

DOCUMENT CONTROL DATA - R&D		
<small>(Security classification of title, body of abstract and indexing annotation must be entered when the overall report is classified)</small>		
1. ORIGINATING ACTIVITY (Corporate author)		2. REPORT SECURITY CLASSIFICATION
Aerojet-General Corporation Liquid Rocket Operations Sacramento, California		<del>Confidential</del>
3. REPORT TITLE		4. GROUP
Advanced Propellant Staged Combustion Feasibility Program		4
5. DESCRIPTIVE NOTES (Type of report and including dates)		
Technical Report - Final, Phase II (Rough Draft)		
6. AUTHOR(S) (Last name, first name, initial)		
Kuntz, Robert J., PE Sjogren, Roy G.		
7. REPORT DATE	7a. TOTAL NO. OF PAGES	7b. NO. OF REFS.
August 1967	293	17
8a. CONTRACT OR GRANT NO.	9. ORIGINATOR'S REPORT NUMBER(S)	
AF 04(611)-10785	AFRPL-TR-67-204	
8. PROJECT NO.	9b. OTHER REPORT NO(S) (Any other numbers that may be assigned this report)	
	10785-F, Phase II	
10. AVAILABILITY/LIMITATION NOTES		
Qualified requestors may obtain copies of this report from DDC		
11. SUPPLEMENTARY NOTES		12. SPONSORING MILITARY ACTIVITY
		Air Force Rocket Propulsion Laboratory Edwards Air Force Base, California
13. ABSTRACT The major objective of this program was the definition of problems associated with the use of 98% hydrogen peroxide (H <sub>2</sub> O <sub>2</sub> ) and Alumizine-43 in a staged-combustion rocket engine system. In the cooled version of the engine conceived, all of the H <sub>2</sub> O <sub>2</sub> is used to regeneratively cool a secondary combustor (in which Alumizine-43 is burned) before the H <sub>2</sub> O <sub>2</sub> passes through the preburner catalyst pack and the turbine. Conditions associated with operating this engine cycle that require investigation are (1) the ability of H <sub>2</sub> O <sub>2</sub> to cool the secondary combustor, (2) integrity of the catalyst (activity, durability) at higher temperature, (3) heat-transfer characteristics of 98% peroxide, and (4) the effect that thermal decomposition of H <sub>2</sub> O <sub>2</sub> vapor may have on the engine design. The program was divided into two phases. Phase I (of six months duration) consisted of design and analysis, 98% H <sub>2</sub> O <sub>2</sub> experimental technology, and critical hardware procurement for Phase II. This phase of the contract was conducted from June to December 1965. The results of Phase I indicated that 98% H <sub>2</sub> O <sub>2</sub> would be a satisfactory coolant and oxidizer for an Alumizine-fueled engine.		

(Continued on attached sheet)

DD FORM 1473

Unclassified

Security Classification

KEY WORDS	LINK A		LINK B		LINK C	
	ROLE	WT	ROLE	WT	ROLE	WT
Peroxide						
Alumizine-43						
Staged Combustion...						
Preburner						
Secondary Combustor						
Catalyst						
Heat Transfer						
Performance						
Decomposition						
Combustion Stability						

**INSTRUCTIONS**

1. **ORIGINATING ACTIVITY:** Enter the name and address of the contractor, subcontractor, grantee, Department of Defense activity or other organization (Corporate author) issuing the report.

2a. **REPORT SECURITY CLASSIFICATION:** Enter the even all security classification of the report. Indicate whether "Restricted Data" is included. Marking is to be in accordance with appropriate security regulations.

2b. **GROUP:** Automatic downgrading is specified in DoD Directive 5200.10 and Armed Forces Industrial Manual. Enter the group number. Also, when applicable, show that optional markings have been used for Group 3 and Group 4 as authorized.

3. **REPORT TITLE:** Enter the complete report title in all capital letters. Titles in all cases should be unclassified. If a meaningful title cannot be selected without classification, show title classification in all capitals in parentheses immediately following the title.

4. **DESCRIPTIVE NOTES:** If appropriate, enter the type of report, e.g., interim, progress, summary, annual, or final. Give the inclusive dates when a specific reporting period is covered.

5. **AUTHOR(S):** Enter the name(s) of author(s) as shown on or in the report. Enter last name, first name, middle initial. If military, show rank and branch of service. The name of the principal author is an absolute minimum requirement.

6. **REPORT DATE:** Enter the date of the report as day, month, year, or month, year. If more than one date appears on the report, use date of publication.

7a. **TOTAL NUMBER OF PAGES:** The total page count should follow normal pagination procedures. I.e., enter the number of pages containing information.

7b. **NUMBER OF REFERENCES:** Enter the total number of references cited in the report.

8a. **CONTRACT OR GRANT NUMBER:** If appropriate, enter the applicable number of the contract or grant under which the report was written.

8b. c. & d. **PROJECT NUMBER:** Enter the appropriate military department identification, such as project number, subject number, system number, task number, etc.

9a. **ORIGINATOR'S REPORT NUMBER(S):** Enter the official report number by which the document will be identified and controlled by the originating activity. This number must be unique to this report.

9b. **OTHER REPORT NUMBER(S):** If the report has been assigned any other report numbers (either by the originator or by the sponsor), also enter this number(s).

10. **AVAILABILITY/LIMITATION NOTICES:** Enter any limitations on further dissemination of the report, other than those imposed by security classification, using standard statements such as:

- (1) "Qualified requesters may obtain copies of this report from DDC."
- (2) "Foreign dissemination and dissemination of this report by DDC is not authorized."
- (3) "U. S. Government agencies may obtain copies of this report directly from DDC. Other qualified DDC users shall request through \_\_\_\_\_."
- (4) "U. S. military agencies may obtain copies of this report directly from DDC. Other qualified users shall request through \_\_\_\_\_."
- (5) "All distribution of this report is controlled. Qualified DDC users shall request through \_\_\_\_\_."

If the report has been furnished to the Office of Technical Services, Department of Commerce, for sale to the public, indicate this fact and enter the price, if known.

11. **SUPPLEMENTARY NOTES:** Use for additional explanatory notes.

12. **SPONSORING MILITARY ACTIVITY:** Enter the name of the departmental project office or laboratory sponsoring (paying for) the research and development. Include address.

13. **ABSTRACT:** Enter an abstract giving a brief and factual summary of the document indicative of the report, even though it may also appear elsewhere in the body of the technical report. If additional space is required, a continuation sheet shall be attached.

It is highly desirable that the abstract of classified reports be unclassified. Each paragraph of the abstract shall end with an indication of the military security classification of the information in the paragraph, represented as (TS), (S), (C), or (U).

There is no limitation on the length of the abstract. However, the suggested length is from 150 to 225 words.

14. **KEY WORDS:** Key words are technically meaningful terms or short phrases that characterize a report and may be used as index entries for retrieving the report. Key words must be selected so that no security classification is required. Identifiers, such as equipment model designation, trade name, military project, code name, geographic location, may be used as key words but will be followed by an indication of technical context. The assignment of links, roles, and weights is optional.



UNCLASSIFIED ABSTRACT (cont.)

Phase II was initiated immediately following the conclusion of Phase I and consisted of a series of 20,000-lbf preburner and staged-combustion evaluation tests. The Phase II technical achievements included the completion of a  $H_2O_2$  experimental heat-transfer program, a preburner test program, and a staged-combustion test program. Satisfactory operation of a 98%  $H_2O_2$  preburner was demonstrated at throughputs from 48 to 108.2 psia for two catalyst configurations. Staged combustion at 3000 psia with 98%  $H_2O_2$ /Alumizine-43 was demonstrated satisfactorily with two secondary injector concepts. Heat-transfer data on critical areas of the chamber and throat were obtained. The experimental performance of the propellant combination was determined over a range of mixture ratios with two different  $L^*$  chambers. The performance of 90%  $H_2O_2$ /Alumizine-43 was determined and compared to the 98%  $H_2O_2$ /Alumizine-43 propellant combination.

UNCLASSIFIED